CHARACTERISATION OF PSEUDOGENE-LIKE EP400NL IN CHROMATIN REMODELLING AND TRANSCRIPTIONAL REGULATION

A thesis presented in partial fulfilment of the requirements for the degree of

Doctor of Philosophy (Ph.D.)

in Biochemistry

At Massey University, Manawatū,
New Zealand

Zidong Li (Andy Li)
2022

"Nothing in life is to be feared. It is only to be understood. Now is the time to understand more, so that we may fear less"

Maria Skłodowska-Curie
(7 November 1867 – 4 July 1934)

ABSTRACT

EP400 is an ATP-dependent chromatin remodelling enzyme that has been implicated in DNA double-strand break repair and transcription regulation including Myc-dependent gene expression. It was previously shown that the ectopic expression of the N-terminal domain of EP400 increases the efficacy of chemotherapeutic drugs against cancer cells. This prompted the question of whether the EP400 N-terminal-Like (EP400NL) gene, which resides next to the EP400 gene locus, also plays a similar role in epigenetic transcriptional regulation to the full-length EP400 protein.

To characterize the function of the EP400NL nuclear complex, a stable cell line expressing TAP-tagged EP400NL was established, and the EP400NL complex was affinity purified and analyzed by mass spectrometry. EP400NL was found to form a human NuA4-like chromatin remodelling complex that lacks both the TIP60 histone acetyltransferase and EP400 ATPase. However, despite no histone acetyltransferase activity being detected, the EP400NL complex displayed H2A.Z deposition activity on a chromatin template comparable to the human NuA4 complex, suggesting another associated ATPase such as BRG1 or RuvBL1/RuvBL2 catalyses the reaction.

In addition to a role in H2A.Z deposition, it was also determined that the transcriptional coactivator function of EP400NL is required for serum and IFNγ-mediated transcriptional activation of the immune checkpoint gene PD-L1. EP400NL, cMyc and multiple identified ATPases such as BRG1, RuvBL1/RuvBL2 were shown to be recruited to the promoter region of PD-L1. To further demonstrate the importance of EP400NL in regulating Myc and IFNγ-mediated PD-L1 expression, CRISPR/Cas9 mediated EP400NL indels were introduced in H1299, a human non-small cell lung carcinoma cell line. These EP400NL indel cell lines show compromised gene induction profiles with significantly decreased PD-L1 expression from both Myc and IFNγ stimulation

experiments. In contrast to full-length EP400NL, two deletion mutants (Δ246-260 and Δ360-419) lacked the ability to enhance the expression level of PD-L1 mRNA or protein, indicating that these regions are important for coactivator activity.

Collectively, these data show that EP400NL plays a role as a transcription coactivator for cMyc-mediated gene expression and provides a potential target to modulate PD-L1 expression in cancer immunotherapy.

ACKNOWLEDGEMENTS

Pursuing a PhD in Biochemistry and Molecular Biology has been my dream ever since the first day I stepped into graduate school. It has been an adventure, after senior high in China I started my tertiary education in Japan, followed by Australia. I had never thought that I could have the opportunity to do my PhD here in New Zealand, a beautiful country with so much to offer. Personally, the acknowledgements are the hardest part of my thesis as deep emotion and gratitude for my friends, colleagues, and family need to be summarised within one to two pages and I realise that my way with words is not the best and I owe everyone more than I can say.

First and foremost, appreciation goes to my previous main supervisor Senior Associate Professor Jeong Hyeon Park. You chose me from many applicants and nudged me into the scientist I am today with constant support and patience. The daily meetings were crucial to my understanding of the field, and I will be forever grateful for the skills you have taught me and your guidance throughout this project.

To my current main supervisor Dr Helen Fitzsimons, you have been much more than a supervisor to me. You adopted me from the middle of my second year and together we waded our way through multiple Covid lockdowns due to the global pandemic, and you offered me a place to excel in my lab techniques as a research technician in the Massey Neurogenetics lab. Your encouragement, support, patience, and insight were more than I could have ever expected. Thank you.

To my co-supervisor Dr Tracy Hale, my sincere appreciation for all the invaluable advice, guidance, and patience. Thank you for always making time to help me along the way and always being happy to provide your expertise and vital feedback throughout my PhD journey.

A huge thank you to Professor Kathryn Stowell, who has been a great mentor for me during the first half of my PhD journey and offered me tremendous helpful research and life suggestions. I would also like to thank Dr Anja Schiemann for lab induction and frequent technical support; Trevor Loo, for performing the mass spectrometry analysis as well as providing help and advice along the way and lending me several reagents that were not readily available to me; the Manawatū Microscopy and Imaging Centre for training and assistance with microscopy techniques; the administration team in the School of Fundamental Sciences for their assistance and help. Furthermore, I have been fortunate to receive the Massey University Doctoral Scholarship to fund me through my research.

To all my lab members past and present in the biomedical research group: Jeremy Stephens, Sophie Burling, Shannon Ormond, Ruby Roach, Aseel Mohammad, Liam Hewson, Jennifer Tu, and Maia Smart, it has been a wonderful time working with you all, particularly thanks to Peter Gardner for teaching me many of the basics when I was new to the lab. Also thanks to my new research family members: Hannah Hawley, Sarah Wilson, Tan Wei Jun, Madeleine Palmer, and Ana Claasen for their inspiration, laughter, humour, kindness, and everlasting friendships.

Finally, a massive thanks to my family and friends for their constant encouragement over the years. Mum and Dad, you have always believed in me and given me the greatest support, particularly my Mum, who is my source of unconditional love, wisdom, and inspiration, I hope I have made you proud. Love you.

ABBREVIATIONS

aa.	Amino acids
ATPase	Adenosine Triphosphatase
ATM/PI-3 kinase	Ataxia telangiectasia/phosphatidylinositol-3 kinase
BAF	BRG1-associated factor
BrD.	Bromodomain
BR -HLH-LZ	Basic-Helix-Loop-Helix-Leucine Zipper
CBP	Calmodulin-binding peptide
ChIP	Chromatin immunoprecipitation
ChIP-qPCR	Chromatin immunoprecipitation-quantitative PCR
CMV promoter	Cytomegalovirus promoter
Co-IP	Co-immunoprecipitation
CRISPR	Clustered regularly interspaced short palindromic repeats
CRISPR/Cas9	CRISPR-associated protein 9
DBS	DNA binding site
DMAP1	DNA methyltransferase 1-associated protein 1
DSBs	DNA double-strand breaks
E-boxes	Enhancer boxes
EGF	Epidermal growth factor
EGFR	Epidermal growth factor Receptor
EP400	E1A binding protein P400
EP400NL	EP400 N-terminal-Like
Esa1	Essential Sas2-related acetyltransferase-1
ESCs	Embryonic stem cells
ET	E1A-TRRAP
FBS	Fetal bovine serum
FDA	U.S. Food and Drug Administration

FRTs	Flip recombination target site
GTFs	General transcription factors
GUSB	Glucuronidase beta
HAT	Histone acetyl transferase
HEK293T	Human embryonic kidney 293 cells
HAS	Helicase/SANT-associated
H3K27me	Histone H3 lysine 27
H3K9me	Methylation of histone H3 lysine 9
H3K4me3	Histone H3 lysine 4 trimethylation
H3K4me2/3	Di- or trimethylation of lysine 4 on histone H3
HLH	Helix-loop-helix
HR	Homologous recombination
LAR II	Luciferase Assay Reagent II
LZ	Leucine zipper
MED30	Mediator of RNA polymerase II transcription subunit 30
NPV	Nuclear pellet volume
NSCLC	Non-small cell lung cancer
NuA4	Nucleosome acetyltransferase of H4
PD-L1/PD-1	Programmed death ligand-1/programmed death-1
PEI	Polyethylenimine
PHD	Plant homeodomain
PIC	Preinitiation complex
pNTAP vector	N-terminal tandem affinity purification tagged vector
Pol II	RNA polymerase II
RAREs	Retinoic acid recognition elements
RT-qPCR	Reverse transcription polymerase chain reaction
RUVBL1/2	RuvB-like 1/2
SAGA	Spt-Ada-Gcn5 Acetyltransferase

SANT	Swi3-Ada2-NCoR-TFIIIB
SBB buffer	Streptavidin binding buffer
SBP	Streptavidin-binding peptide
SDS-PAGE	Sodium dodecyl sulfate – polyacrylamide gel electrophoresis
SNPs	Single nucleotide polymorphisms
SRCAP	Snf2 Related CREBBP Activator Protein
SV40	Simian virus 40 promoter
SWI2/SNF2	SWItch 2 /Sucrose NonFermentable 2
Swr1	Swi2 ATPase domain-related-1
TBP	TATA-binding protein
TBST	Tris-buffered saline (TBS) and Polysorbate 20
TetR	Tet repressor
TIP60	Tat-interactive protein 60
TRRAP	Transformation/transcription domain-associated protein
YEATS	YNK7-ENL-AF9-TFIIF small subunit

Table of Contents

TABLE OF FIGURES

TABLE OF TABLES

1. INTRODUCTION

1. 1 The molecular basis of chromatin structure

Inside the nucleus, eukaryotic DNA condenses into chromatin by associating with four evolutionarily conserved histone proteins H2A, H2B, H3, and H4. Two copies of each of these histones form an octamer, which is comprised of a tetramer of H3 and H4 and two H2A and H2B heterodimers. The octamer is wrapped around by 1.7 turns of approximately 147 bp of DNA to form a nucleosome. There are 14 contact points between the histone proteins and DNA within the nucleosome which is the basic unit of chromatin (Luger et al., 1997) (Figure 1. 1). These multiple interactions enable DNA to be packaged into the nucleus and make the nucleosome one of the most stable protein-DNA complexes under physiological conditions. However, the nucleosome is not a simple static unit, it possesses dynamic properties that are tightly regulated by various functional protein complexes.

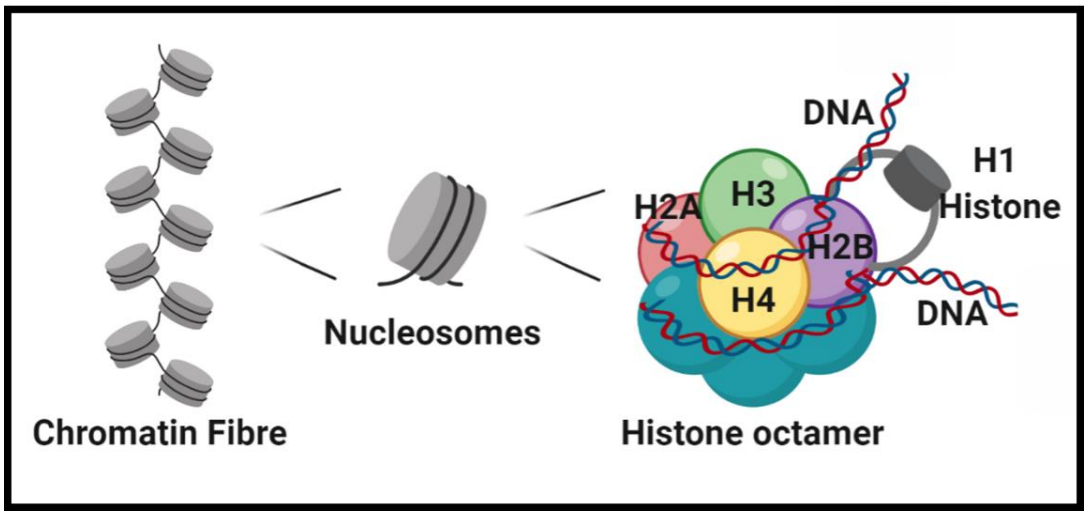

Figure 1. 1 Fundamental unit of chromatin

The chromatin fibre consists of a repeating array of nucleosomes that each contains 147 bp of DNA wrapped around an octamer of histone proteins. The fundamental unit of chromatin is the nucleosome, which consists of two copies each of H2A, H2B, H3, and H4 histones, eukaryotic DNA condenses into chromatin by specific interaction with histone proteins. This is an original artwork by Z.L.

1. 2 Transcriptional regulation

The basic mechanism of transcription is similar between eukaryotes and prokaryotes; The initiation of the RNA polymerase II (Pol II) transcription cycle begins with the binding of activators upstream of the core promoter. This event leads to the recruitment of TATA-binding protein (TBP) which then facilitates the subsequent binding of the general transcription factors including TFIIA, TFIIH, and RNA polymerase II at the transcription start site (Imbalzano et al., 1994, Thomas and Chiang, 2006). These factors and polymerase II constitute the preinitiation complex (PIC), where approximately 11-15 bp of DNA are melted around the transcription start site to generate an open complex for RNA synthesis. During transcription of the first 30 bp, the carboxyl-terminal domain of polymerase II is phosphorylated by the TFIIH subunit which allows the recruitment of regulatory factors that coordinate the mRNA elongation and processing (McCracken et al., 1997, Komarnitsky et al., 2000, Schroeder et al., 2000, Krogan et al., 2003).

Since none of these transcriptional activities can occur in a static chromatin environment, a better understanding of the enzyme activities that mediate chromatin dynamics can provide insightful information about the mechanisms of gene transcription and regulation. The dynamics of chromatin structure are tightly regulated through multiple mechanisms including histone modifications and chromatin remodelling. For instance, the analysis of the ATP-dependent SWI/SNF complex, which is a prototypical chromatin remodelling complex, revealed the importance of chromatin-remodelling enzymes in altering chromatin structure and also regulating multiple nuclear activities such as transcription, translation, DNA replication, and DNA damage repair (Stern et al., 1984, Carlson et al., 1984, Hirschhorn et al., 1992, Peterson and Herskowitz, 1992, Cote et al., 1994, Kwon et al., 1994).

1. 2. 1 Histone modifications

Epigenetic modifications of histones can alter the compaction of the nucleosomal array. Both histone tails and globular domains can be altered by post-translational modifications including methylation, acetylation, phosphorylation, and sumoylation, amongst others (Li et al., 2007). Histone modifications can be generally categorized into two major functional groups based on their transcriptional activities; (a) A condensed form of chromatin called heterochromatin is enriched in modifications such as methylation of histone H3 lysine 9 (H3K9me) and histone H3 lysine 27 (H3K27me) that result in transcriptional silencing and inactivation (Figure 1. 2, top panel), and (b) A lightly packed form of chromatin called euchromatin which is transcriptionally active and enriched with modifications such as acetylation of histone H3 and histone H4 or di- or trimethylation of lysine 4 on histone H3 (H3K4me2/3) (Figure 1. 2, bottom panel) (Brown et al., 2000, Strahl et al., 2002, Li et al., 2007).

In general, histone acetylation of H3 and H4 increases the accessibility of nucleosomal DNA due to a weaker interaction between DNA and histone proteins by neutralizing the basic charge of histones, resulting in a relaxed open chromatin structure. Reader proteins (effector proteins) can then specifically recognize and bind to covalently modified histone tails for recruiting components of the transcriptional machinery and chromatin remodelling complexes. Histone methylation, on the other hand, retains the electron charge of Lys residue and exhibits no ability in the alteration of electrostatic properties of histone proteins and has been found predominantly in gene repression (Allis and Jenuwein, 2016). However, depending on the binding of different panels of transcriptional factors or reader proteins, histone methylation is not always associated with gene repression; for example, methylations of Lys and/or Arg amino acids on histones tails alter their association with reader proteins that result in either transcriptional repression or activation (Teperino et al., 2010). In summary, the polypeptide chain of the histone tail which emanates from the nucleosome core

can be subjected to multiple covalent modifications including acetylation and methylation. These epigenetic modifications play a role as the prerequisite markers for either repression or activation of the genes neighbouring the region containing modified histones.

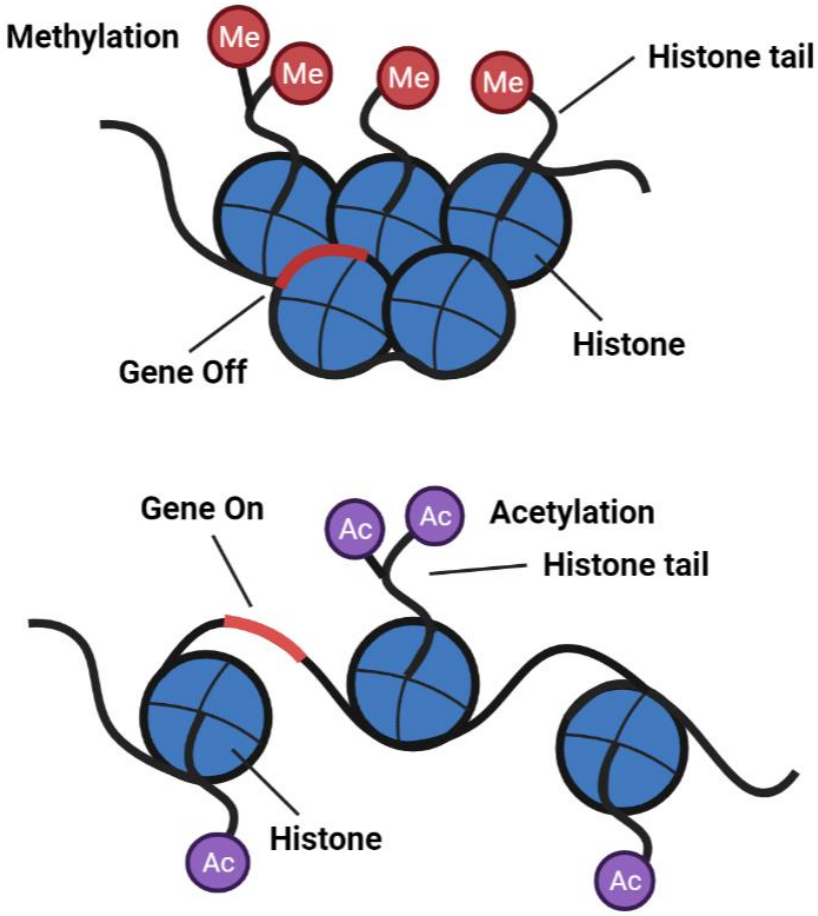

Figure 1. 2 Epigenetic modifications of histones.

(Top panel) DNA inaccessibility leads to gene inactivation. Gene expression is switched off due to the tightly packed heterochromatin enriched by histone methylation. (b) DNA accessible leads to gene activation. Gene expression is switched on due to nucleosomes being spaced far apart as euchromatin enriched in histone acetylation (Ac, acetylation; Me, methylation). This is an original artwork by Z.L.

1. 2. 2 Histone variants and their role in transcription

In addition to the canonical histones, H2A, H2B, H3, and H4, several histones' variants are integral to a variety of nuclear events including DNA repair and transcriptional regulation. A phenomenon in which histones H2A and H3 are replaced by their respective histone variants H2A.Z and H3.3 has been implicated in transactional activation (Figure 1. 3) (Jin et al., 2009). H1 is a linker histone that facilitates the compaction of the chromatin, allowing the formation of a higher-ordered chromatin structure that is transcriptionally inactive.

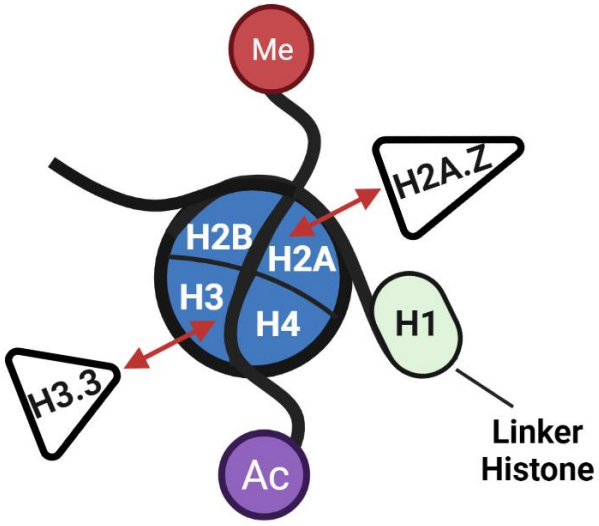

Figure 1. 3 Schematic of histone variant exchange in a nucleosome

Examples of histone tail modifications (Ac, acetylation; Me, methylation) and histone variants (H2A.Z and H3.3) are shown. Arrows indicate the replacement of canonical histones with histone variants. This is an original artwork by Z.L.

H2A.Z and H3.3 have been reported to be enriched in transcriptionally active genes and enhancers (Mito et al., 2005, Jin et al., 2009, Yukawa et al., 2014). Similarly to other histone variants, H3.3 differs from its canonical counterpart by four or five amino acids and can be incorporated into the nucleosomes in a replication-independent manner (Ahmad and Henikoff, 2002, Tagami et al., 2004) A salt-dependent disruption experiment revealed that nucleosomes containing

H3.3 variant exhibit less stability compared to those with canonical H3 (Jin and Felsenfeld, 2007), suggesting that H3.3 may play a key role in generating a relaxed open chromatin structure. Further studies have validated this point by showing H3.3 is enriched in transcriptionally active genes in a genome-wide analysis, and this enrichment is positively correlated with gene transcriptional levels (Goldberg et al., 2010, Kraushaar et al., 2016). H3.3 not only can be found in the adjacent areas towards the transcription start sites (TSSs) but is also enriched at active enhancers and insulators (Jin et al., 2009, Chen et al., 2013b).

H2A.Z has been studied in multiple model organisms such as yeast, Drosophila, and mammalian cells in which its loading mechanism has been partially identified. H2A.Z variants share about 90% similarity among the various higher eukaryotes. H2A and H2A.Z differ in amino acid sequence and only share about 60% identity (Jackson et al., 1996). Thus, a unique chromatin structure can be formed by the enrichment of the H2A.Z variant within nucleosomes. H2A.Z exhibits an additional docking domain and an extended acidic patch for controlling chromatin factor binding and activity in its C-terminus. This unique structure allows an efficient deposition of H2A.Z into the chromatin (Jensen et al., 2011, Wang et al., 2011). Yeast protein SWR1 (a yeast homologue of mammalian EP400) is a member of the SNF2 family of ATPases that is responsible for incorporating H2A.Z into the nucleosome (Mizuguchi et al., 2004b, Li et al., 2005b, Buchanan et al., 2009, Altaf et al., 2010). SWR1 complex is preferentially localized within the nucleosome depleted regions (NDRs) specifically at the first nucleosome in the direction of transcription, this particular NDR downstream nucleosome is referred to as the $+1$ nucleosome that contains the transcription start sites (TSSs) (Iyer, 2020). Interestingly, the H2A.Z-containing nucleosomes are occupying the NDR displaying promoters for the assembly of the transcription pre-initiation complex (Yague-Sanz et al., 2017). In line with this, H2A.Z appears to be deposited by ATPases and is enriched near the TSSs of transcriptionally active genes and enhancers to positively regulate their gene expression (Mizuguchi et al., 2004b,

Jin et al., 2009, Yukawa et al., 2014). In addition, H2A.Z incorporation has been reported to be coupled with H3.3 incorporation, the double variant incorporation synergistically altering the landscape of the chromatin and severely destabilized chromatins containing either one of those variants (Jin and Felsenfeld, 2007, Jin et al., 2009, Yukawa et al., 2014).

A study investigating the relationship between H2A.Z deposition and RNA polymerase demonstrated that the incorporation of H2A.Z reduced pol II stalling in the transcription initiation step and facilitated pol II elongation (Weber et al., 2014). As H2A.Z is predominantly repositioned by the SWR1 complex and its two mammalian homologs EP400 or SRCAP chromatin remodelling complexes, the inhibition of H2A.Z incorporation was observed on the deletion of the SRCAP complex, which resulted in transcriptional suppression of target genes (Wong et al., 2007). However, several studies have raised the possibility that in certain circumstances, H2A.Z deposition is negatively correlated with gene transcription. H2A.Z was reported to decrease the transcriptional activity by increasing nucleosome stability *in vitro* (Chen et al., 2013b) and no differences in nucleosome stability were observed between the H3.3/H2A and H3.3/H2A.Z containing nucleosomes as opposed to the concept that destabilized chromatin structure is a hallmark for transcriptional activation (Thakar et al., 2009). Thus, these studies remain controversial and reveal that the role of histone variant H2A.Z in gene regulation is complex.

1. 2. 3 Chromatin remodelling

Chromatin remodelling regulates the accessibility of nucleosomal DNA to transcription factors for transcriptional initiation by altering the interaction of histone and DNA. ATP hydrolysis, an enzymatic reaction that is often utilized by chromatin remodelling protein complexes such as SWI/SNF (SWItch/Sucrose Non-Fermentable), is used to change the contact points between histone proteins and DNA (Flaus and Owen-Hughes, 2004, Clapier et al., 2017). This event temporarily unwraps one end of DNA from the histone octamers to form a

transitional DNA loop or slides the nucleosomes off the transcriptional regulatory territories where the accessibility between nucleosomal DNA and transcription factors can be increased (Flaus and Owen-Hughes, 2004, Saha et al., 2006). Histone displacement has been characterized as one of the critical cellular activities in chromatin remodelling. A dynamic and flexible mechanism of histone displacement is catalyzed by the participation of ATP-dependent chromatin-remodelling enzymes (Owen-Hughes et al., 1996). Histone H2B can be frequently exchanged from nucleosomes (Kimura and Cook, 2001), and H2A/H2B are preferentially and rapidly exchanged in and out of nucleosomes as histone dimers (Ito et al., 2000, Bruno et al., 2003). In addition to H2A/H2B dimer displacement, an entire octamer can also be evicted under some specific conditions (Engeholm et al., 2009). Histone eviction facilitates transcription factor binding to the nucleosomal DNA to initiate transcription (Owen-Hughes et al., 1996, Workman, 2006). The dysregulation of chromatin remodelling complexes occurs by the translocations, mutations, or deletions of the complex subunits and has been implicated in multiple human diseases and cancers (Orlando et al., 2019).

1. 2. 4 Transcription factor recruitment for transcriptional initiation

Compared to prokaryotes, eukaryotes exploit multiple sophisticated strategies for transcription factor binding, particularly when the binding sites are hidden within chromatin (Hahn, 2004). While chromatin remodelling and histone modifications can alter the conformation of nucleosomal DNA to enhance the binding of transcription factors, it is a complex process that is not entirely dependent on the disruption of histone-DNA contacts. Efficient interaction between sequence-specific transcription factors and nucleosomal DNA also increases the binding affinity and serves as a foundation for loading additional cooperative regulatory factors (Taylor et al., 1991, Adams and Workman, 1995). Conformational changes such as the unwrapping of nucleosomes are integral to many cellular processes including DNA replication, DNA repair, and transcriptional initiation (Annunziato, 2005, Shivaswamy et al., 2008, Zhang et al., 2011). Histone

acetylation is known to play a major role in the regulation of eukaryotic transcription as the acetylated histone tails are the binding target of multiple bromodomain-containing chromatin remodelling complexes (Sterner and Berger, 2000, Josling et al., 2012). These chromatin remodelling complexes alter nucleosome structure to promote DNA - transcription factor binding and provide DNA access to additional regulators for gene activation (Workman and Kingston, 1998, Zhang et al., 2016).

Recent studies have shown that the nucleosome density at the promoter region bound by transcription factors is relatively lower than the coding region of the genome (Lee et al., 2004, Sekinger et al., 2005). For instance, a 200 bp nucleosome-free region was detected in the yeast promoter region that was flanked by H2A.Z-containing nucleosomes (Yuan et al., 2005, Billon and Cote, 2012), and transcription factor binding sites tend to be positioned in the region with a low level of nucleosome occupancy in most eukaryotic cells. A genome-wide chromatin immunoprecipitation (ChIP) study revealed a high level of histone H3K4/79me and H3ac were required for the binding of transcriptional activators such as Myc, indicating that presence of histone post-translational modifications within chromatin can influence the binding of transcription factors (Guccione et al., 2006a).

Based on the transcription studies in eukaryotes, it has been proposed that a nucleosome-free region must form at the promoter, comprising approximately 200 bp of nucleosome-free DNA which can be flanked by a high level of H2A.Z-containing nucleosomes in yeast. The H2A.Z variant can be escorted by histone chaperones to large ATP-dependent chromatin remodelling enzymes such as the SNF2 family ATPase SWR1 containing complex, which is responsible for its deposition (Figure 1. 4, A). This process occurs at the nucleosome-free region (NFR) which is the TSS-containing region sandwiched by -1 and +1 nucleosomes for the preparation of gene transcription (Figure 1. 4, B and C). Since high

occupancy of the H2A.Z-containing nucleosomes are not likely to be modified for the binding of effector proteins and Zhang et al suggested that the H2A.Z-bearing nucleosomes tend to be deposited at repressed/basal promoters (Li et al., 2005a, Zhang et al., 2005). Thus, to facilitate the exposure of the promoter DNA, it is essential to evict the H2A.Z variant upon transcription activation (Figure 1. 4, D). H2A.Z is dissociated from the nucleosomes on acetylation, active transcription ensures following its eviction (Zanton and Pugh, 2006). Studies suggest that H2A.Z-containing nucleosomes need to be removed to provide enough space for PIC formation, but this is not essential to create a complete nucleosome-free zone. Instead, the accumulation of acetylated histones (H3 and H4) are predominantly located in the promoter region after H2A.Z eviction for gene activation (Pokholok et al., 2005). Therefore, the removal of H2A.Z-containing nucleosomes can be seen as a strategy to provide enough space for the translocation of other residual nucleosomes as well as to increase the accessibility of the underlying DNA (Zhang et al., 2005).

Increased histone acetylation is positively correlated with transcriptional initiation (Pokholok et al., 2005), and histone acetyltransferase (HATs) such as GCN5, ESA1, and its mammalian homolog, TIP60 are recruited to the global promoter region together with SAGA (SPT-ADA-GCN5 Acetyltransferase), which is an evolutionarily conserved transcription coactivator, prior to PIC formation (Bhaumik and Green, 2001, Han et al., 2014). Although the functions of many components of the SAGA complex remain unknown, the 1.8 MDa acetyltransferase complex contains approximately twenty other proteins including TRRAP, the ATM-related cofactor TRA1, and GCN5, a histone acetyltransferase within the SAGA protein complex. Therefore, acetylation of histones H3 and H4 is crucial for transcription initiation, especially for the preparation of PIC assembly before transcription elongation.

In conclusion, once transcriptional activators bind to their cognate DNA binding sites occurs, a set of coactivators such as SWI/SNF or SAGA will be recruited to

enhance activator – DNA binding (Raisner et al., 2005, Yuan et al., 2005). These coactivators are generally chromatin remodelling complexes, histone modification enzymes, and mediators, which not only enhance the activator binding efficiency but are also able to increase the accessibility of nucleosomal DNA to general transcription factors.

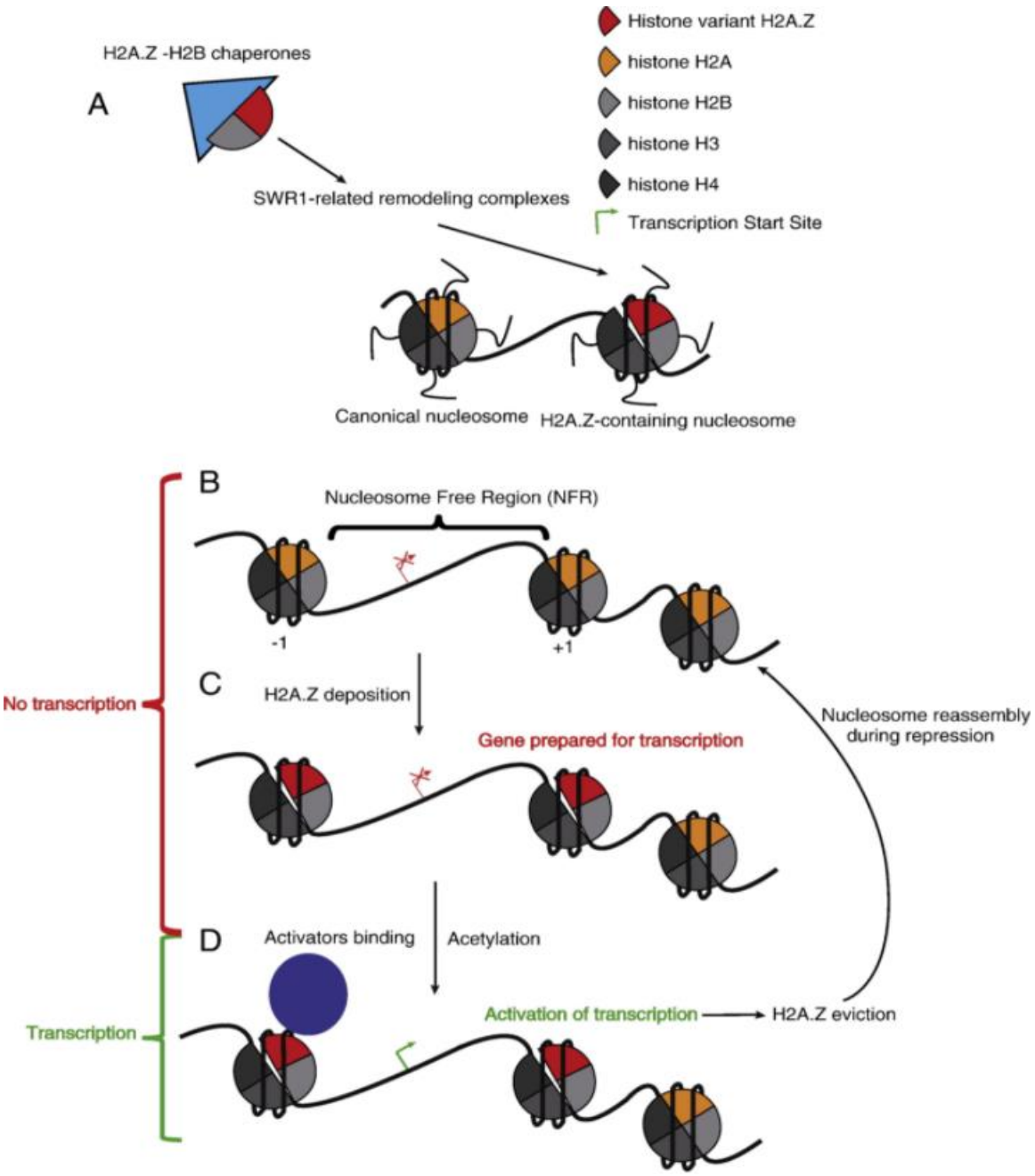

Figure 1. 4 Schematic representation of histone H2A.Z in gene activation

(A) H2A.Z incorporation in chromatin by the replacement of H2A–H2B dimers with H2A.Z–H2B dimers. The ATP-dependent exchange event is coordinated by

H2A.Z–H2B chaperones and Swr1-related complexes which results in a less stable chromatin structure. (B and C) A nucleosome-free region (NFR) is sandwiched by two well-positioned nucleosomes in the yeast promoter. Chromatin-containing incorporated H2A.Z is the prerequisite for the preparation steps of transcriptional activation. (D) H2A.Z acetylation occurs upon the binding of transcriptional activators. Transcription initiation leads to the eviction of H2A.Z containing nucleosomes. Figure modified from (Billon and Cote, 2012), reproduced with permission.

1. 2. 5 Summary of histone variants in transcriptional regulation

In brief, the regulation of eukaryotic chromatin depends on multiple processes including the covalent modifications of histones, and the incorporation of histone variants. Histone variant incorporation plays key roles in a variety of nuclear events such as DNA replication and repair, transcription, and chromosome packaging and segregation (Li et al., 2007, Euskirchen et al., 2012b, Venkatesh and Workman, 2015, Clapier et al., 2017). Some of the histone variants are also implicated in diseases such as cancer when their expression is dysregulated (Vardabasso et al., 2014, Giaimo et al., 2019). As high-order nucleosomes assembled by canonical histones H3, H4, H2A, and H2B are generally depleted in transcription regulatory regions such as enhancers and promoters, and ultimately form a highly repressive chromatin structure that is not accessible to RNA polymerase II (RNAP II) and correspondent transcription factors (Figure 1. 5, left panel). Thus, transforming the tightly compacted chromatin to its relaxed open form is essential for transcriptional activation.

Despite most nucleosomes being comprised of canonical histones, some nucleosomes contain variant histones such as H3.3 and H2A.Z instead of canonical forms (Figure 1. 5, middle panel) (Hake et al., 2006, Buschbeck and Hake, 2017). Canonical histones and their variants are generally sharing high sequence identities with minor changes in amino acids sequence (e.g., canonical H3 and H3.3) (Maze et al., 2014, Mattiroli et al., 2015). These structural differences trigger the alteration of chromatin dynamics and flexibilities which influence gene transcription by associating with chromatin modifiers such as SWI/SNF complex

(Figure 1. 5, middle panel) (Volle and Dalal, 2014, Buschbeck and Hake, 2017). Double variants (H2A.Z and H3.3) containing nucleosomes can be evicted by interacting with their correspondent histone chaperone which leads to the assembly of the pre-initiation complex onto the underlying DNA (Figure 1.5, right panel) (Jiang and Pugh, 2009). Therefore, histone variants are necessary for altering the landscape of the chromatin and interacting partners of the nucleosome by its distinctive biochemical properties which ultimately leads to the transactivation of targeted genes.

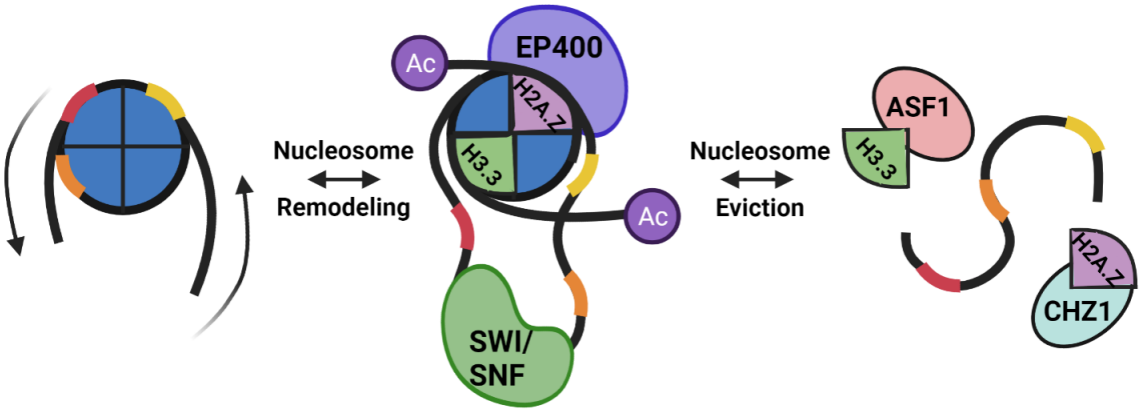

Figure 1. 5 Brief summary of double variants in transcription

(Left panel) A stable nucleosome with less DNA accessibility. (Middle panel) A remodelled nucleosome with relatively higher DNA accessibility. (Right panel) An evicted nucleosome with full DNA accessibility is ready for the binding of transcriptional activators. Three transcription factor binding sites are the orange, red, and yellow boxes, these sites are not available for binding in the left panel but being exposed in the middle panel due to the nucleosome being slide away as indicated by the arrow or modified by chromatin remodelers (green and purple complexes) and histone modification such as acetylation indicated as Ac. (Right panel) Anti-silencing function 1 (ASF1) and H2A.Z-specific chaperone (CHZ1) are examples of histone chaperones that can assist the eviction of variants containing nucleosomes for the preparation of transcriptional initiation. This figure is an original artwork created by Z.L. with referenced to (Jiang and Pugh, 2009).

1. 3 Activation of transcription by E1A binding protein P400 (EP400)

EP400 was first characterised as a subunit of a protein complex that can interact with adenovirus E1A oncoprotein for onco-transformation. E1A oncoprotein elicits abnormal biological effects including the promotion of cell cycle progression, immortalization, and blockade of differentiation by targeting the specific cellular proteins (Fuchs et al., 2001). Binding of E1A to its targeted cellular protein such as E1A-pRb (A tumour suppressor) or E1A-p300/ CREB-binding protein (Transcriptional coactivator/signal integrating proteins) can lead to local chromatin conformation changes and therefore, exhibit transcriptional regulatory effect (Nevins, 1992, Goodman and Smolik, 2000).

EP400 is a multidomain protein that contains four functional domains; an HSA (Helicase and SANT Associated) domain, a SWI2/SNF2 (SWItch 2/Sucrose Non-Fermentable 2) homology domain, a poly Q (poly-glutamine), and a SANT (Swi3-Ada2-N-Cor-TFIIIB) domain (Figure 1. 6) (Aasland et al., 1996). The HSA domain is a primary binding platform for nuclear actin-related proteins (ARPs) which are the core components of multiple chromatin remodelling complexes and have been implicated in transcriptional control. Thus, HSA domains are necessary for the assembly of its specific ARP–actin modules and the HSA bound ARPs can further regulate chromatin remodelling ATPases (Szerlong et al., 2008). Physical interaction analysis of EP400 and SOX10 revealed that EP400 can interact with transcription factor SOX10 and binds to the regulatory regions of the MYRF gene, and this process is achieved by interacting with the HSA and the SANT domains of EP400, but not to the N-terminal region, the ATPase domain or the glutamine-rich C-terminal region (Elsesser et al., 2019). The SWI2/SNF2 domain is a well-characterized region in many ATPases which has been shown to exhibit an ATP-dependent histone exchange activity, but little has been reported regarding the other domains of the EP400 (Fuchs et al., 2001, Mizuguchi et al., 2012).

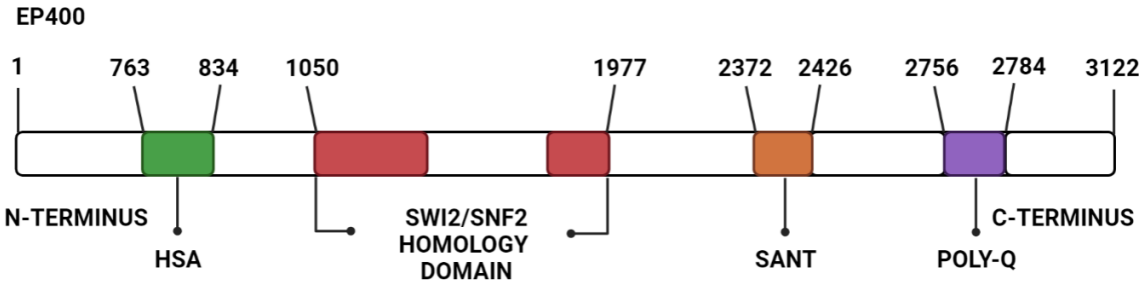

Figure 1. 6 Schematic representation of full-length EP400

Scheme of EP400, its functional HSA, bipartite ATPase, SANT, and Q-rich domains. Full-length EP400 is 3122 amino acids in length. It contains several functional domains including the HSA domain (763 aa. -834 aa.), the SWI2/SNF2 homology domain (Bipartite ATPase) (1050 aa. -1977 aa.), the SANT domain (2372 aa. – 2426 aa.), and the poly-Q domain (poly-glutamine) (2756 aa. -2784 aa.). This is the original work by Z.L.

EP400 is a component of two multi-protein complexes known as the EP400 complex and the TIP60 complex, which is also referred to as the hNuA4 complex (Ikura et al., 2000, Fuchs et al., 2001). These two complexes share the same composition of the subunit proteins except for TIP60, which is not in the EP400 complex. Other subunit proteins that are shared by both EP400 and TIP60 complex include TRRAP (Transformation/transcription domain-associated protein), BAF53 (53 KDa BRG1-associated factor), RuvBL1, and RuvBL2 (TATA-binding protein (TBP)-interacting protein). Unlike the TIP60 complex, the EP400 complex does not exhibit histone acetylase activity, however, given their similar composition, it is feasible to suggest a possible dynamic exchange of the subunit proteins within the two complexes (Ikura et al., 2000, Fuchs et al., 2001, Park et al., 2010).

The human NuA4 (hNuA4) histone acetyltransferase (HAT) complex regulates transcription through chromatin remodelling of target genes (Doyon et al., 2004, Yamada, 2012). It consists of approximately 16 subunits including the phosphatidylinositol 3-kinase family protein kinase homolog TRRAP, TIP60 histone acetyltransferase, EP400, and BRD8 (Figure 1. 7) (Yamada, 2012). The

NuA4 complex was initially purified from *Saccharomyces cerevisiae* to study its nucleosomal H4/H2A HAT activity (Grant et al., 1997) in which an ESA1 protein, a yeast counterpart of human TIP60, was found to be the catalytic HAT component (Allard et al., 1999). In addition to its HAT activity, yESA1 or hTIP60 also contain a chromodomain (CHD) which has been suggested to bind specific methylated histone isoforms or RNA-binding modules (Akhtar et al., 2000, Vaquero et al., 2003). EP400 in the TIP60 protein complex is an ATP-dependent chromatin remodeler that exhibits multiple functions specifically in regulating gene expression and DNA double-strand break repair (Lu et al., 2009, Xu et al., 2012). Unlike canonical chromatin, chromatin containing acetylated H2A.Z and H3.3 double variants stimulates transcription *in vitro* (Mizuguchi et al., 2004a, Ruhl et al., 2006, Gevry et al., 2007), and higher occupancy of these histone variants at the promoter and enhancer region is positively correlated with gene activation (Ahmad and Henikoff, 2002, Chen et al., 2013a). EP400 is required for the activation of gene expression by assisting the deposition of H2AZ/H3.3 onto the promoter and enhancer regions which is an essential process in regulating transcription *in vivo* (Pradhan et al., 2016a, Pradhan et al., 2016b). Higher enrichment of EP400 is also found within the preinitiation complex and this facilitates the exchange of canonical histones with variant histones to trigger gene transcription. (Pradhan et al., 2016b). Taken together, EP400 is a chromatin-remodeler, which plays a critical role in promoting transcriptional initiation.

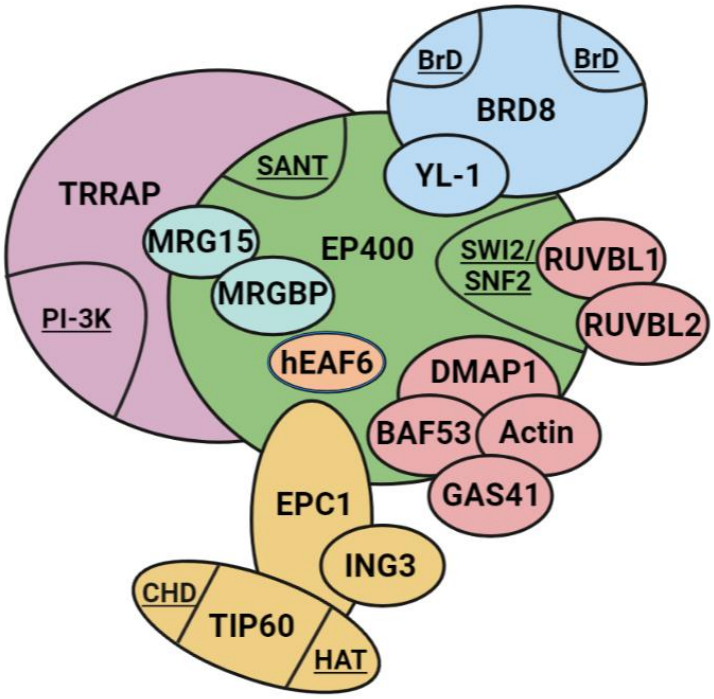

Figure 1. 7 Schematic representation of human NuA4 HAT complex

The Human NuA4 complex consists of approximately 16 subunits including TRRAP, EP400, BRD8 EPC1/EPC-like, TIP60, DMAP1, ING3, YL-1, RUVBL1, RUVBL2, BAF53, Actin, MRG15, GAS41, MRGBP, and hEAF6. A SWI2-related ATPase (EP400) and a histone acetyl transferase (TIP60) present in the human NuA4 complex are homologous to the subunits of the yeast SWR1 complex and ESA1. Other subunits such as double-bromodomain factor (BRD8) and RuvB-like helicases (RUVBL1, RUVBL2) are also essential subunits for recognizing acetylated histones tails via its bromodomains and displaying ATPase activity via its ATPase domain respectively. This complex can be divided into two modules based on its nuclear functions. (Top) A module involved in transcription, DNA repair, and recruitment of functional proteins (purple, green, red, and blue); (Bottom) A module associated with nucleosomal HAT activity and recognition of epigenetically modified histones (yellow). Domains are indicated with underlines. This figure is an original artwork created with referenced to (Doyon and Cote, 2004b).

1. 4 EP400 is implicated in multiple cellular functions

1. 4. 1 EP400 in DNA double-strand break repair

Chromatin is a highly dynamic structure that is altered during transcription and DNA break repair. An expansion of chromatin was observed at sites neighbouring DNA break which is presumably due to the additional space required by the repair proteins. This chromatin expansion ensures higher DNA accessibility and leads to an efficient DNA double-strand break repair. EP400, as an ATPase, facilitates changes in chromatin conformation via nucleosome destabilisation at the break sites, and knock down or loss of EP400 activity increases the cellular sensitivity to radiation which results in chromosomal aberrations (Jiang et al., 2010, Xu et al., 2010). Additionally, the EP400-containing TIP60 complex is required for the acetylation of both H2A.X and H4 histones at the DNA break sites in order to promote an open chromatin structure (Bird et al., 2002, Murr et al., 2006). Additionally, EP400 is required for DNA repair by homologous recombination (HR). EP400 has been shown in the same complex with RAD51 (a key component of HR) and can recruit RAD51 to DNA double-strand break sites for homology-directed repair (Courilleau et al., 2012). Therefore, the interaction between EP400 and Rad51 is required for chromatin remodelling and decompaction around DNA double-stranded breaks, and loss of EP400 causes defects in the DNA double-stranded break repair (Courilleau et al., 2012).

1. 4. 2 EP400 in carcinogenesis

The name of EP400 originated from the specific binding to adenovirus E1A oncoprotein, which is required for viral replication and cellular transformation of primary rodent cells (Bayley and Mymryk, 1994, Fuchs et al., 2001). A mutant of E1A with no EP400 binding site is defective in cellular transformation, which suggests that EP400-E1A binding is essential for oncogenic transformation (Fuchs et al., 2001). An *in vitro* study revealed that the ratio of EP400 and TIP60 expression is crucial to carcinogenesis, given the fact that either overexpression or

siRNA knockdown of EP400 or TIP60 results in the apoptosis of colon cancer cells indicating the importance of balanced expression of EP400/Tip60 in cancer progression (Mattera et al., 2009).

1. 4. 3 EP400 in stem cell maintenance and embryonic development

An *in vivo* study demonstrated the importance of EP400-TIP60 in stem cell maintenance and embryonic development; RNAi screening of 1008 loci encoding chromatin-related proteins in mouse ESCs identified seven subunits of the TIP60-EP400 complex (TRRAP, TIP60, EP400, DMAP1, RuvBL1, RuvBL2, and GAS41) that resulted in diverse phenotypes upon knockdown. ESCs depleted of these EP400-TIP60 subunits exhibited phenotypes consistent with a defect in maintaining the identity of the ESCs including impairment of colonies formation, defects in embryoid bodies (EBs) aggregation, dysregulation of the cell cycle, cellular proliferation, and poor expression of Alkaline phosphatase (AP) activity, which normally is high in undifferentiated ESCs and becomes weaker upon differentiation (Martin and Evans, 1975, Fazzio et al., 2008). The screening also indicates that histone H3 lysine 4 trimethylation (H3K4me3) is indispensable for EP400 localization within the promoter region of both active and silent genes. Embryonic developmental regulators are predominantly deregulated upon TIP60-EP400 knockdown (Fazzio et al., 2008). Nanog, a transcription factor involved in embryonic development, is associated with EP400 and depletion of Nanog can decrease the binding of EP400 to promoters, which inhibits the transcription of Nanog targeted genes that are essential for embryonic development (Fazzio et al., 2008). In short, TIP60-EP400 orchestrates the gene expression in ESCs by processing signals from both Nanog and H3K4me3. The study also showed that homozygous TIP60-EP400 knock-out mice cannot survive after embryonic day 11.5 (E11.5). When the phenotypic analysis was undertaken, an incomplete neural tube maturation and an anaemic appearance potentially caused by a defect in embryonic haematopoiesis were observed. These abnormal phenotypic characteristics are likely brought by the deregulation of genes that are responsible

for embryonic development such as the Hox gene cluster (Ueda et al., 2007, Fazzio et al., 2008). In conclusion, in addition to the role of EP400 associated protein complex in cancer progression, it is also necessary to maintain stemness in embryonic stem cells (ESCs) *in vivo* (Fazzio et al., 2008).

1. 4. 4 Summary

In addition to DNA breaks repair and cancer progression, the EP400 containing TIP60 complex is also involved in a variety of biological processes and cellular activities such as cell cycle progression, stem cell maintenance and differentiation, cell migration, and invasion (Yamada, 2012). The EP400-associated protein complexes are essential for normal transcriptional regulation within cells, but also help to maintain cell homeostasis, and their dysregulation contributes to malignancy.

1. 5 The transcription factor Myc

One of the cellular candidates that is targeted by EP400 is the oncoprotein Myc, which is a global transcription factor that is implicated in 10-15% of genes in humans (Fernandez et al., 2003, Li et al., 2003). Hence, the interrelationship between EP400 and Myc and the mechanisms of Myc-mediated transcriptional regulation require further investigation.

Myc has been investigated for decades due to its importance in many of the molecular biological networks it regulates to orchestrate tissue homeostasis. The Myc family contains three evolutionary conserved transcription factors cMyc, nMyc, and lMyc (Soucek and Evan, 2010). They are functionally similar and coordinate a variety of cellular activities such as cell proliferation, cell cycle progression, biosynthetic metabolism, and apoptosis (Gallant, 2005). Myc protein, as a transcription regulator, can regulate a large number of genes for diverse activities such as somatic cell proliferation, stem cell maintenance and even triggering cancer progression (Lotterman et al., 2008, Lin et al., 2009). In normal

cells and tissues, Myc function is tightly regulated by developmental signals. These signals facilitate mitosis and ensure the appropriate regulation of somatic cell expansion and germ cell proliferation (Soucek and Evan, 2010). Fibroblasts that lack cMyc have a significant decrease in the rate of proliferation and the deletion of either cMyc or nMyc results in embryonic death around E11 (Cavalheiro et al., 2017). Therefore, Myc is essential in maintaining normal tissue homeostasis and embryonic development. In contrast, the deregulation of Myc has been pinpointed as a fundamental yet universal mechanism of tumorigenesis.

1. 5. 1 The deregulation of Myc in cancer development

Overexpression of Myc proto-oncogene is one of the most common routes for driving cancer development (Land et al., 1983). More than 50% of human cancers involve Myc overexpression, which may contribute to the low survival rate of cancer patients (Vita and Henriksson, 2006). Although increased Myc copy numbers do not correlate with Myc overexpression, the frequency of Myc gene amplification has been seen as one of the indicators of metastatic disease and poor prognosis (Singhi et al., 2012). Myc overexpression can result from several biological processes; For example, the deregulation of Myc is often accompanied by the occurrence of a common retroviral promoter insertion which leads to the significant gene activation of Myc family members (Hayward et al., 1981). Increased synthesis of Myc mRNA can also be induced by genomic changes such as single nucleotide polymorphisms (SNPs)(Stine et al., 2015); an inherited nucleotide variant rs6983267 appeared more than one mega-base away from the Myc gene on chromosome 8q24 is a typical risk indicator for causing colorectal and prostate cancer (Haiman et al., 2007). Despite the remote distance, this polymorphism exhibits a tumour-promoting trait that can assist the binding of a transcription activator TCF-4 to a distal Myc enhancer. This would ultimately result in an increased Myc transcription.

Thus, the Myc overexpression is caused by a dynamic and sophisticated mechanism that can be mediated not only by a higher frequency of the Myc gene amplification but also by the genomic alteration and rearrangements.

1. 5. 2 Transcriptional functions of Myc

Transcriptional regulation via Myc is often achieved by a variety of nuclear transcription cofactors to promote either normal cellular proliferation or oncogenic transformation (Cowling and Cole, 2006, Stine et al., 2015). Both the C-terminus and N-terminus of Myc are essential for Myc functions including transcriptional regulation (Oster et al., 2003). The Leucine zipper (LZ) and a helix-loop-helix (HLH) are the evolutionarily conserved DNA binding domains in the C-terminus of Myc. The transactivation domain was identified by fusing the Myc N-terminus to the Gal4 DNA-binding domain, which demonstrated that Myc N-terminus is also a transactivator (Cowling and Cole, 2006). Despite being a global transcriptional activator, the majority of Myc targeted genes can only be upregulated by an average of two-fold which suggests a relatively weak transcriptional activity of Myc compared to other transcription factors (Patel et al., 2004).

1. 5. 3 Myc binding for the transcription of its targeted genes

The studies of the transcription function of Myc have been thriving since the discovery of its interacting partner Max. Unlike Max, which can homodimerize, Myc cannot and must heterodimerise with Max for recognizing and binding to a specific DNA binding sequence (Blackwood and Eisenman, 1991). Myc binding is influenced by several factors: Firstly, Myc/Max dimers preferentially bind to the canonical sequence (CACGTG) called an E-boxes (enhancer box), which is present in approximately 15% of human genes. This E-box sequence exists throughout the genomic DNA and appears on an average of every 4kb (Eilers and Eisenman, 2008). It can be recognized not only by Myc but also by any other

proteins that have the basic-Helix-Loop-Helix-Leucine Zipper (BR-HLH-LZ) structure (Jones, 2004).

Secondly, in addition to the E-box sequence, the binding of Myc also depends on the permissive status of the chromatin. Dimerised Myc can preferentially bind to CpG rich islands near proximal promoter regions which are associated with open and active chromatin (Kundu and Rao, 1999, Zeller et al., 2006). In addition, Myc binding is also enhanced by the posttranslational modifications on nucleosomes. Histone H3 methylation at lysine residues 4 and 79 facilitates the transformation from heterochromatin into euchromatin, which allows those buried E-boxes to be recognized and detected by the potential interacting transcription factors (Lin et al., 2012, Guccione et al., 2006b).

Thirdly, the abundance of Myc also influences where the binding occurs. When Myc levels are low, the Myc/Max dimers bind primarily to the E-boxes containing promoters upon the induction of mitogenic signals (Fernandez et al., 2003). In addition to binding the proximal canonical E-boxes, when Myc levels are high, it will also bind to E-boxes located at distal enhancer sequences or imperfect E-box binding sequences (Lin et al., 2012).

Lastly, Myc can interact with other DNA binding transcription factors to enhance transcription. This mechanism was discovered as a general strategy in most eukaryotic organisms (Gerstein et al., 2012). Myc/Max dimers can be recruited by retinoic acid receptor-α for regulating downstream cellular responses and further activating retinoic acid recognition element (RARE)-containing promoters that lack the E-box sequences. This process maintains a balance between proliferation and differentiation of leukemia cells in a hormone-dependent manner (Uribesalgo et al., 2011).

Taken altogether, these data show that the Myc/Max dimers can bind to the specific E-box sequences (CACGTG) and activate gene transcription. However,

this is not the only pathway for triggering transcription activation of all Myc targeted genes. The permissive status of chromatin is also a key factor, which includes inherited epigenetic, posttranslational modifications, doses of Myc expression, and CpG islands. These are unique conditions that change across different cell types. Indeed, the discovery of Myc co-binding transcription factors has also opened new ideas and avenues of investigation for understanding Myc mediated transcriptional regulation.

1. 5. 4 Myc and its nuclear cofactor TRRAP

TRRAP (Transactivation/transformation Associated Protein) is a highly conserved 434 kDa protein that has been biochemically identified as a direct binding partner of Myc from purified Myc/cofactors protein complex (McMahon et al., 1998). An internal domain of TRRAP binds directly to Myc, and the strength of the specific binding correlates with the Myc oncogenic transformation activity (Park et al., 2001). Moreover, reduction of TRRAP expression by antisense RNA inhibits Myc-mediated oncogenic transformation, suggesting that TRRAP is an important co-factor for mediating Myc function (Park et al., 2001).

Myc is well known for its capability of recruiting HATs protein complexes to its target genes, and although TRRAP does not contain a HATs catalytic domain, it does interact with the histone acetyltransferase GCN5, the recruitment of which is increased by Myc under serum stimulation (Bouchard et al., 1999, Liu et al., 2003).

1. 5. 5 Myc interacts with human NuA4 (hNuA4) complex by binding to TRRAP

TRRAP is one of the evolutionarily conserved subunits found in the histone acetylase TIP60/NuA4 complex (Cai et al., 2003b). It can be specifically recruited to chromatin by Myc for acetylation of histone H4; H4 hyperacetylation and targeted gene expression were found to be significantly reduced in Myc-deficient cells (Frank et al., 2001). This result proved the post-translational acetylation of

the histone H4 N-terminal tail by the hNuA4 histone acetyltransferase complex is required for hNuA4-mediated transcriptional regulation (Xu et al., 2016). Furthermore, overexpression of an enzymatically inactive form of TIP60/NuA4 resulted in an hour delay of the Myc mediated H4 acetylation compared to the wild-type TIP60 containing complex (Frank et al., 2003). On the contrary, Myc repression positively correlates with the loss of histone H4 acetylation (Xu et al., 2001). Myc can recruit TIP60 to the cellular chromatin *in vivo* where its responsive genes are located, and this recruitment event requires additional subunits of the NuA4/TIP60 HAT complex: TRRAP, EP400, TIP48, and TIP49 (Frank et al., 2003). Therefore, the histone acetyltransferase (HAT) complex appears to play a critical role in assisting Myc function. A recent study revealed the association of Myc with the hNuA4 complex can be enhanced by the interaction between E1A oncoprotein and the TRRAP subunit within the HAT complex (Zhao et al., 2017). Specifically, the N-terminal domain of E1A can target TRRAP and form an E1A-TRRAP targeting (ET) domain for enhancing the interaction between Myc and the hNuA4 complex. A global gene expression analysis comparing wild type and E1A N-terminal mutants revealed the interaction of Myc with the hNuA4 complex resulted in higher enrichment in a panel of genes which involved in cell cycle processes, ribosome biogenesis, gene expression, and also genes highly expressed in cancer cells (Ben-Israel and Kleinberger, 2002, Zhao et al., 2017).

1. 5. 6 EP400 is critical in promoting Myc dependent gene transactivation

In addition to examining the role of the ET domain in facilitating the expression of Myc targeted genes, data from a decade ago already pointed out that EP400 is an essential factor for the regulation of E1A activity (Tworkowski et al., 2008). E1A-mediated oncogenic transformation cannot occur without binding to EP400. Since adenovirus E1A drives oncogenesis by interacting with transcription factor Myc and other signalling pathways that control cell growth and proliferation (Chakraborty and Tansey, 2009), it is critical to uncover the potential interacting

partners of E1A and the downstream mechanisms, such as how the associated intracellular signalling and nuclear transfer of these E1A-bound functional protein complexes contribute to oncogenesis. Previous studies demonstrated that E1A stabilises Myc protein via EP400 and enhances the association between Myc and EP400 at Myc target genes to activate transcription (Figure 1. 8) (Tworkowski et al., 2008). These findings indicate a crucial mediating role of EP400 in consolidating the stability between E1A and Myc in promoting their targeted gene expression (Tworkowski et al., 2008).

Taken together, a higher level of Myc expression leads to increased histone acetylation of Myc target genes. Myc recruitment of these histone acetyltransferases contributes to increased transcription by creating an open, and relaxed form of chromatin structure. Moreover, this process is heavily influenced by E1A stabilization with the cooperation of EP400 in adenovirus E1A-mediated oncogenesis (Tworkowski et al., 2008). Since the expression of Myc is tightly linked to oncogenesis and it is overexpressed in a variety of cancers, identification of the potential Myc-associated cofactors and how they regulate Myc-dependent transcription may shed light on the mechanisms through which Myc contributes to oncogenesis.

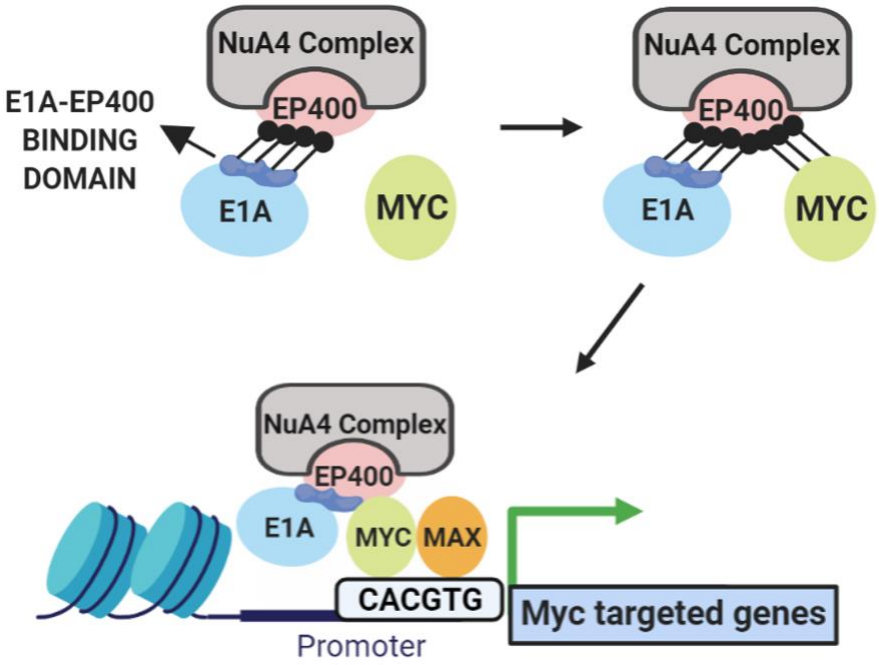

Figure 1. 8 E1A stabilized Myc via EP400 in promoting Myc targeted genes

EP400, a subunit of the hNuA4 HAT complex, can associate with E1A oncoprotein for stabilizing Myc, ultimately, enhancing Myc targeted gene expression. This is an original artwork by Z.L.

1. 6 PD-L1 in cancer immune evasion

The immune system is an efficient and powerful biological tool to fight foreign pathogens, viruses, bacteria, and mutated cells that are programmed to become cancerous. However, in battle with cancer, the immune system that serves as our bodyguard does not always win as cancer cells have their specific defence strategies to hide or even compromise the armies developed from our immune responses. The immune system is a complex apparatus that relies on a coordinated balance between activating and inhibitory mechanisms to counteract foreign invasion of viruses, infections, or cancer formation without causing excessive damage to the healthy cells and tissues. The concept of an immune check has become a hot topic due to its crucial role in orchestrating the balance in the immune system and its relevance in cancer immunotherapy (Schildberg et al., 2016, Antonangeli et al., 2020).

Immune checkpoints are groups of inhibitory receptor/ligand pairs that serve as gatekeepers of the immune response; they can regulate multiple signalling pathways including self-tolerance, which prevents the immune system from attacking cells indiscriminately (He and Xu, 2020). This mechanism can be adopted and taken advantage of by cancerous cells for cancer immune escape. Cytotoxic T lymphocytes can directly trigger apoptosis of tumour cells through granule exocytosis (perforin, granzyme) or death-ligand–death receptor (Fas–FasL, TRAIL) systems (Martinez-Lostao et al., 2015, Tokarew et al., 2019), however, cancer cells can protect themselves from recognition and elimination by the cytotoxic T lymphocytes via stimulating immune checkpoint targets. Among these immune checkpoints, the blockade of programmed death-protein 1 (PD-1) and its ligand (PD-L1) has attracted much attention and has been utilized as one of the major treatments in cancer immunotherapy by enhancing T cell immune responses against tumour cells (Wu et al., 2019).

The PD-L1/PD-1 immune checkpoint inhibits the activation of effector T lymphocytes to enhance the immune tolerance of tumour cells, and ultimately leads to tumour immune escape (Jiang et al., 2019a). Tumour immune escape is a phenomenon in which tumour cells can grow and metastasize indefinitely without being recognized and attacked by the immune system. Among all the checkpoints, PD-L1 has been focused on for years due to its abnormally high expression in cancer cells (Qin et al., 2015, Tang et al., 2017, Lin et al., 2015, Zhou et al., 2017), and its widespread expression through a diverse range of other cell types (Keir et al., 2008, Yamazaki et al., 2002).

On the other hand, PD-1 is a transmembrane protein that is expressed predominantly in a wide range of immune cells, and when it binds PD-L1, it activates its intracellular signalling pathways for inhibiting the activities of the immune cells (Figure 1. 9). This results in a decrease in antibody production and cytokine secretion for maintaining the homeostasis of the immune system. In addition, the specific PD-L1/PD-1 binding can subsequently trigger the apoptosis

of lymphocytes in facilitating the immune evasion process by allowing tumour cells to escape or suppress the host immune surveillance (Jiang et al., 2019b). Based on this concept, anti-cancer drugs such as Nivolumab, Pembrolizumab that work as PD-L/PD-L1 antagonists were previously approved by the FDA and are currently in clinical trials (Gong et al., 2018). Further, blocking immune checkpoints with monoclonal antibodies would potentially allow a proportion of patients to gain significant survival benefits.

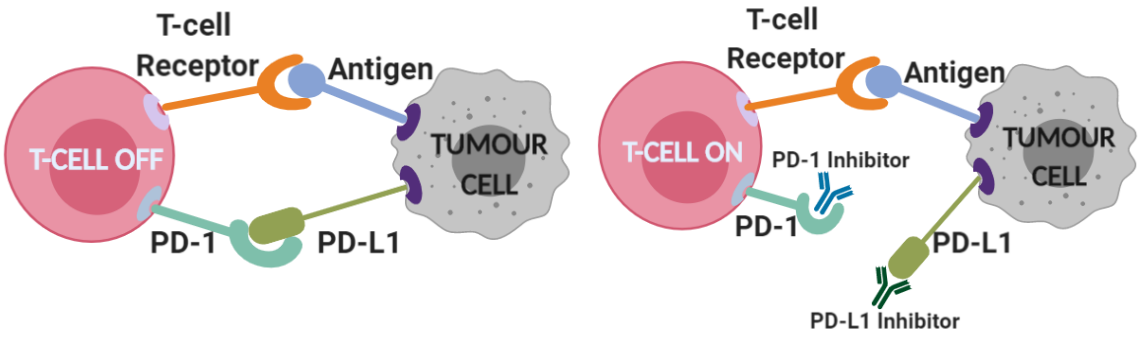

Figure 1. 9 Schematic of cancer cell immune escape by expressing PD-L1

The suppression of T cell activation and apoptosis is triggered by the specific PD-1/PD-L1 binding between T-cells and tumour cells. The interaction between the programmed death 1 (PD-1) receptor, and its ligand PD-L1, is one of the most important immune checkpoints. The activity of T-cells will be switched on once the binding is interrupted by their inhibitors/antibodies which leads to the elimination of tumour cells targeted by T cells. This is an original artwork by Z.L.

1. 6. 1 Myc mediated PD-L1 expression

According to the national cancer institute report from the U.S. Department of Health and Human Services, cancer immunotherapy is one of the major treatments that modulate the immune system to fight cancer. Interestingly, it has recently been shown that Myc is involved in preventing immune cells from attacking tumour cells by inducing PD-L1 gene expression (Sun et al., 2018). The ligand-receptor interaction between PD-L1 and PD-1 has been extensively studied as a target of cancer immunotherapy ever since it was implicated in the suppression of T lymphocytes and immune tolerance, ultimately leading to a

tumour immune escape (Jiang et al., 2019a). cMyc has been demonstrated to bind to the PD-L1 gene promoter and induce expression, however, the molecular mechanisms through which this occurs are not well understood (Casey et al., 2016, Kim et al., 2017).

Casey et al. (Casey et al., 2016) suggest that Myc can bind to the PD-L1 promoter region directly and promote PD-L1 expression in a dosage-dependent manner, with higher Myc expression leading to higher PD-L1 expression *in vitro*. Similar results were also validated from tissues that were isolated from non-small cell lung cancer (NSCLC) patients in which Myc expression was significantly correlated with PD-L1 expression (Kim et al., 2017). When Myc expression was suppressed, both RNA and protein expression levels of PD-L1 decreased accordingly and further enhanced the anti-tumour immune response. In addition, when Myc was inactivated under the overexpression of PD-L1, the anti-tumour immune response remained inhibited, and the tumour cells continued to grow. Indeed, Myc inactivation in mouse tumour models results in the recruitment of immune cells to the tumours for initiating proper immune responses (Rakhra et al., 2010). These reports indicate that Myc can associate directly with the PD-L1 promoter for transcription regulation and participate in the process of manipulating immune regulatory molecules (Casey et al., 2016).

1. 6. 2 Interferon-gamma (IFNγ) mediated PD-L1 expression

The pro-inflammatory cytokine interferon-gamma (IFNγ) is also known to induce PD-L1 expression in a variety of tumours including melanoma, non-small cell lung cancer (NSCLC), and renal cell carcinoma (Seliger, 2019, Karachaliou et al., 2018). This phenomenon has been referred to as innate immune resistance which is a survival strategy of tumour cells to escape immune surveillance (Chen et al., 2016, Jiang et al., 2019b, Keir et al., 2008). IFNγ activates the IFNγ receptor, which further activates various signalling pathways such as PI3K/AKT/mTOR and JAK-STAT (Lastwika et al., 2016, Moon et al., 2017). The activation of these pathways can ultimately recruit downstream transcription factors such as IRF1,

HIF-1α/2α, STAT1 dimers, STAT3, Myc, and NF-ϰB to the interferon-gamma activated site elements or other regulatory sites within the promoter region of PD-L1 to induce expression (Gowrishankar et al., 2014, Lastwika et al., 2016, Moon et al., 2017, Gong et al., 2018, Sun et al., 2018, Garcia-Diaz et al., 2019, Antonangeli et al., 2020).

Taken together, these data indicate that deciphering the molecular mechanisms of PD-L1 induction by oncogenic Myc and IFNγ as well as seeking other cofactors that potentially affect the immune suppression mechanism warrants further investigation.

1. 7 EP400NL, a step away from EP400

EP400, as a member human NuA4 chromatin remodelling complex, has been implicated in transcription regulation and DNA double-strand break repair. As mentioned earlier in this report, EP400 facilitates the deposition of double variant H2AZ/H3.3 onto promoter and enhancer regions for transcriptional activation (Pradhan et al., 2016a, Pradhan et al., 2016b). Previous data from this laboratory identified that EP400 can interact with ATM kinase (a major DNA damage responsive protein) for efficient DNA double-strand break response and repair (Smith et al., 2016). These results indicated that the N-terminal fragments of EP400 interact specifically with ATM and lead to an increased susceptibility to bleomycin without affecting ATM phosphorylation. Bleomycin is a known chemotherapy drug that induces DNA damage including DSB (Chen and Stubbe, 2005). Furthermore, a bleomycin sensitivity assay using U2OS tumour cells that express the N-terminal fragment of EP400 (1aa. -719aa.) displays normal cellular growth without bleomycin treatment, however, they are sensitised upon bleomycin treatment as observed by the reduced proliferation pattern (Smith et al., 2016). Bleomycin binds to the DNA of tumour cells for preventing cellular growth and proliferation, as well as causing free radicals inside the cell nucleus by

acting as a DNA damaging agent. Thus, it has been utilized as a medication for multiple cancer treatments (2000, Chen and Stubbe, 2005). In brief, Smith et al suggest that the N-terminal domain of EP400 is not only crucial for maintaining the integrity of DNA but is also able to enhance the susceptibility of tumour cells toward potential anticancer drugs.

Interestingly, an EP400 N-terminal-Like (EP400NL) gene resides downstream of the EP400 gene on chromosome 12q24.33 (Figure 1. 10 A). After the polypeptide sequences of EP400 and EP400NL were aligned, nine fragment matches were found (Figure 1. 10, B). The sequence alignment of EP400 and EP400NL shows that the N-terminal fragment of EP400 (131-490 amino acid sequence) is almost identical to EP400NL (51-404 amino acid sequence), sharing the highest sequence similarities (92%) over 84.5% of the total EP400NL amino acids sequence (Figure 1. 10, B). Despite its initial annotation as a pseudogene that has no obvious functional domain, EP400NL gene expression appears to be regulated by an independent promoter sequence, and the exon regions are highly conserved in many vertebrates (UCSC genome browser). Compared to EP400 (ENSG00000183495.13) which exhibits a high expression pattern throughout various tissue samples, the gene expression profile of EP400NL (ENSG00000185684.12) displays a higher tissue-specific expression pattern in the pituitary gland and testis, indicating a potential regulatory role of EP400NL in these two annotated tissues (Figure 1. 11). Given their adjacent genetic location and sequence similarity, we hypothesized that EP400NL may have a unique regulatory function distinct from its homolog EP400 in the regulation of EP400-target genes.

A

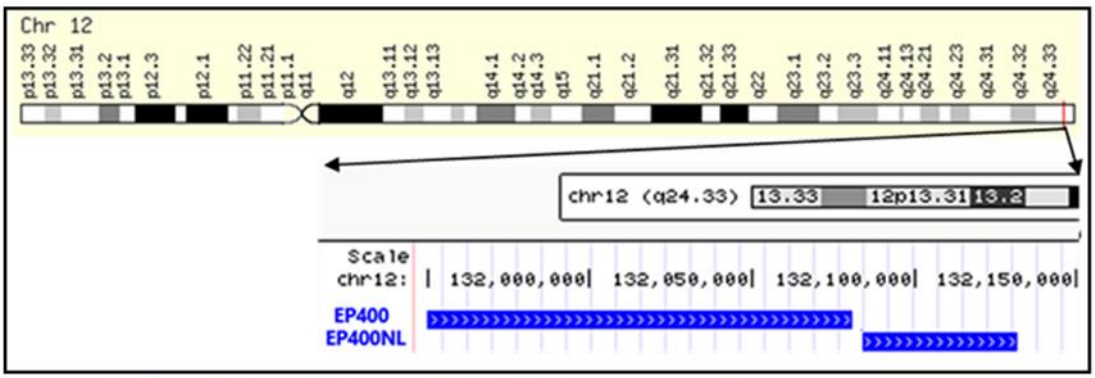

B **Sequence ID: Query_209577 Length: 419 Number of Matches: 9**

Range 1: 51 to 404 Graphics ▼ Next Match

Score	Expect	Method	Identities	Positives	Gaps
560 bits(1444)	0.0	Compositional matrix adjust.	332/360(92%)	337/360(93%)	6/360(1%)

```
EP400     131  VQTQSPTQPSPGPGQALQNVRAGAPGPGLGLCSSSPTGGFVDASVLVRQISLSPSSGGHF  190
               VQTQSPTQPSPGPGQALQNVRAGAPGPGLGLCSSSPTG FVDASVLVRQISLSPSSGGHF
EP400NL   51   VQTQSPTQPSPGPGQALQNVRAGAPGPGLGLCSSSPTGDFVDASVLVRQISLSPSSGGHF  110

EP400     191  VFQDGSGLTQIAQGAQVQLQHPGTPITVRERRPSQPHTQSGGTIHHLGPQSPAAAGGAGL  250
               VFQDGSGLTQIAQGAQVQLQHPGTPITVRERRPSQPHTQSGGTIHHLGPQSPAAAGGAGL
EP400NL   111  VFQDGSGLTQIAQGAQVQLQHPGTPITVRERRPSQPHTQSGGTIHHLGPQSPAAAGGAGL  170

EP400     251  QPLASPSHITTANLPPQISSIIQGQLVQQQQVLQGPPLPRPLGFERTPGVLLPGAGGAAG  310
               QPLASPSHITTANLPPQISSIIQGQLVQQQQVLQGPPLPRPLGFERTPGVLLPGAGGAAG
EP400NL   171  QPLASPSHITTANLPPQISSIIQGQLVQQQQVLQGPPLPRPLGFERTPGVLLPGAGGAAG  230

EP400     311  FGMTSPPPPTSPSRTAVPPGLSSLPLTSVGNTGMKKVPKKLEEIPPASPEMAQMRKQCLD  370
               FGMTSPPPPTSPSRTAVPPGLSSLPLTSVGNTGMKKVPKKLEEIPPASPEMAQMRKQCLD
EP400NL   231  FGMTSPPPPTSPSRTAVPPGLSSLPLTSVGNTGMKKVPKKLEEIPPASPEMAQMRKQCLD  290

EP400     371  YHYQEMQALKEVFKEYLIELFFLQHFQGNMMDFLAFKKKHYAPLQAYLRQNDLDIEEEEE  430
               YH+QEMQALKEVFKEYLIELFFLQHFQGNMMDFLAFK++ Y PLQAYLRQNDLDIEEEEE
EP400NL   291  YHHQEMQALKEVFKEYLIELFFLQHFQGNMMDFLAFKERLYGPLQAYLRQNDLDIEEEEE  350

EP400     431  EEEEEEEKSEVINDEVKVVTGKDGQTGTPVAIATQLPPKVSAAFSSQQQPFQQALAGSLV  490
               E         EVINDEVKVV  K GQ GTPVAIATQLPP+ SAAF +QQQP Q    GS V
EP400NL   351  EH------FEVINDEVKVVARKHGQPGTPVAIATQLPPRTSAAFPAQQQPLQVLSDGSTV  404
```

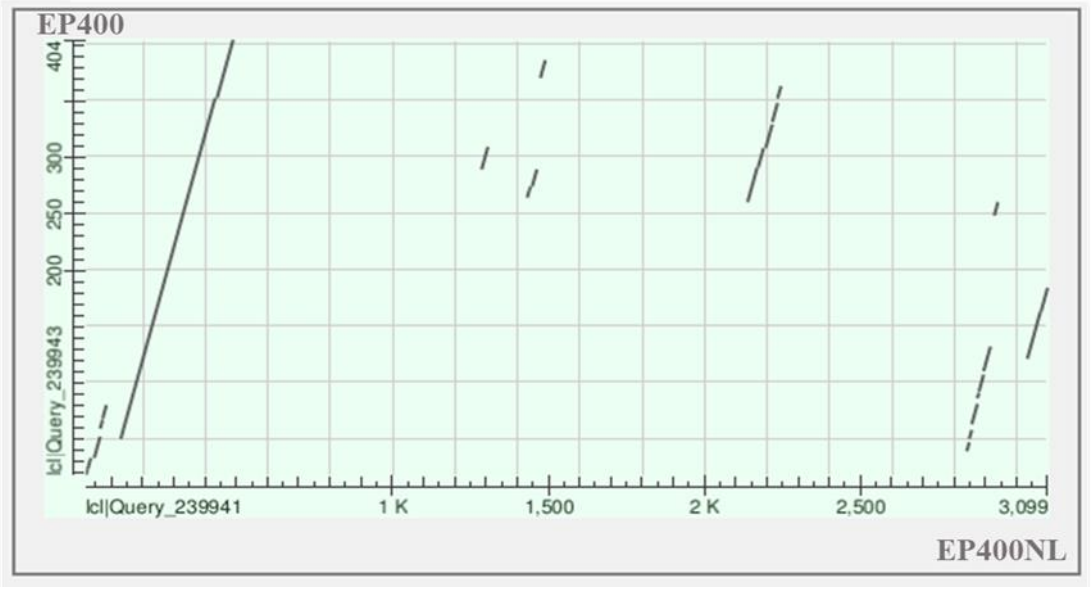

Figure 1. 10 The genetic localization and sequence alignment of EP400 and EP400NL

(A) EP400NL (EP400 N-terminal-Like) gene resides right next to the EP400 gene locus on 12q24.33 which produces a protein of 419 amino acids. (B) Amino acid sequence alignment between EP400 and EP400NL. Nine matches were detected from the sequence alignment. The Y-axis and x-axis of the dot plot show the amino acid sequence number of EP400NL and EP400 respectively. A double-headed arrow indicates the sequence alignment between EP400 (131aa. -490aa.) and EP400NL (51aa. -404aa.) which displays the highest protein sequence similarity up to 92%.

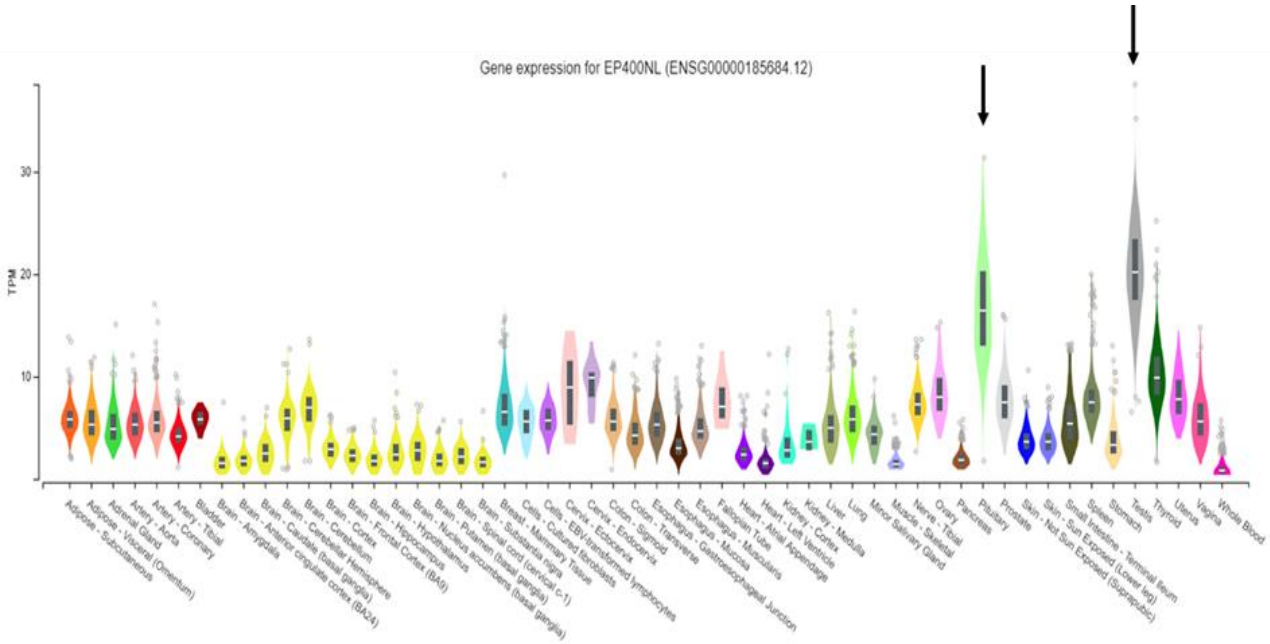

Figure 1. 11 Gene expression pattern of EP400NL in 54 tissues

RNA-sequencing data showing the relative expression of EP400NL across 54 human tissues. Dots represent the biological replicates, and the median TPM (transcript per million) reads are indicated as the horizontal white bar in each sample. Two black arrows indicate the pituitary gland (N=283; Median TPM=16.52) and testis (N=361; Median TPM=20.23) respectively which exhibit significantly higher EP400NL expression up to approximately 17 and 20 times compared to the baseline. GTEx RNA-sequence from GTEx portal.

1. 8 Motivation of the work presented in the thesis

PD-L1 overexpression is a predictor of recurrent cancer incidence and is associated with a poor prognosis in cancer patients (Wang et al., 2016, Casey et al., 2016). Recent studies have shown that Myc directly binds to the promoter region of PD-L1 to facilitate increased expression (Casey et al., 2016), and Myc expression correlates with PD-L1 expression in non-small cell lung cancer (Kim et al., 2017). Multiple transcription factors and epigenetic protein complexes such as TRRAP, EP400, and TIP60. have been identified as interacting partners with Myc to induce and maintain cancerous phenotypes. But little is known about the role of EP400NL, as well as how these individual proteins or complexes contribute to the Myc-targeted PD-L1 gene expression and oncogenic Myc functions (Figure 1. 12).

Considering its potential interaction with EP400-related epigenetic protein complexes, the role of EP400NL in Myc mediated PD-L1 targeted transcriptional regulation was investigated. Furthermore, elucidating the association between PD-L1 and EP400NL may shed a light on strategies for developing new cancer therapeutics and provide meaningful insights for cancer immunotherapy.

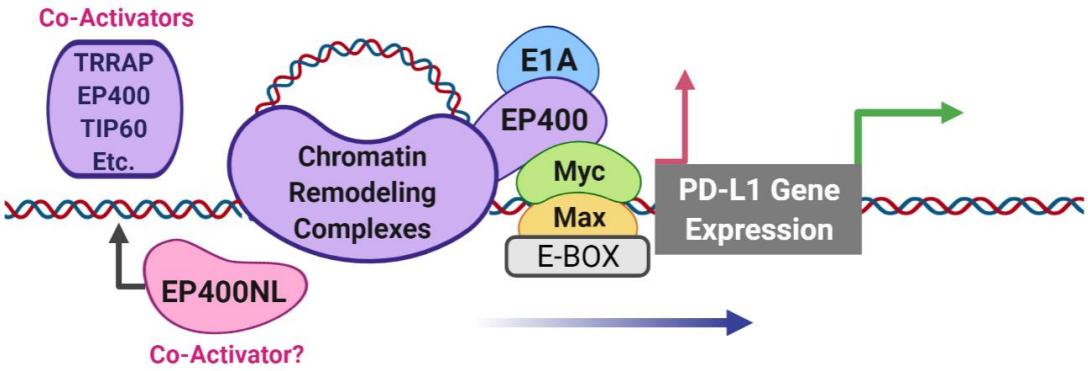

Figure 1. 12 Chromatin remodeling complexes in regulating PD-L1 gene expression

Epigenetic protein complexes serve as transcription coactivators of Myc in upregulating PD-L1 expression. Multiple epigenetic protein complexes such as TRRAP, EP400, TIP60. have been identified as interacting partners with Myc for driving PD-L1 expression, E1A-EP400 binding can stabilize Myc to the promoter region to maintain the consistent expression of Myc targeted genes.

EP400NL, a protein of our interest, can be another coactivator for regulating PD-L1 expression. This is the original work by Z.L.

1. 9 Hypothesis

- ❖ EP400NL forms a unique chromatin remodelling complex and regulates PD-L1 gene expression

1. 10 Aims of the project

To determine whether EP400NL interacts with Myc to regulate PD-L1, it is crucial to identify other functional proteins which contribute to the formation of the EP400NL-containing nuclear complex. Therefore, a series of biochemical assays in characterising the enzyme activities associated with EP400NL are attempted for the confirmation of its role as a potential chromatin remodeler. Functional characterization of the EP400NL complex is subsequently conducted to investigate its role in Myc mediated transcriptional regulation.

Objective 1. Purification of EP400NL complex

- ❖ Establish a stable cell line expressing TAP-tagged EP400NL using Flp-In™ T-REx™ system
- ❖ Determine the subcellular localization by cellular fractionation
- ❖ Purify the EP400NL-containing protein complex by affinity purification and size exclusion chromatography
- ❖ Identify EP400NL interacting proteins by mass spectrometry
- ❖ Confirm EP400NL interacting protein candidates by co-immunoprecipitation

Objective 2. Characterisation of EP400NL complex associated enzymatic activities

- ❖ Determine whether the EP400NL complex is associated with HAT activity
- ❖ Determine whether the EP400NL complex is associated with H2A.Z deposition activity

Objective 3. Functional characterisation of the EP400NL complex in transcriptional regulation

- ❖ Investigate the transcriptional activity of EP400NL using the GAL4-DBS system

- ❖ Investigate if EP400NL can be recruited to the GAL4-DBS in a Myc dependent manner by Chromatin Immunoprecipitation Assay (ChIP)

- ❖ Determine whether EP400NL and Myc physically interact

- ❖ Investigate the alteration of protein interactions and transcriptional coactivator activities using EP400NL deletion mutants

Objective 4. Elucidating the role of EP400NL complex in PD-L1 expression

- ❖ Investigate the role of EP400NL in Myc mediated PD-L1 transcription using RT-qPCR

- ❖ Investigate if EP400NL and other EP400NL interacting functional proteins can be recruited to the PD-L1 promoter in a Myc dependent manner by Chromatin Immunoprecipitation Assay (ChIP)

- ❖ Investigate the role of EP400NL in PD-L1 gene transcription

  1) EP400NL deletion mutants by InterPro bioinformatic prediction tool

  2) Indel mutated EP400NL by CRISPR/Cas9 genomic editing

2. Materials and Methods

2. 1 Mammalian cell culture for providing experimental materials

FLP-In T-REX cells were maintained in Dulbecco's Modified Eagle's Medium (5% FBS, 4.5 g/l D-Glucose, 25 mM HEPES, Gibco/Life Technologies) with 15 μg/ml blasticidin and 100 μg/ml Zeocin. FLP-In T-REX cells that stably express EP400NL were maintained in the same media with 15 μg/ml blasticidin and 30 μg/ml hygromycin. All other cell lines were maintained in Dulbecco's Modified Eagle's Medium (4.5 g/l D-Glucose, 25 mM HEPES, Gibco/Life Technologies) supplemented 5% fetal bovine serum (FBS) and 0.5% Penicillin-Streptomycin in a 5% CO_2 incubator. For serum starvation, cells were grown for 48 h in the DMEM medium containing 1% FBS and then stimulated with 20% fetal bovine serum (FBS) or IFNγ (5 ng/ml and 20 ng/ml). All the untreated cells were maintained at 37 °C in a humid atmosphere of 95% air and 5% CO_2 with 5% fetal bovine serum (FBS).

2. 2 Methods for the purification of EP400NL complex

2. 2. 1 Generation of a stable cell line stably expressing EP400NL

Cells that stably expressing EP4000NL were generated using the Flp-In™ T-REx™ System (Invitrogen). Flp-In™T-REx™ cells are HEK 293-T cells with a stably integrated flip recombination target (FRT) site which allows for the integration of a gene of interest with homogenous and robust expression. These cells stably express the lacZ-Zeocin fusion and an FRT site at a transcriptionally active locus. EP400NL was previously cloned into the pcDNA5/FRT/TO expression vector, and when co-transfected with pOG44, which contains a recombinase. The inserted cDNA of EP400NL can flip into the host genome by homologous recombination. The expression of the EP400NL is under the control of a tetracycline-inducible promoter, allowing for induced expression with tetracycline treatment at a final concentration of 1 μg/ml. Cells were selected by the addition of 30 μg/ml hygromycin to the media as the expression plasmid encodes a hygromycin

resistance cassette linked to FRT under the control of a cytomegalovirus (CMV) promoter. 48 hours post-transfection, non-transfected cells died within a week, monoclonal EP400NL integrated cell lines were selected using single-cell cloning rings. A western blot was used to examine the EP400NL protein expression of each clone.

2. 2. 2 Subcellular fractionations

Cells that stably express EP4000NL were generated using the Flp-In™ T-REx™ System (Invitrogen). Flp-In™ T-REx™ cells were washed and scraped after tetracycline induction. Cells were pelleted and resuspended with hypotonic buffer (10 mM Tris pH 7.3, 1 mM KCl, 1.5 mM $MgCl_2$, 0.01 M KCl) and the supernatant was removed after centrifugation. Hypotonic buffer was then added and homogenized with size B pestle of Dounce homogenizer. Cells were spun at 4000 rpm (1500 rcf) for 15 min and the supernatant was used as the cytosolic fraction. The nuclear pellet was then resuspended with low salt buffer (20 mM Tris pH 7.3, 12.5% Glycerol, 1.5 mM $MgCl_2$, 0.2 mM EDTA, 20 mM KCl) and transferred for homogenization. High salt buffer (20 mM Tris pH 7.3, 12.5% Glycerol, 1.5 mM $MgCl_2$, 0.2 mM EDTA, 1.2 M KCl) was added to the homogenized nuclear pellet at 4°C and stirred for 30 min followed by 30 min centrifugation at 30,000 rpm (40,320 rcf). After taking the supernatant as the nuclear soluble fraction, the nuclear pellet was then resuspended and centrifuged at the same speed for the nuclear pellet fraction.

2. 2. 3 Western-Blot Analysis

Whole-cell extract was lysed using F-buffer (25 mM Tris pH 7.05, 50 mM sodium chloride, 30 mM sodium pyrophosphate, 50 mM sodium fluoride, 10% Glycerol, 0.5% Triton X-100) with 1× protease inhibitor cocktail (cOmplete™, Mini, EDTA-free Protease Inhibitor Cocktail, Sigma-Aldrich), then protein concentrations were measured by NanoDrop Protein Quantification. Protein lysates were separated by 10–15% SDS-PAGE for HAT assay, 5–15% SDS-PAGE for colloidal staining and either 5% or 10% SDS-PAGE for Co-immunoprecipitation assays, all others were

conducted using 10% SDS-PAGE. Separated proteins were then transferred to a nitrocellulose blotting membrane (GE Healthcare Life Sciences), which was blocked in 5% skim milk in TBST plus 0.02% sodium azide for 30 minutes at room temperature. Membranes were incubated with primary antibodies overnight at 4°C in TBST and washed with TBST three times before the incubation with secondary antibodies for 1 hour at room temperature. All secondary antibodies were diluted at 1:10000. Membranes were imaged using the Azure c600 (Azure Biosystems). Target proteins were detected by Western blot analysis with antibodies listed in the table below.

Table 2. 1 Source and dilution of the antibodies used for western-blot analysis
Anti-BAF53 antibody was received from Dr Michael Cole, Department of Molecular Biology, Princeton University, Princeton, NJ.

Antibodies	Dilution in TBST	Information
Anti-EP400NL	1:1000	HPA068417, Sigma-Aldrich
Anti-CBP	1:500	Sc-32998, Santa-Cruz Biotechnology
Anti-FLAG	1:1000	A8592, Sigma-Aldrich
Anti-BRG1	1:1000	ab70558, Abcam, USA
Anti-BRD8	1:10000	ab17969, Abcam, USA
Anti-BAF53	1:100	A kind gift from Dr Cole
Anti-cMyc	1:500	MCA1929, Bio-Rad
Anti-PPM1B	1:500	AF4396, R&D System Minneapolis, USA
Anti-β-actin	1:5000	NB600-501, NOVUS, USA
Anti-Lamin A/C	1:10000	ab108595, Abcam, USA
Anti-TIP48	1:500	A kind gift from Dr Cole
Anti-MED30	1:500	MBS9609934, MYBioSource
Anti-TIP49	1:500	A kind gift from Dr Cole
Anti-PD-L1	1:500	#14-5982-82, Invitrogen

2. 2. 4 Size exclusion chromatography

EP400NL complex was isolated from the established EP400NL expressing FLP-In T-REX cell line after tetracycline induction. Flp-In™ T-REx™ cells were harvested from 40 × 15 cm plates. Nuclear soluble samples were fractionated and used as the input for size exclusion chromatography. Bio-Gel A1.5 gel is an agarose-based size-exclusion resin that provides high resolving power, the gel media consists of spherical beads containing pores of the specific size distribution for separating protein complexes based on their molecular weight. The gel was washed with distilled water and packed into a column. The packed column was then equilibrated 3 volumes of streptavidin binding buffer (10 mM Tris pH 8.0, 150 mM sodium chloride, 2 mM EDTA pH 8.0, 0.1% NP40, and 10 mM 2-Mercaptoethanol). The nuclear soluble fractionated protein sample was applied to the column inlet using the SBB buffer (0.3 ml/min). The UV absorbance and conductivity curve from the chromatogram were monitored, each fraction was separately collected into a 15 ml tube (3 ml/Fraction). A total of 60 tubes (180 ml) were collected and stored at 4°C for further analysis.

2. 2. 5 Purification and elution of EP400NL complex

Tetracycline-induced EP400NL protein from the pNTAP vector (N-terminal tandem affinity purification tagged vector) is tagged with both streptavidin-binding peptide (SBP) and calmodulin-binding peptide (CBP) and can be purified by using streptavidin-conjugated agarose beads (EZview™ Red Streptavidin Affinity Gel, Sigma-Aldrich). Streptavidin affinity beads were equilibrated with streptavidin binding buffer and reconstituted as a 50% slurry before use. Fractions that contain proteins were identified from the peaks from the size exclusion chromatography. The fractions of both parental Flp-In™ T-REx™ and established Flp-In™ T-REx™ cells were collected and pooled together respectively after the size exclusion chromatography. Every 12 ml collected fractions were incubated with 500 µL of 50% slurry (streptavidin affinity beads) with constant rotation at 4°C overnight. The beads were collected by centrifugation at 3000 rpm (800 rcf)

for 5 minutes at 4°C and were washed 3 times with streptavidin binding buffer (10 mM Tris pH 8.0, 150 mM sodium chloride, 2 mM EDTA pH 8.0, 0.1% NP40, and 10 mM 2-Mercaptoethanol), one last wash with PBS buffer and eluted by biotin elution buffer (50 mM Biotin, 10 mM EDTA pH 8.0, 1.5% SDS, 1×PBS) that had been reconstituted with 1× PMSF and 1× protease inhibitor (cOmplete™, Mini, EDTA-free Protease Inhibitor Cocktail, Sigma-Aldrich). Streptavidin bound EP400NL protein was eluted twice with 200 μL of elution buffer rotating constantly overnight at 4°C. Eluted protein samples were utilized as an input source for mass spectrometric analysis.

2. 3 Methods for the identification of EP400NL interacting candidates

2. 3. 1 Mass spectrometry

Protein samples were separated by SDS-PAGE, the gel was fixed in 10 % (v/v) acetic acid, 40 % (v/v) methanol for one hour at room temperature and washed three times in distilled water. The gel was stained overnight in colloidal Coomassie blue (75.6 mM ammonium sulphate, 2 mL 5 % Coomassie G250, 1.2 mL phosphoric acid, distilled water to a final volume of 100 mL). The gel was destained in distilled water at room temperature. Protein bands were excised from the gel in the safety cabinet and all stain was removed by three 30-minute washes in 50 mM ammonium bicarbonate, 50 % methanol (v/v) at 37 °C with a final wash in 80 % acetonitrile. All liquid was removed, and the gel pieces were dried in a centrifugal evaporator. The gel pieces were rehydrated in 10 mM DTT in 50 mM ammonium bicarbonate and incubated at 37 °C for one hour. The gel pieces were then washed three times in 50 mM ammonium bicarbonate and once in 80 % acetonitrile, then dried in a centrifugal evaporator. The gel pieces were rehydrated in 0.5 mM iodoacetamide in 50 mM ammonium bicarbonate for one hour in the dark. The gel pieces were washed three times in 50 mM ammonium bicarbonate and once in 80 % acetonitrile then dried in a centrifugal evaporator. The gel pieces were eventually rehydrated in 20 ng/μL trypsin in 50 mM ammonium bicarbonate and incubated overnight at 37 °C for proper trypsin digestion. Trypsin digested

samples were sonicated in an ultrasonic bath for 2 minutes twice and centrifuged for final collection. Protein peptides were first extracted by 2 minutes sonication with 50 µL 5% formic acid in 50% MeCN buffer, and then ultra-sonicated for 2 minutes in 50 µL 0.1% formic acid, 80% acetonitrile. A total of 100 µL collection for each sample was dried in a centrifugal evaporator and reduced to around 50 µL and stored at -80°C until analysis was performed. Proteome Discoverer™ Software (Thermo Scientific™) was utilized for the identification and quantification of peptide sequences.

2. 3. 2 PEI transient transfection for Co-IP assays

HEK-293T cells (1.5×10^7) were seeded into four 15 cm cell culture dishes (Greiner Bio-One). After 24 hours, cells were transfected with 16 µg plasmid DNA to express HA-tagged GST, FLAG-tagged EP400NL, FLAG-tagged DMAP1, and FLAG-tagged TIP60 respectively using polyethyleneimine (PEI) transient mammalian cell transfection. PEI transfection was conducted with transfection reagent in 2% FBS without antibiotics. 40 hours post-transfection, cells were lysed using 500 µL of lysis buffer containing 25 mM Tris pH 7.05, 50 mM sodium chloride, 30 mM sodium pyrophosphate, 50 mM sodium fluoride, 10% Glycerol, and 0.5%v/v Triton X-100. The lysis buffer was reconstituted with 1× PMSF and 1× protease inhibitor (cOmplete™, Mini, EDTA-free Protease Inhibitor Cocktail, Sigma-Aldrich) just before use. 50 µL of cell lysate from each of the four samples was saved separately as input controls for western blot. The remaining 450 µl cell lysate was mixed with 30 µL of anti-FLAG® M2 Affinity Gel (Sigma-Aldrich) that was equilibrated in BC50/1%NP40 (50 mM KCl, 50 mM Tris pH 7.5, 0.2mM EDTA, 10%v/v Glycerol, 1%v/v NP40) and rotated constantly overnight at 4°C. Beads were washed with F-buffer once, BC300 (300 mM KCl, 50 mM Tris pH 7.5, 0.2 mM EDTA, 10% v/v Glycerol, 1% v/v NP40) 3 times, and final wash with 1×PBS. Beads from each sample were then eluted in 50 µL FLAG peptide elution buffer (1 mg/ml FLAG peptide, 1×protease inhibitor mix, in PBS). thirteen microliters out of the 50 µL of immunoprecipitates was used for HAT (histone

acetyltransferase) assays (described below), 37 µL was used for western-blot analysis to confirm protein-protein interactions.

2. 4 Methods for the characterization of EP400NL associated enzymatic activities

2. 4. 1 Histone acetyltransferase assay

As described in the above section (2.3.2), 13 µL out of the 50 µL immunoprecipitates was used for HAT (histone acetyltransferase) assays, 16 µL of 2 × HAT buffer (40Mm Tris pH 9.0, 100mM KCl, 1mM EDTA, 10mM DTT, 20mM sodium butyrate, 10% glycerol), 1 µg Hela free histones as substrate protein, and 0.02 mci of [^{14}C]- acetyl-coenzyme A was used for each reaction. 2 × HAT buffer, substrate histone protein, and immunoprecipitated protein were initially incubated for 10 minutes at 30°C, followed by the addition of [^{14}C]-Acetyl-Coenzyme and incubated for another one hour at 30°C. The reactions were inactivated by the addition of 6 µL of 6 × SDS sample buffer. Samples were boiled at 90°C for 5 minutes before 10-15% SDS-PAGE analysis. Proteins were transferred onto a membrane blot by semi-dry and immediately stained with Ponceau for detecting histone proteins. Membranes were air-dried in the air circulating safe cabinet overnight and exposed to Biomax MS film at -80°C for 5 days for radioactive signal exposure.

2. 4. 2 H2A.Z deposition assay

Plasmids that contain nineteen repeats of 601-Widom nucleosome positioning sequences (pUC19/19x601) were utilized for generating multi-nucleosomes by interacting with wild-type free histones. The template utilized in the experiment was biotin-labelled chromatin assembly, non-labelled ones serve as the negative control. MNase digestion revealed a pattern of periodic spacing of both wild-type and biotinylated chromatins which represents the properly assembled chromatins. Biotin labelling of the nucleosome assembly was conducted using the EZ-Link™

Psoralen-PEG3-Biotin kit (Thermo Scientific™) following the manufacturer's protocol. EP400/TIP60 complex was purified from HeLa cell nuclear extracts which TIP60 is HA/FLAG-tagged. Individually aliquoted HeLa nuclear extracts (5 mL) were mixed with same volume of F-lysis buffer (25 mM Tris pH 7.05, 50 mM sodium chloride, 30 mM sodium pyrophosphate, 50 mM sodium fluoride, 10% Glycerol, 0.5% Triton X-100). Ten microlitres of the HeLa nuclear extracts was mixed with 100 µL of anti-FLAG® M2 Affinity Gel (Sigma-Aldrich) that had been equilibrated in BC50/1%NP40 (50 mM KCl, 50 mM Tris pH 7.5, 0.2mM EDTA, 10%v/v Glycerol, 1%v/v NP40) and rotated constantly overnight at 4°C. M2 Affinity Gel were washed with F-buffer once, BC300 (300 mM KCl, 50 mM Tris pH 7.5, 0.2 mM EDTA, 10% v/v Glycerol, 1% v/v NP40) four times, and final wash with 1×PBS. M2 Affinity Gel from the sample was then eluted in 100 µL FLAG peptide elution buffer (1 mg/ml FLAG peptide, 1×protease inhibitor mix, in PBS) and preserved in 25% glycerol at -20°C for future use. Transient transfection of FLAG-EP400NL and HA-GST constructs into HEK293T cells for protein expression was conducted using Effectene Transfection Reagent (QIAGEN), followed by the affinity binding of the anti-FLAG M2 agarose beads. samples were then eluted in 50 µL FLAG peptide elution buffer (1 mg/ml FLAG peptide, 1×protease inhibitor mix, in PBS) and preserved in 25% glycerol at -20°C for future use. The expression of EP400 and EP400NL was confirmed by western blot. An equivalent of 500 ng of DNA was preincubated for 15 min at 30°C with or without apyrase (1 U) and all components including 1×protease inhibitor mix, substrates (FLAG-H2A.Z/H2B dimers), and exchange buffer (25 mM HEPES-KOH at pH 7.6, 0.1 mM EDTA, 5 mM $MgCl_2$, 10% glycerol, 0.02% NP-40, 1 mM DTT, 0.1 mg/mL BSA, 70 mM KCl) were added and mixed. Enzyme preps which previously purified from the HEK293T cells were included at the final stage. After the preincubation step, exchange reactions were assayed for 1 hour at 30°C in the absence or presence of 1 mM ATP, exchanged FLAG-H2A.Z were investigated by anti-FLAG immunoblots.

2. 5 Methods for the characterization of EP400NL associated transcriptional activity

2. 5. 1 Dual-luciferase reporter assays

HEK293TGal4-Luciferase cells were established by the incorporation of a Gal4 luciferase reporter into HEK 293T cells, the Gal4-Myc fusion protein can specifically target and bind to the Gal4 DNA binding site within the Gal4 luciferase reporter for driving downstream gene expression. Thus, to test if the following co-activators can show a positive effect in up-regulating Myc targeted gene expression, cells were seeded in 24-well plates, co-transfections of the CbF-GaL4-Myc construct (20 ng), pRenilla-CMV vector (1 ng) together with the appropriate transcription co-factors, which include CbS-GST (200 ng), CbF-TRRAP (Full-length 1-3830aa.) (200 ng), CbF-TRRAP-Deletion (1-3760aa.) (200 ng), CbF-EP400 (Full-length 1-3122aa.) (200 ng), CbF-EP400-Mutated (ATPase mutated EP400, 200 ng) and CbF-EP400NL (200 ng) were conducted. Plasmids were added to each well simultaneously using Effectene Transfection Reagent (QIAGEN). After 48 hours, firefly luciferase and renilla luciferase activities were measured using the Dual-Luciferase® Reporter Assay System (Promega). Each sample was measured in triplicate and three independent experiments were conducted. The firefly luciferase reporter is measured first by adding Luciferase Assay Reagent II (LAR II) to generate a stabilized luminescent signal. After quantifying the firefly luminescence, this reaction is quenched, and the Renilla luciferase reaction is simultaneously initiated by adding Stop & Glo® Reagent to the same sample. The Stop & Glo® Reagent also produces a stabilized signal from the Renilla luciferase, which decays slowly throughout the measurement. The luminescent signals are measured and recorded every 0.5 seconds in intervals from 2 seconds to 20 seconds, once both reagents were added, data were selected from the last 10 intervals and averaged. Averaged firefly activity was normalized by the averaged corresponding Renilla activity. The luminescent activity was measured using the POLAR star Omega plate reader (BMG LABTECH),

collected data was processed by the MARS Data Analysis Software (BMG LABTECH). For final data analysis, the relative Firefly activity of the internal control (cells co-transfected with CbF-GST and Gal4-Myc) was set as 1, all tested samples were subsequently normalized against the internal control.

2. 5. 2 Cell cycle analysis by flow cytometry

Cells were harvested by trypsinization and washed with ice-cold PBS (PH 7.4). The cells were then resuspended into 2 mL PBS to a final concentration of 1×10^6/mL. 1 mL of cell suspension was then aliquoted into individual 15 mL tubes. three volumes of ice-cold 100 % ethanol were added dropwise into tubes and mixed with cells in suspension by slow vortexing. After ethanol fixation for 1 hour at 4°C, the cells were centrifuged (400 g, 5 min) and washed in the PBS buffer twice. Fifty microlitres of 1 mg/mL RNase A (EN0531, Thermo Fisher Scientific) was then added to each sample and the samples were incubated at 37 °C for 30 min. After incubation, 1 mL of 50 μg/mL propidium iodide (P1304MP, Thermo Fisher Scientific) was added to each tube for 30 min to provide the nuclear signal for flow cytometry.

2. 6 Methods for elucidating the role of EP400NL on PD-L1 expression

2. 6. 1 Real-Time qRT-PCR (Real-Time Quantitative Reverse Transcription PCR)

Total RNA was extracted from H1299 and FLP-In T-REX cells with TRIzol reagent (Invitrogen) following the manufacturer's instructions, and 4 μL of 20 ng/μL of RNA was then reversely transcribed to single-stranded cDNA and subsequently quantitatively analyzed by real-time PCR using the SensiFAST™ SYBR® No-ROX One-Step Kit (Bioline) according to the manufacturer's instructions. The sequences of the primer set of GUSB (housekeeping gene) and PD-L1 (target) are bioinformatically validated and provided by QuantiTect Primer Assays (QIAGEN). Reverse transcribed cDNA was used as a DNA

template for amplification using both GUSB and PD-L1 primer sets by the light cycler 480 II (Roche). Instead of using the ΔΔCT method, a standard curve method for relative quantification was utilized to minimize errors caused by different amplification efficiencies from different primer sets. Non-diluted (100 ng/μL) and a serial dilution consisting of 1:5 (20 ng/μL) and 1:25 (4 ng/μL) concentrated RNA extracted from control cells were prepared for both GUSB and PD-L1, the average Cp value from the non-diluted and two serial diluted samples were used to draw the standard curve for both GUSB and PD-L1 with the average of Cp value on the X-axis and log100, log20, log4 on the Y-axis. The Cp value from the GUSB samples was averaged and normalized first based on the standard curve of its own for calculating the baseline expression level. The Cp value from the PD-L1 samples was also averaged and normalized by its standard curve for the calculation of the raw expression level and then normalized against the expression level of GUSB for calculating the relative expression level of PD-L1 (14. APPENDIX 6).

Table 2. 2 QIAGEN catalogue number of GUSB and PD-L1 for Real-Time qRT-PCR assay. The primer sequences of the genes are proprietary.

Genes	QIAGEN Catalogue Number
GUSB	QT00046046
PD-L1	QT00082775

2. 6. 2 Chromatin immunoprecipitation-quantitative PCR (ChIP-qPCR) assay

Chromatin immunoprecipitation (ChIP) assays were performed according to the protocol obtained from Abcam high-sensitivity ChIP kit (ab185913, Abcam) with several modifications. 1×10^7 HEK-293TGal4-Luciferase cells were treated with formaldehyde at a final concentration of 1% for 5 min at room temperature for the prevention of over-crosslinking. Glycine was added to a final concentration of 0.125 M for 5 min at room temperature. Cells were washed with cold 1×PBS twice

and lysed with F-buffer, DNA was then sonicated to a size of approximately 500 bp. The concentration of sonicated DNA fragments was measured using the Nanodrop, and 0.2 µg of sonicated DNA was used as 1% input control, 20 µg of sonicated DNA per reaction was immunoprecipitated overnight with antibodies against FLAG (A8592, Sigma-Aldrich), CBP (sc-33000, Santa Cruz Biotechnology), BRG1 (# 710894, Invitrogen), TIP48, TIP49 (kind gifts from Dr. Cole) and IgG which was included in the Abcam high-sensitivity Chip kit (ab185913). Immune complexes were collected using a protein A/G PLUS-Agarose beads (sc-2003, Santa Cruz Biotechnology), washed once with F-buffer (25 mM Tris pH 7.05, 50 mM sodium chloride, 30 mM sodium pyrophosphate, 50 mM sodium fluoride, 10% Glycerol, 0.5% Triton X-100) and once with LiCL2 buffer and eluted in 50 µL fresh elution buffer (v/v1% SDS, 50mM Tris pH 7.0, 10mM EDTA). The DNA was reverse cross-linked by incubating with 0.5 µL RNase A (10 mg/mL) per reaction at room temperature for 1 hour followed by 0.5 µL proteinase K (50 mg/mL) per reaction overnight at 65°C. Reverse cross-linked DNA was then extracted using phenol-chloroform and ethanol. Protein was removed by incubating with proteinase K at 65°C for 3 hours. All chromatin samples were sonicated and pulled down by six antibodies (anti-cMyc, anti-CBP, anti-BRG1, anti-TIP48, anti-TIP49, and IgG). ChIP-qPCR was performed on the Light cycler 480 II (Roche). Immunoprecipitated DNA was quantified using the Luna® Universal qPCR Master Mix (NEB) and qPCR was carried out to and amplify the specific targeted regions of the Gal4DNA binding site within the promoter regulatory region and PD-L1 promoter region respectively. The coding region of p21 and GAPDH which are the non-specific binding sites that serve as negative controls were examined correspondently. Single melt curve and melt peak of GUSB and PD-L1 are used to validate a single PCR product. Primer sets designed to amplify regions of luciferase transcription start site (TSS) that are also being recognized as the Gal4-DNA binding site, p21 gene, PD-L1 promoter

region, and GAPDH gene are listed in Table 2. 2 and the sequences of the primers are referenced from the following sources (Kufe, 2020, Ghosh et al., 2018).

Serial dilutions consisting of 0.2% and 0.04% from the 1% input control of the sonicated DNA were prepared and examined on the Light cycler 480 II (Roche) together with all samples. The average Cp value from the input controls was used to draw the standard curve with the average Cp value on X-axis and log100, log20, log4 correspondently on Y-axis. The Cp value from the samples was also averaged and normalized based on the standard curve for calculating the relative enrichment compared to the input controls. All reactions were carried out in duplicate.

Table 2. 3 Information of the primers used for ChIP qPCR assay

P21 (Non-specific)	**Forward Primer**	**5'-CACTGCAATTTGGCCCAGA-3'**
	Reverse Primer	**5'-GTGCAGTAGAGAATTATTCCACATTTG-3'**
Gal4-DNA binding site	**Forward Primer**	**5'-CTTATGGTACTGTAACTGAGCTAAC-3'**
	Reverse Primer	**5'-GCGGGACTATGGTTGCTGAC-3'**
GAPDH (Non-specific)	**Forward Primer**	**5'-TACTAGCGGTTTTACGGGCG-3'**
	Reverse Primer	**5'-TCGAACAGGAGGAGCAGAGAGCGA-3'**
Promoter region of PD-L1	**Forward Primer**	**5'-CATATGGGTCTGCTGCTGAC-3'**
	Reverse Primer	**5'-CAACAAGCCAACATCTGAAC-3'**

2. 6. 3 Tetracycline induction for co-IP and reverse co-IP assays

FLP-In T-REX cells (Invitrogen) were seeded into four 10 cm cell culture dishes (Greiner Bio-One). All cells were serum-starved (1% FBS) for 24 hours and followed by a combination of treatments of 1 μg/mL tetracycline induction and serum stimulation (20% FBS) for 24 hours. Cells were scraped and lysed in 500 μL F-lysis buffer which was described in the previous Co-IP section followed by either Co-IP or reverse Co-IP assays. In Co-IP analysis, 20 μL streptavidin-conjugated agarose beads (EZview™ Red Streptavidin Affinity Gel, Sigma-Aldrich) was added into each cell lysis for overnight precipitation at 4°C and further denatured by boiling at 90°C in 2× SDS sample buffer. All denatured

immunoprecipitated samples were examined by SDS-PAGE followed by western blotting for protein detection (EP400NL, BRG1, TIP48, and TIP49). In reverse Co-IP analysis, cells of each treatment were lysed in 1000 µL F-lysis buffer and separated evenly into two portions for overnight precipitation with 2 µL antibodies (anti-BRG1/anti-TIP48/anti-TIP49) and IgG negative controls. Protein A/G PLUS-Agarose beads (sc-2003, Santa Cruz Biotechnology) were utilized the following day for immunoprecipitation for one hour at room temperature. The expression of EP400NL was examined from each of the immunoprecipitated samples using both anti-EP400NL and anti-CBP immunoblots. 50 µL of cell lysate from each sample was saved separately as input controls for western blot.

2. 6. 4 Generation of indel mutated EP400NL cell lines by CRISPR/Cas9

Guide RNAs were designed based on a Toronto KnockOut (TKO) CRISPR Library and the fourth exon of the EP400NL genomic sequence was specifically targeted. EP400NL targeted guide RNA sequence (AGGTTGTGGCCAGAAAGCAC), luciferase targeted guide RNA sequence (AACGCCTTGATTGACAAGGA), and scrambled guide RNA sequence (AAACATGTATAACCCTGCGC) were submitted to GenScript and engineered into enhanced specificity CRISPR/Cas9 plasmids (eSpCas9-LentiCRISPR,v2) which are structurally engineered for improved target specificity by Feng Zhang laboratory at the broad institute (Slaymaker et al., 2016). HEK293T cells were seeded in a 10 cm plate at a density of 1×10^6 cells/plate and incubated for one day followed by the co-transfection of lentiviral packing plasmids and EP400NL-sgRNA-LentiCRISPR plasmids by Effectene Transfection Reagent (QIAGEN). 10 mL fresh DMEM media supplemented with 5% FBS, 0.5% Pen/Strep, and 0.5mM Caffeine was changed after 17 hours of transfection in order to increase the virus titre. The lentiviral medium was collected twice after 41 hours and 65 hours post-transfection respectively as a total of 20 mL for each co-transfection. The lentiviral medium was subsequently concentrated using Lenti-X™

Concentrator (Takara Bio) following the manufacturer's protocol. Individual transfection of Luciferase-sgRNA-LentiCRISPR plasmid and Scrambled-sgRNA-LentiCRISPR plasmid was carried out using the same procedure as described above. H1299 cells were then infected with these concentrated lentiviruses respectively for 24 hours and selected with 2ug/mL puromycin for a week. High-Resolution Melt (HRM) was utilized for the detection of created mutations within the EP400NL coding region. sgRNAs specifically recognize and bind the exon 4 of the protein-coding region of EP400NL (Figure A.1), gRNA-Cas9 complexes subsequently digest the targeted sequences upon specific binding which leads to non-homologous DNA end joining (NHEJ). NHEJ resulted in either insertions or deletions at the Cas9 targeted EP400NL coding region and ultimately introduced indel mutations.

HRM analysis was performed on double-stranded genomic DNA samples. Real-time PCR was utilized before HRM analysis to amplify the DNA region in which EP400NL indel mutation lies. The process involves increasing the temperature of the amplicon DNA from approximately 50 °C up to around 95 °C. When the melting temperature of the amplicon is reached, the two strands of DNA melt. The melting temperature of the amplicon was monitored by using a DNA intercalating dye. The fluorescence of the dye was monitored and plotted by the HRM capable light cycler 480 II (Roche) for generating melt curves and melt peak shifts. Western blot was used to examine EP400NL protein expression in the polyclonal indel mutation cells.

2. 6. 5 Confocal microscopy

Cells were seeded in a 6 well plate at a density of 1.5×10^5/mL together with two UV sterilized coverslips in each well. Cells were allowed to adhere overnight before serum starvation followed by treatments such as serum stimulation and tetracycline induction as appropriate. Cells were washed three times for 5 minutes with PBS and fixed with 2% paraformaldehyde in PBS for 15 minutes at room temperature. There was no shaking in all the above processes. Cells were then

washed with PBS twice for 5 minutes each and permeabilized with 0.2% Triton X-100 in PBS for 5 minutes with a gentle mix every few minutes. Cells were blocked for 60 minutes (PBS, 5% BSA, 0.05% Tween-20) with gentle shaking after two 10 minutes washes by PBS. Coverslips were overlaid with primary antibodies diluted in blocking buffer and incubated overnight at 4°C. The primary antibody solution was removed the next morning, coverslips were washed three times for 5 minutes each in PBS with 0.1% Triton X-100. Coverslips were kept in dark from this point on to prevent photo-bleaching. Coverslips were overlaid with secondary antibodies diluted in blocking buffer and incubated for 60 minutes at room temperature. Coverslips were then washed three times for 5 minutes each with 0.1% Triton X-100 in PBS and once in PBS followed by the fixation in 2% paraformaldehyde in PBS for 15 minutes at room temperature. Coverslips were washed three times with PBS followed by the final rinse with ddH_2O before being mounted on a slide glass using 50 µL antifade and fixed using nail polish. Samples were examined by Zeiss LSM900 confocal laser scanning microscope. The dye and absorption wavelengths used are shown in table 2. 3.

Table 2. 4 Dyes used during confocal microscopy

Dye	Excitation (nm)	Absorption (nm)
DAPI	405	450
Alexa Fluor® 555	555	565
Alexa Fluor® 647	652	668

2. 7 Statistical analyses

Statistical analysis was performed using GraphPad Prism software version 8.0 (GraphPad Software Inc., San Diego, CA, USA). Data were compared with a two-way ANOVA statistical test followed by Tukey's multiple comparisons test for cell cycle analysis and cell proliferation assays, Sidak's multiple comparisons test for ChIP-qPCR assays in Myc-dependent EP400NL recruitment, and Tukey's

multiple comparisons test for the recruitment of other candidates. Data were compared with one-way ANOVA statistical test followed by Dunnett's multiple comparisons test in investigating the Dual-luciferase reporter activity of both titrated EP400NL and multiple coactivators, two-way ANOVA followed Dunnett's multiple comparisons test were used for comparing the reporter activity of EP400NL mutants. Data on H2A.Z deposition activity were compared by one-way ANOVA followed by Tukey's multiple comparisons test. RT-qPCR data from the EP400NL inducible Flp-In™ T-REx™ cell line and H1299 cell line were compared with ordinary one-way ANOVA and two-way ANOVA statistical test respectively, but all followed by Tukey's multiple comparisons test. P values less than 0.05 were considered statistically significant. (N.S. $P > 0.05$, * $P \leq 0.05$, ** $P \leq 0.01$, *** $P \leq 0.001$, **** $P \leq 0.0001$). All data shown were determined for the independent experiments and presented as the mean $\pm$ SD.

3. INVESTIGATION OF THE EP400NL COMPLEX

To study the function of EP400NL, the first approach was to determine and identify proteins in complex with EP400NL. A method was developed for the affinity purification of epitope tagged EP400NL and its associated proteins from cultured human cells, followed by mass spectrometry to determine the identity of these proteins. The first goal of this strategy was to develop a stable cell line for the inducible expression of EP400NL.

3. 1 Establishment of a stable cell line expressing TAP-tagged EP400NL

To generate a stably transfected cell line for inducibly expressing EP400NL, a pNTAP vector expresses EP400NL with an in-frame N-terminal streptavidin-binding peptide (SBP) and a calmodulin-binding peptide (CBP) epitope tag was obtained from Dr. Park (Figure 3. 1). The Flp-In™ T-REx™ System was used for inducible expression of EP400NL, as it is designed for the rapid generation of stable cell lines that ensure stable expression of the protein of interest. The cells were modified from a human epithelial HEK293T cell line carrying an Flp Recombination Target (FRT) site in which the expression vector containing EP400NL was used to integrate into the genome via Flp recombinase-mediated DNA recombination at the FRT site (Ogorman et al., 1991). To generate the target protein expression vector, TAP-EP400NL was excised from the pNTAP vector with Not1 and Apa1 and inserted into pcDNA5/FRT/TO vector.

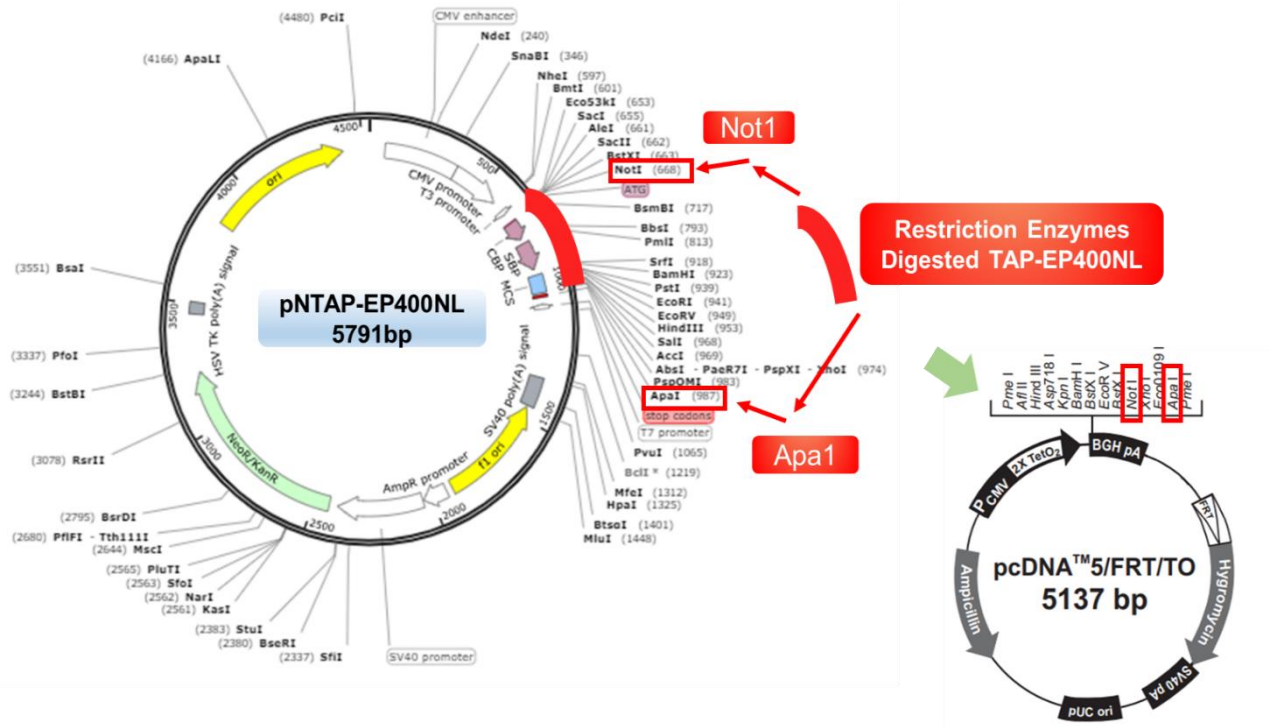

Figure 3. 1 pNTAP vector (N-terminal tandem affinity purification tagged vector)

The red DNA fragment indicates the EP400NL TAP-tagged sequence that was digested by Not1 and Apa1. The digested sequence was then inserted into pcDNA5/FRT/TO vector that had been digested by the same restriction enzymes.

pcDNA5/FRT/TO and pOG44 (which constitutively expresses FLP recombinase under the control of the human CMV promoter) was co-transfected into the FLP-In T-REX cell line (Figure 3. 2). TAP-EP400NL is integrated into the genome of the host Flp-In™ T-REx™ cells via site-specific recombination between FRT sites in the host cell genome, which is mediated by the FLP recombinase.

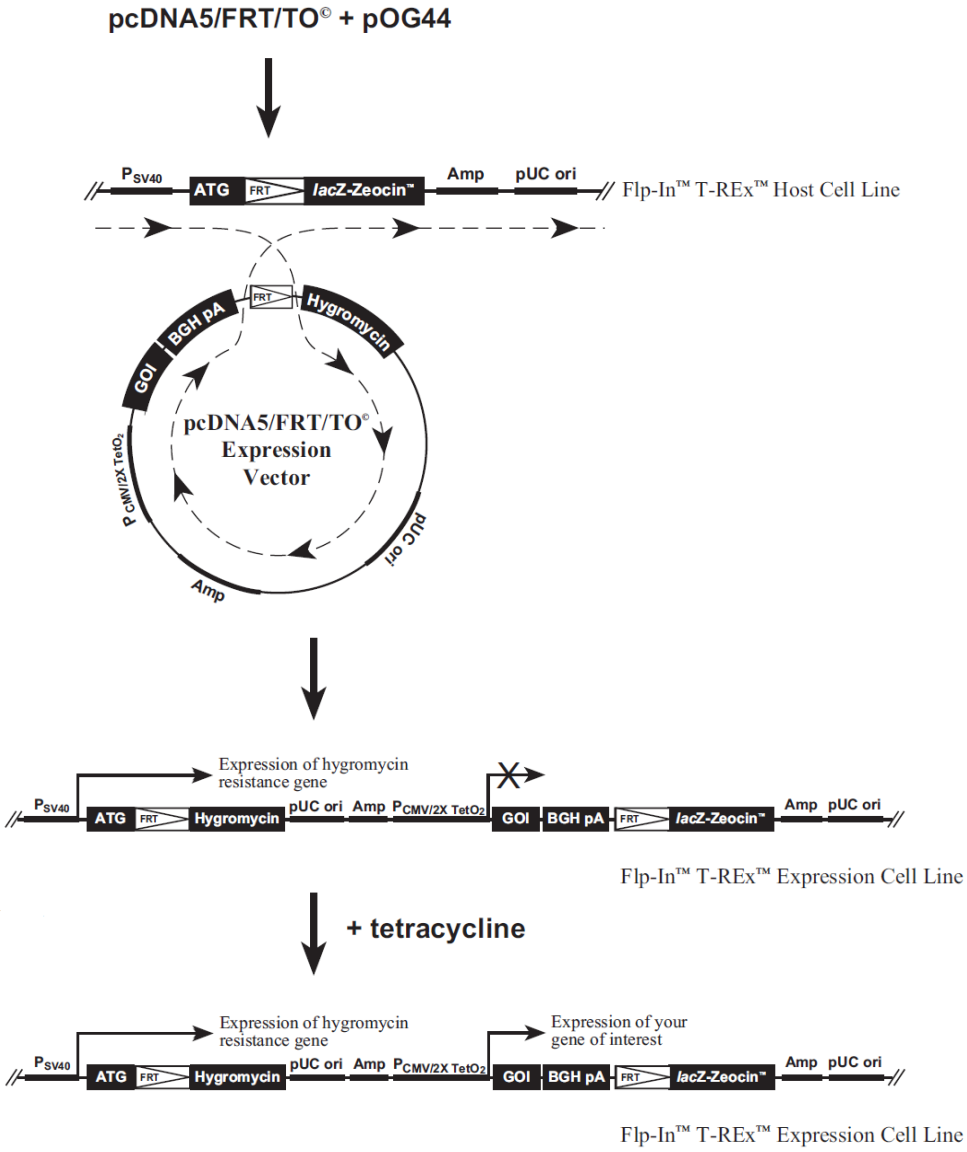

Figure 3. 2 Flp-In™ T-REx™ System for generating stable EP400NL expressing cell line.

pcDNA5/FRT/TO-TAP-EP400NL vector was co-transfected with pOG44 into the Flp-In™ T-REx™ cells for homologous recombination into the FRT site. Cells with genomic integration of pcDNA5/FRT/TO-TAP-EP400NL were selected by resistance to hygromycin, and expression of TAP-EP400NL can be induced by the addition of tetracycline. Figure modified from Thermo Fisher Scientific, reproduced with permission.

After the co-transfection of pcDNA5/FRT/TO-TAP-EP400NL and pOG44, the Flp-In™ T-REx™ cells were cultured in the presence of hygromycin for two weeks to select for genomic integration of pcDNA5/FRT/TO-TAP-EP400NL. Following the establishment of the TAP-EP400NL inducible Flp-In™ T-REx™ cells,

individual cells were isolated with cloning rings to obtain monoclonal cell lines, which then could be characterised to identify the suitable incubation time and the line with the highest expression level of TAP-EP400NL on induction. As the Tet repressor (TetR) binds the operator (TetO2) and represses the expression of EP400NL. Therefore, upon addition of tetracycline, TetR disassociates from TetO2 and allows expression of EP400NL (Figure 3. 2).

The optimal induction time point was investigated by incubating established cells with 1 μg/ml tetracycline and harvested at the selected intervals over a 96-hour time course (Figure 3. 3, top panel). Maximum expression of EP400NL was achieved after 48 hours therefore this time point was used in all subsequent experiments. Three individual cultures were treated with 0 or 1 μg/mL tetracycline for 48 hours, then harvested and processed for western blotting. Clone #3 exhibited the highest TAP-EP400NL level after tetracycline induction and was selected for further analysis. The lower bands around 52kDa indicate the endogenous expression of EP400NL (Fig 3. 3 bottom panel).

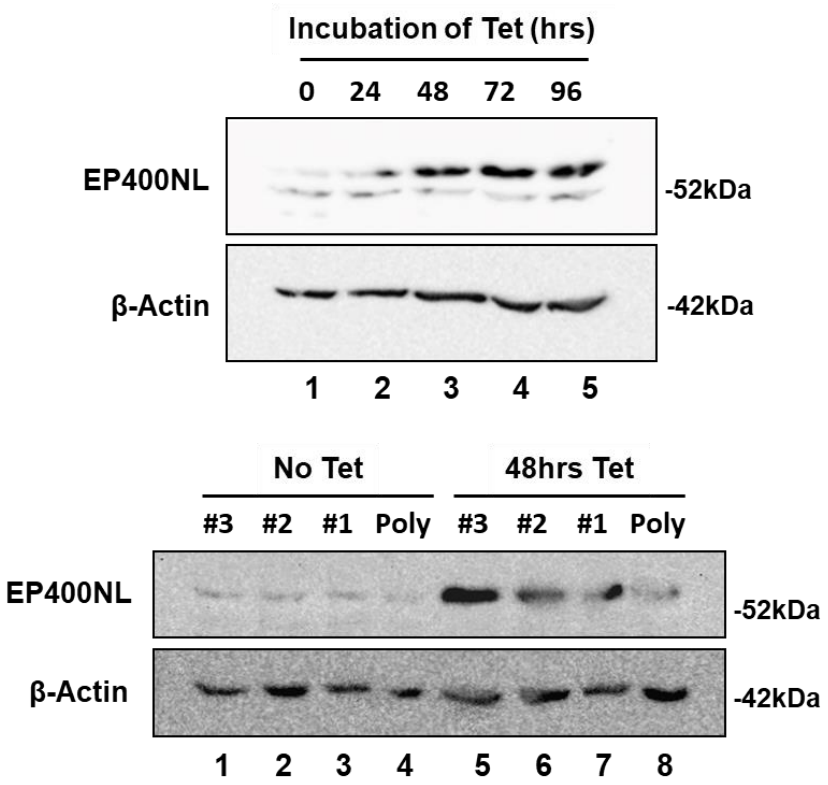

Figure 3. 3 Optimisation of tetracycline induction

(Top) An interval of 24 hours of tetracycline induction from 0 to 96 hours was tested. 48 hours of tetracycline induction were able to produce sufficient expression of TAP-EP400NL. (Bottom) Clone #3 exhibits the highest EP400NL expression compared to other clones. Tet: Tetracycline; hrs: hours; Poly: Polyclonal cells. 1 μg/mL of tetracycline was added for the optimal induction followed by the manufacturer's protocol, 50 μg of protein was loaded after extraction from the whole cell lysate, protein expression was subsequently confirmed by anti-EP400NL immunoblots.

To distinguish the expression of TAP-EP400NL from endogenous EP400NL, both the parental cell line (Flp-In™ T-REx™) and the stably EP400NL expressing cell line (hereafter referred to as the "established EP400NL" cell line) were cultured in the presence and absence of 1 μg/mL tetracycline and harvested 48 hours later. The molecular weight of both EP400NL and TAP-EP400NL was estimated by first constructing a standard curve using the protein marker. The molecular weight of the protein marker was then transformed into log10 value for generating a linear correlation, the coefficient of the linear correlation was subsequently calculated for the molecular weight estimation of these proteins (endogenous

EP400NL, 51kDa; TAP-EP400NL, 68kDa) (Figure 3. 4). Inducible expression of the TAP-EP400NL was confirmed by immunoblotting. A band was detected at a molecular weight of approximately 68kDa, which corresponds to the estimated size of EP400NL of 51 kDa plus a 17kDa of the TAP tag (SBP and CBP) and it was only detected in lysates of the established cells in the presence of tetracycline, as expected (Figure 3. 5, lane 4). The endogenous expression of EP400NL was also detected in all cell lysates, and the co-detection of the 68 kDa band in the established cell line treated with tetracycline confirmed the identity of this protein as EP400NL (Figure 3. 5).

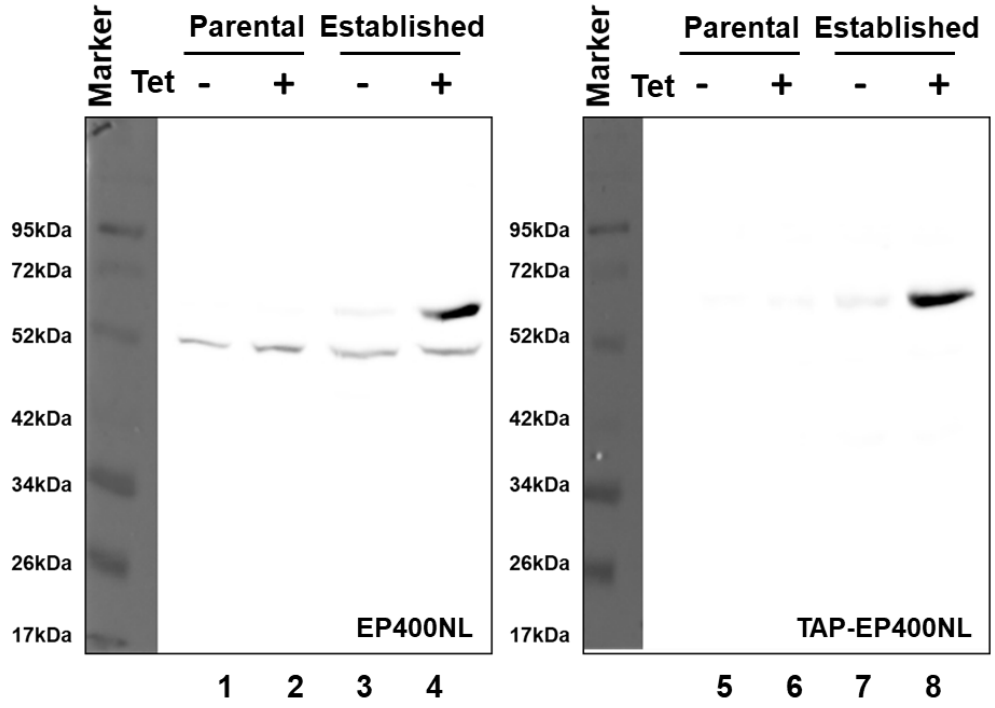

Protein marker		
Migration (cm)	MW (kDa)	Log value
0.5	260	2.4149733
1.2	140	2.146128
2.2	95	1.9777236
2.8	72	1.8573325
3.8	52	1.7160033
4.2	42	1.6232493
5.5	34	1.5314789
6.7	26	1.4149733
8	17	1.2304489

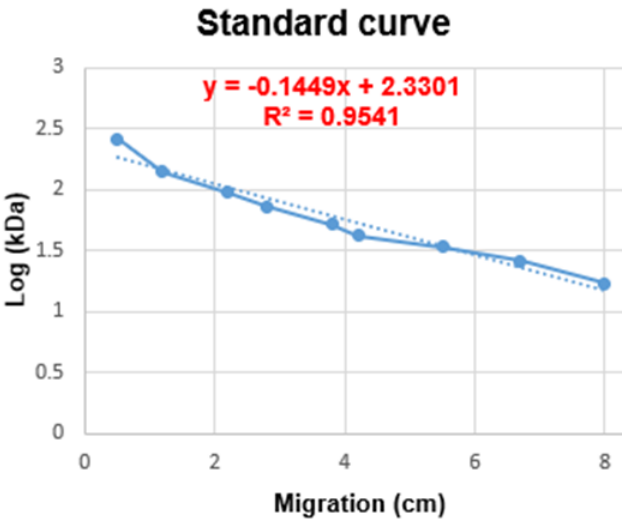

Proteins	Migration (cm)	Log10	MW (kDa)
TAP-EP400NL	3.45cm	1.830195	67.6
EP400NL	4.3cm	1.70703	50.9

Figure 3. 4 Molecular weight estimation of EP400NL and TAP-EP400NL

(Top panel) Immunoblots of anti-EP400NL and anti-CBP (TAP-EP400NL detection) after 48 hours of 1 µg/mL tetracycline induction based on the manufacturer's protocol using both parental and established EP400NL cells. 50 µg of whole-cell lysate was loaded after extraction from the whole cell lysate. (Middle panel) Standard curve construction. Migration of each band of the protein marker was measured (cm), the molecular weight of the protein marker was transformed into Log value (middle panel, left) for generating a linear correlation

between the Log (kDa) and protein band migration (cm). (Bottom panel) migration of both EP400NL and TAP-EP400NL was measured, and the corresponding Log value was calculated based on the equation y = -0.1449x +2.3301, R^2 = 0.9541. (Log10 value: TAP-EP400NL, 1.83; EP400NL, 1.71), the molecular weight of these proteins was subsequently calculated (TAP-EP400NL, $10^{1.83}$=67.6 kDa; EP400NL, $10^{1.7}$=50.9kDa). Tet: Tetracycline; MW: molecular weight.

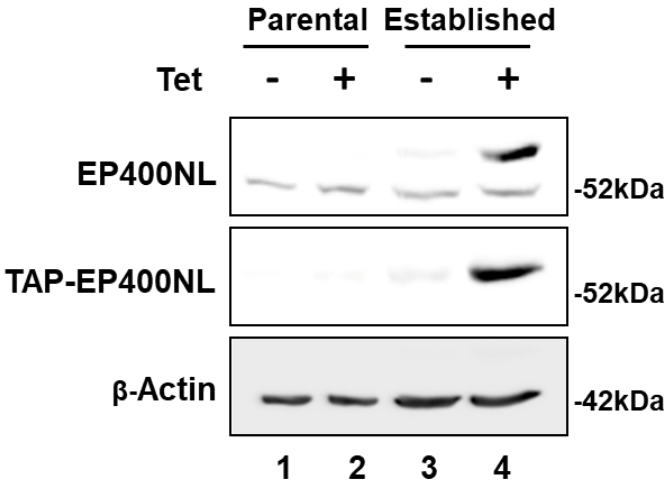

Figure 3. 5 Confirmation of tetracycline induced expression of TAP-EP400NL

After 48 hours of tetracycline induction (1 μg/mL), TAP-EP400NL was only detected from the established EP400NL cells followed by hygromycin selection. The protein bands at approximately 52kDa are endogenous EP400NL. The expression of TAP-EP400NL is the protein band about 68 kDa. The expression of TAP-EP400NL and endogenous EP400NL was detected by anti-CBP and anti-EP400NL, respectively. Tet: Tetracycline.

The established EP400NL cell line was then characterised to determine the subcellular distribution of TAP-EP400NL via cellular fractionation (methods and materials section 2. 2. 2) and immunocytochemistry. Following tetracycline induction, cells were harvested, and the cytosolic (CT), soluble nuclear (SN), and insoluble nuclear fractions (IN) were isolated and analysed by immunoblotting to identify the subcellular localization of TAP-EP400NL (Figure 3. 6, left panel). The same blots were also probed with antibodies for three proteins PPM1B, MED30, and Lamin A/C of known subcellular distribution to verify the accuracy of the fractionation: PPM1B is a cytosolic marker, (Bruce et al., 2012), MED30

(mediator of RNA polymerase II transcription subunit 30) is a subunit of the nuclear mediator complex and thus a nuclear marker (Baek et al., 2006, Baek et al., 2002), and Lamin A/C is an intermediate filament protein that is a part of the nuclear lamina and a marker for the insoluble component of the nucleus (Alvisi et al., 2018, Muchir et al., 2004). EP400NL was found to localize predominantly to the soluble nuclear fraction. TAP-EP400NL also colocalized with DAPI stained cell nuclei of Flp-In™ T-REx™ HEK293 cells, which supports the subcellular fractionation results that the endogenous EP400NL localises predominantly to the

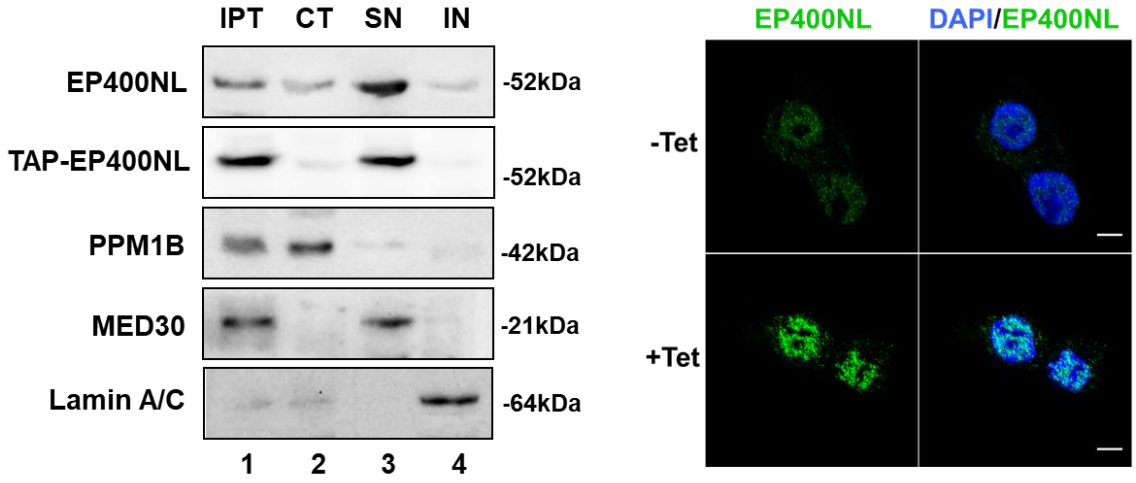

Figure 3. 6 Subcellular localization of TAP-EP400NL

nucleus (Figure 3. 6, right panel).

Cellular fractionation of TAP-EP400NL. Whole-cell lysate (IPT), cytosolic fraction (CT), soluble nuclear fraction (SN), and insoluble nuclear pellet (IN) were analysed by immunoblotting (left panel). Subcellular localization of TAP-EP400NL was analysed by immunocytochemical analysis (right panel). TAP-EP400NL inducible Flp-In™ T-REx™ cell line was treated with or without tetracycline. Scale bar denotes 10 µm.

3. 2 Purification of EP400NL protein complexes

To identify associated proteins with EP400NL, a strategy was developed in which TAP-EP400NL and associated proteins would be purified and isolated via size fractionation and affinity chromatography and subjected to mass spectrometry (Figure 3. 7)

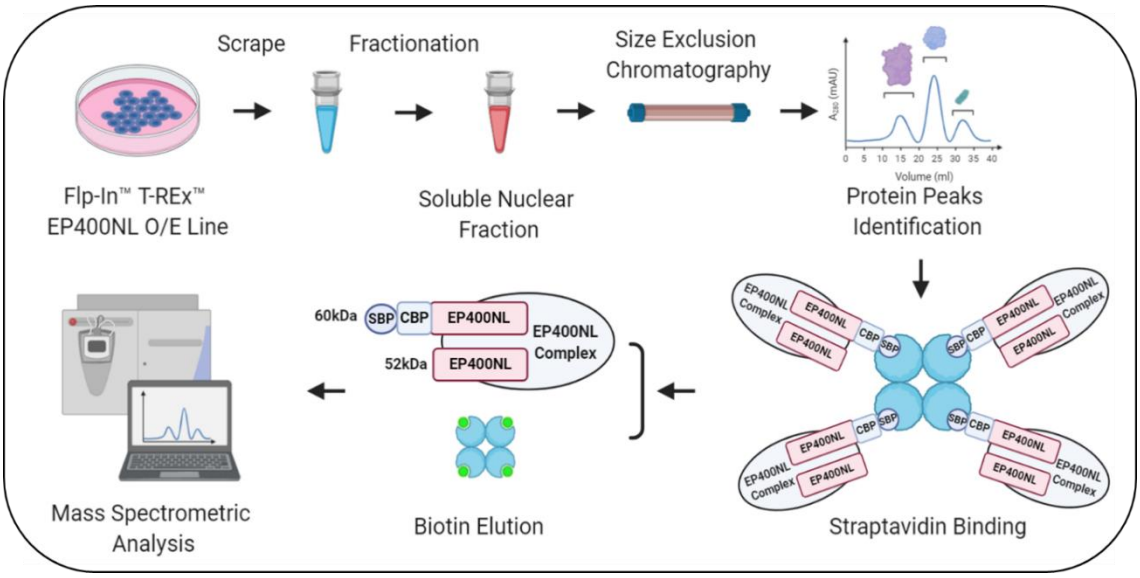

Figure 3. 7 Proposed workflow of TAP-EP400NL complex isolation using multistep purification.

This process includes size exclusion chromatography for the detection of specific protein peaks and streptavidin binding of those detected proteins followed by biotin elution of the targeted EP400NL complex for mass spectrometric analysis. This is an original artwork by Z.L.

3. 2. 1 Isolation of TAP-EP400NL complexes from the inducible Flp-In™ T-REx™ cells

To identify proteins in complex with EP400NL, TAP-tagged EP400NL associated complexes were isolated from the soluble nuclear fraction of the established EP400NL cells by a combination of size exclusion chromatography and affinity purification. After the fractionation of the cell lysates, the soluble nuclear fraction was collected then subjected to size exclusion chromatography. This protocol was first carried out on the parental Flp-In™ T-REx™ cells to determine the elution profile of endogenous EP400NL.

The elution of protein complexes was detected by monitoring the UV absorbance at A280 nm and the salts were detected by monitoring the conductivity of the buffer. The protein elution profiles indicated that large protein complexes were eluted right after the void volume (V_0), whereas small protein complexes or protein monomers were eluted later. Finally, salts from the input sample that potentially have full access to the resin pores indicated the total bed volume (Vt) of the column. Agarose-based size exclusion gel (Bio-Gel A1.5) was used at a flow rate of 0.3 mL/min. A total of 3 mL 60 fractions were collected (Figure 3. 8).

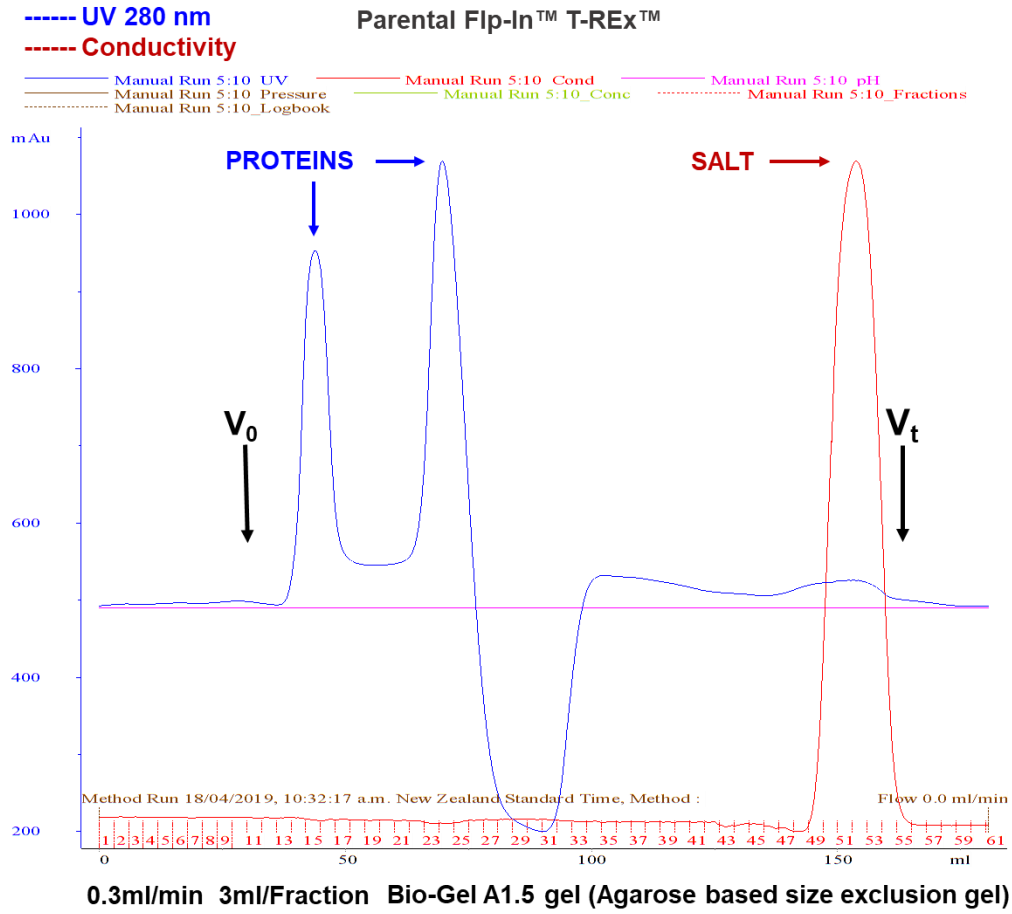

Figure 3. 8 Chromatogram of parental Flp-In™ T-REx™ cells

This chromatogram shows the elution profile of the nuclear soluble fraction isolated from the parental HEK293 Flp-In™ T-REx™ cells which serve as an internal negative control. Y-axis refers to the UV absorbance, X-axis refers to the fraction number in red and volume of the eluted buffer in black (ml). V_0: void volume; Vt: total bed volume.

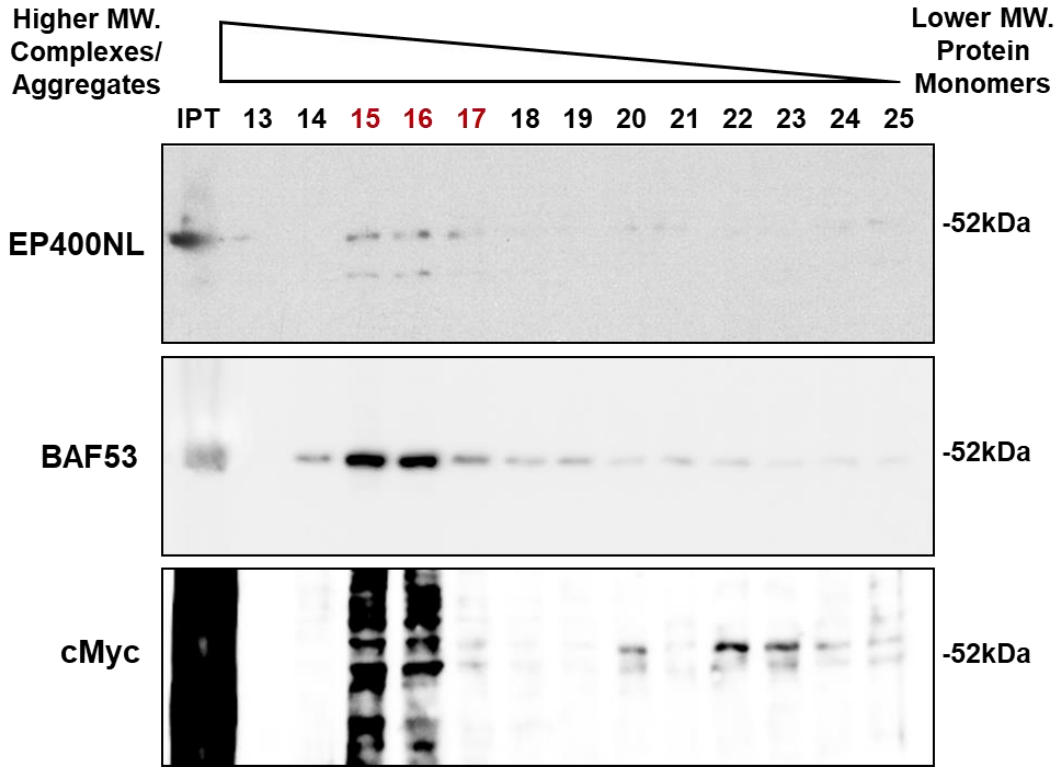

Figure 3. 9 Confirmation of EP400NL in the detected protein peaks (Parental Flp-In™ T-REx™ cells)

Fractions from 13 to 25 were sampled and probed with antibodies against EP400NL, BAF53, and cMyc. Three factions (15, 16, and 17 in red) contain the endogenous EP400NL (52kDa). IPT: Input.

Two protein peaks corresponding to fractions 13 to 25 were detected from the parental Flp-In™ T-REx™ cells by measuring the UV absorbance at A280 nm (Figure 3. 8), which were then analysed by immunoblotting to determine whether any of the peaks contain EP400NL.

Figure 3. 9 shows three fractions contain EP400NL, given that BAF53 is a common subunit of several multi-subunit chromatin remodelling complexes containing TIP60 and EP400 (Fuchs et al., 2001, Ikura et al., 2000), thus, it was of interest to determine that EP400NL eluted in the same fraction as BAF53, indicating they are in a similar-sized complex. To examine if the lower molecular weight fractions contain proteins as a protein peak around fraction 23 was detected, a widely expressed global transcription factor cMyc was utilised to

confirm protein presence in these fractions. Since cMyc cannot homodimerize and the cMyc-Max heterodimer is unstable, which leads to higher populations of dissociated cMyc monomers (Mustata et al., 2009), thus the presence of cMyc represents protein fractions with lower molecular weight monomers. Based on this, cMyc should be detected at higher levels as the fraction number increases from 13 to 25, because higher molecular weight proteins or complexes elute in early fractions followed by the elution of smaller proteins or monomers in relatively late fractions. EP400NL containing complexes were collected from the fractions 14, 15, 16, 17 which corresponded to the first protein peak with relatively higher molecular mass detected from the chromatogram (Figure 3. 8). This step also eliminated most of the smaller proteins fractionated at the second peak.

After determining the fractions that contained endogenous EP400NL and associated proteins including BAF53 and cMyc, soluble nuclear fraction from the established EP400NL were collected for size exclusion chromatography. Similar to the chromatogram of the parental cells, two protein peaks were detected from the established EP400NL cells by measuring their UV absorbance at A280nm (Figure 3. 10). Immunoblotting was carried out to examine whether these fractions also contain the same protein complexes as the parental cell line (Figure 3. 11). Since fractions 13 to 25 overlap with the protein peaks, the fraction pattern of EP400NL, BAF53, and cMyc was subsequently examined. The presence of EP400NL, BAF53, and cMyc was detected across fractions 14, 15, 16, and 17. cMyc was detected in the relatively late stage of the elution ranging from fraction 20 to 24 which corresponds to the second protein peak (Figure 3. 10). cMyc was also present in fractions 14 to 16, suggesting that the EP400NL complex may interact with cMyc under physiological conditions. Since both EP400NL and BAF53 were detected in fractions 14, 15, 16, and 17 (Figure 3. 11), these fractions were pooled together for subsequent streptavidin affinity purification.

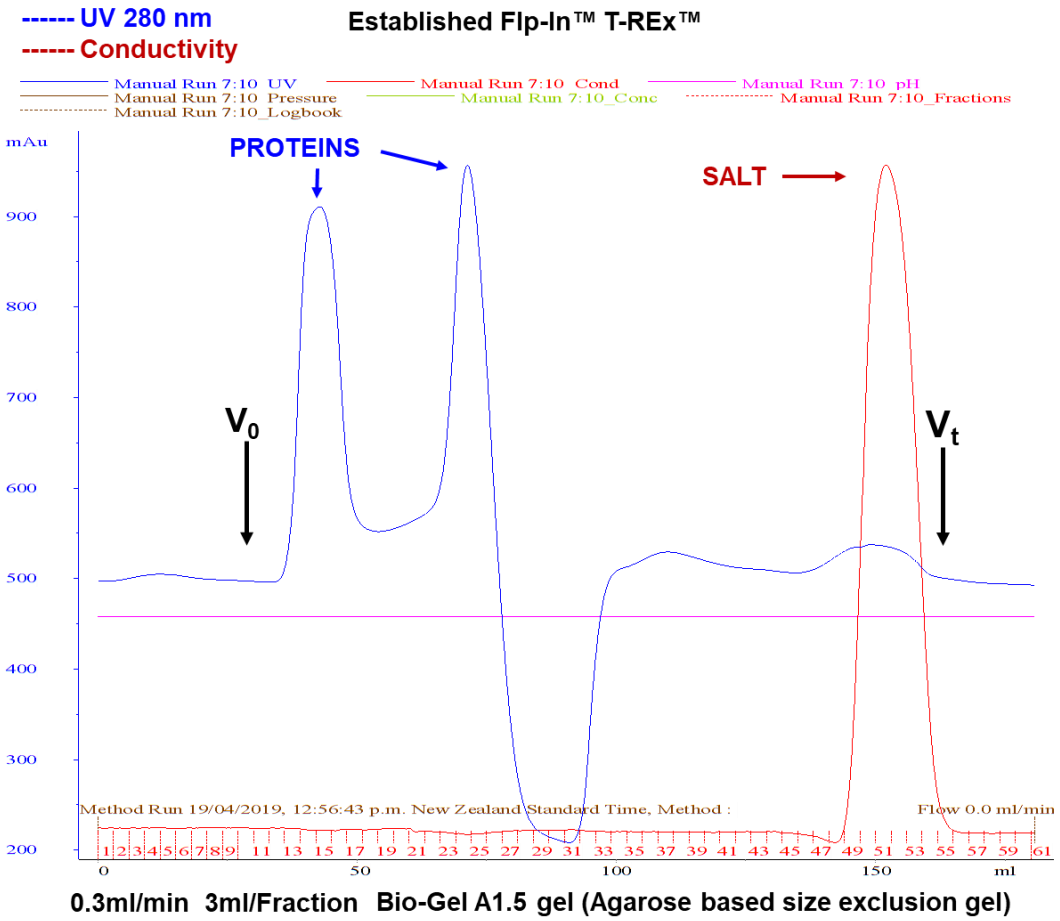

Figure 3. 10 Chromatogram of the established EP400NL cells stably expressing TAP-EP400NL

Two protein peaks (blue) were detected from this chromatogram. The presence of proteins was detected by monitoring their UV absorbance at A280nm and the salts were detected by monitoring the conductivity of the buffer. Y-axis refers to the UV absorbance, X-axis refers to the fraction number in red and volume of the eluted buffer in black (ml). V0: void volume; Vt: total bed volume.

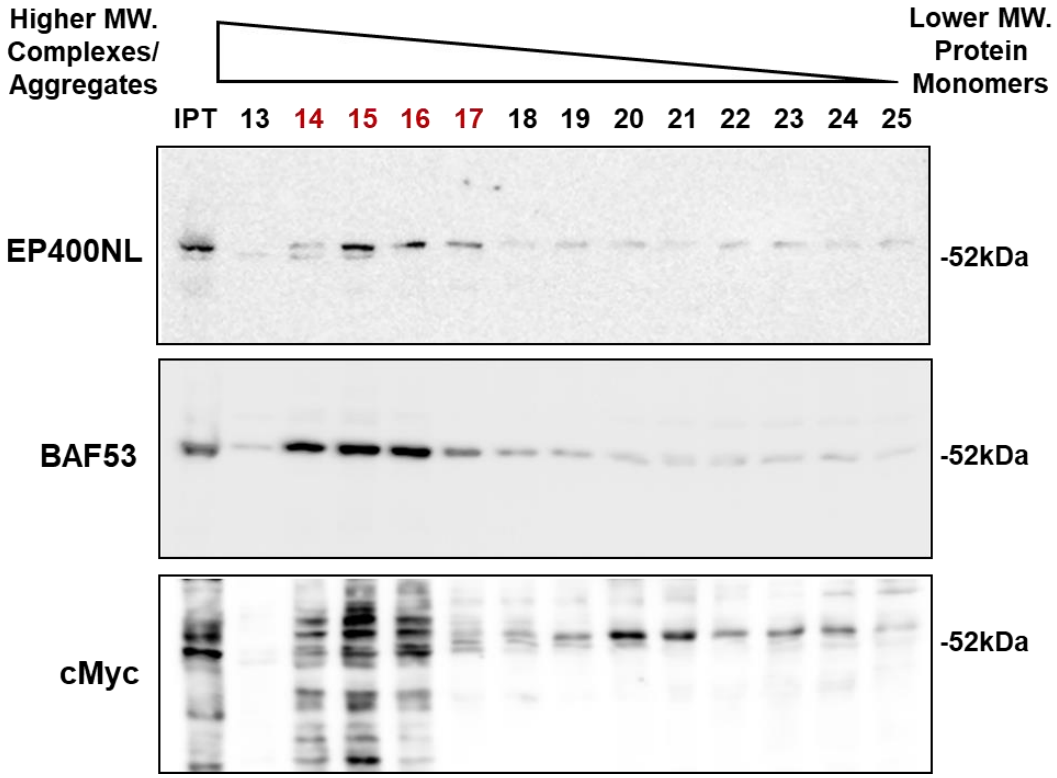

Figure 3. 11 Confirmation of proteins from the detected protein peaks (Established EP400NL cells)

Fractions from 13 to 25 were sampled and probed with anti-EP400NL, anti-BAF53, and anti-cMyc antibodies. Four fractions (14, 15, 16, and 17) containing TAP-EP400NL (68kDa), BAF53, and cMyc were identified. IPT: Input.

3. 2. 2 Streptavidin affinity purification and biotin elution of the EP400NL complex

TAP-EP400NL tagged with the streptavidin binding peptide (SBP) binds to streptavidin resin through its SBP tag and is dissociated from the resin by the addition of excess biotin. Fractions from 14 to 17 from either parental or established EP400NL cells were pooled together and incubated overnight with streptavidin beads for optimal streptavidin binding and followed by the biotin elution. Endogenous EP400NL was detected in both input and flow-through samples from the parental and the established Flp-In™ T-REx™ cells (Figure 3. 12, top panel, IP and FT), showing the requirement of SBP tag in the binding to the streptavidin resin. TAP-EP400NL was detected in the eluent from established cells only after tetracycline induction (Figure 3. 12 middle panel, lane 5, 6, 7, and 8) and with the highest amount of protein level from the biotin eluted fraction (Figure 3. 12 middle panel, lane 7). BAF53 was also detected in the eluent from established cells expressing EP400NL, suggesting that it interacts with EP400NL (Figure 3. 12, bottom panel, lane 7).

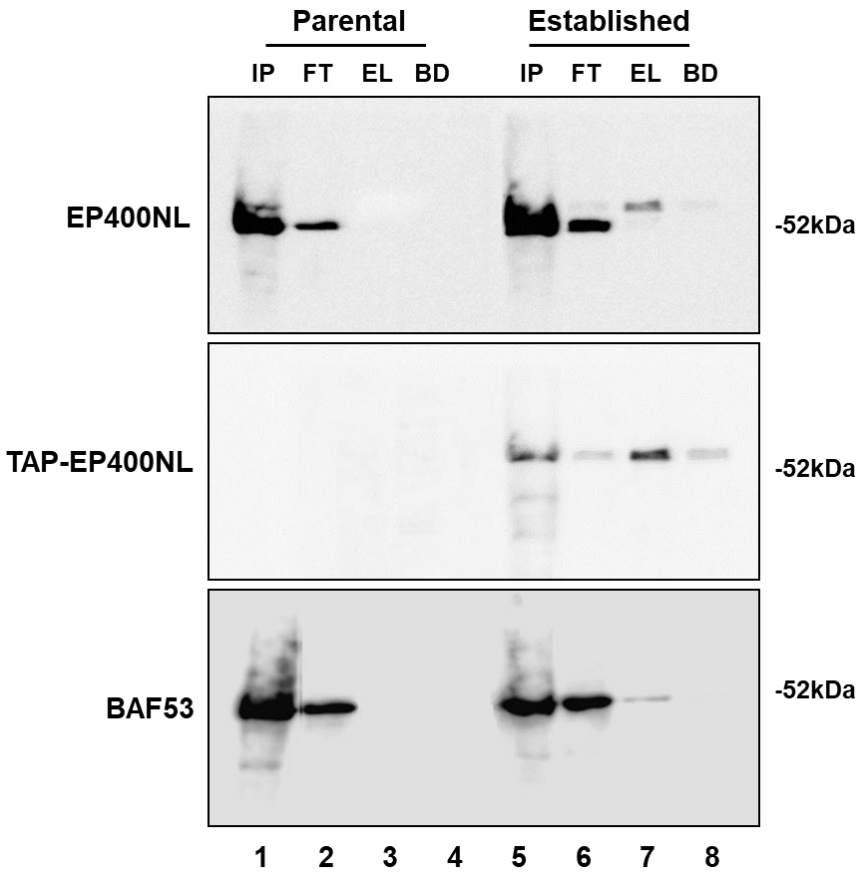

Figure 3. 12 Verification of biotin eluted proteins from streptavidin affinity purification

Eluted proteins from the parental and the established EP400NL cells were detected by anti-EP400NL immunoblot (top panel), anti-CBP immunoblot (middle panel), and anti-BAF53 immunoblot (bottom panel) respectively. IP: Input; FT: Flow-through; EL: Eluent; BD: Streptavidin beads.

3. 3 Identification of EP400NL interacting proteins by mass spectrometry

Following optimisation of the procedure for purification of TAP-EP400NL-containing nuclear complex, the purified protein samples derived from parental and established EP400NL cells were resolved by SDS-PAGE (Figure 3. 13) and the protein gel was stained with Coomassie Brilliant blue. The whole length of the protein gel from the established cells was excised and separated into 17 gel slices and processed for mass spectrometry (2. 3. 1). (Table 3. 13).

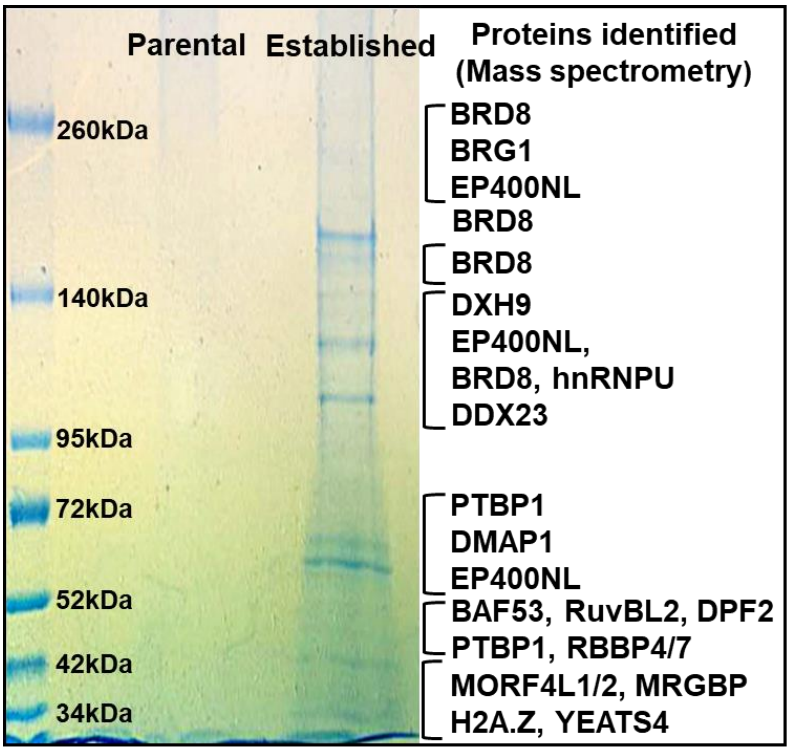

Figure 3. 13 Colloidal Coomassie Blue G250 staining of EP400NL nuclear complex.

Protein samples were purified from Flp-In™ T-REx™ cell lines either expressing TAP-EP400NL or parental control, respectively. The gel slices were excised and processed for mass spectrometry. Identified proteins are indicated on the right side of the stained gel.

Gel No.	MW ranges	Proteins identified (EP400NL complex)	# Unique Peptides	MW [kDa]
1	>300			
2	>300			
3	~260	BRD8	3	135.3
4	<260	BRD8	5	135.3
	<260	BRG1	5	188.7
	<260	EP400NL	1	51.7
5	140-260	BRD8	2	135.3
6	140-260	BRD8	1	135.3
7	140	BRD8	6	135.3
8	95-140	DHX9	11	140.9
	95-140	EP400NL	1	51.7
	95-140	BRD8	1	135.3
9	95-140	hnRNPU	6	90.5
10	95-140			
11	95-140	DDX23	4	95.5
12	72-95			
13	52-72	EP400NL	6	51.7
14	52-72	DMAP1	6	53
	52-72	PTBP1	4	62.4
	52-72	EP400NL	2	51.7
15	42-52	BAF53 (ACTL6A)	8	47.4
	42-52	TIP48 (RuvBL-2)	2	51.1
	42-52	DPF2	3	45.8
	42-52	PTBP1	3	62.4
	42-52	RBBP7	2	47.8
	42-52	RBBP4	3	47.6
16	42	MORF4L1	13	40
	42	MORF4L2	1	32.3
17	<34	MORF4L2	7	32.3
	<34	MORF4L1	2	40
	<34	MRGBP	2	22.4
	<34	Histone H2A.Z	1	13.5
	<34	YEATS4	1	26.5

Table 3. 1 Summary of EP400NL associated protein candidates identified via mass spectrometry.

Seventeen gel slices were digested by trypsin and analysed by mass spectrometry. The column in the middle shows the identified proteins, number of their identified unique peptides on the right. The right column indicates the molecular weight of each protein that was identified from the analysis.

Eighteen specific peptides of the EP400NL interacting protein candidates were identified, six of which (BAF53 (ACTL6A), BRD8, BRG1, DMAP1, H2A.Z, and RuvBL2 (TIP48)) were selected for further analysis, based on the criteria that they are either involved in transcriptional regulation or members of multiple chromatin remodelling complexes (Yamada, 2012).

As expected, BAF53 (ACTL6A) is not only an essential component of the hNuA4 complex but also a key subunit of the SWI/SNF chromatin remodelling complex for transcriptional activation or repression (Doyon and Cote, 2004b, Euskirchen et al., 2012a). The presence of BAF53, a BRG1-associated factor, is essential to the ATPase activity of BRG1 and promotes the interaction between the BRG1-containing modifying complex and the chromatin matrix (Zhao et al., 1998). The identification of BAF53 from mass spectrometry also coherent to the results of the detection of protein presences (Figure 3. 9 and Figure 3. 11, anti-BAF53 immunoblots).

BRD8 is a transcriptional co-activator recruited by hormone nuclear receptors and has been identified as a subunit of the hNuA4 histone acetyltransferase (HAT) complex for transcriptional activation. Nucleosomal histones H4 and H2A can be modified by BRD8 associated HAT activity and the modified histones can further recruit other regulatory proteins such as transcriptional activators for promoting gene transcription (Monden et al., 1997, Yamada, 2012). Interestingly, three other identified proteins, DMAP1, BAF53, and RuvBL2 were also previously shown as the key components of the hNuA4 histone acetyltransferase complex for transactivation through histone modification and chromatin remodelling (Doyon et al., 2004, Yamada, 2012).

DMAP1 (DNA methyltransferase 1-associated protein 1) was initially identified as a transcriptional corepressor by interacting with HDAC2 for histone deacetylation (Rountree et al., 2000). However, it is also a subunit of the hNuA4 complex (Doyon et al., 2004).

RuvBL2 is an ATPase that not only positively regulates gene transcription as a component of the HAT complex but is also involved in the removal of histone H2A.Z from the nucleosome when it forms an SWR-1 like complex (Alatwi and Downs, 2015). H2A.Z is a histone variant of H2A that is commonly incorporated into nucleosomes in place of the canonical histone H2A. RuvBL2 is also an ATP-dependent DNA helicase that can be recruited to the sites of damaged DNA to facilitate the DNA double strand break repair. (Lans et al., 2012). The identification of RuvBL2, as well as a unique peptide of H2A.Z in the mass spectrometry data, warrants further investigation into whether H2A.Z deposition can be catalysed by the EP400NL-containing complex.

BRG1 is a critical enzymatic subunit of SWI/SNF chromatin remodelling complexes that associate with chromatin conformation changes by altering the DNA-histone interactions in an ATP-dependent manner (Trotter and Archer, 2008, Wu et al., 2017). However, unlike BRD8, DMAP1, RuvBL2, and BAF53, which are all found as subunits of the hNuA4 histone acetyltransferase complex, BRG1 has not been reported to interact with this complex, thus this interaction warrants further characterisation. (Doyon and Cote, 2004b, Yamada, 2012).

3. 4 Confirmation of EP400NL interacting protein candidates

Following mass spectrometric identification of putative EP400NL-interacting proteins, co-immunoprecipitation was carried out to confirm the individual interactions. Three FLAG-tagged proteins (EP400NL, DMAP1, and TIP60) were transiently expressed separately in HEK293T cells and partially purified by anti-FLAG M2 agarose beads (Figure 3. 14). Consistent with the results obtained from the mass spectrometry, BRG1, BRD8, BAF53, and RuvBL2 all coimmunoprecipitated with EP400NL (Figure 3. 14). Although RuvBL1 was not identified by the mass spectrometry, since it forms a hetero-oligomeric complex with RuvBL2 in most human nuclear complexes (Lopez-Perrote et al., 2014), the

blot was also probed with an anti-RuvBL1 antibody and it was also found to interact with EP400NL (Figure 3. 14). On the other hand, TIP60 and EP400 were not detectable in the immunoprecipitates (Figure 3. 14).

The interaction between BRG1 and EP400NL was also confirmed by co-immunoprecipitation (Figure 3. 14). These data suggest that while BRG1 has not been reported to interact with the hNuA4 complex (Doyon and Cote, 2004b, Doyon et al., 2004, Yamada, 2012), it may interact in a unique complex containing EP400NL and DMAP1 (Figure 3. 14).

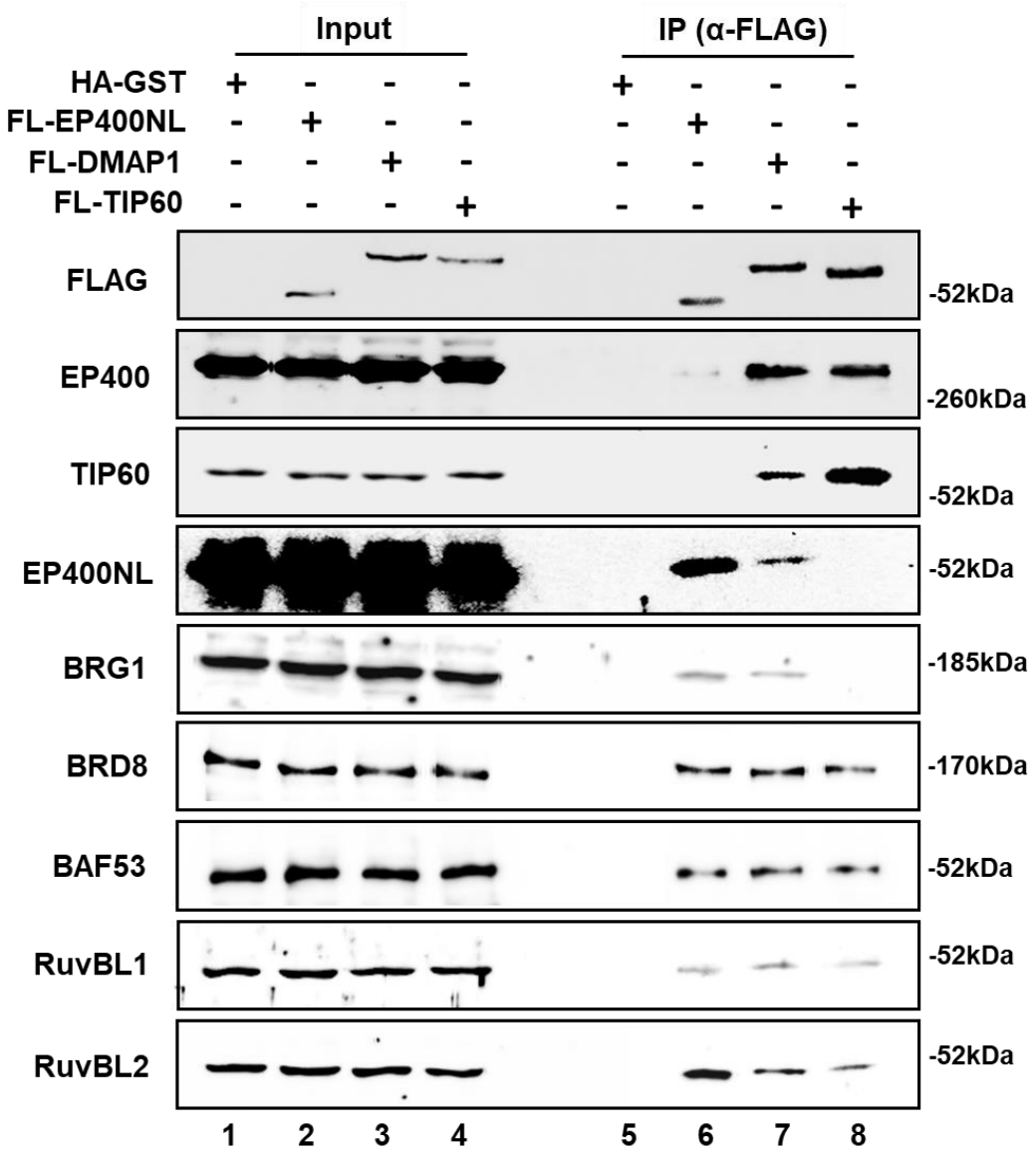

Figure 3. 14 Interaction of EP400NL with the candidate proteins by co-immunoprecipitation assay.

HEK293T cells were transiently transfected with plasmids expressing HA-GST, FLAG-EP400NL, FLAG-DMAP1, or FLAG-TIP60 and the whole-cell lysates were immunoprecipitated by anti-FLAG antibody. The immunoprecipitates were analyzed by immunoblots using anti-FLAG, anti-EP400, anti-TIP60, anti-EP400NL, anti-BRG1, anti-BRD8, anti-BAF53, anti-RuvBL1, and anti-RuvBL2 antibodies.

3. 5 Discussion

A stable cell line for tetracycline-inducible expression of TAP-EP400NL was successfully generated and the TAP-EP400NL associated proteins were purified and subjected to mass spectrometry. Several proteins that were identified to associate with EP400NL are also shared with the hNuA4 complex, including DMAP1, BRD8, RuvBL1, RuvBL2, BAF53, MRGBP, MRG15(MORF4L1), and YEATS4 (GAS41) (Doyon and Cote, 2004a, Yamada, 2012). According to a protein-protein interaction (PPI) network and functional enrichment analysis tool (STRING bioinformatical analysis from ELIXIR's Core Data Resources), multiple known and predicted protein-protein interactions were further revealed (Figure 3. 15).

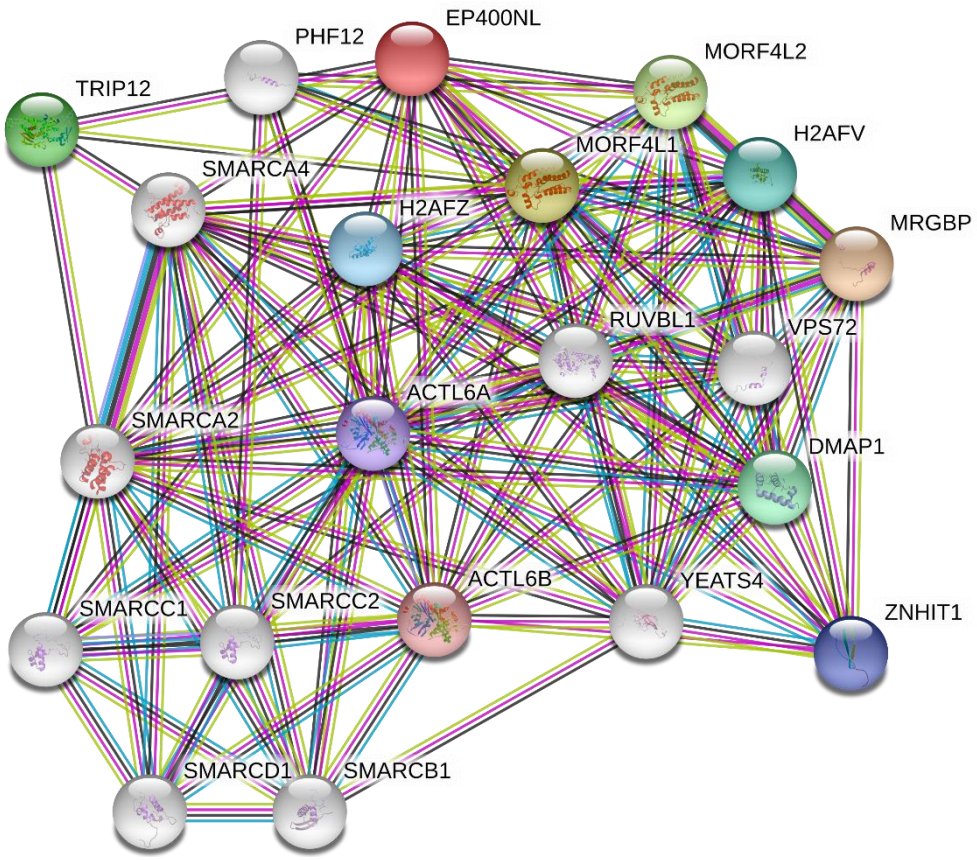

Figure 3. 15 String analysis for known and predicted EP400NL interactors

Predicted and known protein interactions were summarized and visualized as nodes that are connected by coloured lines. Presence of fusion evidence (red line); neighbourhood evidence (green line); cooccurrence evidence (blue line); experimental evidence (purple line); text mining evidence (yellow line); database

evidence (light blue line); co-expression evidence (black line). The physical distances between two nodes along an edge in a graph have no meaning and only represent connections between proteins.

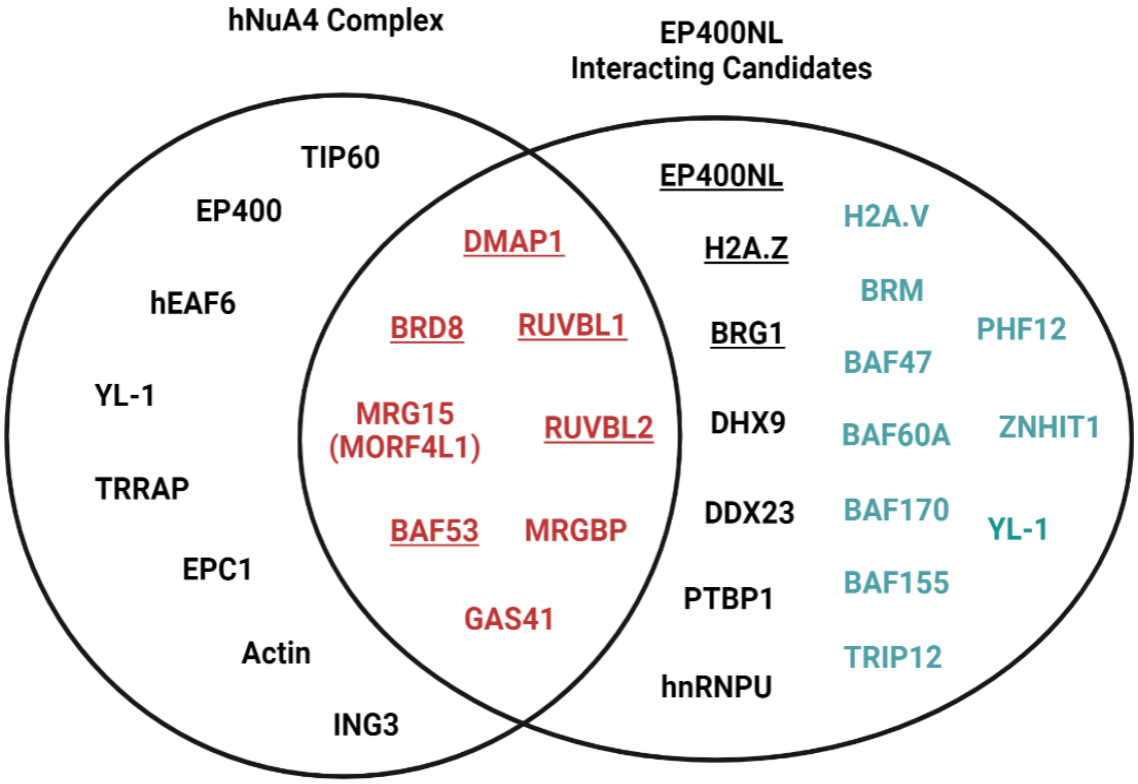

Figure 3. 16 Venn diagram showing the overlap of hNuA4 complex and EP400NL interacting candidates.

The hNuA4 complex contains 16 subunits with eight of them shared by the EP400NL containing complex (es) (red labelled proteins in EP400NL circle), seven additional EP400NL interacting candidates were identified from the mass spectrometric analysis (black labelled proteins in EP400NL circle), the underlined candidates were confirmed by immunoprecipitation after the identification by mass spectrometry. String predicted another ten EP400NL interacting candidates (blue labelled proteins in EP400NL circle).

In addition to the previously identified protein candidates from the mass spectrometry (Figure 3. 16, EP400NL interacting candidates, labelled in black), 10 new protein candidates (H2A.V (H2AFV), BRM (SMARCA2), BAF47 (SMARCB1), BAF60A (SMARCD1), BAF170 (SMARCC2), BAF155 (SMARCC1), TRIP12, PHF12, ZNIT1, and YL-1 (VPS72)) are predicted to interact with EP400NL directly or indirectly (Figure 3. 16, EP400NL interacting

candidates, labelled in blue). Similar to H2A.Z, H2A.V, also known as H2A.Z2, is another histone variant of the canonical histone H2A encoded by a separate gene. There are only three amino acids differences between H2A.Z and H2A.V and currently, no antibodies are available to distinguish between them (Dryhurst et al., 2009, Matsuda et al., 2010, Dunn et al., 2017). There has been little study to date on H2A.V, however, it has been observed to be overexpressed in many cancers including breast, prostate, bladder, and lung cancer. H2A.Z has been shown to replace conventional H2A in a subset of nucleosomes for altering DNA accessibility, which modulates a variety of processes such as transcription regulation, DNA repair, DNA replication, and chromosomal stability (Farris et al., 2005, Gevry et al., 2007, Jin and Felsenfeld, 2007, Billon and Cote, 2012, Xu et al., 2012, Alatwi and Downs, 2015, Giaimo et al., 2019). Therefore, it will be of interest to investigate the importance of the interactions between EP400NL and H2A.Z/H2A.V in these processes and whether EP400NL influences the deposition of these histone variants.

YL-1 (VPS72) was also identified as a potential interactor with EP400NL. YL-1 is a shared subunit of both the hNuA4 complex as well as the chromatin remodelling SRCAP-containing complex. Both these complexes catalyze H2A.Z exchange (Ruhl et al., 2006, Wong et al., 2007, Giaimo et al., 2019). Moreover, the ATPases BRG1 and RuvBL2 have also been reported to reside in multiple chromatin remodelling complexes that promote H2A.Z exchange events in an ATP-dependent manner, therefore, the role of EP400NL in the deposition of H2A.Z is the focus of the next chapter.

Nine protein candidates identified by either mass spectrometry or STRING bioinformatical analysis are shared by both the EP400NL containing complex and the hNuA4 complex. Of these, the five underlined candidates were confirmed by the coimmunoprecipitation (Figure 3. 16, labelled in red). DMAP1, BRD8, BAF53, and two ATPases (RuvBL1/2) are components of the hNuA4 complex. Together with other interacting partners such as the catalytic subunits TIP60 and EP400,

these proteins synergistically orchestrate the conformation changes of the chromatin through acetylation of nucleosomal histones H4 and H2A, ATP-dependent deposition or eviction of histones, and ultimately leads to transcriptional activation of those select genes (Murr et al., 2006, Yamada, 2012, Wang et al., 2018).

The bromodomain specifically binds to acetylated lysine residues on histone tails, resulting in the targeted recruitment of the bromodomain-containing protein complexes towards the acetylated chromatin for the transcription regulation (Fujisawa and Filippakopoulos, 2017). BRD8 (Bromodomain-containing protein 8) is a transcriptional coactivator recruited by hormone nuclear receptors, in which isoforms of BRD8 were reported as the subunit of hNuA4 histone acetyltransferase complex for transcriptional activation (Cai et al., 2003a, Yamada, 2012).

The evolutionarily conserved BRG1, as the core catalytic ATPase in multiple BAF complexes, was initially confirmed as one of the interacting candidates of EP400NL. Interestingly, another core ATPase: BRM, and additional subunits of the mammalian BAF complexes: BAF47, BAF60A, BAF170, and BAF155 were also predicted to interact with EP400NL from the STRING bioinformatical analysis. BAF complexes are important because it is a subfamily of SWI/SNF ATP-dependent chromatin remodelers that dynamically modulate chromatin structure to regulate fundamental cellular processes including gene transcription, cell cycle control, and DNA damage response (Hodges et al., 2016, Yan et al., 2017, Watanabe et al., 2017). Moreover, variant subunits can assemble into different combinations that contain either BRG1 or BRM as the catalytic ATPase, of which, four of them (BAF47, BAF60A, BAF170, and BAF155) were predicted to interact with EP400NL. BAF47, BAF170, and BAF155 are the core components of the BAF complex that act as scaffolds for the assembly, maintenance, and stability of the complex formation (Chen and Archer, 2005, Muratcioglu et al., 2015). On the other hand, BAF60A, a member of the BAF60

subfamily, is one of the accessory subunits of the BAF complex. The expression of BAF60 proteins changes in a tissue-dependent manner and the proteins from the BAF60 family can bridge the interaction between the transcription factors and the core BAF complexes (Wang et al., 1996, Wang and Crabtree, 1997, Lickert et al., 2004). Therefore, an association between EP400NL and the BAF complexes requires further investigation to consolidate the role of EP400NL in transcriptional regulation.

A total of 24 protein candidates that potentially interact with EP400NL were identified through a combination of mass spectrometry and bioinformatic prediction, seven of which were confirmed by coimmunoprecipitation. PHD Zinc Finger Transcription Factor (PHF12) and Zinc finger HIT domain-containing protein 1 (ZNHIT1) are transcriptional repressor/mediators that were also identified in the STRING bioinformatical analysis, however, whether they do interact with EP400NL is yet to be confirmed.

Mass spectrometric data also indicated that EP400NL interacts with a multifunctional ATP-dependent nucleic acid helicase DHX9 and a probable ATP-dependent RNA helicase DDX23. DHX9 unwinds DNA and RNA in a 3' to 5' direction that plays important roles in many processes including DNA replication, mRNA translation, and post-transcriptional RNA regulation and stability (Lee and Pelletier, 2016, Zhang and Grosse, 1994). DDX23, on the other hand, was reported to be involved with pre-mRNA splicing and its phosphorylated form (by SRPK2) is required for spliceosomal B complex formation (Mathew et al., 2008) Coincidently, a nucleic acid-binding protein hnRNPU (Heterogeneous Nuclear Ribonucleoprotein U) and an RNA binding protein PTBP1 (Polypyrimidine tract-binding protein 1) which binds specifically to the polypyrimidine tract of introns in premature mRNAs were also identified from the mass spectrometry. These pre-mRNA binding proteins play roles in several cellular processes such as transcription, mRNA alternative splicing and stability (Xiao et al., 2012, Yugami et al., 2007, Weidensdorfer et al., 2009, Oberstrass et al., 2005, Xue et al., 2009).

Additionally, MRG15(MORF4L1) was reported to serve as a chromatin-binding protein that can recruit splicing regulators such as polypyrimidine tract binding proteins (PTBPs). MRG15 specifically recognizes the methylated H3K36 and recruits PTBP isoforms including PTBP1/2 at intronic splicing silencer elements near an exon to suppress exon insertions into mRNA (Wang and Manley, 1997, Luco et al., 2010).

Both PTBP1 and MRG15 are essential for pre-mRNA splicing events during spermatogenesis. Germline-specific MRG15 Conditional KO (cKO) males display spermatogenic arrest at the round spermatid stage (Iwamori et al., 2016). PTBP1, on the other hand, contributes to spermatogenesis through the regulation of spermatogonia proliferation. PTBP1 cKO mice exhibit a significantly decreased sperm count at six months old with severe degenerations in seminiferous tubules in the testis. *In vitro* models using germline stem cells also revealed a retarded proliferation accompanied by an increase of apoptotic cell death when PTBP1 was deleted (Senoo et al., 2019). Gene expression profiling of 54 tissues from the GTEx RNA-sequence shows that EP400NL is expressed at the highest level in the testis, suggesting a specialized function of EP400NL in the tissue. Therefore, the specific identification of hnRNPU, MRG15, and PTBP1 as interactors of EP400NL suggest it would be of interest to investigate whether EP400NL plays a role in mRNA splicing and whether it is involved in the pre-mRNA splicing during spermatogenesis.

In summary, by combining these previously published results with the identification of EP400NL interacting candidates from our mass spectrometry, it is feasible to suggest that EP400 and EP400NL complexes share both bromodomain-containing candidates (BAF53 and BRG1) and the ATPase proteins (RuvBL1, RuvBL2, and BRG1) may exhibit some similar nuclear functionalities specifically for chromatin remodelling and transcriptional regulation. Thus, the next chapter will focus on investigating the role of EP400NL in histone acetylation and H2A.Z deposition.

4. THE INVESTIGATION OF EP400NL-ASSOCIATED ENZYMATIC ACTIVITIES

4. 1 Characterization of EP400NL complex -associated HAT activity

While EP400NL complex lacked a HAT (TIP60), since this complex has multiple proteins in common with hNuA4 histone acetyltransferase complex such as BAF53, BRD8, DMAP1, GAS41, RuvBL1, and RuvBL2. It was investigated whether the EP400NL complex was also associated with HAT activity.

In this method, radioactive isotope ^{14}C -labelled acetyl function group of coenzyme A is transferred to the ε -Nitrogen of the lysine residues on the histone tails by histone acetyltransferases, which leads to a conformational change from closed chromatin to a form of relaxed open chromatin (Figure 4. 1, top panel). If a transiently expressed enzymatic protein exhibits HAT activity, the radioactive signal on the histone tails can be detected using a maximum sensitivity radioisotope film (Figure 4. 1, bottom panel).

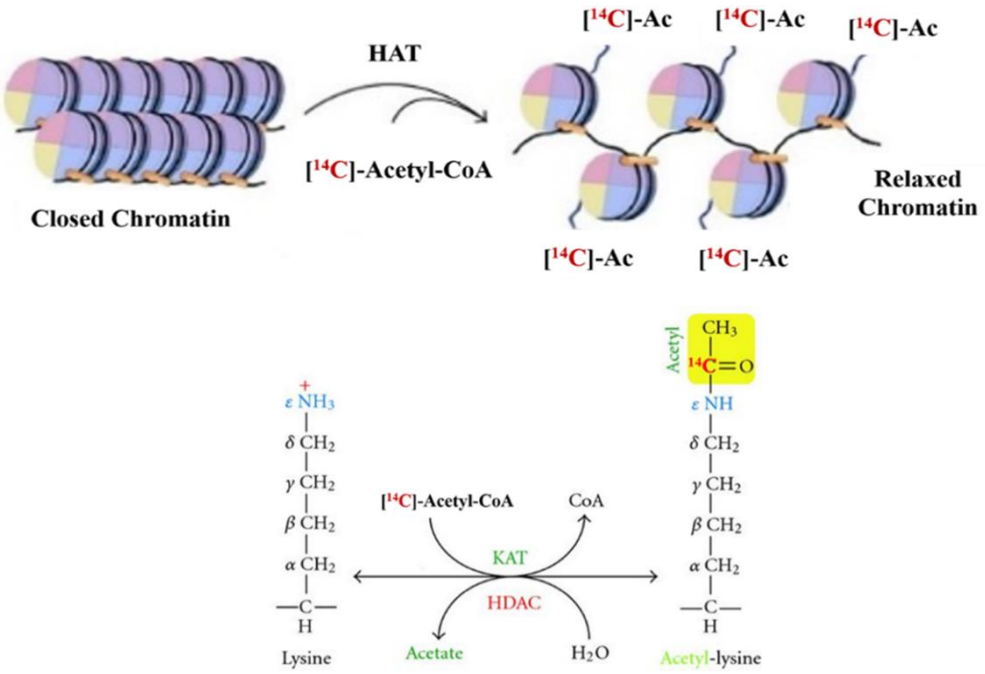

Figure 4. 1 [^{14}C]-Acetyl-Coenzyme A-based EP400NL HAT assay

Closed chromatin can transform to relaxed chromatin by histone acetylation, which leads to transcriptional activation (top panel). Radioactive isotope ^{14}C

incorporated into the acetyl function group of the coenzyme A is transferred to histones (ε-Nitrogen of the lysine residues) by histone acetyltransferases (HAT) (bottom panel).

4. 1. 1 Preparation of chromatin and protein complexes for the HAT enzymatic assay

The HAT assay is typically carried out by incubating the HAT catalytic domain-containing enzymes with histone H3 or histone H4 peptide in the presence of Acetyl-Coenzyme A. The HAT catalyses the transfer of acetyl groups from Acetyl-Coenzyme A to the histone peptide, resulting in the generation of acetylated peptide and CoA-SH. However, instead of using a single histone substrate peptide, plasmid DNA assembled with histone octamers (artificial nucleosomes) was utilized for better mimicking a physiological substrate.

Three plasmids that express FLAG-EP400NL, FLAG-DMAP1, and FLAG-TIP60 were transiently transfected into HEK293T cells, and anti-FLAG® M2 Affinity Gel was used to partially purify the proteins bound to FLAG-tagged EP400NL, DMAP1, and TIP60 respectively under native condition by FLAG peptide elution (Figure 4. 2). Partially purified DMAP1 and TIP60 protein complexes are the two positive controls as they are the core subunits of the TIP60 histone acetyltransferase (HAT) complex (Figure 4. 2) (Yamada, 2012, Lu et al., 2009) and HA-GST serves as a negative control (Figure 4. 2). EP400NL complex-associated HAT activity was then assayed with assembled nucleosomes as a substrate. A plasmid that contains nineteen repeats of 601-Widom nucleosome positioning sequences (pUC19/19x601) was used to generate the chromatin assembly by incubation with wild-type core histones. The proper assembly of histone proteins into chromatin was assessed via micrococcal nuclease (MNase) analysis. The micrococcal nuclease preferentially cleaves linker DNA between nucleosomes. Thus, MNase digestion should reveal a pattern of 200 bp periodic spacing from the assembled nucleosomes (Bulger et al., 1995) (Figure 4. 3).

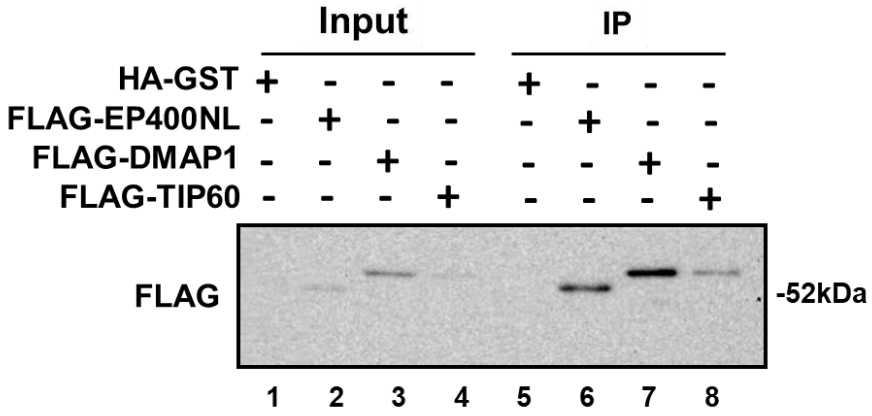

Figure 4. 2 Confirmation of expression of partially purified proteins after FLAG peptide elution

Confirmation of the transiently expressed proteins (FLAG-EP400NL, FLAG-DMAP1, and FLAG-TIP60) from the input controls and immunoprecipitates after FLAG peptide elution by using anti-FLAG immunoblot.

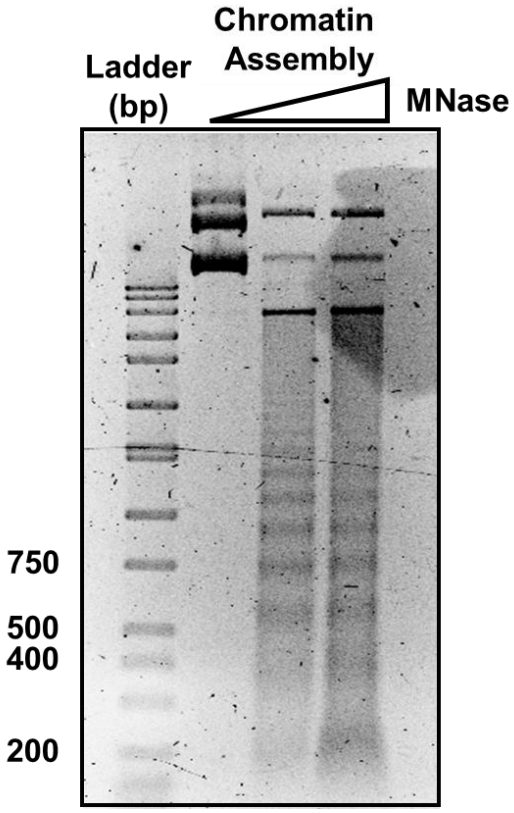

Figure 4. 3 Micrococcal nuclease (MNase) digestion for HAT assay

Micrococcal nuclease (MNase) assay to assess the assembly of chromatin by detecting a periodic spacing after digestion with MNase. Chromatin was incubated with MNase at 0, 3.75 $\times 10^{-3}$ U and 1.5 $\times 10^{-2}$ U, then digested chromatin was analysed by 1% agarose gel electrophoresis.

4. 1. 2 EP400NL has no associated HAT activity

Partially purified enzymatic protein complexes were incubated with the chromatin assembly in the presence of [^{14}C]-Acetyl-Coenzyme A, radioactive isotope ^{14}C - labelled acetyl function group of coenzyme A can be transferred to the histone tails only if these purified complexes exhibit histone acetyltransferases activity. The presence of Hela core histones was first examined and the transferred ^{14}C - labelled acetyl function group was subsequently detected on a radioisotope film with maximum sensitivity. The equivalent loading of HeLa core histones was confirmed by Ponceau staining (Figure 4. 4, top panel) followed by the examination of EP400NL complex-associated HAT activity (Figure 4. 4, bottom panel). Chromatin assemblies are acetylated by DMAP1-containing TIP60 complexes (Lalonde et al., 2014), and the TIP60 complex possesses high HAT catalytic activity on all histones substrates (Figure 4. 4), validating the ability of this assay to detect histone acetylation. However, a partially purified EP400NL complex did not show any HAT activity (Figure 4. 4).

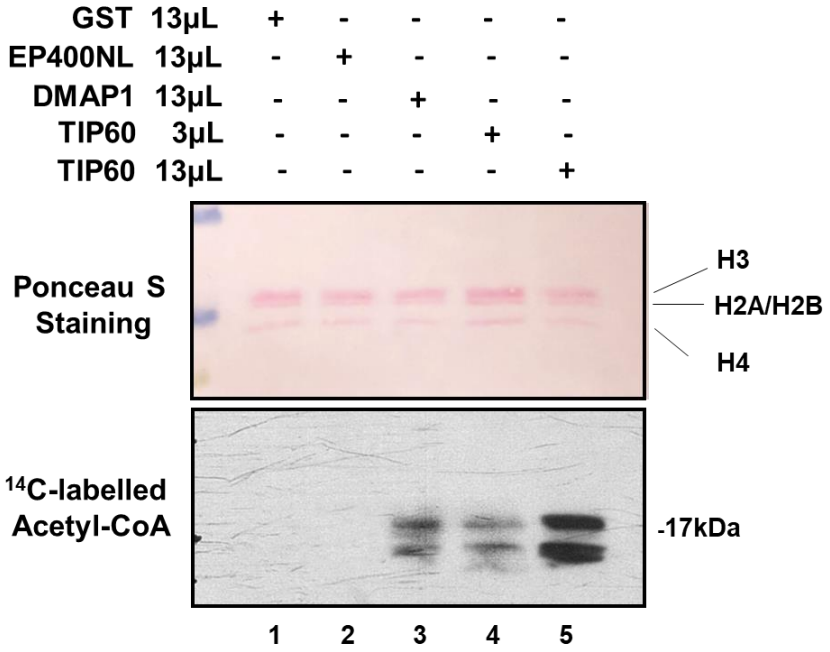

Figure 4. 4 Detection of EP400NL associated HAT activity

(Top) validation of equivalent loading of Hela histone proteins by Ponceau staining. (Bottom) detection of the radioactively labelled histones. Thirteen (µL) of EP400NL and DMAP1 were added to each reaction, TIP60 was tested using both 3 µL and 13 µL to confirm that the increased HAT activity is dose dependent.

4. 2 Characterization of EP400NL associated H2A.Z deposition activity

The identification of H2A.Z as an EP400NL interacting protein suggested that the EP400NL-complex may mediate ATP-dependent H2A.Z deposition as previously shown by the EP400 complex (Mizuguchi et al., 2004a, Xu et al., 2012). FLAG-tagged H2A.Z/H2B histones were used as a substrate to investigate if a partially purified FLAG-tagged EP400NL complex could catalyse H2A.Z deposition into chromatin (Figure 4. 5). Biotinylated pUC19/19x601 plasmids were assembled with recombinant canonical histones. Following assembly of H2A/H2B-containing histone octamers, they were incubated with the purified EP400NL-complex. If this complex exhibits H2A.Z deposition activity, the H2A/H2B dimers would be replaced with the FLAG-H2A.Z/H2B dimers. The biotinylated chromatin assemblies deposited with FLAG-tagged H2A.Z can then be affinity isolated with streptavidin beads and the deposition activity is assessed by the presence of FLAG-H2A.Z.

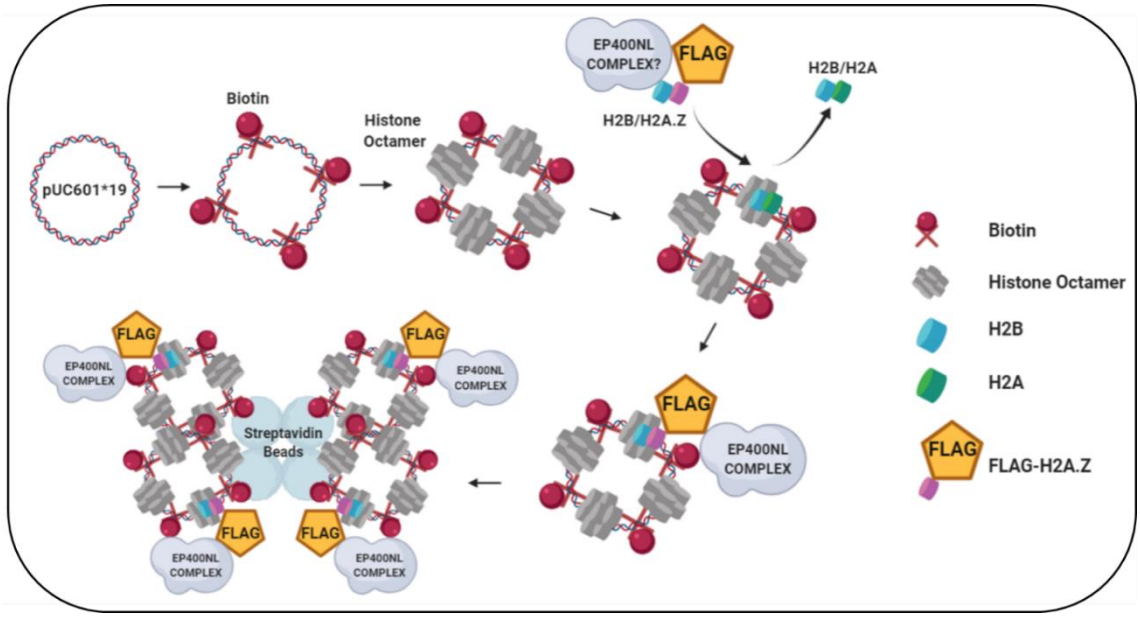

Figure 4. 5 Schematic illustration of H2A.Z deposition assay

Biotinylated chromatin assemblies (pUC19/19x601 with core histones) were incubated with the purified EP400NL-complex. The H2A/H2B dimers can be replaced with the FLAG-H2A.Z/H2B dimers if this complex exhibits H2A.Z deposition activity. The biotinylated chromatin assemblies with FLAG-tagged H2A.Z can be affinity isolated with streptavidin beads

4. 2. 1 Material preparation for the H2A.Z deposition assay

To obtain the substrate to be used in the deposition assay, recombinant histone FLAG-H2A.Z/H2B dimers were reconstituted and purified by gel filtration chromatography after individual core histone expression in *Escherichia coli* cells. The protein expression of FLAG-H2A.Z and H2B was first visualized by Coomassie blue staining and the identity of H2A.Z was confirmed by immunoblot with the anti-FLAG antibody (Figure 4. 6).

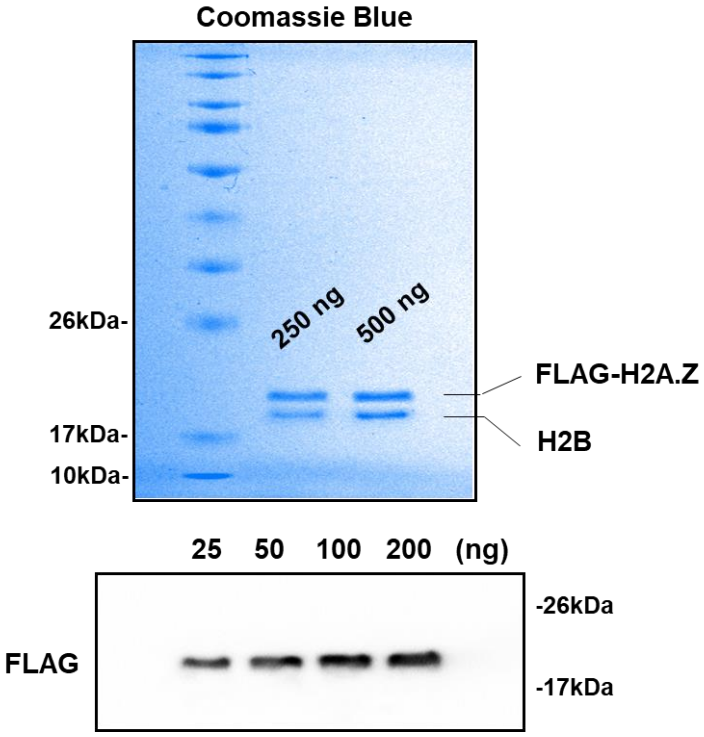

Figure 4. 6 Confirmation of the substrate expression of FLAG-H2A.Z/H2B dimers

250ng and 500ng of recombinant histone FLAG-H2A.Z/H2B dimers were visualized by Coomassie blue staining (top panel), and the expression of an increased amount of FLAG-H2A.Z/H2B from 25 ng to 200 ng was confirmed by an anti-FLAG immunoblot (bottom panel)

For this deposition assay, two major protein complexes (EP400 containing hNuA4 complex and EP400NL associated complex) need to be purified. The hNuA4 complex, a functional protein complex that contains both TIP60 and EP400 enzymatic subunits, served as a positive control as it has been reported to catalyse H2A.Z deposition in an ATP-dependent manner (Altaf et al., 2010, Yamada, 2012). The hNuA4 complex was purified from HeLa nuclear extract using FLAG-

tagged TIP60 followed by the confirmation using both anti-FLAG and anti-EP400 immunoblots (Figure 4. 7, top panel, red arrows). The FLAG-EP400NL-containing complex was partially purified by transiently expressing EP400NL in HEK293T cells followed by FLAG peptide elution. Expression of FLAG-EP400NL was confirmed by both anti-FLAG and anti-EP400NL immunoblots (Figure 4. 7, bottom panel). The plasmids containing the 601-Widom repeats (pUC19/601x19) were biotinylated and used to generate synthetic chromatin with recombinant canonical core histones. Synthetic chromatin assemblies were validated by MNase digestion that showed a 200bp spaced ladder (Figure 4. 8).

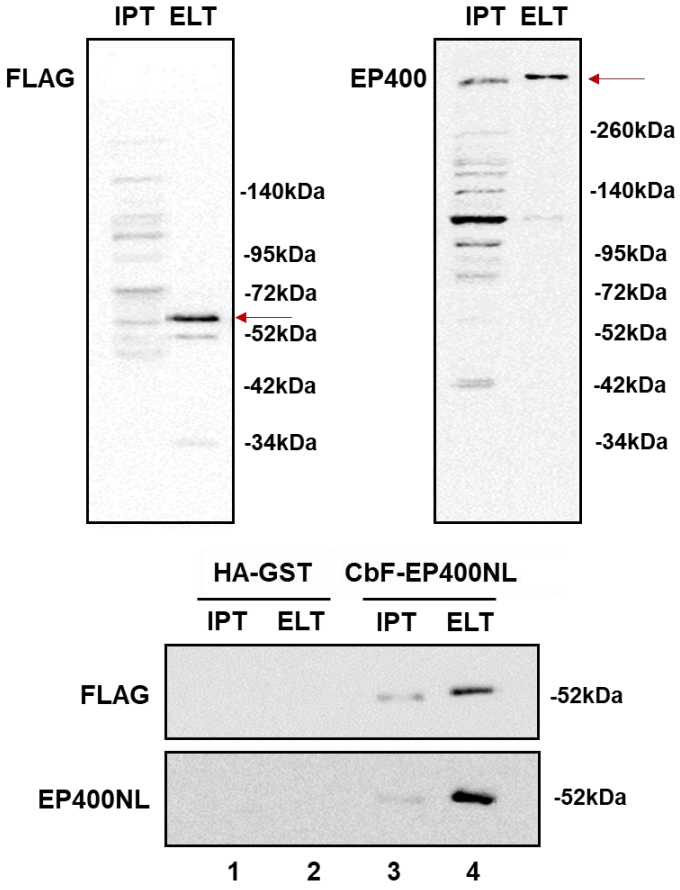

Figure 4. 7 Confirm the expression of TIP60/EP400 containing protein complex

The expression of FLAG-tagged TIP60 and EP400-containing protein complex were validated by anti-FLAG and anti-EP400 immunoblots, in which the expression of these proteins is indicated by red arrows (top panel). Expression of the FLAG peptide-eluted EP400NL was confirmed by both anti-FLAG and anti-EP400NL immunoblots, HA-GST was transiently expressed in HEK293T cells and serves as a negative control after FLAG-peptide elution (bottom panel). IPT: Input; ELT: Eluent.

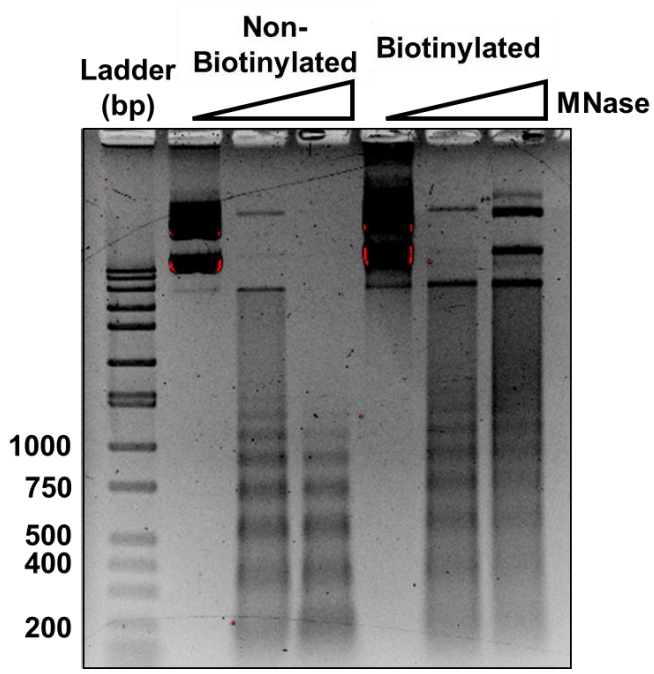

Figure 4. 8 MNase digestion assay of the assembled chromatin

Chromatin substrates assembled with either biotin-labelled pUC19/601x19 or unlabelled plasmid DNA (wild type) were digested with an increased concentration of MNase (3.75×10^{-3} U (low); 1.5×10^{-2} U (high)) and analysed by 1% agarose gel electrophoresis.

4. 2. 2 Optimization of substrate addition and non-specific binding of the substrate (FLAG-H2A.Z/H2B dimers) to the chromatin assemblies

To perform H2A.Z deposition assay, several steps need to be optimised. The amount of the substrate (FLAG-H2A.Z/H2B dimers) used in the deposition assay is critical and needs to be initially determined. This ensures the non-specific binding of the substrates to the chromatin assemblies is avoided. Secondly, to eliminate non-specific binding to the streptavidin beads, high salt wash steps with Tris/KCl-EDTA buffer (BC-Buffer) are necessary. However, high salt concentration can disrupt the biochemical interactions between the substrate histone dimers and either chromatin assemblies or their associated enzymatic protein complexes. Thus, the optimal concentrations of the substrate and the washing buffer needs to be empirically determined.

In the preliminary H2A.Z deposition assays, substrate histone dimers (FLAG-H2A.Z/H2B dimers) ranging from 50 ng to 500 ng were tested without the addition of any chromatin assemblies. Theoretically, no FLAG-tagged protein expression should be detected due to neither enzymatic proteins nor chromatin assemblies were added. The purpose is to provide enough substrate in the reaction without causing non-specific binding of the substrate to the streptavidin beads and consequently determine an appropriate amount of FLAG-H2A.Z/H2B dimers used in the follow up H2A.Z deposition assay. Increasing amount of the FLAG-H2A.Z/H2B dimers (1 ng, 5 ng, and 10 ng) were utilized as loading controls. After confirming the accuracy of the H2A.Z./H2B dimer (Figure 4. 6), a control needs to be included when investigating the non-specific binding of the substrate to the streptavidin beads to understand if those non-specific binding is from the overloaded substrates. A faint band can be detected from loading 10 ng of the substrate (Figure 4. 9), but 1 ng and 5 ng of substrate cannot be detected on the immunoblot which means a minimum of 10 ng of protein needs to be loaded to serve as the loading controls (Figure 4. 9). Among all four loaded substrates, 500 ng shows the highest level of non-specific binding to the streptavidin beads followed by the loading of 200 ng substrate. To avoid the risk of low detection, 100 ng of the FLAG-H2A.Z/H2B dimers was utilized for the following experiments (Figure 4. 9).

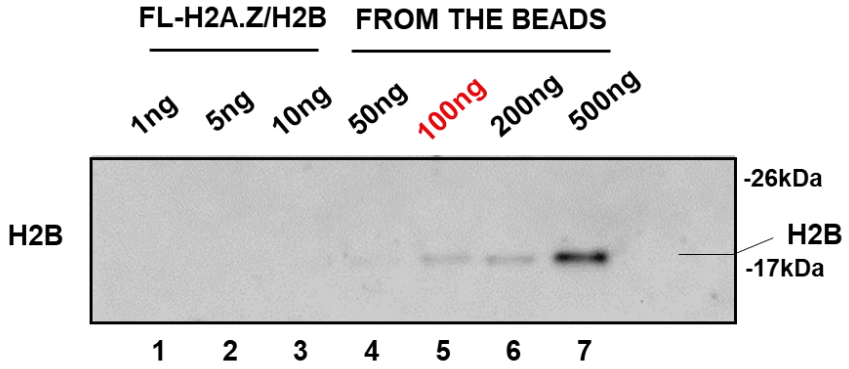

Figure 4. 9 Optimize the amount of the substrate loading

The elimination of the non-specific binding of substrate (FLAG-H2A.Z/H2B dimers) to the streptavidin beads. 100 ng was determined as the appropriate

amount of loading substrate, the ideal amount of the substrate is labelled in red. 1 ng, 5 ng, and 10 ng of the FLAG-H2A.Z/H2B dimers are the loading controls.

Next, two different salt concentrations of the washing buffer BC500 (500 mM KCl in 1% v/v NP40) and BC750 (750 mM KCl, in 1% v/v NP40) (reference to section 2. 4. 2) were tested. Histone substrate (100 ng) was included in each reaction with either non-labelled or biotinylated chromatin assemblies, initially in the absence of the EP400NL or hNuA4 complexes. Given the previous results (figure 4. 9), an increased amount of substrate ranging from 10 ng to 30 ng was used for the loading control (figure 4. 10). As expected, no H2B can be detected from the non-labelled chromatin assembly as no chromatin assemblies could bind to the streptavidin beads (Figure 4. 10, lane 4 and 5). In contrast, H2B can be detected from the biotinylated assemblies which represents the non-specific binding as no EP400NL complex was present for the deposition of FLAG-H2A.Z. (Figure 4. 10, lane 6 and 7). Washing with BC750 significantly reduced the non-specific binding of the FLAG-H2A.Z/H2B dimers to the chromatin assemblies isolated by the streptavidin beads compared to washing with BC500, this reduced level of H2B may come from the biotinylated chromatin assembly itself rather than the deposited H2B histones (Figure 4. 10, lane 7).

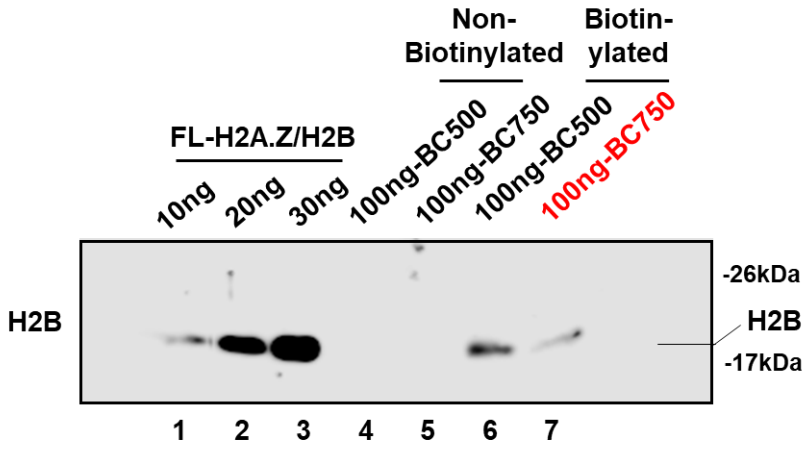

Figure 4. 10 Optimization of the concentration of the washing buffer

The washing procedure was optimized to eliminate the non-specific binding of substrate (FLAG-H2A.Z/H2B dimers) to the chromatin assemblies. Washing with

BC750 eliminated most of the non-specific binding and was determined as the appropriate concentration for the washing procedures, the ideal concentration of the washing buffer is labelled in red. 10 ng, 20 ng, and 30 ng of the FLAG-H2A.Z/H2B dimers are the loading controls, the blot was probed with anti H2B antibody.

This experiment was repeated, and the blot was probed with the anti-FLAG antibody to further confirm that non-specific binding to chromatin assemblies by substrate dimers was minimised by washing with BC750 (Figure 4. 11. Lane 5 and 7). Therefore, a combination of 100 ng of histones substrate (FLAG-H2A.Z/H2B dimers) with the BC750 washing step was used in the following H2A.Z deposition assay.

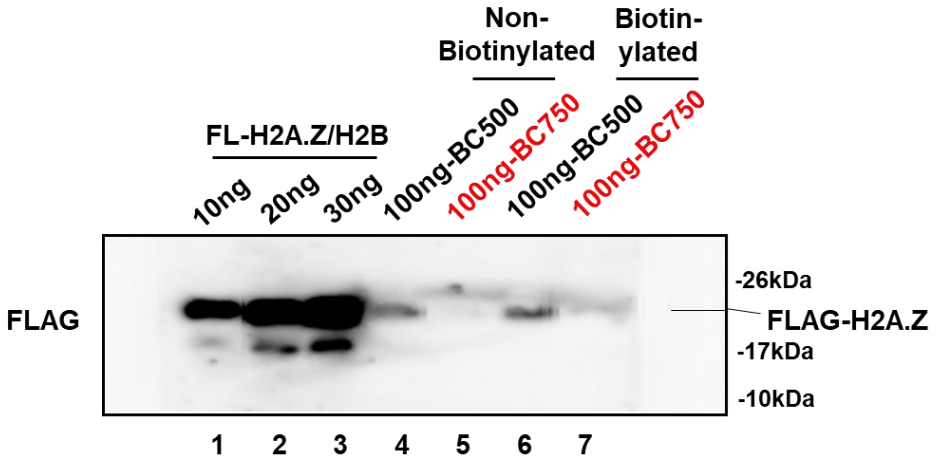

Figure 4. 11 Final validation of the experimental optimization

Addition of FLAG-H2A.Z/H2B dimers (100 ng) followed by washing with BC750 reduced most of the non-specific binding of the histone substrate to either the chromatin assemblies or the streptavidin beads, the ideal combination is labelled in red. 10 ng, 20 ng, and 30 ng of the FLAG-H2A.Z/H2B dimers are the loading controls. The blot was probed with anti-FLAG to detect FLAG-H2A.Z.

4. 2. 3 Evaluation of EP400NL complex-associated H2A.Z deposition activity

The hNuA4 complex, which serves as a positive control in the assay, was initially examined to determine whether it could catalyse an efficient incorporation of H2A.Z to the chromatin. The hNuA4 complex was purified from a HeLa cell line that stably expressed FLAG-TIP60. Mock purification from parental HeLa cells

served as a negative control. Following immunoprecipitation of FLAG-TIP60, the presence of the eluted hNuA4 complex was confirmed by both anti-EP400 and anti-FLAG immunoblots, in which the two major catalytic subunits EP400 and TIP60 were detected (Figure 4. 12, red arrows for lane 4 of each blot).

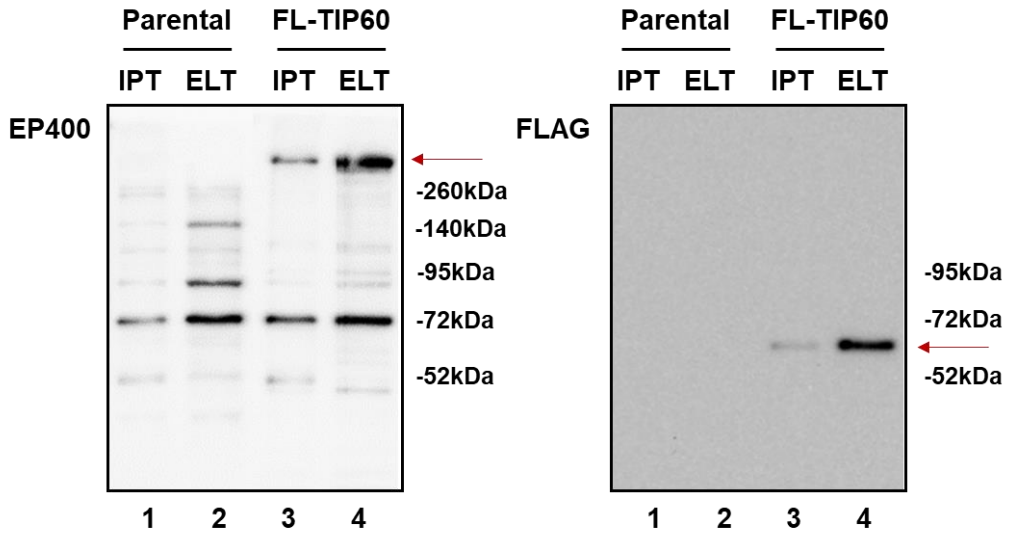

Figure 4. 12 Immunoprecipitation of the hNuA4 complex

Affinity purification of the hNuA4 complex from the FLAG-TIP60 expressing cell line was validated by the presence of its two major components (EP400 and FLAG-TIP60) using anti-FLAG and anti-EP400 immunoblots respectively. Neither protein was isolated from the parental cell line. Proteins are indicated by red arrows. FL-TIP60: FLAG-tagged TIP60; IPT: Input; ELT: Eluent.

To establish the H2A.Z deposition assay, substrates (FLAG-H2A.Z/H2B dimers) were incubated with either biotinylated or non-labelled chromatin assemblies in the presence of partially purified hNuA4 complex containing TIP60 and EP400. The hNuA4 complex was tested for the presence of H2A.Z deposition activity in preliminary experiments using biotinylated chromatin assemblies. Non-labelled chromatin assemblies served as a negative control. FLAG-H2A.Z was detected in biotinylated chromatin assemblies incubated with the hNuA4 complex via anti-FLAG immunoblot (Figure 4. 13, top panel, anti-FLAG immunoblot lane 3). Faint bands were detected in the other lanes which are considered to be non-specific binding, as it was detected in the parental cell line which does not express

FLAG-TIP60 and in the non-biotinylated chromatins (Figure 4. 13, top panel, anti-FLAG immunoblot lane 1, 2, and 4). H2B detection serves as an internal control as the amount of H2B remains constant before and after H2A.Z exchange (Figure 4. 13, top panel, anti-H2B immunoblot lane 3 and 4). Therefore, the level of FLAG-H2A.Z can be normalized against the reference of H2B.

To test if the EP400NL-containing protein complex can catalyse the exchange of H2A with H2A.Z, similar experiments were performed as described above with chromatins incubated with the EP400NL complex. HA-GST, which serves as a negative control for indicating background presence of H2A, was transiently expressed in HEK293T cells and isolated by FLAG-peptide elution (Figure 4. 13, bottom panel). A similar amount of FLAG-H2A.Z was detected in the reactions with the EP400NL complex as those incubated with the hNuA4 complex, indicating that the EP400NL complex also exhibits H2A.Z deposition activity (Figure 4. 13, bottom panel, anti-FLAG immunoblot lane 6). H2B was not detected in the non-labelled chromatin assemblies as only the biotinylated chromatin assemblies can be harvested after incubation with streptavidin beads (Figure 4. 13, bottom panel, anti-H2B immunoblot). And as an internal control, the expression of H2B remained consistent throughout the assay (Figure 4. 13, bottom panel, anti-H2B immunoblot).

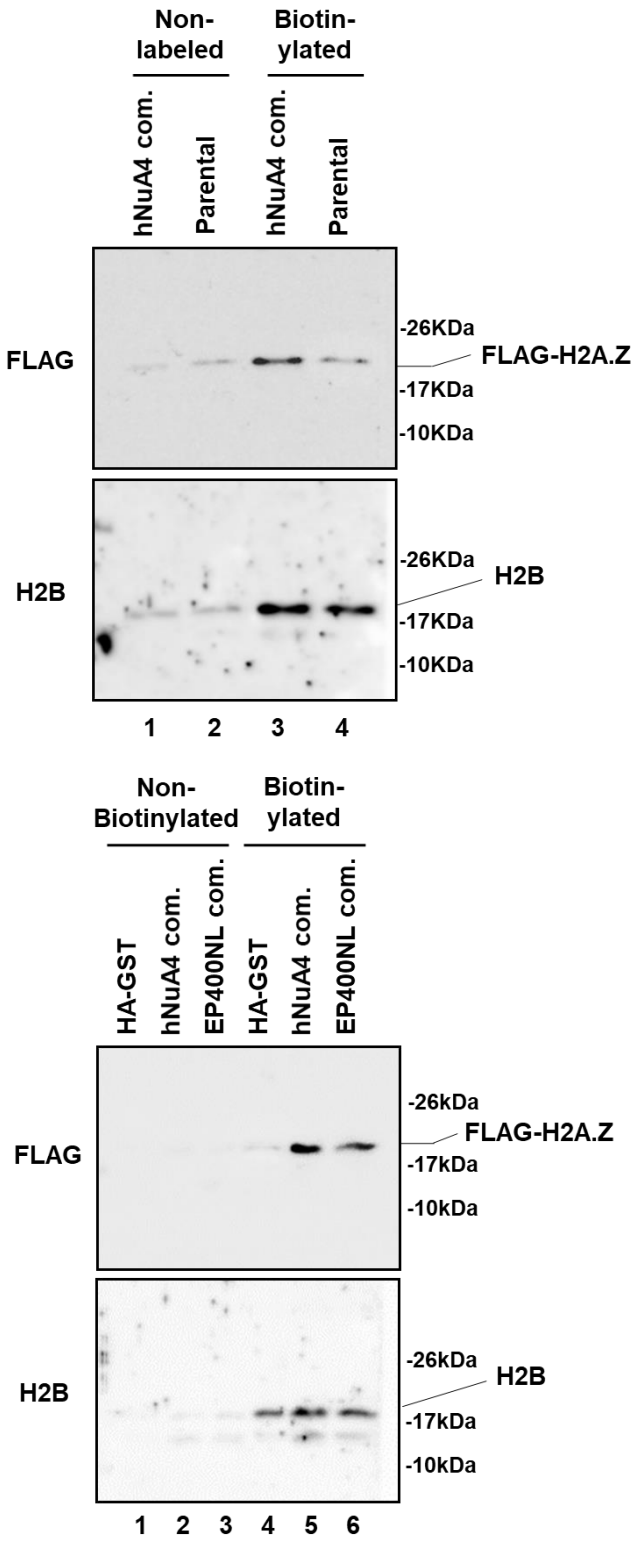

Figure 4. 13 Examination of the H2A.Z activity in hNuA4 and EP400NL

Detection of FLAG-H2A.Z incorporation into the chromatin substrate by immunoblotting. The reactions were resolved by SDS-PAGE and H2A.Z deposition was analyzed by anti-FLAG immunoblot. Examination of the hNuA4 complex (top panel) and EP400NL complex (bottom panel) associated enzymatic activity. hNuA4 com.: hNuA4 complex; EP400NL com.: EP400NL complex.

Since EP400 is an ATPase within the hNuA4 complex and displays the H2A.Z deposition activity through ATP consumption (Mizuguchi et al., 2004a, Xu et al., 2012), further investigation was conducted to determine whether the EP400NL complex catalyses the H2A.Z deposition in an ATP-dependent manner. As a positive control, the hNuA4 complex was purified from HeLa nuclear extract using FLAG-tagged TIP60, and the presence of each core protein (RuvBL1, RuvBL2, BRG1, and BAF53) was confirmed by immunoblotting (Figure 4. 14). Consistent with the mass spectrometry data, the hNuA4 and EP400NL complexes share multiple common protein subunits, however, BRG1 was only present in the EP400NL complex, not the hNuA4 complex (Figure 4. 14, anti-BRG1).

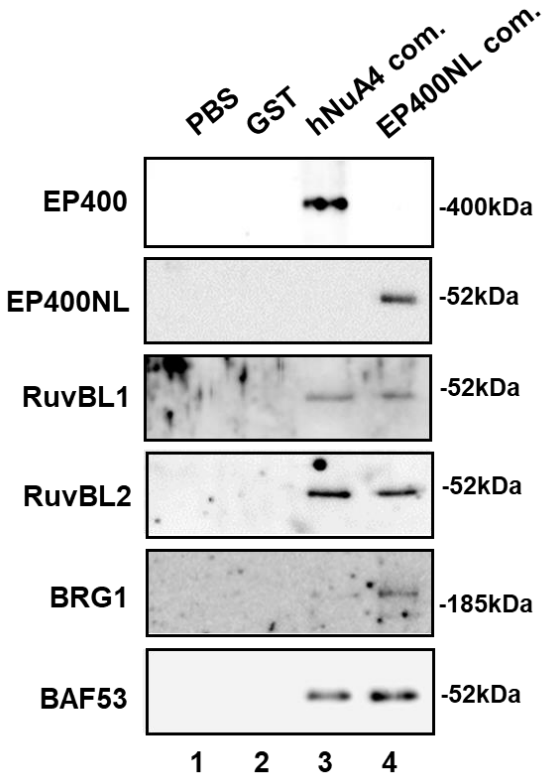

Figure 4. 14 Identification of protein candidates from the hNuA4 and EP400NL complexes

Protein preparation used in the H2A.Z deposition assay was analyzed by immunoblots for the core components of the protein complexes including EP400, EP400NL, RuvBL1, RuvBL2, BRG1, and BAF53. Negative controls in lane 1 and lane 2 were supplemented with PBS and GST respectively. hNuA4 com.: hNuA4 complex; EP400NL com.: EP400NL complex.

The H2A.Z deposition assay was repeated with the EP400NL complex in the presence and absence of ATP. As expected, the hNuA4 complex catalysed the deposition of H2A.Z, with the highest incorporation of FLAG-H2A.Z. The presence of the EP400NL complex, which contains the ATPases BRG1, RuvBL2, and RuvBL1, also increased FLAG-H2A.Z deposition activity (Figure 4. 15), as did the hNuA4 complex in the presence of ATP (Figure 4. 15). In the presence of Apyrase (1 U), which degrades residual ATP that might still have been associated with the purified enzymatic protein complexes, H2A.Z deposition was no different from controls (Figure 4. 15). Thus, these results collectively show that the EP400NL complex catalyses H2A.Z deposition in an ATP-dependent manner.

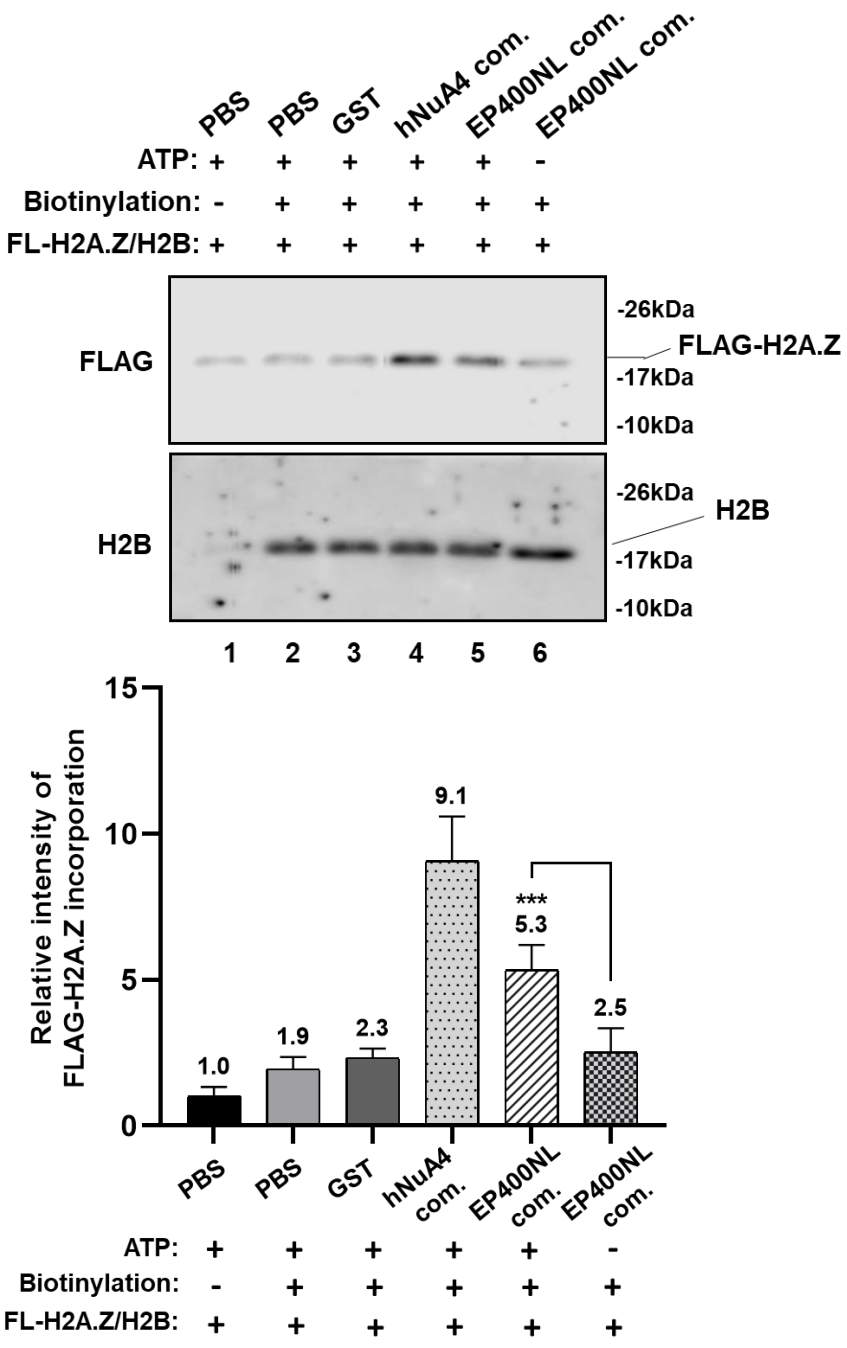

Figure 4. 15 Examination of an ATP-dependent H2A.Z deposition activity in EP400NL complex

Detection of FLAG-H2A.Z incorporation into the chromatin substrate by immunoblotting (top panel). The reactions were resolved by SDS-PAGE and H2A.Z deposition activities were analyzed by anti-FLAG immunoblot (immunoblots). The relative intensity of FLAG-H2A.Z was initially normalized by the H2B signals and the normalized value from the negative control (PBS and non-biotinylated chromatin) was set to one and the relative activities from other samples were plotted (bar graph) (bottom panel) [Ordinary one-way ANOVA, $F_{(3,24)} = 65.75$, $p < 0.0001$; post-hoc Tukey's HSD, $***p < 0.001$]. hNuA4 com.: hNuA4 complex; EP400NL com.: EP400NL complex

4. 3 Discussion

Previous studies have shown that chromatin remodelling complexes with either HAT or histone variant deposition activity are critical for cellular functions such as the regulation of gene transcription, differentiation, and proliferation (Frank et al., 2003, Mizuguchi et al., 2004b, Saha et al., 2006, Wong et al., 2007, Mattera et al., 2009, Yamada, 2012, Pradhan et al., 2016b, El Hadidy and Uversky, 2019). One of the key components of these complexes is the ATPase subunits that serve as energy providers for these cellular functions. Given the importance of understanding how these specific biological traits are orchestrated, exploring and understanding these functional protein complexes is essential. EP400NL appears to form a nuclear complex like the TIP60-deficient EP400 complex but also contains the BRG1 ATPase. The association of multiple identified ATPases such as BRG1, RuvBL1, and RuvBL2 with the EP400NL complex may be critical for conferring the regulatory functions of EP400NL.

The hNuA4 complex not only exhibits HAT activity but also catalyses histone acetylation induced H2A.Z deposition (Mizuguchi et al., 2004a, Altaf et al., 2010, Ranjan et al., 2013, Giaimo et al., 2019). Specifically, the acetylated histone tails can stimulate and enhance the H2A.Z exchange by a cooperative action of RuvBL1 and RuvBL2 via their ATPase activities (Puri et al., 2007, Choi et al., 2009).

HATs play key roles in the epigenetic modulation of gene transcription by modifying histone proteins. TIP60 is the enzymatic subunit of the hNuA4 HAT complex, even though no specific peptides of TIP60 were detected from the EP400NL containing complex, the detection of multiple subunits that are shared by both the hNuA4 and the EP400NL containing complexes prompted an investigation into whether the EP400NL-containing complex also displays some levels of HAT activity. However, no HAT activity was detected.

This was consistent with the lack of identification of HAT(s) in the mass spectrometric analysis (Chapter 3. 3), The EP400NL complex did however exhibit ATP dependent H2A.Z deposition activity. This was a lower exchange efficiency only about 58% compared to the hNuA4 complex, but it was significantly higher compared to the reactions either with the addition of GST or PBS, which serve as two negative controls with a background expression level of incorporated FLAG-H2A.Z. Mechanistically, the acetylated histone tails are recognized by bromodomain-containing proteins and the bromodomain-containing hNuA4 complex is recruited to stimulate H2A.Z deposition by acetylation of H4 and H2A histone tails within the nucleosome (Choi et al., 2009, Altaf et al., 2010, Ranjan et al., 2013). Since the synthetic chromatin in the H2A.Z deposition assay was prepared using recombinant core histones expressed in *Escherichia coli* lacking acetylation, it will be interesting to test if acetylated H2A or H4 would further increase the EP400NL complex-mediated H2A.Z deposition activity. In brief, acetylation of histones is critical for the enhancement of the activity but may not necessarily be the prerequisite in the EP400NL mediated H2A.Z deposition, the investigation of EP400NL associated complex(es) remains superficial and further exploration needs to be carried out to piece together the jigsaw puzzle of the EP400NL associated chromatin remodelling mechanisms.

In this chapter, a partially purified EP400NL complex exhibited H2A.Z deposition activity using chromatin assemblies *in vitro,* to further confirm the viability of these results, *in vivo* experiments using cell cultures would be one of the most straightforward methods to tackle this problem. The established EP400NL cells can be transiently transfected with FLAG-H2A.Z when an EP400NL targeted gene is transcriptionally active. Subsequently, the detection of FLAG-H2A.Z enrichment by ChIP analysis which can specifically detect the recruitment of H2A.Z would reveal if the H2A.Z deposition activity of the EP400NL complex can be achieved.

Since EP400 and EP400NL complexes are of similar composition, it seems feasible to predict that EP400 and EP400NL may be interchangeable in some specific circumstances of the chromatin remodelling process in the cell nucleus but need to be further confirmed in the future.

The bromodomain-containing BRD8 and BRG1 of the EP400NL complex can be recruited by a DNA-binding transcription factor and the interaction would be significantly enhanced by acetylated chromatin. Interestingly, the BRG1-containing BAF complex is known to play a role in H2A.Z deposition in embryonic stem cells but little is understood about its molecular mechanism (Hainer and Fazzio, 2015). It is tempting to speculate that the EP400NL complex is a carrier of BRG1 in certain genomic regions of H2A.Z deposition activity, however, the connection between BRG1 and EP400NL complex-mediated H2A.Z deposition and the coactivator function remains to be further elucidated.

5. Characterisation of the role of EP400NL in transcriptional regulation

5. 1 Functional analysis of EP400NL in Myc-mediated transcriptional regulation

Following the demonstration that EP400NL is associated with transcriptional regulators, the role of EP400NL as a transcriptional coactivator was investigated. As EP400 is a known coactivator of Myc-targeted gene expression (Zhao et al., 2017), it was first investigated as to whether EP400NL is also a coactivator of Myc.

5. 1. 1 Model for investigating the transcriptional regulatory activity of EP400NL

To examine whether EP400NL induces gene expression in a Myc-dependent manner, a luciferase reporter system was developed using 293TGAL4-Luciferase cells (Figure 5. 1). This cell line contains a GAL4 DNA binding site upstream of the firefly luciferase reporter gene. The GAL4 DNA binding domain fused to a transcriptional activator such as Myc can induce transcription of luciferase, and the transcriptional activity can be further enhanced by the addition of multiple co-activators (Figure 5. 1).

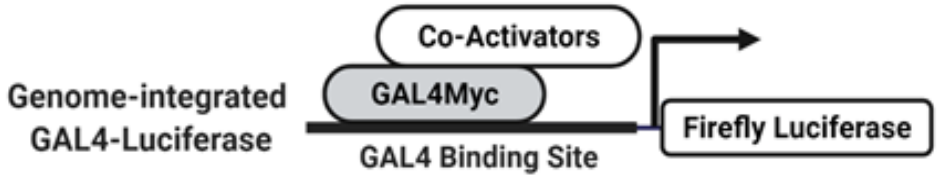

Figure 5. 1 Model of GAL4Myc luciferase system

GAL4Myc binds to the GAL4 DNA binding site to induce the expression of the luciferase gene. The expression of additional co-activators can further enhance luciferase expression.

5. 1. 2 EP400NL upregulates Myc-mediated gene expression

Activation of luciferase expression by GAL4Myc was quantitatively assessed in the presence of EP400NL in 293TGAL4-Luciferase cells. As a control, previously known coactivators of the hNuA4 complex (TRRAP, EP400, and their defective

mutants) were included to compare to EP400NL. These coactivators were transiently expressed in 293TGAL4-Luciferase cells and the ectopic expression was confirmed by immunoblot to detect their FLAG tags (Figure 5. 2).

Consistent with the coactivator role of TRRAP and EP400 (McMahon et al., 1998, Nikiforov et al., 2002, Liu et al., 2003), TRRAP stimulated luciferase expression up to two-fold, whereas a C-terminal deletion mutant of TRAAP failed to promote similar gene activation. EP400 also significantly induced luciferase expression, whereas the ATPase-deficient EP400 did not. EP400NL induced reporter activity up to 2.2-fold, indicating that EP400NL activates transcription at a level comparable to that of TRRAP (Figure 5. 3).

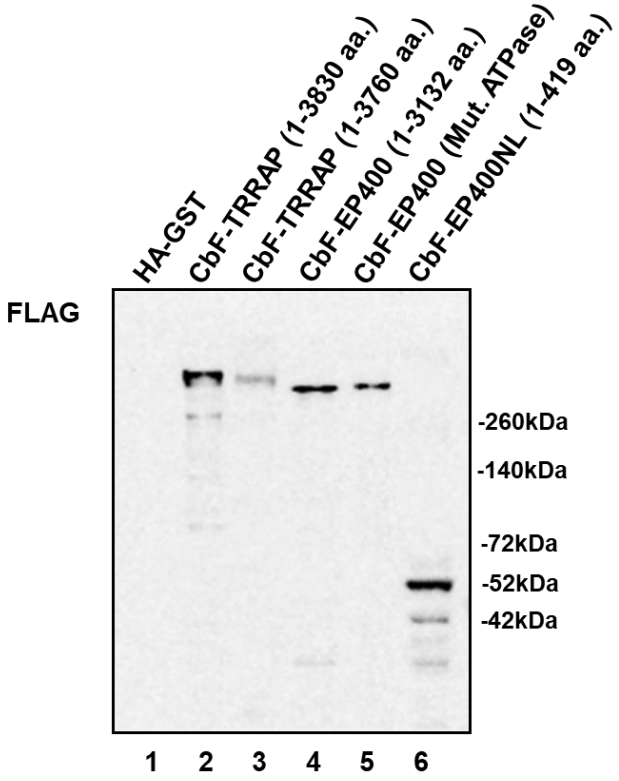

Figure 5. 2 Confirmation of the ectopic expression of the FLAG-tagged coactivators

Plasmids encoding FLAG-tagged full-length TRRAP (1-3830 aa.), full-length EP400 (1-3132) and their defective mutants TRRAP (1-3760 aa.) and ATPase defective EP400 and EP400NL were transfected into 293TGAL4-Luciferase cells, then lysates were subjected to SDS-PAGE and immunoblotting with anti-FLAG to confirm expression. HA-GST serves as a negative control. The expected size of TRRAP (1-3830 aa.), full-length EP400 (1-3132), TRRAP (1-3760 aa.), ATPase defective EP400 and EP400NL are approximately 440kDa, 430kDa, 400kDa, 400kDa, 52kDa respectively.

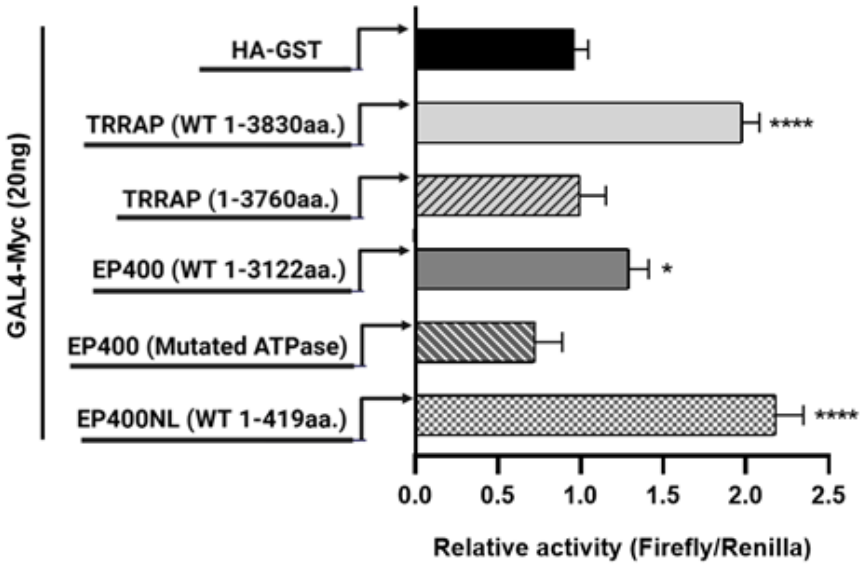

Figure 5. 3 Assessment of co-activator activity of EP400NL in comparison to known coactivators of Myc.

293TGAL4-Luciferase cells were transfected with each construct expressing either HA-GST (control), wild type TRRAP (1-3830aa.), TRRAP C-terminal deletion mutant (1-3760aa.), wild type EP400 (1-3122aa.), ATPase mutated EP400, and wild type EP400NL (1-419aa.) together with a plasmid expressing GAL4Myc, respectively. After normalisation to renilla luciferase activity, firefly luciferase activity of the control (HA-GST) was set to one and the relative values for other samples were calculated [One-way ANOVA, $F_{(5,12)} = 55.96$, $p < 0.0001$; Dunnett's post-hoc test, $^{*}p < 0.05$, $^{****}p < 0.0001$].

To examine whether EP400NL serves as a bona fide co-activator of Myc, luciferase expression was examined in the presence of increasing amounts of EP400NL in 293TGal4-Luciferase cells (Figure 5. 4, top panel). In the presence of the same amount of GAL4Myc, there was a dose-dependent increase in luciferase expression of up to three-fold upon increased EP400NL level (Figure 5. 4, bottom panel).

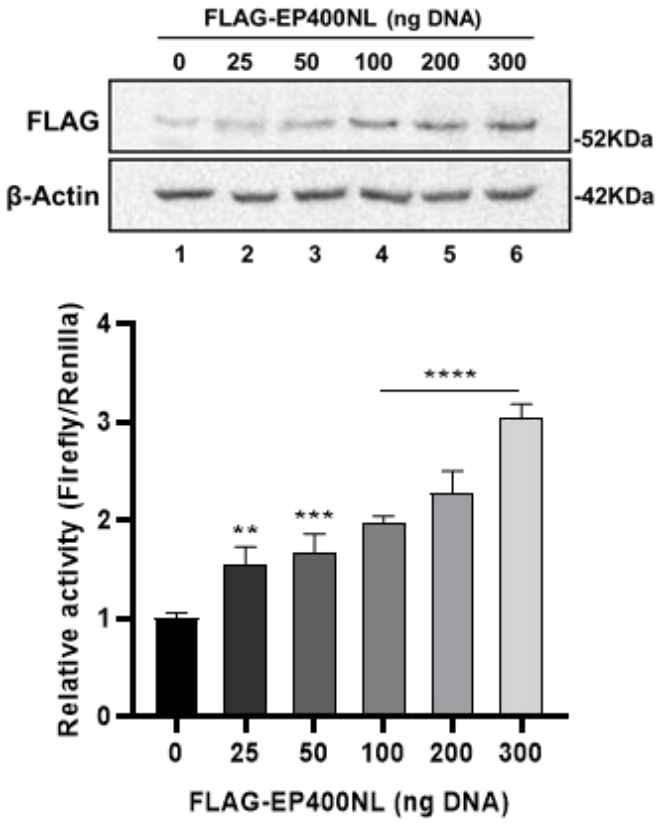

Figure 5. 4 Titration of EP400NL expression

Transient transfection of FLAG-EP400NL (0 ng, 25 ng, 50 ng, 100 ng, 200 ng, 300 ng) into 293TGAL4-Luciferase cells followed by the dual-luciferase reporter assay [One-way ANOVA, $F(5,12) = 61.11$, $p < 0.0001$; Dunnett's post-hoc test, $^{**}p < 0.01$, $^{***}p < 0.001$, $^{****}p < 0.0001$]. Protein expression of EP400NL was confirmed by anti-FLAG immunoblot (top panel) and the relative luciferase activity was plotted against the amount of DNA used in the transfection (bottom panel).

5. 1. 3 EP400NL can be recruited in a Myc-dependent manner

The previous experiment showed that EP400NL acts as a transcriptional co-activator of Myc-dependent transcription. To confirm the recruitment of EP400NL to the promoter, chromatin immunoprecipitation (ChIP-qPCR) was performed. In this experimental model, FLAG-GAL4Myc and TAP-EP400NL were transiently co-expressed in 293TGal4-Luciferase cells followed by immunoprecipitation using anti-FLAG and anti-CBP antibodies. When both FLAG-GAL4Myc and TAP-EP400NL are expressed, FLAG-GAL4Myc binds to the DBS (DNA Binding Site) and recruits its corresponding co-activators (Figure

5. 5, top panel). 293TGal4-Luciferase cells co-expressing HA-GST and TAP-EP400NL serve as the negative control with no specific DNA binding at the promoter region (Figure 5. 5, bottom panel). Chromatin that interacts with either FLAG-GAL4Myc or TAP-EP400NL was precipitated and served as DNA templates in the ChIP-qPCR analysis. The primers were designed to amplify the GAL4 binding site within the promoter region of the Firefly luciferase.

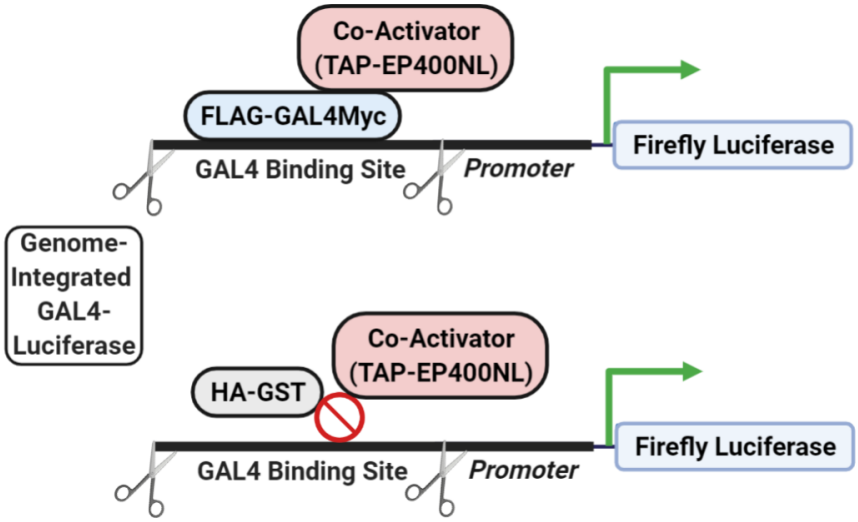

Figure 5. 5 ChIP for demonstrating Myc dependent EP400NL recruitment

GAL4Myc binds to the GAL4 DNA binding site upstream of luciferase and recruits its co-activator EP400NL to activate downstream gene expression (Top panel). HA-GST does not bind, thus EP400NL is not recruited (bottom panel). DNA shearing by sonication is indicated as scissors. TAP-EP400NL can be recruited only when GAL4Myc binding occurs and the enrichment of both FLAG-GAL4Myc and TAP-EP400NL bound chromatin can then be detected by ChIP after sonication.

Before demonstrating an activator-dependent recruitment of EP400NL on target genes, the transiently expressed FLAG-GAL4Myc and TAP-EP400NL need to be initially examined. Expression of TAP-EP400NL, FLAG-GAL4Myc, and endogenous EP400NL was confirmed by immunoblot analysis (Figure 5. 6). ChIP was then performed on chromatin isolated from 293TGAL4-Luciferase cells in the presence or absence of ectopic FLAG-GAL4Myc and TAP-tagged EP400NL.

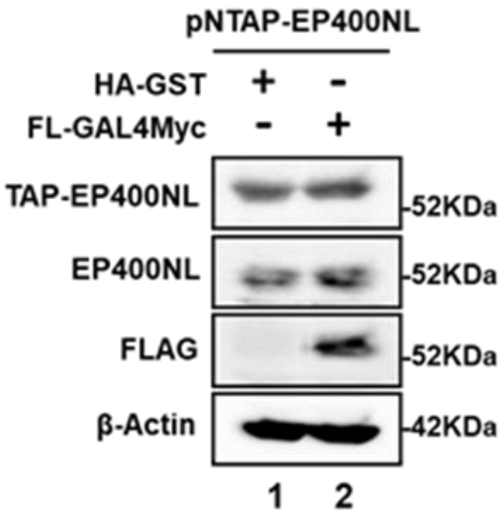

Figure 5. 6 Confirmation of protein expression for ChIP assay

293TGAL4-Luciferase cells were co-transfected with plasmids expressing either HA-GST (control) or FLAG-GAL4Myc together with TAP-EP400NL respectively. Protein expression was confirmed by immunoblotting. TAP-EP400NL was detected by an anti-CBP antibody, the transient expression of FLAG-GAL4Myc was detected by an anti-FLAG antibody.

As TAP-EP400NL is CBP tagged, an anti-CBP antibody was used to immunoprecipitates chromatin bound to TAP-EP400NL and qPCR was conducted with primers designed to the GAL4 binding site to determine whether EP400NL was enriched at the promoter in a Myc-dependent manner. There was minimal TAP-EP400NL at the GAL4 binding site in the absence of GAL4Myc, however, recruitment was increased by approximately 8-fold in the presence of GAL4Myc (Figures 5. 7, left and middle panels, GAL4-DBS). The distal exon region of p21, which is not expected to be bound by Myc, was used as a control to establish the specificity as neither GAL4Myc nor EP400NL were enriched in that region (Figures 5. 7, left and middle panels, p21). Non-specific binding of the IgG to the sonicated chromatin revealed no different enrichment between HA-GST and FLAG-GAL4Myc in the presence of TAP-EP400NL (Figures 5. 7, right panel). Taken together, these results suggest that EP400NL promotes reporter gene expression by the specific recruitment onto the promoter in a Myc-dependent manner.

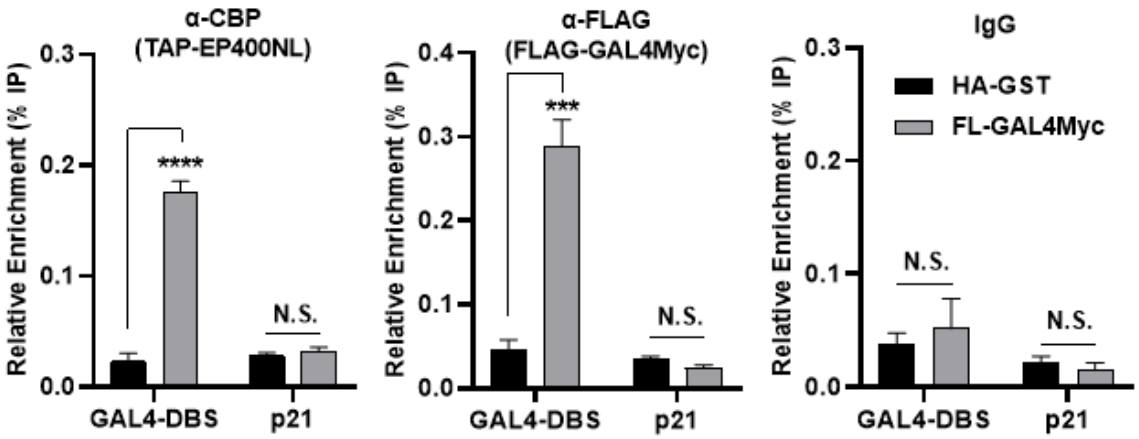

Figure 5. 7 ChIP analysis for investigating the Myc dependent recruitment of EP400NL

ChIP analyses were performed using anti-CBP for TAP-tagged EP400NL (Left panel), anti-FLAG for GAL4Myc (Middle panel), and IgG as a negative control (Right panel). The ChIP data are plotted for relative enrichment of input chromatin from each ChIP reaction over the GAL4 DNA binding site (GAL4-DBS) and p21 distal exon region (p21). [Two-way ANOVA, $F_{(1,4)} = 225.7$, $p = 0.0001$ (CBP), $F_{(1,4)} = 107.0$, $p = 0.0005$ (FLAG); Sidak's post-hoc test, $***p < 0.001$, $****p < 0.0001$].

5. 1. 4 EP400NL physically interacts with cMyc in HEK293 cells

Since EP400NL is recruited by Myc and enhances Myc-dependent transcription in a dose-dependent manner. This suggests that EP400NL may physically interact with Myc, therefore, pull-down assays were performed to test if this was the case. The expression of cMyc is induced by growth factors and studies have shown that the cMyc gene exhibits serum-responsive activity which endogenous Myc expression is increased under conditions of high serum (Dean et al., 1986, Richman and Hayday, 1989b, Schmidt, 1999). Therefore, the stably TAP-EP400NL expressing Flp-In™ T-REx™ cells was induced with tetracycline in high serum condition. After the tetracycline induction and serum stimulation, TAP-EP400NL was isolated by streptavidin beads and successful pulldown was confirmed via immunoblotting with anti-EP400NL and anti-CBP antibodies (Figure 5. 8). Myc was also detected in the precipitates containing EP400NL, confirming that these two proteins interact under physiological conditions.

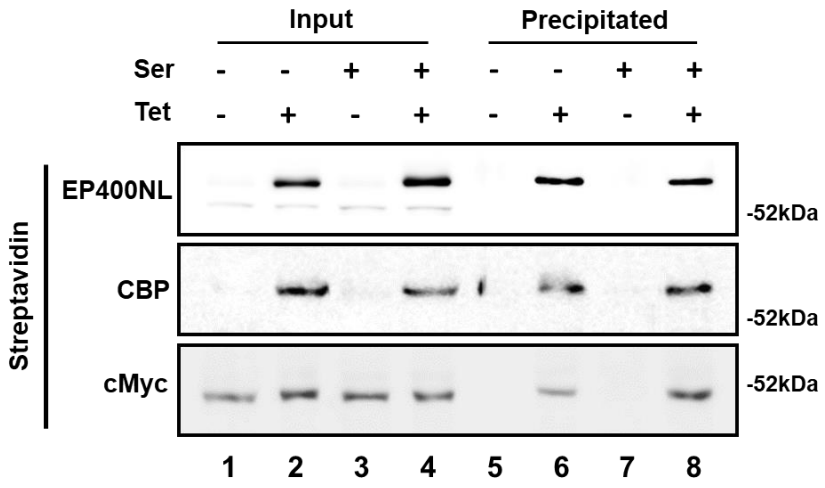

Figure 5. 8 Interaction between EP400NL and cMyc

EP400NL protein complexes were precipitated by streptavidin beads followed by immunoblotting with anti-EP400NL and anti-CBP to confirm successful pulldown. The co-precipitation of cMyc was evaluated by the anti-cMyc immunoblot

5. 2 Functional analyses of EP400NL in GAL4Myc-mediated transcriptional regulation

The results from previous section have shown the coactivator function of EP400NL in Myc-mediated transcription followed by the confirmation of their physical interaction by pull-down assay. Thus, it is of interest to investigate the specific function domain(s) of EP400NL and how these domains are involved with its transcriptional activity.

Furthermore, since Myc is a global transcription factor that regulates growth and cell cycle entry by its ability to induce expression of genes required for these processes (Cole and McMahon, 1999, Schmidt, 1999, Gallant, 2005), cell proliferation assay and cell cycle analysis were subsequently carried out to test if EP400NL plays any role in facilitating the Myc mediated transcriptional network.

5. 2. 1 Identification of the functional domains of EP400NL

Given the detection of three candidates (BAF53, BRD8, and BRG1) that are in complex with EP400NL in the previous mass spectrometric analysis, the interaction between BRD8, BAF53, BRG1, and EP400NL was investigated. BRD8 displayed a variety of nuclear activities and was identified in multiple chromatin remodelling complexes such as the hNuA4 complex. Interestingly BRG1 was revealed as a unique ATPase within many chromatin-modifying complexes but has not been found in the hNuA4 complex (Yamada, 2012, Xu et al., 2016). No specific functional domains within EP400NL have been identified to date, however, the bioinformatic prediction tool InterPro, an integrated database of protein families, domains, and functional sites, predicts seven potential functional regions within EP400NL (Figure 5. 9, white boxes). BAF53, BRD8, and BRG1 have been shown to play key roles in multiple nuclear activities including transcriptional regulation and DNA damage repair, and are also associated with multiple chromatin remodelling complexes (Park et al., 2002, Trotter and Archer, 2008, Yamada, 2012, Chiu et al., 2017, Wu et al., 2017) To investigate the importance of these regions in the interactions with BAF53, BRD8, and BRG1, full-length EP400NL and four FLAG-tagged deletion mutants of EP400NL (Δ1-50, Δ141-156, Δ246-260, Δ360-419) were designed (QIAGEN) and transiently expressed in HEK293T cells (Figure 5. 10).

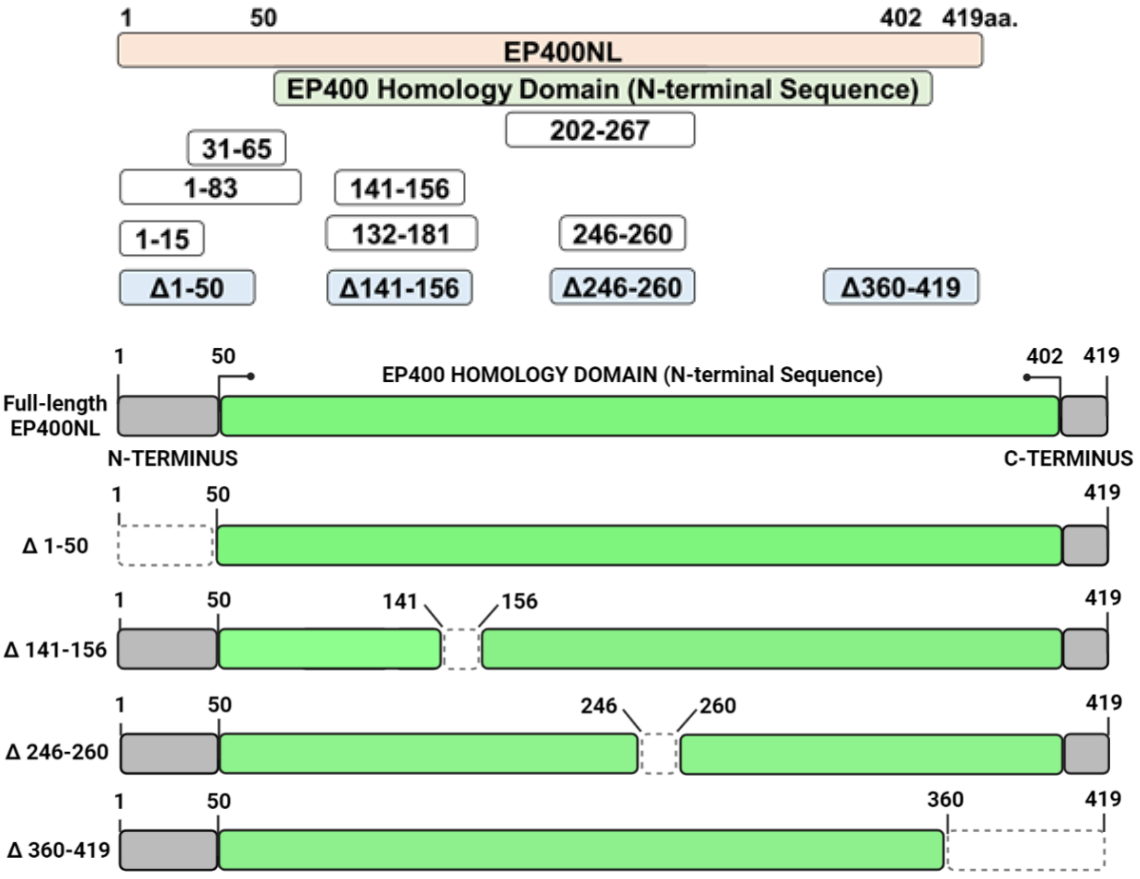

Figure 5. 9 InterPro prediction of potential regions of functional importance in EP400NL

(Top panel) orange box represents the full-length E400NL (1-419aa.), green box represents the EP400 homology domain (50-402aa.), white boxes represent the seven predicted functional sites by the bioinformatic tool (InterPro, not to scale). The regions of EP400NL (Δ1-50, Δ141-156, Δ246-260, and Δ360-419) that were selected for the generation of mutants are shown in blue boxes. (Bottom panel) four constructs of EP400NL deletion mutants (Δ1-50, Δ141-156, Δ246-260, and Δ360-419) were generated based on the InterPro prediction.

Full-length EP400NL and its mutants were cloned into mammalian expression CbF vectors. The CbF backbone was used to express FLAG-tagged proteins (10. APPENDIX 2), thus, plasmids expressing full-length EP400NL, and its deletion mutants were transiently transfected into HEK293T cells, and their expression was confirmed via anti-FLAG immunoblot (Figure 5. 10, Input panel). All four deletion mutants were expressed at a higher level than wild-type EP400NL (Figure 5. 10, anti-FLAG immunoblot).

To determine whether the mutants display altered binding to BAF53, BRD8 or BRG1, which were identified as binding partners of EP400NL via mass spectrometry (Chapter 3. 3), anti-FLAG immunoprecipitation was carried out. All mutants retained the ability to interact BAF53, BRD8, and BRG1. Despite higher levels of mutants were immunoprecipitated with FLAG, they all display a relatively lower interaction with BAF53 compared to the full-length EP400NL (1-419aa.) in which Δ246-260 and Δ360-419 showed a much weaker interaction (Figure 5. 10).

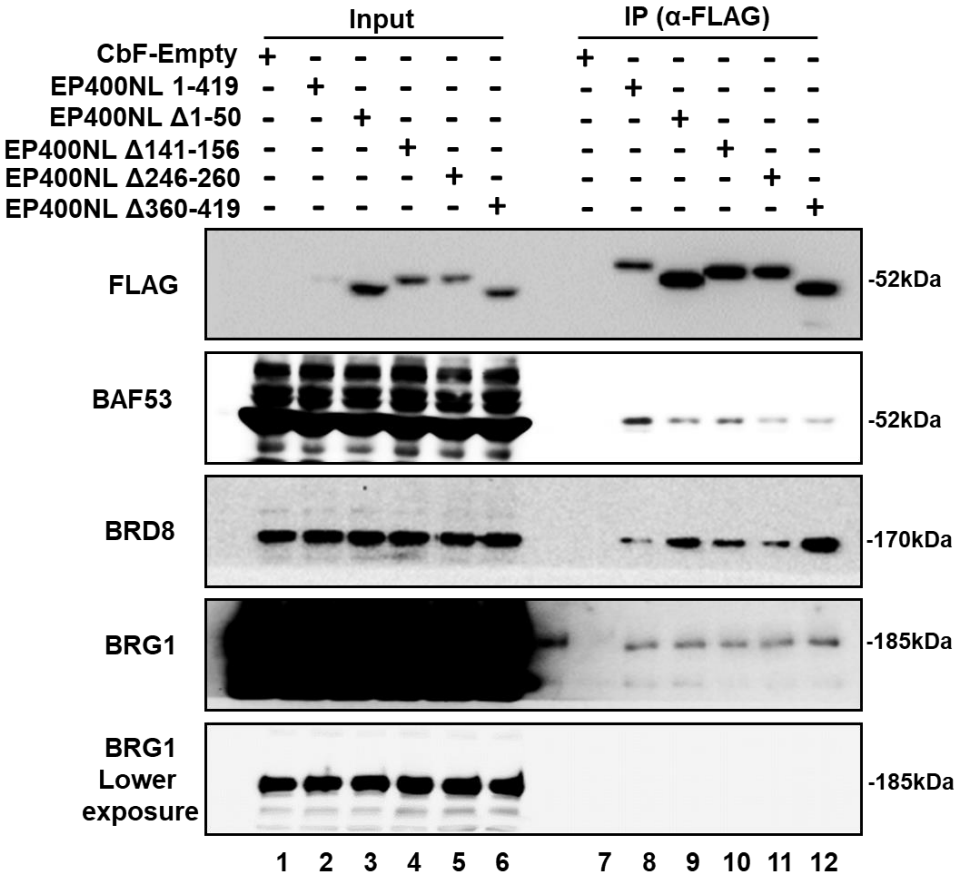

Figure 5. 10 Co-immunoprecipitates of BAF53, BRD8 and BRG1 with wild-type and mutant EP400NL

Co-immunoprecipitation assays of wild type EP400NL and deletion mutants. HEK293T cells were transiently transfected with plasmids expressing FLAG-tagged full length and mutant EP400NL, followed by immunoprecipitation with the anti-FLAG antibody. The co-precipitation of BAF53, BRD8, and BRG1 was examined via immunoblotting with their respective antibodies. Empty vector serves as a negative control. IP, Immunoprecipitation.

5. 2. 2 Investigate the alteration of transcriptional regulation using EP400NL deletion mutants

To examine whether the mutants also retained transcriptional coactivator activity, they were tested for their ability to co-activate GAL4Myc-mediated luciferase reporter expression. The deletion mutants and full-length EP400NL (419aa.) were each co-transfected with FLAG-GAL4Myc and pRenilla-CMV vector followed by luciferase assay. The expression of each construct was confirmed by an anti-FLAG immunoblot (Figure 5. 11). The deletion of either aa246-260 or aa360-419 resulted in the loss of coactivator activity compared to full-length EP400NL, however, the deletion of aa1-50 resulted in a significant enhancement of luciferase activity over full-length EP400NL and other mutants (Figure 5. 12).

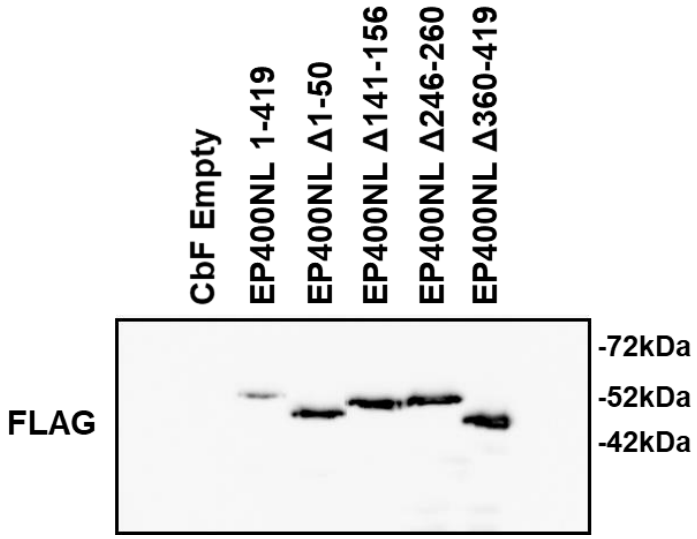

Figure 5. 11 Confirmation of expression of full-length and mutant EP400NL

Transient transfection of full-length EP400NL (1-419aa.) and the four deletion mutants (Δ1-50, Δ141-156, Δ246-260, and Δ360-419) into HEK293TGal4-Luciferase cells, followed by luciferase assay. Transient expression of the FLAG-tagged EP400NL and its deletion mutants was confirmed by anti-FLAG immunoblot.

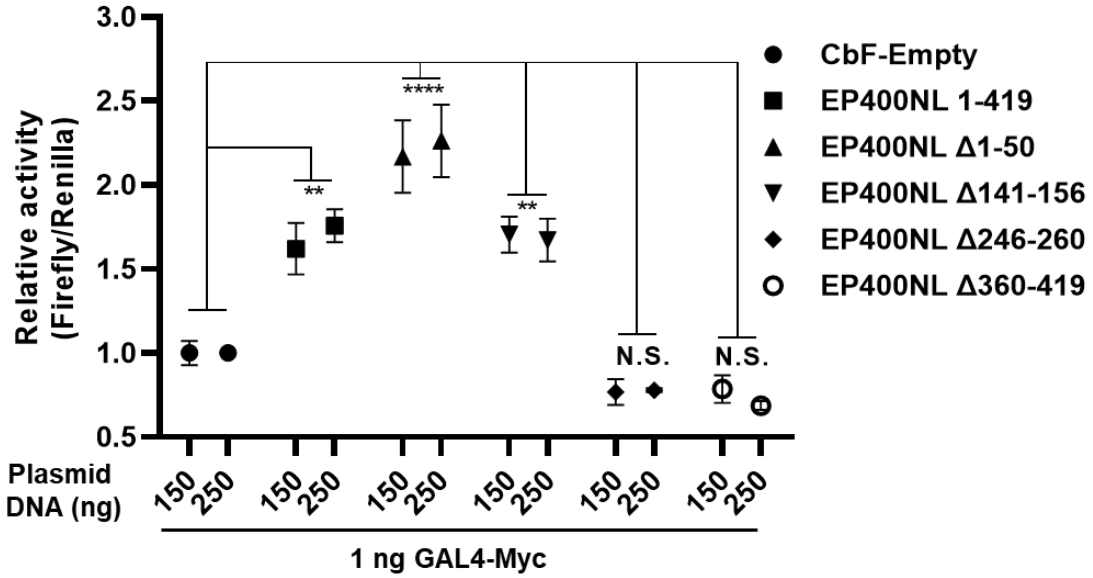

Figure 5. 12 Examine the EP400NL deletion mutants in transcriptional regulation

Firefly luciferase reporter assays in 293TGal4-Luciferase cells. The cells were transfected with either 150 ng or 250 ng of plasmid DNA encoding either wild-type EP400NL or the deletion mutants together with 1 ng of Gal4Myc expression plasmid. After normalisation to renilla luciferase activity, the firefly luciferase activity from the control cells (GAL4Myc expression + CbF empty vector) set to 1 and the relative values of other samples are calculated [Two-way ANOVA, $F_{(5,24)} = 50.28$, $p < 0.0001$; post-hoc Tukey's HSD, $^{**}p < 0.01$, $^{****}p < 0.0001$].

To further confirm the loss of coactivator function of the Δ246-260, and Δ360-419, plasmid DNA encoding either full-length EP400NL or the deletion mutants was titrated to examine a possible dominant-negative effect as they could be impairing endogenous EP400NL activity. As observed in the previous experiment, both the deletion mutants failed to enhance GAL4-Myc activity, however as the amount of plasmid DNA transfected increased, the level of activity did not decrease below the basal level of GAL4Myc-mediated gene expression (Figure 5. 13), thus they do not appear to be acting in a dominant-negative manner. Taken together, these data show that regions within amino acids 246-260 and 360-419 of EP400NL are essential for transcriptional coactivation and whether this is due to reduced interaction with BAF53 warrants further investigation.

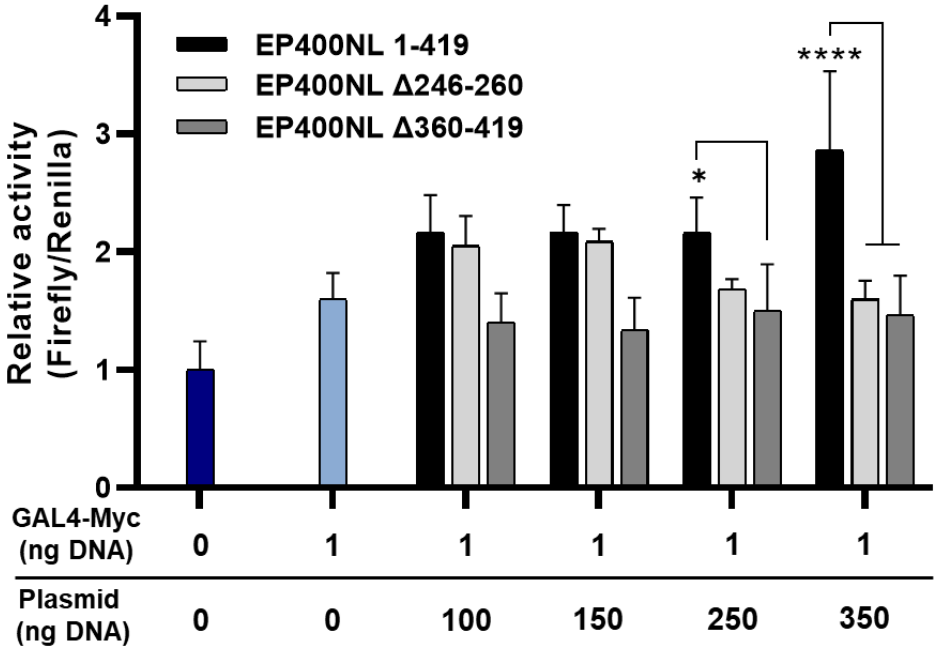

Figure 5. 13 EP400NL deletion mutants Δ246-260, Δ360-419 fail to enhance GAL4-Myc activity

HEK293 cells were transfected with increasing amounts of full length or mutant EP400NL plasmid followed by luciferase assay. After normalization to renilla luciferase, firefly luciferase activity from the control cells (dark blue) was set to 1 and the relative values for other samples are calculated [Two-way ANOVA, $F_{(2,36)} = 21.11$, $p < 0.0001$; post-hoc Tukey's HSD, $*p < 0.05$, $****p < 0.0001$].

5. 3 Investigating the role of EP400NL in cell proliferation

Myc has been depicted as a downstream effector of many signal transduction pathways including WNT, ERK/MAPK, and TGF-beta/SMAD which elicits positive or negative regulation of a series of biological functions (Leon et al., 2009, Dang, 2012, Wolpaw and Dang, 2018). In particular, Myc regulates the expression of genes that promote cell growth and proliferation. Myc induces positive cell-cycle regulators such as several cyclins, CDKs and E2F transcription factors. On the other hand, it also represses genes encoding cell-cycle inhibitors such as p15, p21, or p27 (Cowling and Cole, 2006, Vita and Henriksson, 2006, Soucek and Evan, 2010, Garcia-Gutierrez et al., 2019). Given that EP400NL is a coactivator of Myc, it was of interest to investigate whether EP400NL influences cell proliferation and cell cycle progression.

To investigate whether alteration in the expression level of EP400NL impacts cell growth, a strategy was decided upon whereby cellular proliferation would be assessed in the presence of increased expression of EP400NL via the stably inducible TAP-EP400NL expressing Flp-In™ T-REx™ cell line (as discussed in Chapter 3. 1), and reduced expression via a CRISPR/Cas9 indel mutated a non-small-cell lung carcinoma (NSCLC) cancer cell line (H1299).

5. 3. 1 Establishment of EP400NL indel mutation cell lines by CRISPR/Cas9

H1299 was utilized to establish the EP400NL indel cell lines due to its clinical and research significance in treating non-small cell lung cancer (Zhao et al., 2016). To generate indel mutated H1299 cell lines, a single guide RNA (sgRNA) was designed to specifically target the protein-coding region of EP400NL. After co-transfection of lentiviral packing plasmids and EP400NL-sgRNA-LentiCRISPR plasmids, the lentiviral medium was collected and subsequently concentrated, H1299 cells were then infected with the virus medium followed by seven days of puromycin selection. Multiple trials of cell cloning were conducted but failed to generate monoclonal EP400NL indel mutated cells as some clones became quiescent when being cultured from the cloning rings, and those that did grow expressed a similar level of EP400NL to wild type. Therefore, polyclonal EP400NL indel mutated cells were utilized after being infected with lentiviral medium and puromycin selection. Indel mutation A and Indel mutation B are two biological replicates of EP400NL polyclonal indel mutated cell lines (hereafter called EP400 indel cell lines). Two guide RNAs, Luciferase and Scramble were designed to target the coding sequence of luciferase (which is not present in these cells) and a random sequence within chromosome 10 (Hart et al., 2015) respectively and serve as negative controls.

High-Resolution Melt (HRM) was carried out to determine whether the extracted genomic DNA was altered at the EP400NL locus in the indel cell lines. Both melting peak shifts (Figure 5. 14, A) and changes in fluorescent signals were detected which confirmed the specificity of the EP400NL targeted guide RNA in

creating indels within the EP400NL coding region (Figure 5. 14, B). EP400NL protein expression was also decreased considerably compared to the mock (non-infected wild type H1299) and two negative controls (gRNA-luciferase and gRNA-scrambled random sequence) (Figure 5. 14, C). These results confirm that two CRISPR/Cas9 based EP400NL polyclonal indel cell lines were successfully established.

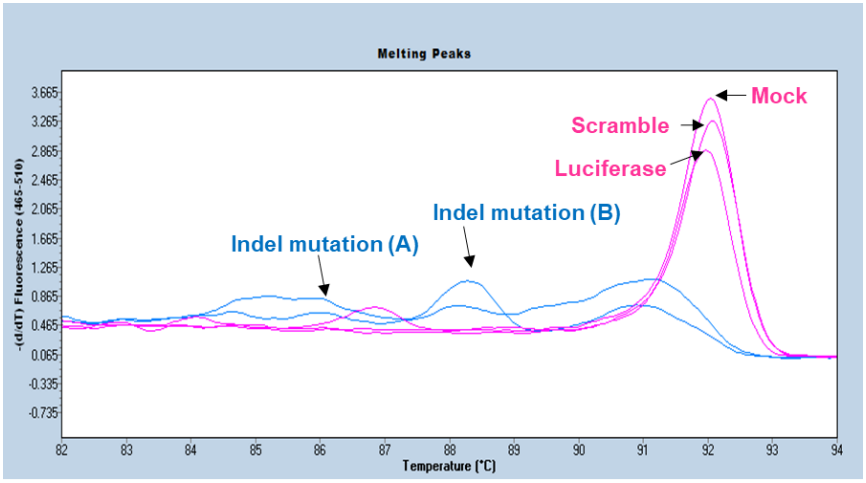

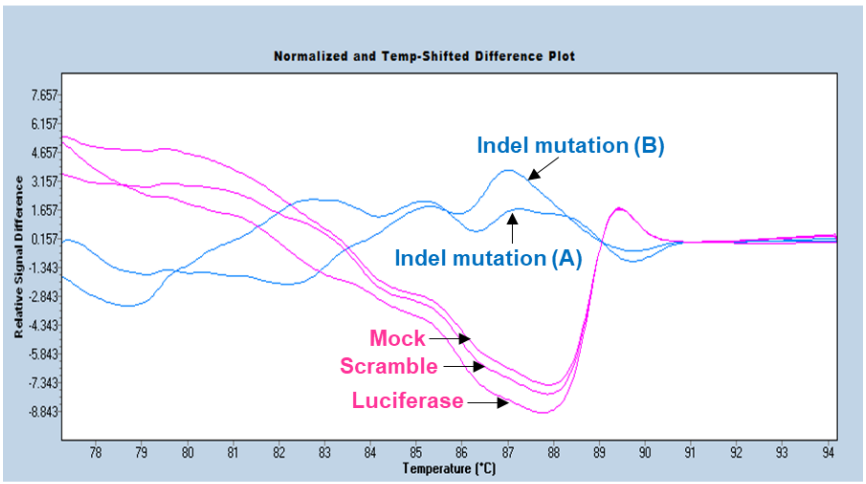

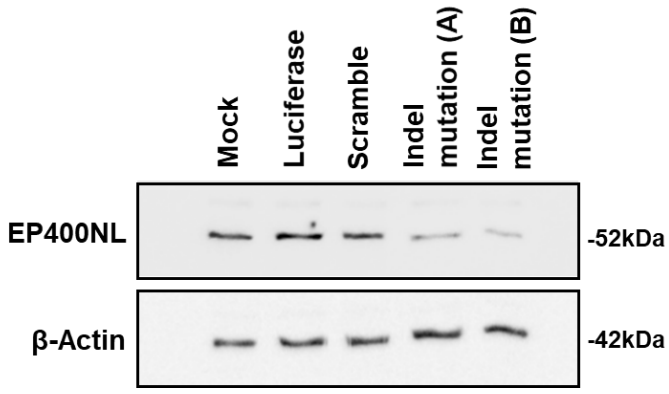

Figure 5. 14 CRISPR/Cas9 mediated EP400NL indel mutation

(Top panel) EP400NL indel mutation confirmed by HRM. Melting peak shifts were identified from the two EP400NL indel cell lines (Indel mutation A, Indel mutation B) compared to the three control cell lines which are Mock, Luciferase, and Scramble respectively. (Middle panel) Normalized and Temp-shifted difference plot of the three control cell lines and the two-biological replicated EP400NL indels cell lines. Mock, Wild type H1299; Luciferase, gRNA-luciferase; Scramble, gRNA-scrambled random sequence; Indel mutation A, gRNA-EP400NL-A; Indel mutation B, gRNA-EP400NL-B. (Bottom panel) Analysis of EP400NL protein levels among the three controls and two EP400NL polyclonal indel cell lines.

5. 3. 2 EP400NL influences cell proliferation

To identify if EP400NL influences cell proliferation, the EP400NL indel cell line and the established EP400NL inducible cell line were utilized in the presence and absence of serum. The established EP400NL cell line was simultaneously induced by tetracycline for overexpressing TAP-EP400NL.

Serum-starved cells exhibited no apparent differences regardless of tetracycline induction, however, the serum-stimulated EP400NL inducible cells proliferated significantly faster than the serum-starved cells. Interestingly, the proliferation rate further increased when serum-stimulated cells were treated with tetracycline (Figure 5. 15, left panel), indicating that induction of EP400NL expression increases proliferation.

Conversely, a significantly decreased proliferation rate was observed in the two EP400NL indel cell lines compared to the mock (wild type H1299) and negative control cell lines (luciferase and scramble) as the incubation extended to 108 hours. (Figure 5. 15, right panel).

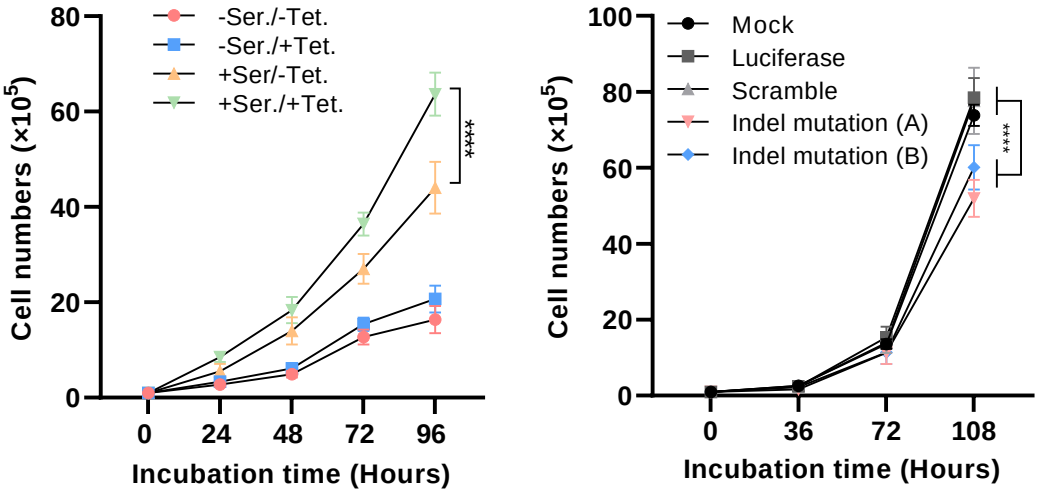

Figure 5. 15 Cell proliferation assay

Cell proliferation analysis using Flp-In™ T-REx™ cells. Flp-In™ T-REx™ cells were treated with a combination of ±serum and ±tetracycline (left panel). Cell proliferation analysis using H1299 (right panel). Two EP400NL indel cell lines (Indel mutation A and B) were compared to the three control cell lines (Mock, Luciferase, Scramble.) under serum stimulation. [Two-way ANOVA, $F_{(12,\ 40)} = 42.09$, $p < 0.0001$ (left panel). $F_{(12,80)} = 15.49$, $p < 0.0001$ (right panel); post-hoc Tukey's HSD, $^{****}p < 0.0001$]. Mock, Wild type H1299; Luciferase, gRNA-luciferase; Scramble, gRNA-scrambled random sequence; Indel mutation (A), gRNA-EP400NL-A; Indel mutation (B), gRNA-EP400NL-B.

Next, cell cycle profile was analysed using flow cytometry. Cells were harvested and fixed with 100% ethanol, after DNA staining with propidium iodide, flow cytometry was utilized to detect level of peaks that indicative of the DNA content. In order to exclude multiplets form the population, cells were first separated digitally by using forward/side scatters as forward scatter indicates cell size whereas side scatter relates to the complexity of the cells. These results were further analysed based on an area-width discrimination method established previously in the lab to eliminate the potential multiplets. Next, single cells were gated after doublets/multiplets discrimination in flow cytometry for the following up cell cycle analysis (13. APPENDIX 5). Similar patterns as the cell proliferation assay were confirmed from the DNA content analysis which gated single cells in the G2/M cell cycle displayed the highest ratio when TAP-EP400NL was induced

with tetracycline (Figure 5. 16, top panel), and the lowest ratio in the indel cell lines (Figure 5. 16, bottom panel). The absolute cell numbers per sample counted vary in the flow cytometry, however, using the same gating strategy to compare the cell population from different samples under normalization mode can resolve this issue. The number of recorded events showing as the specific graph formatting 'Normalized to Mode' allows unification of total cell numbers and visualisation of differences in relative percentages of cell populations of interest (G2/M).

In summary, the results from the TAP-EP400NL inducible Flp-In™ T-REx™ cells showed a faster growth to the highest cell population under both serum stimulation and tetracycline induction (Figure 5. 16, top panel). On the other hand, the polyclonal EP400NL indel mutation cells exhibited the lowest cell population compared to the other control cell lines (Figure 5. 16, bottom panel), which are correspond to the cell proliferation pattern. Collectively, these data suggest that EP400NL regulates cell proliferation in a serum-responsive manner.

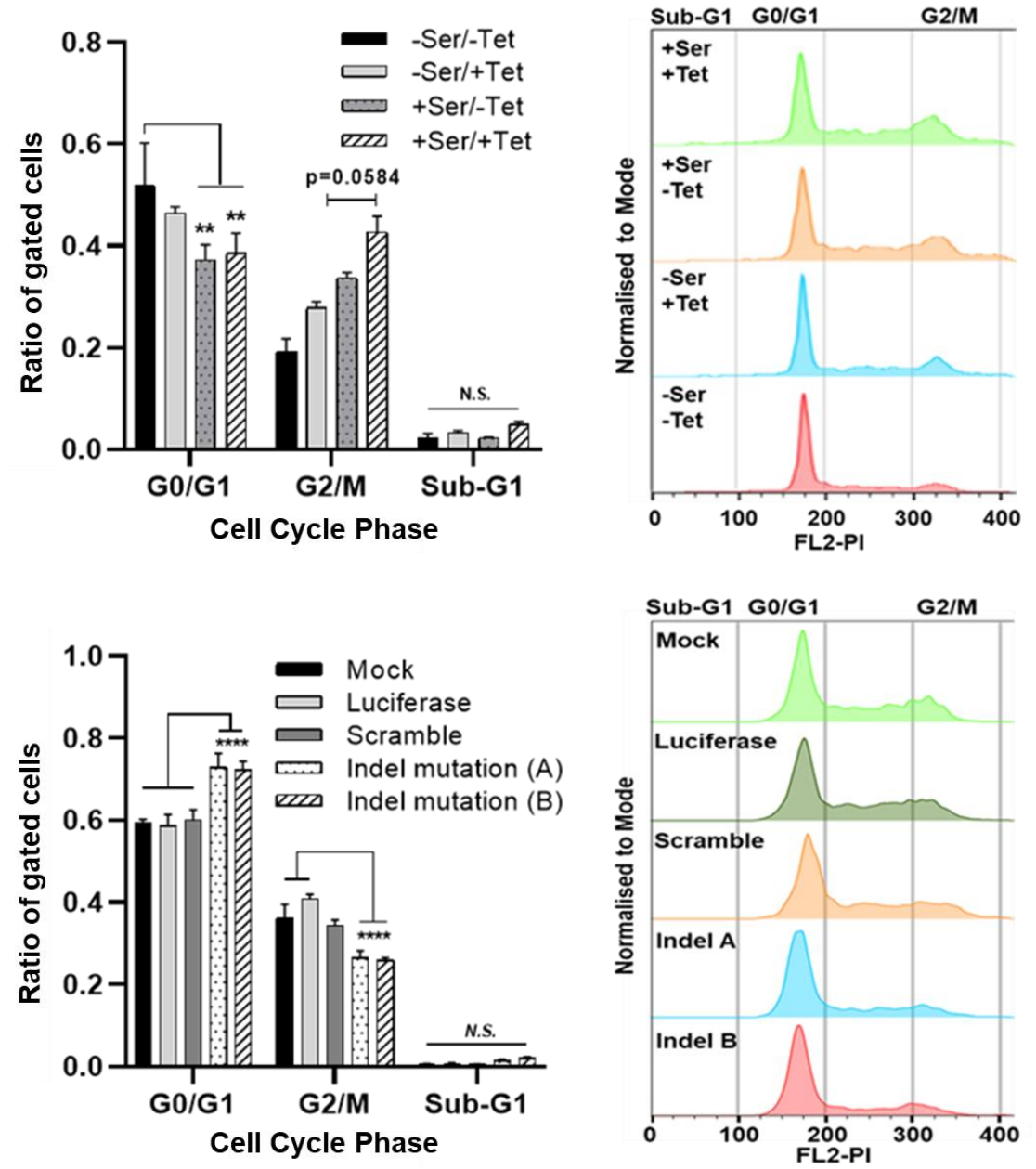

Figure 5. 16 Cell cycle analysis

(Top left panel) cell cycle quantification of the gated Flp-In™ T-REx™ cells in DNA content analysis. (Bottom left panel) cell cycle quantification of the gated H1299 cells in DNA content analysis [Two-way ANOVA, $F_{(6,\ 12)} = 13.76$, $p < 0.0001$ (top left panel). $F_{(8,30)} = 42.08$, $p < 0.0001$ (bottom left panel); post-hoc Tukey's HSD, $^{**}p < 0.01$, $^{****}p < 0.0001$]. (Top right panel) an overlay of four plots under four treatments (a combination of ±serum and ±Tetracycline) which shows the consistency among samples with respect to lack of sub G1 peak and an increased G2/M population from the treatment of -serum/-Tetracycline (red) up to the treatment of +serum/+Tetracycline (green). (Bottom right panel) cells harvested were fixed and stained with propidium iodide, and their DNA contents were analyzed by flow cytometry. An overlay of five plots under serum stimulation

shows the consistency among samples with respect to lack of sub G1 peak and a relatively lower G2/M population in the two polyclonal EP400NL indel mutation cell lines (red and blue) compared to the three control cell lines (brown, dark and light green). x - and y -axes denote DNA content and normalized cell number, respectively.

5. 4 Discussion

Functional characterization of the EP400NL complex revealed its transcriptional regulatory activity. EP400NL was subsequently confirmed as a bona fide co-activator of Myc by using GAL4Myc reporter assays. To further examine if the EP400NL coactivates Myc-mediated transactivation and confirm if EP400NL can be specifically recruited in a Myc-dependent manner, a ChIP assay was conducted using 293TGAL4-Luciferase cells in which a GAL4 DNA binding domain can be targeted by GAL4 fusion proteins. These results showed GAL4Myc can specifically interact with the GAL4 DNA binding site and further recruit the TAP-EP400NL, which indicates that EP400NL is a coactivator of Myc.

After the confirmation of interaction between EP400NL and cMyc, whether the EP400NL deletion mutants are required for Myc-mediated transcriptional coactivity was investigated. FLAG-tagged full-length EP400NL and its four deletion mutants (Δ1-50, Δ141-156, Δ246-260, and Δ360-419) were transient expressed from the 293TGAL4-Luciferase cells followed by the FLAG peptide elution in which the expression of the three major EP400NL interacting candidate proteins (BAF53, BRD8, and BRG1) was examined from the partially purified complexes. BRD8 and BRG1 both retained the interaction with full-length EP400NL and its deletion mutants. Despite a higher protein amount of two EP400NL deletion mutants (Δ246-260, Δ360-419) in the immunoprecipitates, they showed a weaker interaction with BAF53 than the full-length EP400NL and lost the coactivator activity of Myc in the luciferase reporter assay (Figures 5. 12 and 5. 13). Since BAF53 functions as a critical Myc-interacting nuclear cofactor for oncogenic transformation (Park et al., 2002), these regions (246-260aa., 360-

419aa.) of EP400NL are likely to play a role in the association with BAF53 for co-activating Myc-mediated transcription.

Next, the transcriptional regulatory activity of these deletion mutants was investigated. Interestingly, the two EP400NL deletion mutants (Δ246-260, Δ360-419) that are close to the C-terminus exhibited a reduced transcriptional activity compared to both the full-length EP400NL and the deletion mutants that are adjacent to the N-terminus. These results further consolidate the findings in the previous immunoprecipitation assay which a weak interaction with BAF53 was specifically observed from these two EP400NL deletion mutants (Δ246-260, Δ360-419). Contrarily, the N-terminal deletion mutant (Δ1-50) displayed an elevated ability of transactivation despite three functional sites were predicted by the InterPro algorithm (Chapter 5. 2. 1). Given that the only known functional domain in which the EP400 homology domain of EP400NL is from residue 50 (50-402 aa.), it seems like the first 50 amino acids from the N-terminus might not be as essential as the rest of the sequence especially compared to the C-terminus (Chapter 5. 2. 2). These results suggested a possibility that boosting the co-transcriptional activity of EP400NL can be achieved by potentially removing the N-terminus (1-50) while maintaining the C-terminus intact.

As the wild type EP400NL complex exhibits H2A.Z deposition activity (Chapter 4. 2. 3), in addition to the core components (BAF53, BRD8), a unique ATPase BRG1 also interacted with the full-length EP400NL, which has not been found in the hNuA4 complex. Thus, experiments into understanding if the EP400NL deletion mutants, specifically Δ246-260 and Δ360-419, retain the ability to interact with other ATPases such as RuvBL1 and RuvBL2 warrants further investigation. Meanwhile, elucidating the interaction between the N-terminal deletion mutant (Δ1-50) of EP400NL with these three ATPases need to be conducted.

The deleted regions (246-260) and (360-419) of EP400NL were shown to be essential for Myc targeted transcription and binding of BAF53 in this *in vitro* system. Given that EP400NL exhibits the H2A.Z deposition activity, and that transcriptional activity was severely impaired when the two mutants were transiently expressed, this suggests that these two deleted regions might also be crucial for interacting with ATPases for altering chromatin structure.

Myc has been shown to play a critical role in cell proliferation, migration, and an important role in the control of the cell cycle (Schmidt, 1999, Garcia-Gutierrez et al., 2019). Following verification that EP400NL is a bonafide coactivator of Myc, experiments investigating whether manipulation of the expression level of EP400NL alters cell proliferation were subsequently conducted. EP400NL overexpression promoted cell proliferation and increased the cell population in the G2/M cell cycle, whereas a decreased proliferation rate and G2/M cell population were observed in the EP400NL indel mutation cell lines.

In addition to the ChIP data and the evidence for interaction between EP400NL and Myc, combined with the observation that EP400NL overexpression under serum stimulation exhibited the highest proliferation rate, together indicate that EP400NL-mediated coactivation of Myc is important to cellular function. Further studies should also be carried out to investigate the effect of EP400NL in regulating the proliferation of other cancer cell lines

In brief, EP400NL coactivates Myc-mediated transactivation and can interact with Myc by forming a functional epigenetic complex. EP400NL enhanced and further promoted cellular proliferation in a serum-dependent manner. Transcriptional analysis using EP400NL deletion mutants revealed the importance of the two polypeptide regions (246-260, 360-419) adjacent to the C-terminus that are critical for its core transitional activity. It is of interest to narrow down how BAF53 interacts with EP400NL and further clarify if other proteins are required for this interaction in the future.

6. INVESTIGATING THE ROLE OF THE EP400NL COMPLEX IN PD-L1 EXPRESSION

The interaction between the programmed death 1 (PD-1) receptor and its ligand PD-L1 is a well-characterised adaptive immune checkpoint that has been widely targeted in cancer immunotherapy. PD-L1, expressed on the tumour cell surface, is regulated by Myc (Casey et al., 2016), however little is known about the specific mechanism through which Myc regulates PD-L1 expression. The aim of the research in this chapter was to first confirm the transcriptional activation of PD-L1 and then to examine the transcriptional regulatory function of EP400NL in regulating PD-L1 gene expression by either overexpressing or mutating EP400NL in the presence and absence of serum or IFNγ. Myc expression is positively correlated with the amounts of serum in the culture medium (Dean et al., 1986, Richman and Hayday, 1989a) and multiple studies have shown that Myc and IFNγ can both activate the expression of PD-L1 (Casey et al., 2016, Kim et al., 2017, Lastwika et al., 2016, Moon et al., 2017, Nowicki et al., 2018). It was investigated whether EP400NL acts as a coactivator for IFNγ and/or Myc-mediated expression of PD-L1.

6. 1 Myc positively regulates PD-L1 expression

To confirm that Myc regulates PD-L1, FLAG-Myc plasmids range from 0.4 µg to 2.0 µg were transfected into a non-small cell lung cancer cell line (H1299). The increase in plasmid DNA that was transfected correlated with an increase in Myc protein as detected by western blot (Figure 6. 1). Next, RNA was extracted from the transfected cells for measuring PD-L1 mRNA expression level by RT-qPCR assays (Figure 6. 2). HA-GST transiently transfected cells in these assays serves as a negative control. It should be noted that PD-L1 is endogenously expressed in H1299 cells, however, this is at a relatively lower level in comparison to other non-small cell lung cancer cells (Kim et al., 2017), therefore, subtle changes in PD-L1 expression in H1299 can be easily detected compared to those non-small cell lung cancer cell lines such as H157, H441, H1975, and HCC827 which display

extremely higher expression of PD-L1 (Cao et al., 2017a). RT-qPCR data revealed a gradual increase in PD-L1 mRNA level in response to an increased protein expression level of Myc.

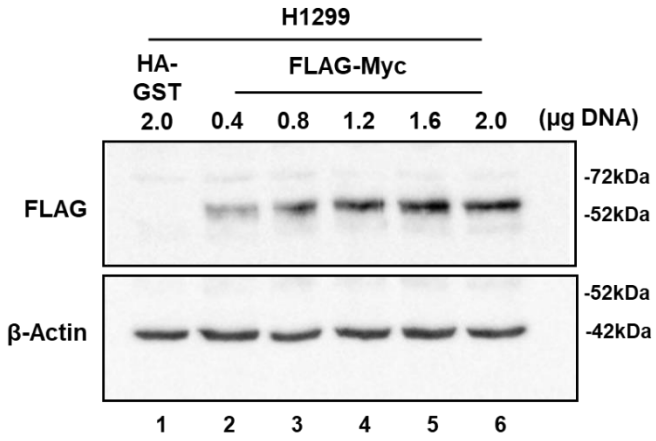

Figure 6. 1 Confirmation of transient Myc expression

Confirmation of Myc protein expression after transient transfection. Lysates were subjected to SDS-PAGE and western blotting with an anti-FLAG antibody. The level of Myc increased with an increasing amount of plasmid ranging from 0.4 µg to 2.0 µg.

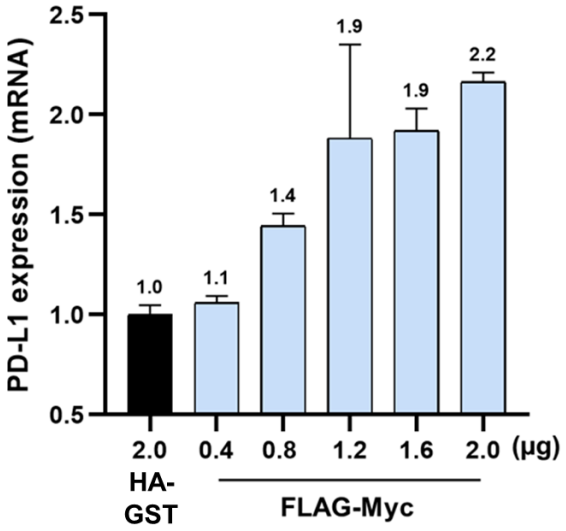

Figure 6. 2 Level of PD-L1 mRNA expression in response to Myc by RT-qPCR

The investigation of PD-L1 mRNA expression level in response to the Myc transient transfection. FLAG-Myc plasmids range from 0.4 µg to 2.0 µg were transiently expressed in H1299 cells. The level of PD-L1 mRNA in cells transfected with HA-GST was set to one and served as a negative control in this experiment. PD-L1 expression in the other samples was normalized against the negative control.

6. 2 Serum stimulation increases PD-L1 expression

Data from chapter 6. 1 indicated that Myc upregulates PD-L1, therefore it is of interest to determine whether this upregulation can be further enhanced by the presence of EP400NL. The PD-L1 expression was initially confirmed to be induced in both H1299 and the established EP400NL Flp-In™ T-REx™ cell lines in the presence of increased serum concentration, and the increased concentration of the serum has been previously shown to induce endogenous cMyc expression (Dean et al., 1986). Cells were serum-starved (1% serum) for 48 hours before serum stimulation (20% serum). RNA and protein samples were prepared after 0 hours, 6 hours, 12 hours, 24 hours, and 36 hours of serum stimulation. PD-L1 mRNA expression level was determined by RT-qPCR. Both cell lines exhibit an increased level of PD-L1 mRNA expression after serum stimulation. The established Flp-In™ T-REx™ cell line displayed increased PD-L1 mRNA expression up to 3.2-fold following 6 hours of serum stimulation and this remained at a relatively stable level over the 36-hour duration of the experiment (Figure 6. 3, top left panel). On the other hand, H1299 displayed a significantly higher level of PD-L1 expression of up to seven-fold following 6-hours of serum stimulation, which then dropped as the incubation time continued (Figure 6. 3, top right panel).

To measure the induction of Myc after serum stimulation, the level of endogenous Myc expression was analysed. Unexpectedly, no detectable alteration was observed on an anti-Myc immunoblot, as the expression level remained consistent in these two cell lines before and after the serum stimulation (Figure 6. 3, bottom panel). Despite this, it was confirmed that serum stimulation leads to an increased level of PD-L1 mRNA in both cell lines, however, the lack of increase in Myc suggests that EP400NL is not acting through Myc to upregulate EP400NL.

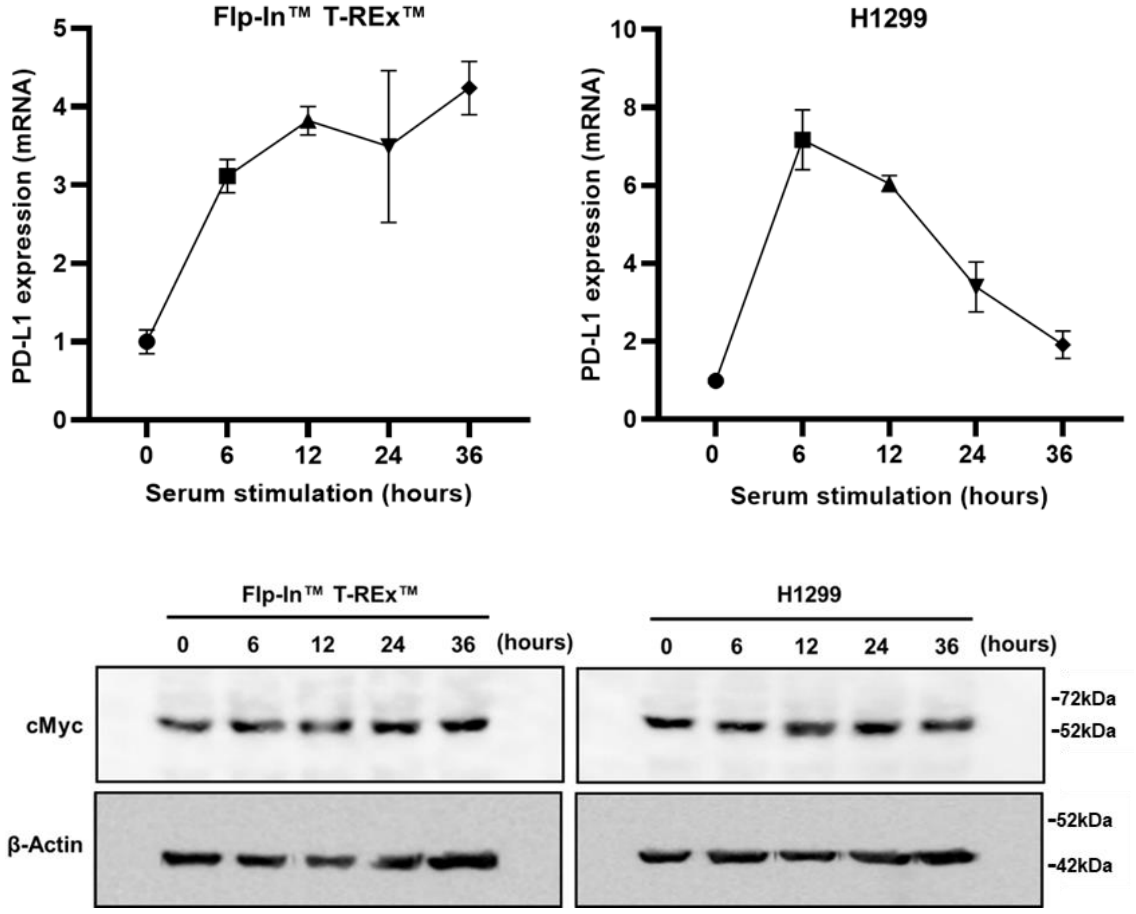

Figure 6. 3 PD-L1 expression pattern in Flp-In™ T-REx™ and H1299 cells

(Top left panel) PD-L1 expression pattern of Flp-In™ T-REx™ cells and (top right panel) H1299 cells under 0 to 36 hours of serum stimulation after serum starvation. (Bottom panel) Immunoblot with anti-Myc showed the cMyc protein levels under serum stimulation in Flp-In™ T-REx™ cells (left) and H1299 cells (right), an equal amount of protein was loaded.

6. 3 EP400NL in serum-mediated PD-L1 expression

6. 3. 1 EP400NL positively regulates serum-mediated PD-L1 expression

To elucidate the role of EP400NL in regulating PD-L1 expression, the inducible EP400NL Flp-In™ T-REx™ cell line was used to determine how the expression of EP400NL affects serum mediated PD-L1 expression. An increase in PD-L1 expression up to 3.8-fold can be achieved after 12 hours of serum stimulation in Flp-In™ T-REx™ cells based on our preliminary experiments (Figure 6. 3 A). Cells were initially serum-starved for 48 hours for cell cycle synchronization

(Khammanit et al., 2008) and followed by 20% serum stimulation for 12 hours in the presence of 1 mg/ml tetracycline for induction of EP400NL expression. PD-L1 expression increased up to approximately 2-fold on serum stimulation and expression was further increased up to 3.2-fold in the presence of both serum stimulation and EP400NL induction (Figure 6. 4, stripped bar). Consistent with the effect on PD-L1 mRNA level, PD-L1 protein expression in the serum-stimulated and tetracycline induced cells was increased up to 2-fold compared to the untreated cells (Figure 6. 5, anti-PD-L1 immunoblot).

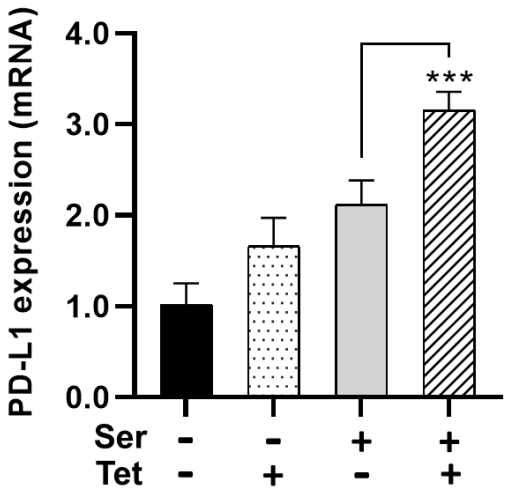

Figure 6. 4 PD-L1 mRNA expression levels in response to serum stimulation and EP400NL induction

Flp-In™ T-REx™ cells were treated with four different conditions (±Ser/±Tet) followed by an analysis of PD-L1 expression via RT-qPCR [One-way ANOVA, $F_{(3,12)} = 48.96$, $p < 0.0001$; post-hoc Tukey's HSD, $***p < 0.001$]. Ser: Serum; Tet: Tetracycline. PD-L1 expression was normalized against GUSB which served as a housekeeping gene.

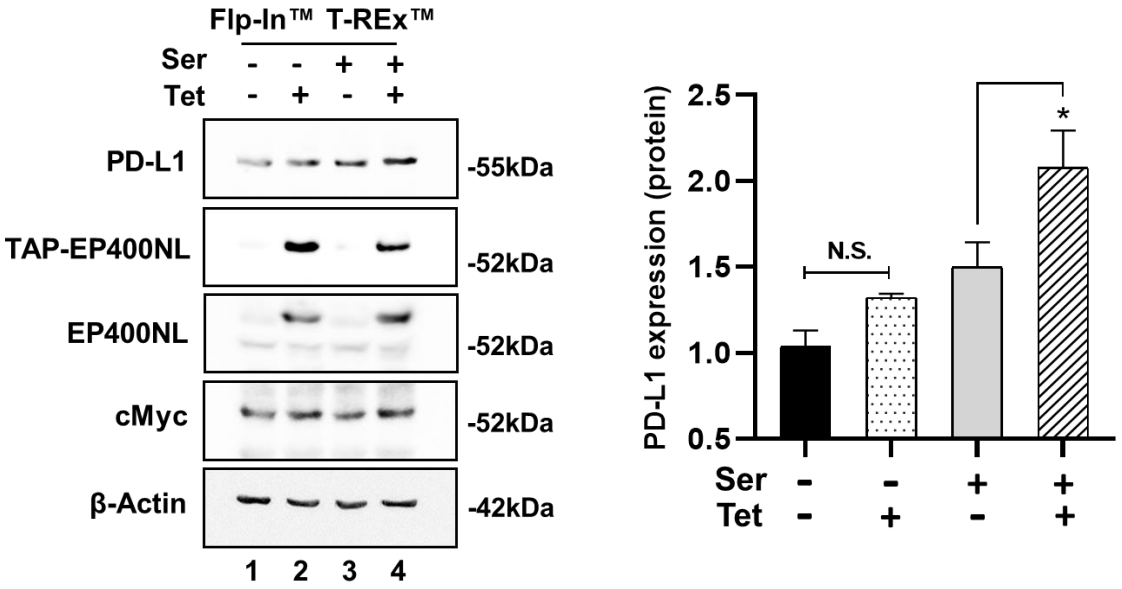

Figure 6. 5 PD-L1 protein expression levels in response to serum stimulation and tetracycline induction

Protein expression levels of endogenous PD-L1 in four different conditions (±Ser/±Tet) were examined by immunoblots (left panel). The relative intensities of PD-L1 protein were quantified and plotted (right panel) [Ordinary one-way ANOVA, $F_{(3,4)} = 20.32$, $p = 0.0070$; post-hoc Tukey's HSD, $^{*}p < 0.05$]. Quantitative data from experiments performed in duplicate. Ser: Serum; Tet: Tetracycline.

PD-L1 upregulation was confirmed via confocal microscopy. Flp-In™ T-REx™ cells were treated with tetracycline to induce EP400NL after serum stimulation then stained with anti-PD-L1, anti-EP400NL, and DAPI. Increased expression of EP400NL was detected after tetracycline induction, but no alteration in PD-L1 expression was observed during serum-starvation regardless of EP400NL induction (Figure 6. 6, top two panels).

On the contrary, all cells expressed a significantly higher level of PD-L1 after serum stimulation, which was further increased when EP400NL was present (Figure 6. 6, bottom two panels). Taken together, these results demonstrate that EP400NL enhances the expression of PD-L1 following serum stimulation.

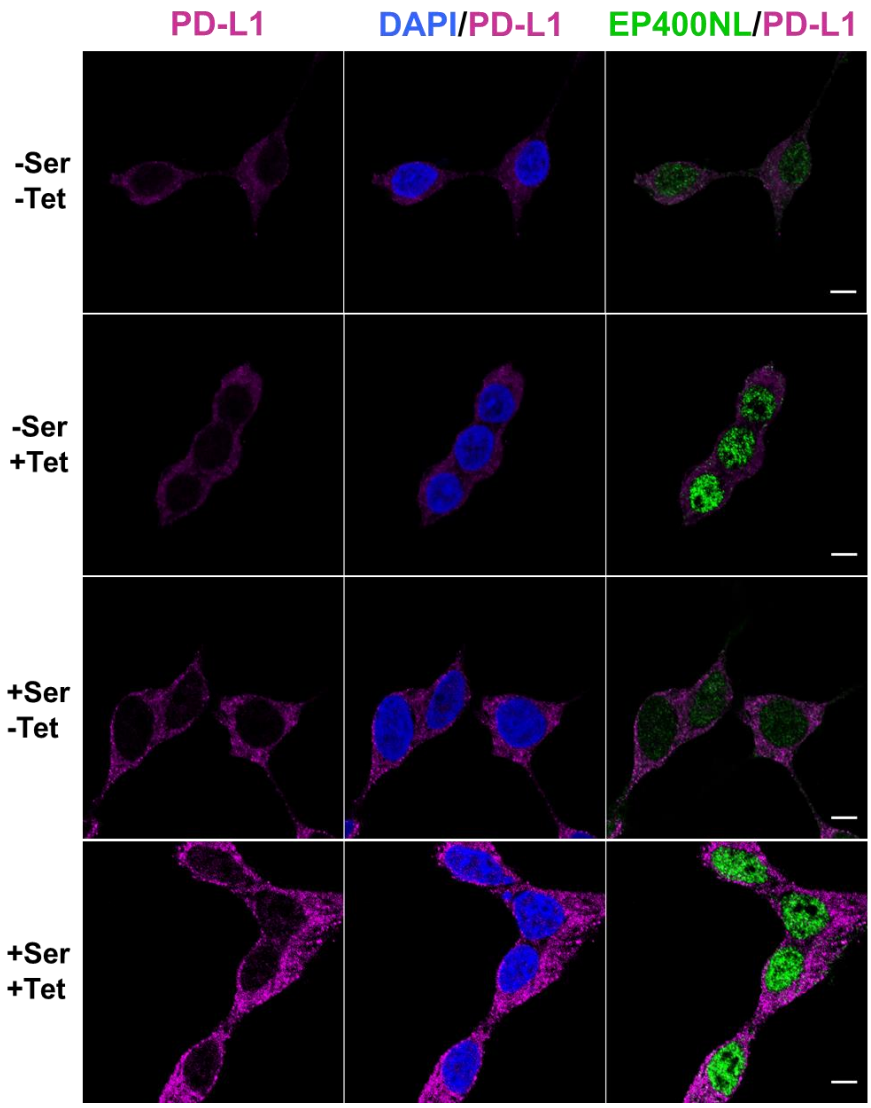

Figure 6. 6 Immunocytochemical analysis of PD-L1 expression in the TAP-EP400NL inducible Flp-In™ T-REx™ cell line

Cells were treated with a combination of serum stimulation and tetracycline as indicated, followed by staining with anti-PD-L1 and anti-EP400NL antibodies. Nuclei were counterstained with 4,6-diamidino-2-phenylindole (DAPI). Scale bar = 5 µm.

6. 3. 2 EP400NL deletion mutants are unable to enhance serum mediated PD-L1 expression

To determine the domains of EP400NL that are required for its coactivator function, the two deletion mutants (Δ246-260 and Δ360-419, Figure 5. 9) that lack coactivator function were transiently expressed and examined for their ability to induce PD-L1 expression in the presence of serum stimulation using H1299

cells. Full-length EP400NL (1-419) and its mutants (Δ246-260 and Δ360-419) were cloned into mammalian expression CbF vectors, the CbF backbone was used to express FLAG-tagged proteins (10. APPENDIX 2). HA-GST transfected H1299 cells were used as a negative control since GST originated from *E. coli* which is not expected to play a role in any transcriptional regulation in mammalian cell lines.

In contrast to wild-type EP400NL, neither mutant induced the expression of PD-L1 mRNA (Figure 6. 7) or protein (Figure 6. 8). These data confirm that the regions of EP400NL between amino acids 246-260 and 360-419 are required for EP400NL to coactivate the expression of PD-L1.

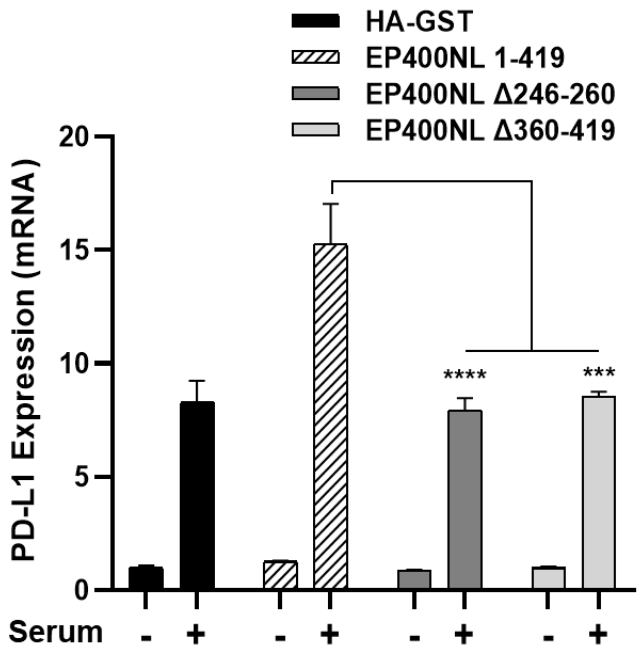

Figure 6. 7 EP400NL mutants lack the ability to coactivate serum mediated PD-L1 expression

H1299 cells were transiently transfected with plasmids expressing either wild type EP400NL or two deletion mutants (Δ246-260 and Δ360-419) and PD-L1 mRNA levels induced by serum stimulation were determined by RT-qPCR [Two-way ANOVA, $F_{(3, 8)} = 18.60$, p=0.0006; post-hoc Tukey's HSD, $^{***}p < 0.001$, $^{****}p < 0.0001$]. HA-GST serves as the negative control. PD-L1 expression was normalized against GUSB which served as a housekeeping gene.

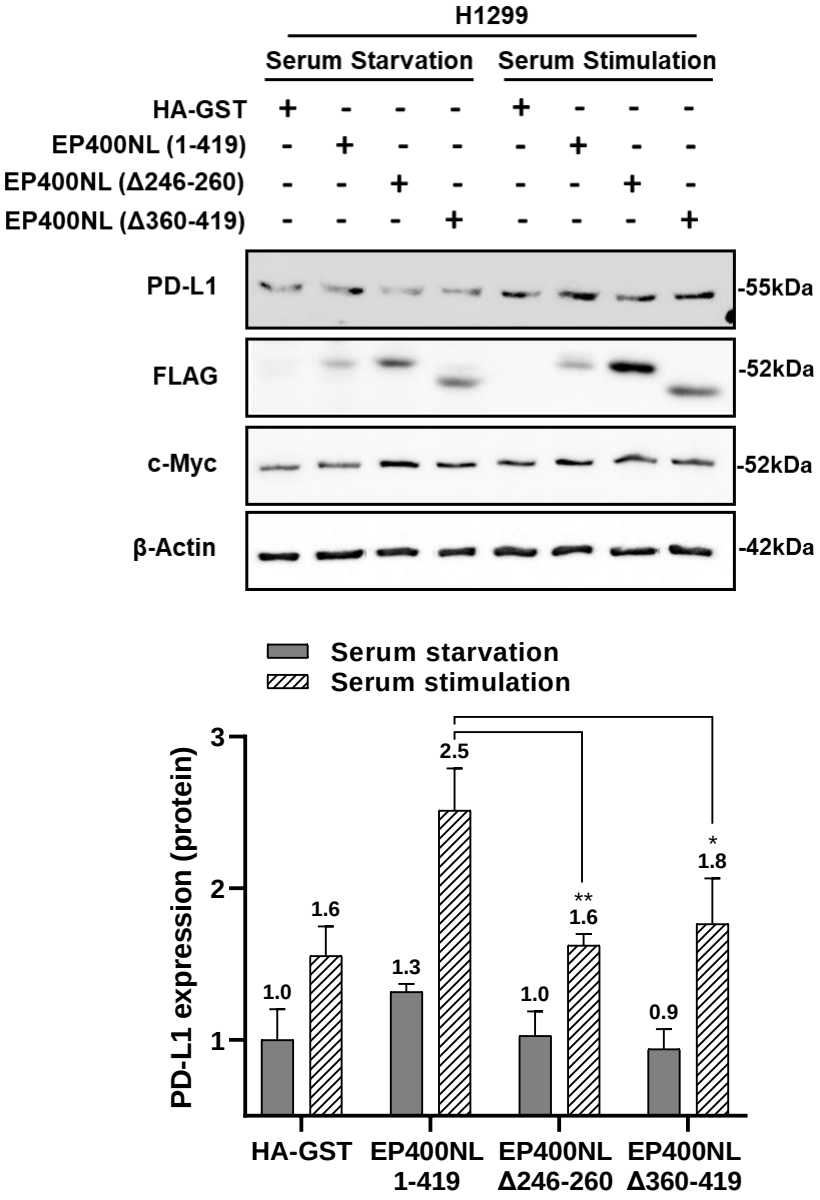

Figure 6. 8 EP400NL mutants lose the coactivator function for serum mediated PD-L1 expression (protein)

(Top panel) H1299 cells were transiently transfected with plasmids expressing either wild type EP400NL or two deletion mutants (Δ246-260 and Δ360-419). Protein expression of PD-L1, transient FLAG-tagged proteins and cMyc was confirmed by immunoblots. (Bottom panel) PD-L1 protein levels induced by serum stimulation were determined by anti-PD-L1 immunoblots [Two-way ANOVA, $F_{(3,\ 8)} = 9.763$, p=0.0047; post-hoc Tukey's HSD, $^{*}p < 0.05$, $^{**}p < 0.01$]. HA-GST serves as the negative control. Immunoblotting was conducted in duplicate.

6. 3. 3 Lack of EP400NL hinders serum-mediated PD-L1 expression

The two EP400NL indel lines (Indel-A, Indel-B) were used to examine PD-L1 expression in the presence of serum stimulation. In comparison to the control H1299 cell line which showed a drastic increase in PD-L1 mRNA of up to approximately 100-fold after six hours of serum stimulation, PD-L1 was induced only 30-fold in the EP400NL indel cells at the same time interval (Figure 6. 9, top panel).

Despite a decreased mRNA expression of PD-L1, there was no significant reduction in PD-L1 protein (Figures 6. 9, bottom panel, anti-PD-L1 immunoblot).

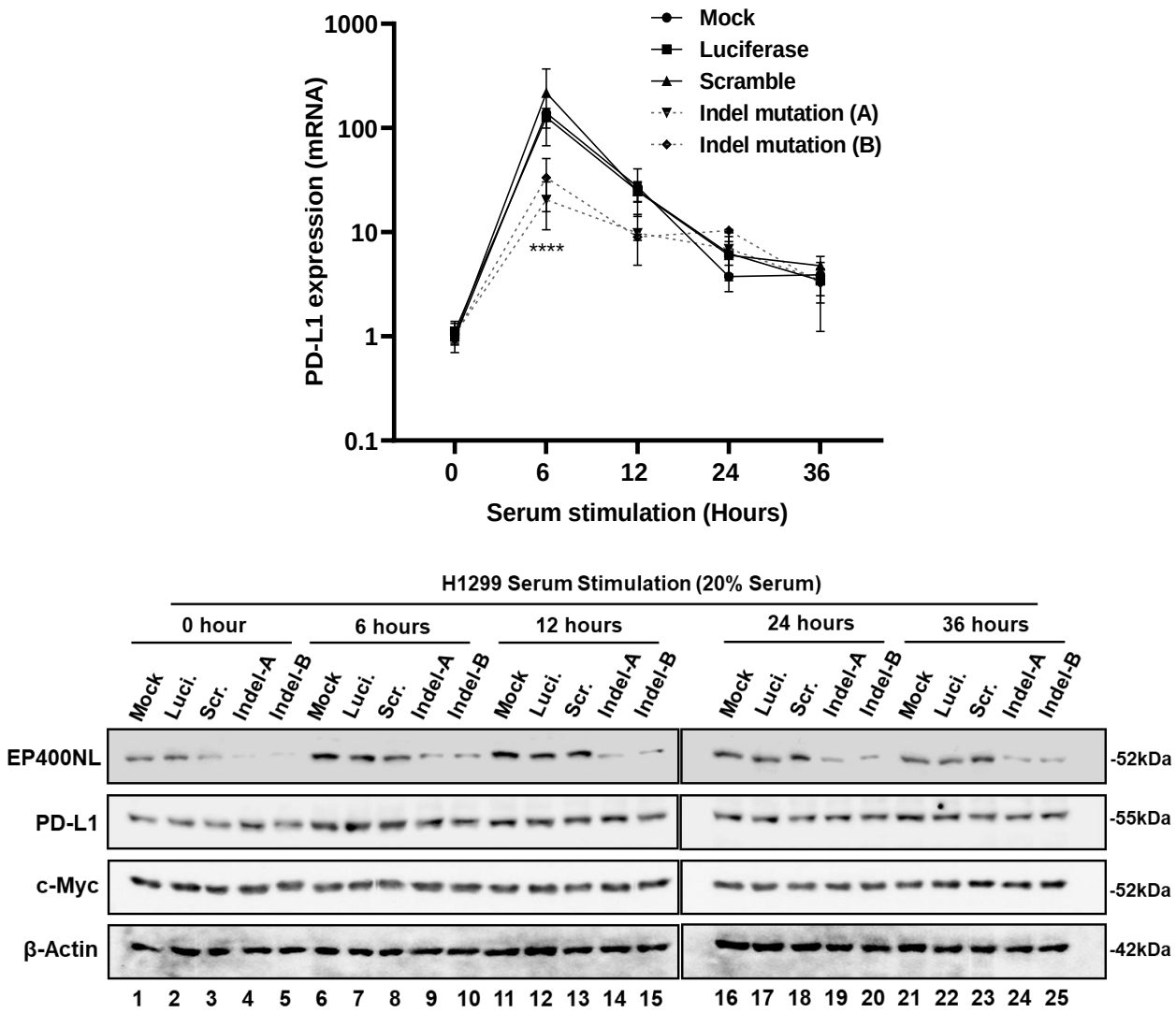

Figure 6. 9 EP400NL enhances serum mediated PD-L1 expression

(Top panel) PD-L1 mRNA expression levels in H1299 cell lines carrying EP400NL indels in the presence of serum stimulation. The level of PD-L1 protein at the zero time point was set to one and the expression levels of PD-L1 were calculated against their basal expression levels [Two-way ANOVA, $F_{(4,25)} = 21.10$, $p < 0.0001$ (Serum stimulation); post-hoc Tukey's HSD, $^{****}p < 0.0001$ (Scr. Vs. Indel-A or Indel-B, serum stimulation)]. (Bottom panel) Immunoblots on lysates generated on cells treated identically to those processed for RT-qPCR: Mock, gRNA-luciferase (Luci.), gRNA-scrambled random sequence (Scr.), gRNA-EP400NL-A (Indel-A), and gRNA-EP400NL-B (Indel-B).

6. 4 EP400NL complex recruitment for induction of PD-L1 expression

To determine whether EP400NL is recruited and enriched at the E-box region, which Myc heterodimers bind by the addition of serum, ChIP was carried out on the established EP400NL cells in the presence and absence of tetracycline and serum stimulation to determine the relative enrichment of EP400NL within the promoter region of PD-L1. (Figure 6. 10).

As BRG1, RuvBL1, and RuvBL2 were identified as EP400NL interactors via mass spectrometric analysis and as components of the purified EP400NL complexes in the H2A.Z deposition assay (Chapter sections 3. 3 and 4. 2. 3), their recruitment to the PD-L1 promoter was also assessed via ChIP-qPCR. In addition, interactions between EP400NL and these candidates were investigated via co-immunoprecipitation.

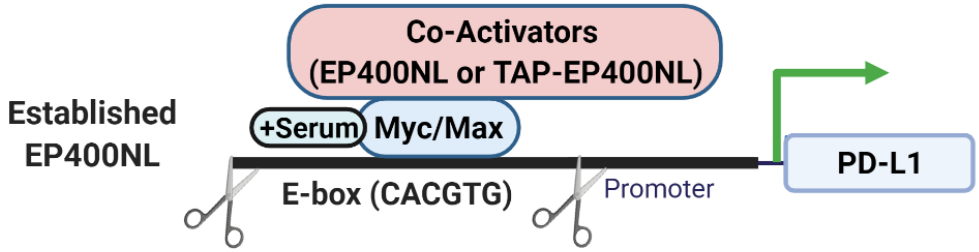

Figure 6. 10 Schematic of PD-L1 promoter containing an E-box region

PD-L1 promoter used in ChIP analysis. Myc/Max binds to the E-box region (Enhancer box: CACGTG) for the recruitment of its co-activators (Endogenous EP400NL and tetracycline induced TAP-EP400NL) for inducing PD-L1 expression under serum stimulation. Scissors represent the sonication of chromatins for subsequent ChIP assay.

6. 4. 1 Optimisation of the ChIP assay

Before demonstrating if EP400NL can be recruited to the PD-L1 promoter with serum stimulation, the established EP400NL cells were used, and the expression of the endogenous EP400NL, induced TAP-EP400NL and cMyc from four combinations of treatment conditions (A: Serum-/Tetracycline-, B: Serum-/Tetracycline+, C: Serum+/Tetracycline-, and D: Serum+/Tetracycline+) was

initially confirmed by immunoblotting (Figure 6. 11). The expression of endogenous EP400NL was detected in samples of all four treatments and TAP-EP400NL was detected via an anti-CBP immunoblot (Figure 6. 11). No alteration in cMyc expression was detected across all four treatments (Figure 6. 11, anti-cMyc immunoblot).

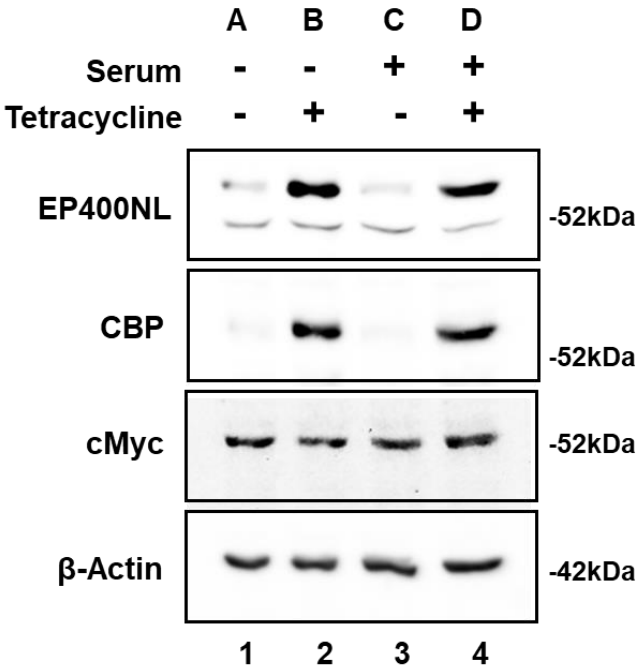

Figure 6. 11 Confirmation of protein expression for ChIP assay

Protein expression of endogenous EP400NL, TAP-EP400NL, and cMyc in four different conditions (±Serum/± Tetracycline) were examined by immunoblots. TAP-EP400NL (CBP tagged) was detected by an anti-CBP antibody.

Furthermore, chromatin was isolated after the four treatments (A: Serum-/Tetracycline-, B: Serum-/Tetracycline+, C: Serum+/Tetracycline-, and D: Serum+/Tetracycline+) and subsequently sonicated. The optimal size of chromatin for ChIP is in the range of 500-700 bp, and this was confirmed following sonication (Figure 6. 12)(Chapter section 2. 6. 2).

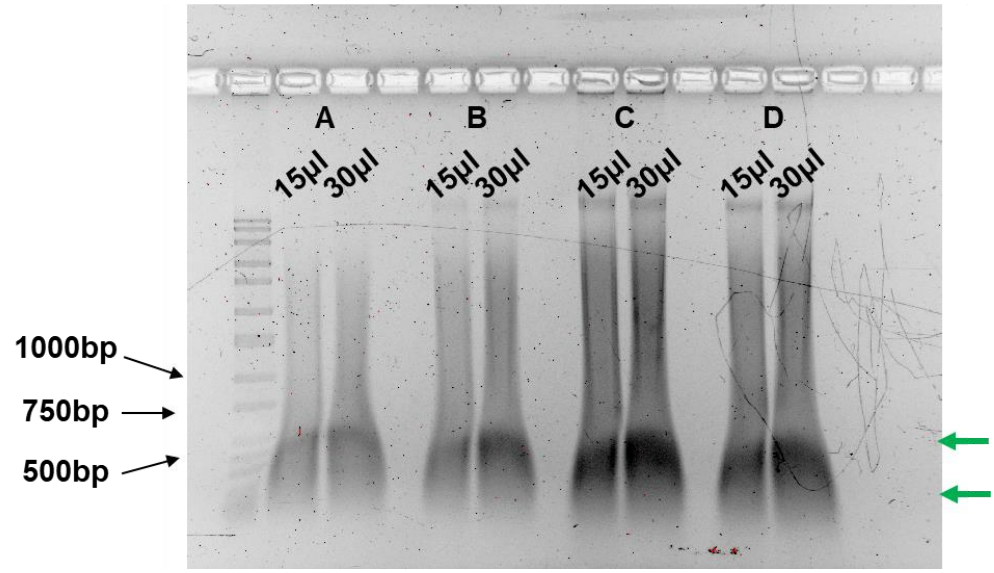

Figure 6. 12 Confirmation of optimal chromatin fragmentation

Chromatin was sonicated for 2 minutes and confirmed by 1% agarose gel electrophoresis. 15 µL and 30 µL of each sonicated chromatin were loaded. Green arrows show the sonicated fragments are in the range of 500bp to 750bp in length. A: Serum-/ Tetracycline-, B: Serum-/ Tetracycline+, C: Serum+/ Tetracycline-, and D: Serum+/ Tetracycline+.

6. 4. 2 The EP400NL complex is targeted to the PD-L1 promoter in a Myc-dependent manner

To investigate whether EP400NL is recruited to the PD-L1 promoter in a Myc-dependent manner, ChIP was performed following induction of TAP-EP400NL expression in Flp-In™ T-REx™ cells. Despite serum stimulation, no significant increase in cMyc enrichment was detected at the PD-L1 promoter (Figure 6. 13, cMyc panel), however, TAP-EP400NL induction enhanced cMyc enrichment upon serum stimulation.

Two potential ATPases (BRG1 and RuvBL2) (Puri et al., 2007, Wu et al., 2017) that were identified as the associated proteins with EP400NL were also examined for enrichment at the PD-L1 promoter. BRG1 and RuvBL2 showed a similar recruitment pattern in which both serum stimulation and tetracycline induction of EP400NL resulted in a higher enrichment than serum stimulation or induction of EP400NL individually (Figure 6. 13, BRG1 and RuvBL2 panels, stripped bars

versus dark or light grey bars). These data indicate that cellular signals induced by serum stimulation are a prerequisite for the enrichment of BRG1 and RuvBL2 ATPases near the E-box of the PD-L1 gene, which can be significantly enhanced by the upregulated EP400NL. Unexpectedly, no specific RuvBL1 enrichment can be detected from our ChIP-qPCR assay given that RuvBL1 and RuvBL2 are the binding partners in most of the chromatin remodelling complexes (Figure 6. 13, RuvBL1 panel) (Lopez-Perrote et al., 2014, Puri et al., 2007, Choi et al., 2009). Taken together, these results indicated that increased EP400NL expression in the presence of serum stimulation enhances recruitment of its interactors including cMyc, BRG1, and RuvBL2.

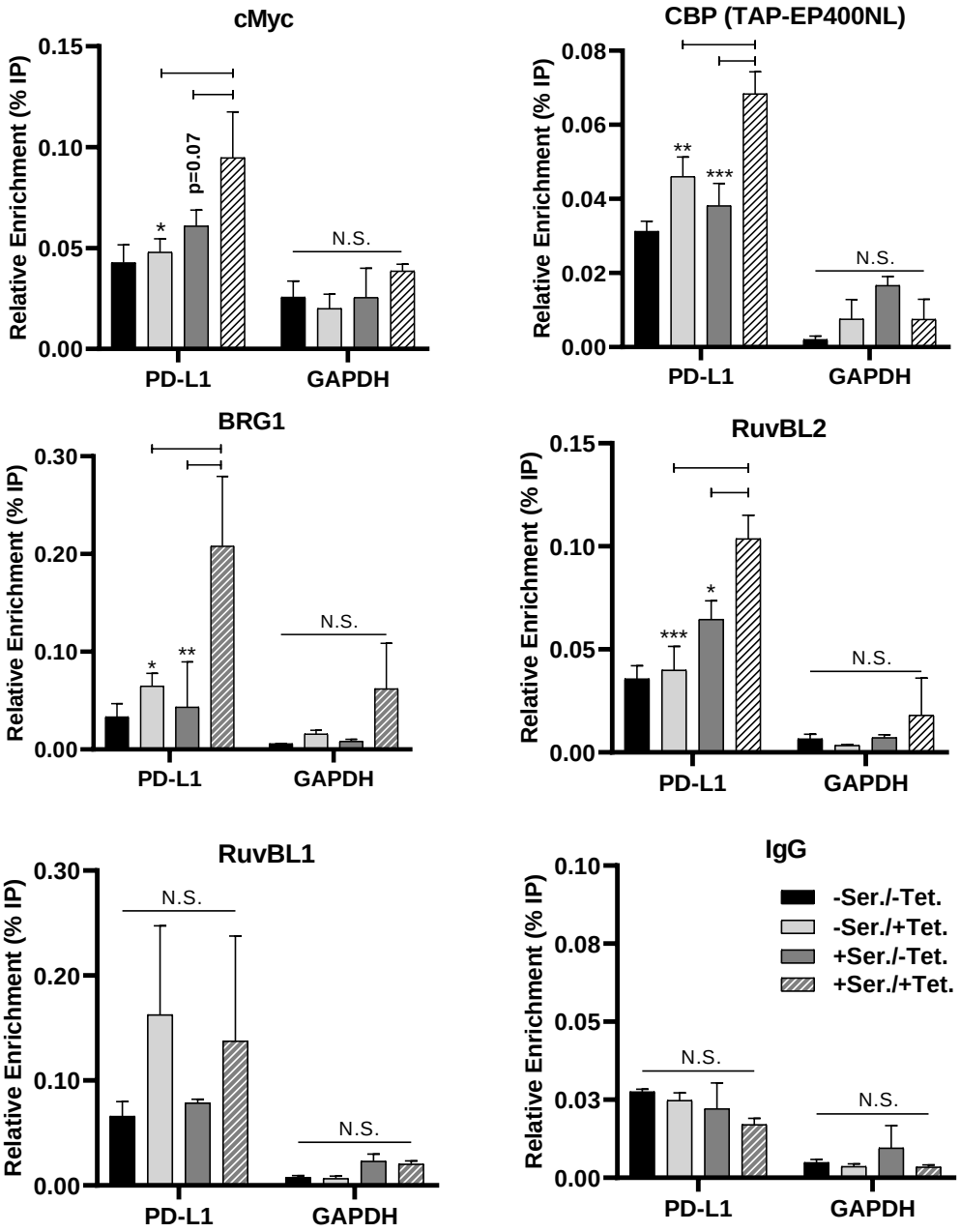

Figure 6. 13 EP400NL complex is recruited at the PD-L1 promoter in a cMyc dependent manner

Enrichment of cMyc, EP400NL, BRG1, RuvBL1, and RuvBL2 at the PD-L1 promoter of Flp-In™ T-REx™ cell line stably expressing tetracycline-inducible EP400NL. The purified DNA after ChIP reactions was analyzed by qPCR over the regions of PD-L1 promoter (Myc binding site) or GAPDH promoter. Four combinations of the experimental conditions (the presence and absence of serum and tetracycline: ±Ser/±Tet) were used in the ChIP analyses [Two-way ANOVA, $F_{(1,8)} = 36.01$, $p = 0.0003$ (cMyc), $F_{(1,8)} = 263.7$, $p < 0.0001$ (CBP), $F_{(1,8)} = 13.57$, $p = 0.0062$ (BRG1), $F_{(1,8)} = 121.5$, $p < 0.0001$ (RuvBL2); post-hoc Tukey's HSD, $^{*}p < 0.05$, $^{**}p < 0.01$, $^{***}p < 0.001$].

6. 4. 3 Investigation of the interaction between EP400NL and associated candidates

To examine if the interaction of EP400NL with associated cMyc, BRG1, RuvBL1, and RuvBL2 occurs under physiological conditions, a serum stimulation experiment was conducted using the stable Flp-In™ T-REx™ cell line expressing tetracycline-inducible TAP-EP400NL.

Following tetracycline induction and serum stimulation, TAP-EP400NL was precipitated by streptavidin beads (Figure 6. 14, top panel) and the presence of endogenous cMyc, BRG1, RuvBL1, and RuvBL2 was detected in the precipitates (Figure 6. 14, top panel, lanes 6 and 8). Then this was reversed, antibodies against cMyc, BRG1, RuvBL1, or RuvBL2 were used to precipitate TAP-EP400NL (Figure 6. 14, bottom panel, lanes 6, 8, 10, and 12). These results further support the hypothesis that cMyc directly interacts with the EP400NL nuclear complexes containing BRG1, RuvBL1, and RuvBL2 and those interactions can be further stabilised by EP400NL.

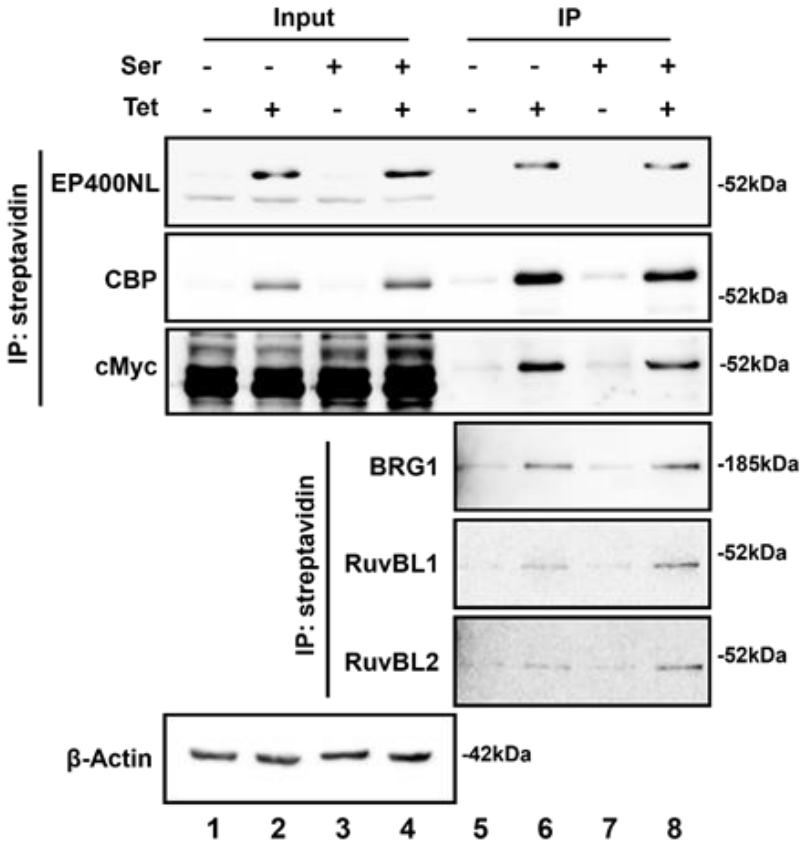

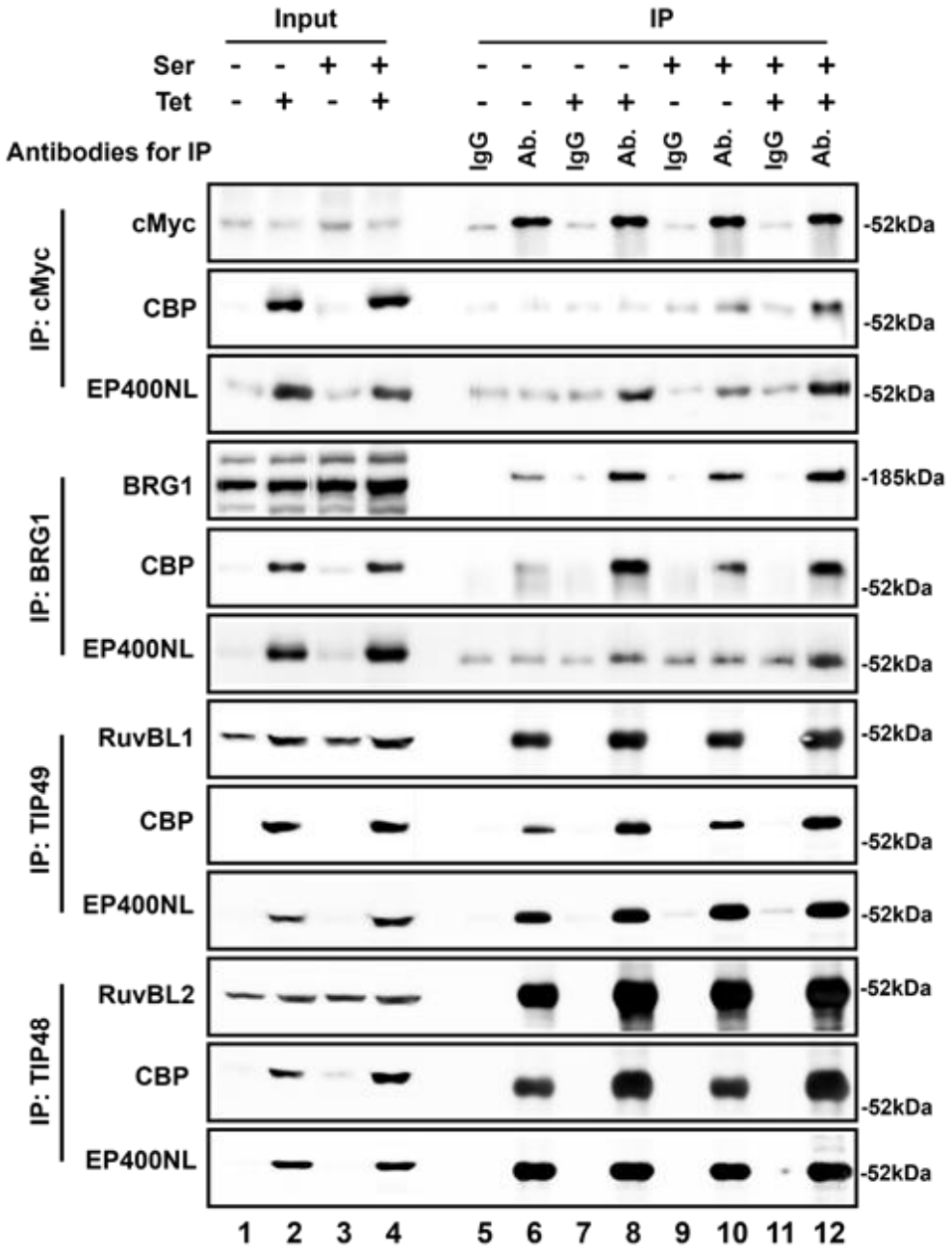

Figure 6. 14 Co-IP experiments for examining the protein-protein interaction between EP400NL and its associated protein candidates

(Top panel) Co-immunoprecipitation experiments for the protein-protein interaction of EP400NL, cMyc, BRG1, RuvBL1, and RuvBL2. EP400NL protein complexes were precipitated by streptavidin beads followed by anti-EP400NL and anti-CBP immunoblots. The co-immunoprecipitations of cMyc, BRG1, RuvBL1, and RuvBL2 were confirmed by the immunoblots. (Bottom panel) Reverse co-immunoprecipitation experiments were performed with the same cell lysates. Immunoprecipitation was carried out using anti-cMyc, anti-BRG1, anti-RuvBL1, and anti-RuvBL2 antibodies (Ab.), and immunoblots were probed with anti-CBP and anti-EP400NL immunoblots. IgG immunoprecipitation serves as a negative control.

6. 5 EP400NL in IFNγ mediated PD-L1 expression

PD-L1 expression is induced in tumours in response to the proinflammatory cytokine IFNγ, which is secreted by tumor-infiltrating T cells (Chen et al., 2016). This induction is mainly associated with the stimulation of multiple pathways such as the JAK/STAT and PI3K-AKT-mTOR signalling pathway (Lastwika et al., 2016). Thus, in addition to coactivating PD-L1 expression, an investigation into whether EP400NL also coactivates IFN-γ mediated PD-L1 expression was conducted.

6. 5. 1 IFNγ mediated PD-L1 expression patterns in Flp-In™ T-REx™ and H1299 cell lines

To examine whether IFNγ upregulates PD-L1 mRNA expression in either Flp-In™ T-REx™ and H1299 cell lines, cells were treated with increasing concentrations of IFNγ followed by RT-qPCR analysis. No significant induction of PD-L1 mRNA expression was detected from Flp-In™ T-REx™ cells until the concentration of IFNγ reached 20 ng/mL (Figure 6. 15, left panel). On the other hand, 5 ng/mL of IFNγ promoted the PD-L1 mRNA expression up to 14-fold in H1299 cells, therefore these cancer cells are extremely sensitive to IFNγ in comparison to the non-cancer epithelial HEK293 cells (Figure 6. 15, right panel). Two minimum concentrations of IFNγ (5 ng/mL for H1299; 20 ng/mL for Flp In™ T-REx™) were adopted for inducing PD-L1 mRNA expression in subsequent experiments.

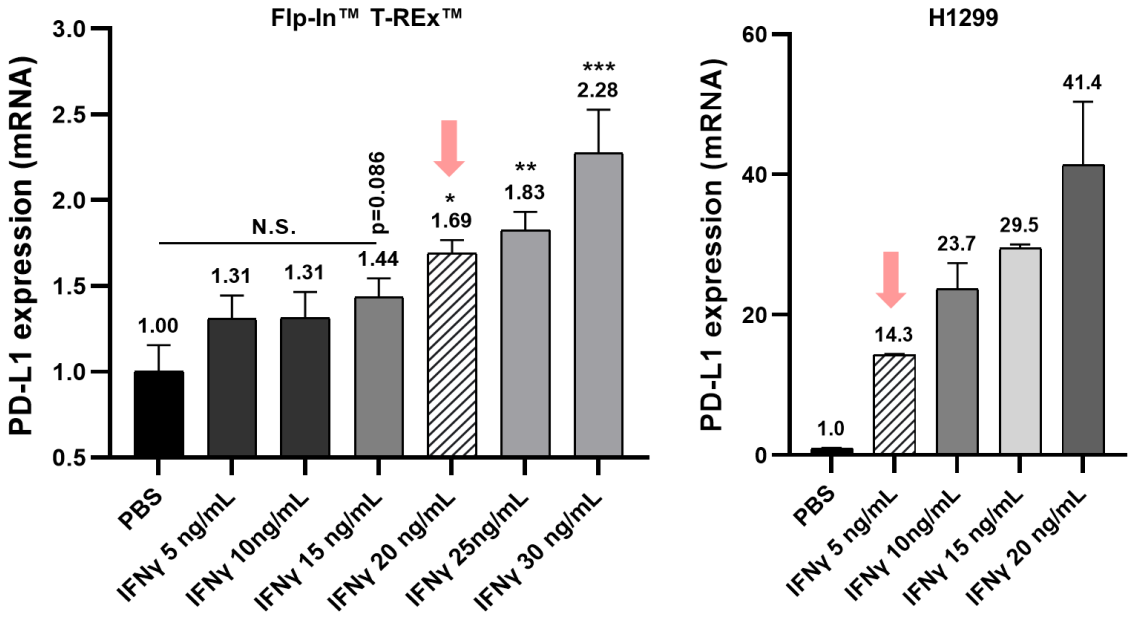

Figure 6. 15 IFNγ mediated PD-L1 expression patterns in Flp-In™ T-REx™ and H1299

PD-L1 mRNA expression pattern in Flp-In™ T-REx™ (left panel) and H1299 cells (right panel) after IFNγ treatment. Pink arrows indicate the selected concentration of IFNγ for subsequent experiments.

6. 5. 2 EP400NL positively regulates IFNγ-mediated PD-L1 expression

To explore the role of EP400NL in regulating IFNγ-mediated PD-L1 expression, the inducible Flp-In™ T-REx™ cell line was used to determine whether TAP-EP400NL coactivates IFNγ mediated PD-L1 expression. Cells for IFNγ-mediated experiments were treated using the same protocol as the serum mediated PD-L1 experiments in the previous section (6. 2. 1) with an additional 20 ng/mL IFNγ treatment in the last 24 hours of incubation.

IFNγ also increased PD-L1 mRNA expression by approximately 2-fold and additional treatment of either serum stimulation or EP400NL induction resulted in an additive effect (Figure 6. 16). Interestingly, PD-L1 gene expression was synergistically upregulated up to eight-fold with IFNγ sensitization, serum stimulation, and tetracycline induction (IFNγ+/Serum+/Tetra+) (Figure 6. 16, stripped bar). A similar pattern of PD-L1 protein expression was observed in the

triple-treated cells (IFNγ+/Serum+/Tetra+) with a 2. 5-fold increase compared to the control cells (Figure 6. 17, anti-PD-L1 immunoblot).

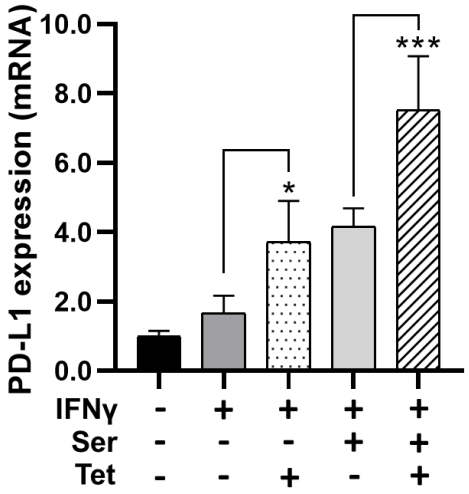

Figure 6. 16 PD-L1 mRNA expression levels in response to IFNγ sensitization, serum stimulation, and tetracycline induction

Flp-In™ T-REx™ cells were treated under five different conditions (±IFNγ/±Ser/±Tet) and PD-L1 expression was analysed by RT-qPCR. PD-L1 mRNA expression level in response to a combination of serum (Ser) stimulation, tetracycline (Tet) induction, and IFNγ sensitization [One-way ANOVA, $F_{(4,15)} = 30.42$, $p < 0.007$; post-hoc Tukey's HSD, $^{*}p < 0.05$, $^{***}p < 0.001$].

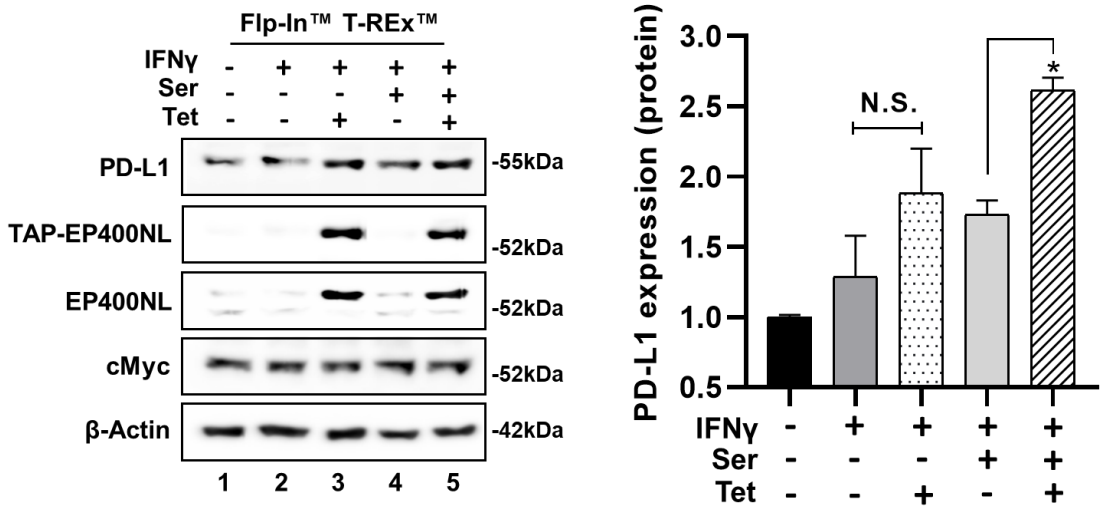

Figure 6. 17 PD-L1 protein expression levels in response to IFNγ sensitization, serum stimulation, and tetracycline induction

Protein levels of endogenous PD-L1 under five different conditions (±IFNγ/±Ser/±Tet) was examined by immunoblots (Left panel). The relative intensities of PD-L1 protein levels are quantified and plotted in the right panel [Ordinary one-way ANOVA, $F_{(4,5)} = 18.81$, $p = 0.0032$; post-hoc Tukey's HSD, $^{*}p < 0.05$]. Immunoblotting was conducted in duplicate.

PD-L1 protein upregulation was subsequently confirmed via confocal microscopy. Flp-In™ T-REx™ cells were cultured in the presence or absence of tetracycline and IFNγ then stained with anti-PD-L1, anti-EP400NL, and DAPI. Increased expression of EP400NL was detected after tetracycline induction, but no alteration in PD-L1 expression was observed following the treatment in the absence of IFNγ even when TAP-EP400NL was induced by tetracycline (Figure 6. 18, top two panels). On the contrary, all cells expressed a significantly higher level of PD-L1 after IFNγ treatment, which was further increased under the induction of EP400NL (Figure 6. 18, bottom two panels). These data demonstrate that the inducing ability of serum and IFNγ requires the presence of EP400NL to increase PD-L1 expression.

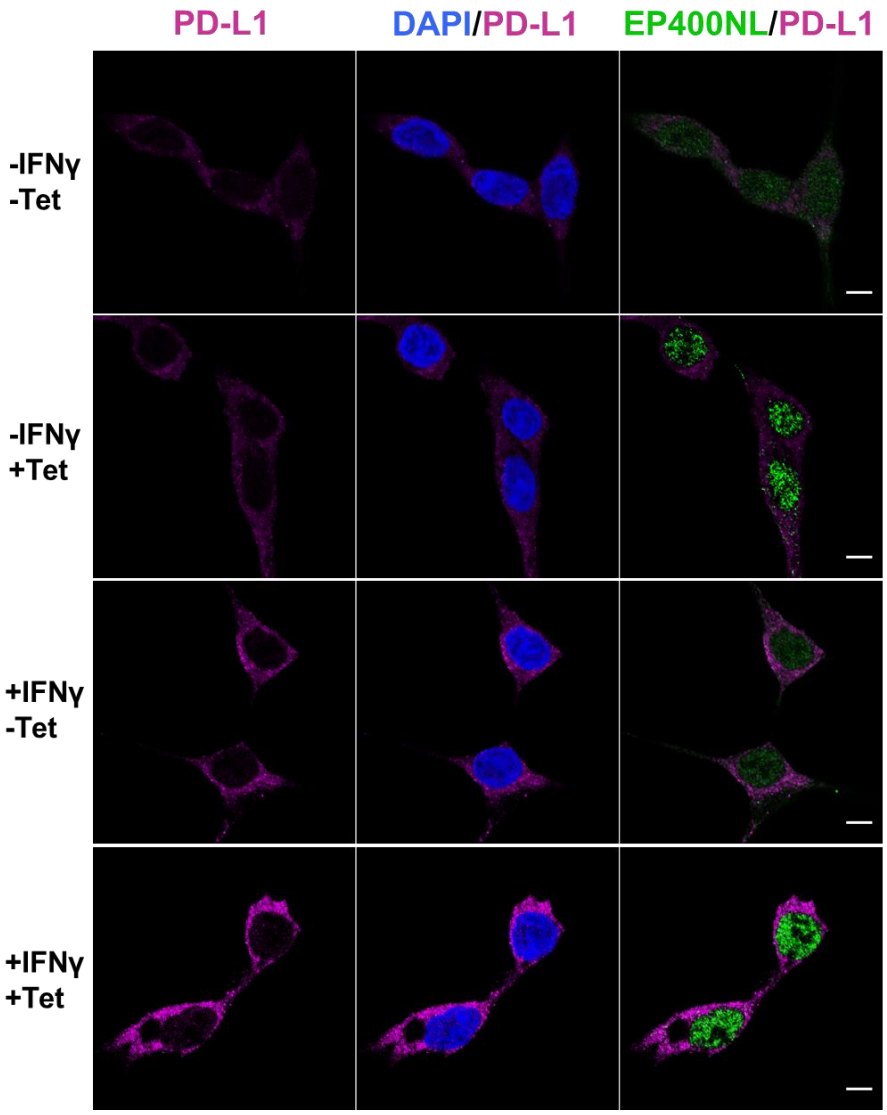

Figure 6. 18 Immunocytochemical analysis of IFNγ mediated PD-L1 in the TAP-EP400NL inducible Flp-In™ T-REx™ cell line

Immunocytochemical analysis of PD-L1 in the TAP-EP400NL inducible Flp-In™ T-REx™ cell line. Cells were treated with either a combination of IFNγ sensitization and tetracycline induction followed by the staining with the anti-PD-L1 and anti-EP400NL antibodies. Nuclei were counterstained with 4,6-diamidino-2-phenylindole (DAPI). Scale bar denotes 5 µm.

6. 5. 3 EP400NL deletion mutants in regulating IFNγ mediated PD-L1 expression

To understand the domains of EP400NL coactivator function in IFNγ mediated PD-L1 expression, the two deletion mutants (Δ246-260 and Δ360-419) that lack the coactivator function were examined for regulating PD-L1 expression in the presence of IFNγ sensitization. In contrast to wild type EP400NL, neither mutant induced expression of PD-L1 mRNA (Figure 6. 19) or protein (Figure 6. 20) in H1299 cells. Taken together, combining the experimental data from inducing PD-L1 mRNA expression under serum stimulation, these data further confirm that the regions of EP400NL between amino acids 246-260 and 360-419 are important in regulating the EP400NL-mediated coactivator function of PD-L1 gene activation.

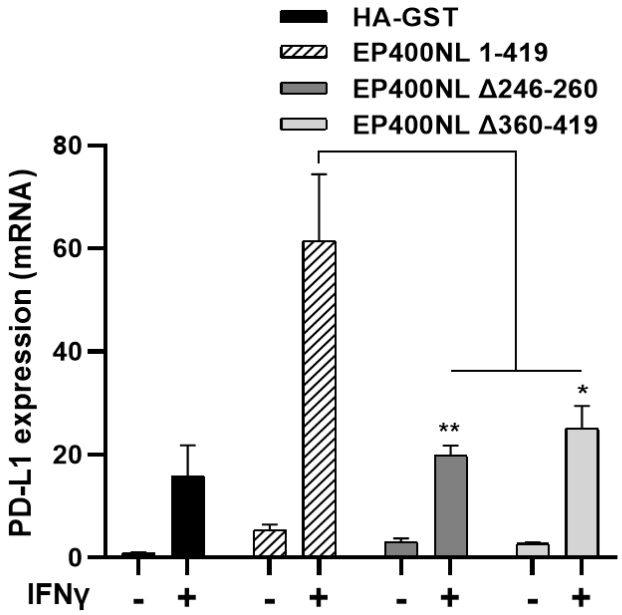

Figure 6. 19 EP400NL mutants lose the coactivator function for IFNγ-mediated PD-L1 expression (mRNA).

H1299 cells were transiently transfected with plasmids expressing either wild type EP400NL or two deletion mutants (Δ246-260 and Δ360-419) and PD-L1 mRNA levels induced by IFNγ sensitization were determined by RT-qPCR assays [Two-way ANOVA, $F_{(3,8)} = 7.112$, $p = 0.012$ (IFNγ sensitization); post-hoc Tukey's HSD, $*p < 0.05$, $**p < 0.01$]. HA-GST serves as the negative control.

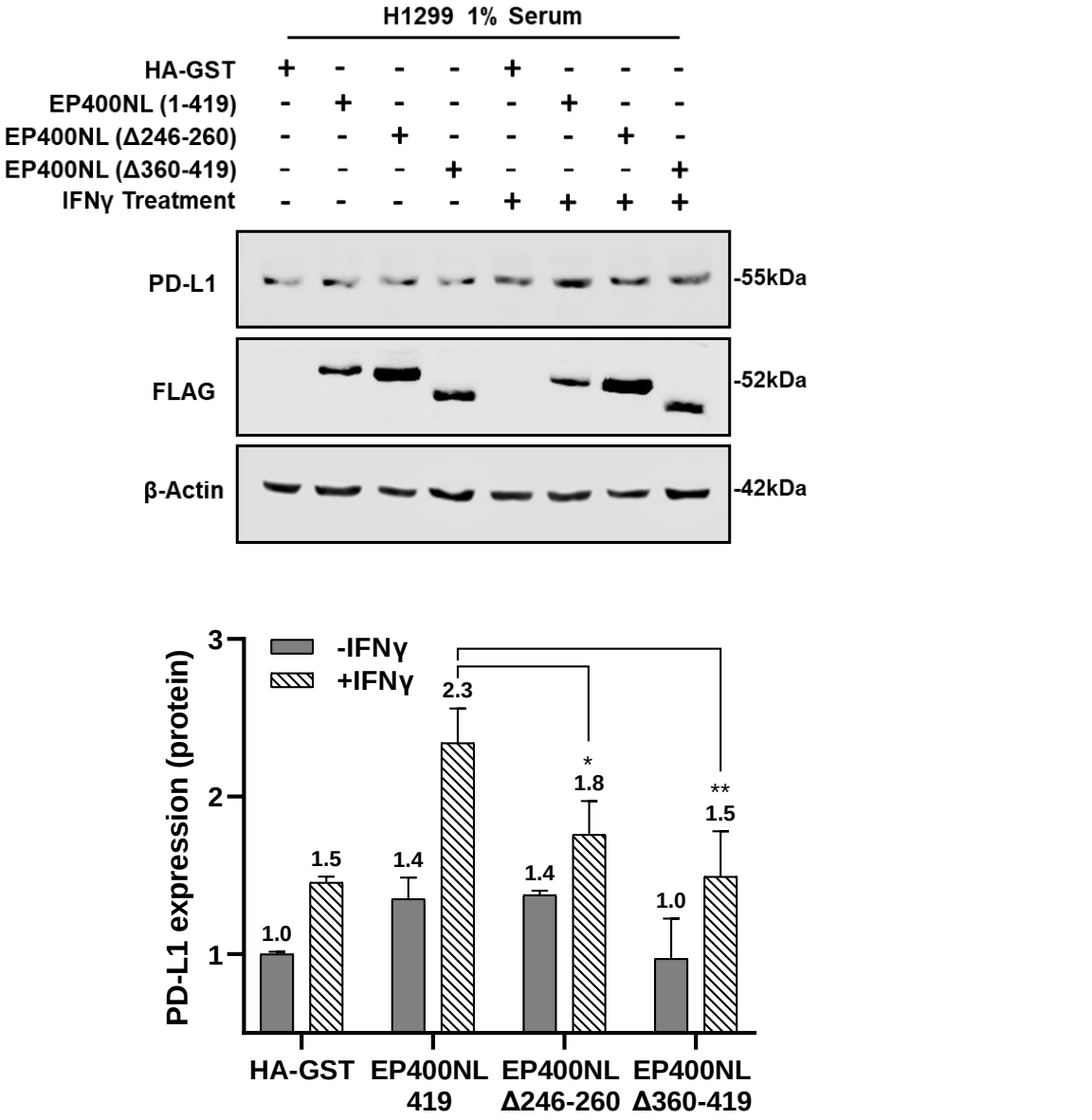

Figure 6. 20 EP400NL mutants lose the coactivator function for IFNγ-mediated PD-L1 expression (protein)

(Top panel) H1299 cells were transiently transfected with plasmids expressing either wild type EP400NL or two deletion mutants (Δ246-260 and Δ360-419). Protein expression of the transient FLAG-tagged proteins and PD-L1 was confirmed by anti-FLAG immunoblot and anti-PDL1 immunoblot respectively. (Bottom panel) PD-L1 protein levels induced by serum stimulation were determined by anti-PD-L1 immunoblots [Two-way ANOVA, $F_{(3,\ 8)} = 2.301$, p=0.1540; post-hoc Tukey's HSD, $^{*}p < 0.05$, $^{**}p < 0.01$]. HA-GST serves as the negative control. Immunoblotting was conducted in duplicate.

6. 5. 4 EP400NL indel mutants in regulating IFNγ mediated PD-L1 expression

To investigate if a reduced expression of EP400NL results in decreased IFNγ mediated PD-L1 expression, the two EP400NL indel lines (Indel-A, Indel-B) were used to examine PD-L1 expression following IFNγ sensitization over a time course of 24 hours. After 9 hours of treatment, IFNγ sensitization resulted in a lower level of PD-L1 expression from the EP400NL indel cell lines compared to the three control cell lines (mock, luciferase, and scramble) (Figure 6. 21).

Taken together, the loss of function studies using CRISPR/Cas9-mediated indels confirmed the critical role of EP400NL in driving both serum and IFNγ-mediated PD-L1 transcriptional activation. However, similarly to that seen with serum mediated PD-L1 protein expression data (6. 3. 3), the weaker transcriptional activity of the PD-L1 gene caused by EP400NL indels failed to show significant downregulation of PD-L1 protein levels (Figures 6. 21, anti-PD-L1 immunoblot).

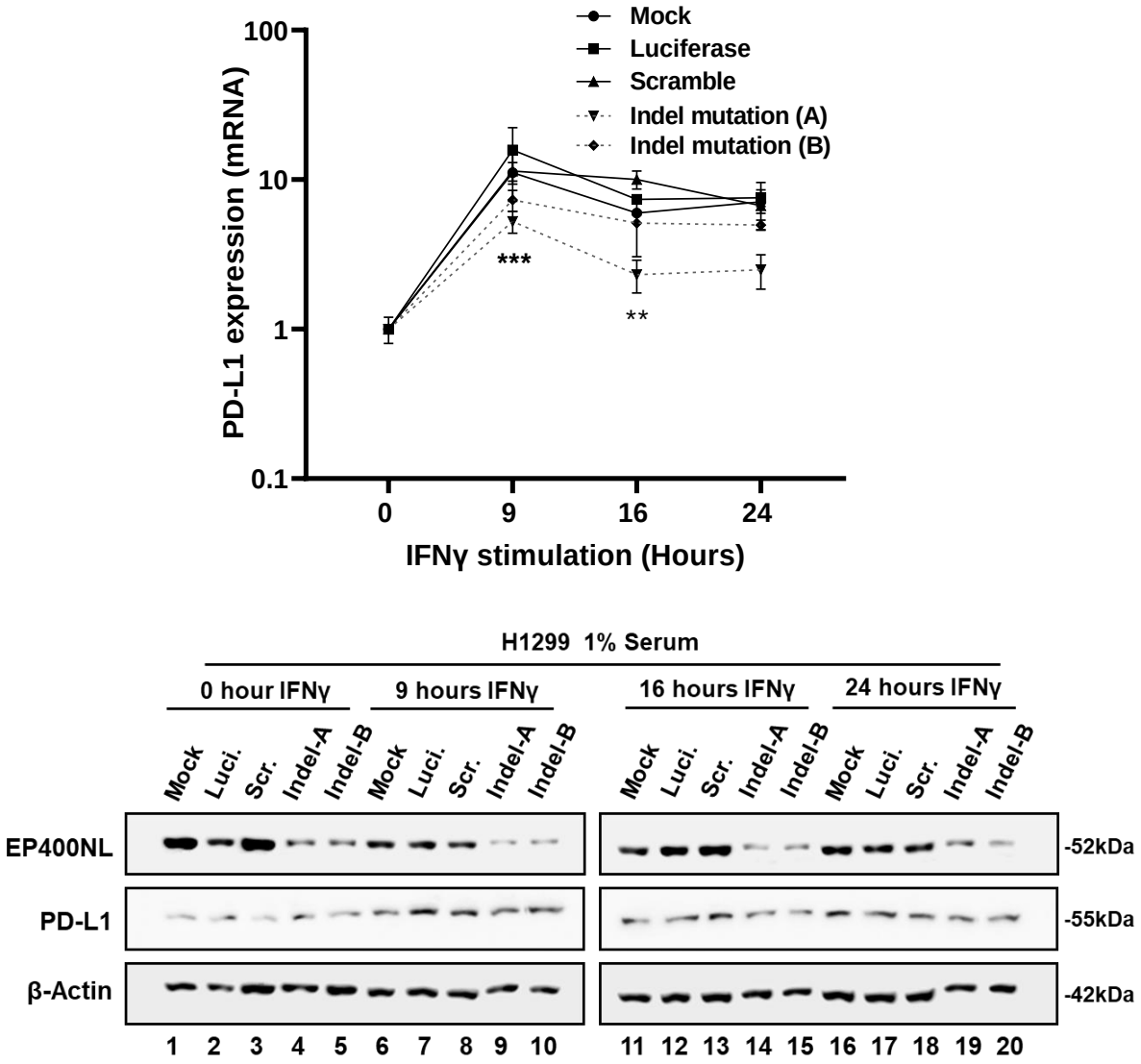

Figure 6. 21 EP400NL enhances IFNγ mediated PD-L1 expression

PD-L1 mRNA expression levels in H1299 cell lines carrying EP400NL indels. (Top panel) This experiment was conducted under the condition of IFNγ sensitization. The basal PD-L1 expression level of each cell line set to one and the expression levels of PD-L1 was calculated against their basal expression levels [Two-way ANOVA, $F_{(3,20)} = 36.56$, $p < 0.0001$ (IFNγ sensitization); post-hoc Tukey's HSD, $^{**}p < 0.001$ (Scr. versus Indel-A, IFNγ sensitization), $^{***}p < 0.001$ (Luci. Vs. Indel-A, IFNγ sensitization)]. (Bottom panel) EP400NL immunoblots for H1299 cell lines established by CRISPR-Cas9 system: Mock, gRNA-luciferase (Luci.), gRNA-scrambled random sequence (Scr.), gRNA-EP400NL-A (Indel-A), and gRNA-EP400NL-B (Indel-B). Protein expression levels of endogenous PD-L1 under IFNγ sensitization were examined by immunoblots.

6. 6 Discussion

EP400NL overexpression studies were conducted using the Flp-In™ T-REx™ cell line as it can stably express TAP-EP400NL in a tetracycline-dependent manner, in which induced expression of EP400NL enhanced the expression of PD-L1 in the presence of serum. A higher level of PD-L1 expression is a predictor of recurrent cancer incidence and is associated with poor cancer prognosis (Qin et al., 2015, Kojima et al., 2021), thus, methodologies to decrease the expression of PD-L1 in cancer cells have become a prominent focus in cancer research. Among all types of cancers, lung cancer remains the leading cause of cancer-related death worldwide, of which NSCLC is one of the most aggressive and devastating malignancies despite the development of targeted therapies (Akbay et al., 2013, DeSantis et al., 2014, Siegel et al., 2014, Cao et al., 2017b). Due to practical and applicational perspectives, it is meaningful to link this research to translational studies by using H1299 which is a non-small cell lung carcinoma (NSCLC) cell line. Compared to other high PD-L1 expressing lung cancer cell lines including H157, H441, H1975, and HCC827, the H1299 exhibits relatively lower PD-L1 expression (Cao et al., 2017a) which is suitable for monitoring subtle changes of expression caused by epigenetic modifications and transcriptional regulation. Therefore, in addition to the Flp-In™ T-REx™ cell line that stably expresses TAP-EP400NL under tetracycline induction, H1299 was exploited to study the loss of coactivator function of EP400NL.

Serum stimulation of both H1299 and Flp-In™ T-REx™ cells induced PD-L1 expression (Figure 6. 3, A and B). Interestingly, despite the transcriptional upregulation of PD-L1 in both cell lines, they exhibit different expression kinetics after serum stimulation. H1299 displayed a significantly higher PD-L1 expression of up to 7.2-fold in an early response to 20% serum incubation and gradually dropped to about 1.5-fold compared to the non-serum stimulated cells. In comparison, the established Flp-In™ T-REx™ cells showed an increase in PD-L1 mRNA expression of up to approximately 3.2-fold after 20% serum stimulation

but remained relatively steady at this level across incubation time. Thus, it is likely that H1299 significantly increases the membranous PD-L1 expression immediately after serum stimulation and exploits this as a protective strategy for the enhancement of immune evasion.

Although Myc expression was not altered significantly by serum stimulation in the EP400NL inducible Flp-In™ T-REx™ cells, serum stimulation in the presence of EP400NL enhances Myc binding to the PD-L1 promoter. ChIP data shows that the recruitment of EP400NL to the target promoter requires the binding of DNA binding transcription factors such as Myc to the promoter (Wang et al., 2021). Myc may be one of the main upregulated factors by the addition of serum which serves as a prerequisite binding partner of EP400NL. Thus, a Myc knockdown experiment may confirm and provide insights into the accuracy of the premises. It is also of interest to investigate if other components in the serum contribute to the PD-L1 induction.

Myc-dependent target gene activation is a multi-step process in which the binding of Myc to the target gene promoter is important but not sufficient to activate target genes. Myc pre-binds its target genes but does not activate them; this requires other cofactors such as P-TEFb, E2F1, and chromatin remodelers (Cole and McMahon, 1999, Kanazawa et al., 2003, Cowling and Cole, 2006, Gargano et al., 2007, Leung et al., 2008). These mechanisms might explain why the level of Myc was unchanged on serum stimulation.

The co-immunoprecipitation of Myc and the EP400NL complex and their enrichment at the Myc binding site of the PD-L1 gene support a model whereby cMyc recruits epigenetic modifying complexes to remodel the target gene promoters for transcriptional activation. Additionally, the PD-L1 expression pattern from cells with EP400NL indels suggests that EP400NL is required at an early stage of the transcriptional activation within 6 hours of serum stimulation (Figure 6. 9, top panel).

PD-L1 overexpression is a predictor of recurrent cancer incidence and is associated with a poor prognosis of cancer patients (Casey et al., 2016, Wang et al., 2016). Consistent with the role in the PD-L1 gene regulation, cMyc expression correlates with PD-L1 expression in NSCLC (Kim et al., 2017). A previous study demonstrated that the tobacco-specific carcinogen NNK can trigger higher PD-L1 expression and cause primarily lung adenoma in mice (West et al., 2004, Lastwika et al., 2016). Moreover, a meta-analysis of mRNA expression profile identified EP400NL being upregulated in lung adenocarcinoma tissue from the cancer patients who have a smoking history (He et al., 2018). Multiple transcription factors and epigenetic protein complexes including the hNuA4, EP400, and BRG1-containing BAF complexes have been identified as interacting partners with Myc to induce and maintain cancerous phenotypes (McMahon et al., 1998, Park et al., 2001, Fuchs et al., 2001, Nikiforov et al., 2002, Park et al., 2002, Frank et al., 2003, Liu et al., 2003, Cowling and Cole, 2006, Vita and Henriksson, 2006, Tworkowski et al., 2008, Yamada, 2012, Zhao et al., 2017).

This research suggests that EP400NL forms a unique nuclear complex with BRG1 and contributes to serum-mediated PD-L1 gene expression, providing a potential therapeutic target to suppress cancer-associated PD-L1 gene expression.

7. SUMMARY

Functional characterization of EP400NL in chromatin remodelling and transcriptional regulation was conducted in this research project. Although previously annotated as a pseudogene, EP400NL encodes an expressed protein that forms a hNuA4-like chromatin remodelling complex. This complex differs from EP400 in that it lacks both the TIP60 histone acetyltransferase as well as the EP400 ATPase. EP400NL displays extremely high protein sequence similarity up to 92% to the N-terminal domain of its homologous gene EP400 and associates with multiple functional proteins found in the hNuA4 complex including BRD8, BAF53, DMAP1, GAS41, MRG15, MRGBP, RuvBL1, and RuvBL2, suggesting the EP400NL complex may share similar nuclear functions to the novel hNuA4 complex.

Despite no histone acetyltransferase activity being detected, which is consistent with the lack of TIP60 histone acetyltransferase in the complex from the mass spectrometric analysis, the novel complex can exchange ATP-dependent H2A.Z-H2B dimers *in vitro.* This further supports the coactivator function of EP400NL under serum stimulation, specifically in serum and IFNγ-mediated PD-L1 gene activation, by depositing the histone variant H2A.Z into an artificial nucleosomal substrate *in vitro.*

EP400 stabilizes Myc to enhance Myc targeted gene expression (Tworkowski et al., 2008, Zhao et al., 2017), therefore, a luciferase reporter system was developed to examine if EP400NL induces gene expression in a Myc-dependent manner. In this reporter assay, four deletion mutants of EP400NL were generated based on InterPro prediction and used to compare with the full-length EP400NL to explore its transcriptional regulatory function. Two deletion mutants (Δ246-260) and (Δ360-419), which overlap with the EP400 homology domain, significantly reduced GAL4-Myc activity compared to the full-length EP400NL (1-419),

indicating that the two deleted regions may be essential for transcriptional coactivation.

Myc directly binds to the promoter region of PD-L1 for increased expression level (Kim et al., 2017), since EP400NL promotes reporter gene activity in a Myc dependent manner, it was investigated whether the EP400NL nuclear complex can be recruited to the PD-L1 promoter in a serum-dependent manner given previous studies had shown serum stimulation positively regulates Myc expression (Dean et al., 1986, Richman and Hayday, 1989a, Perna et al., 2012). ChIP assays confirmed this hypothesis by showing EP400NL and the associated three core ATPases (BRG1, RuvBL1, and RuvBL2) were all significantly enriched at the promoter region of the targeted PD-L1 gene under serum stimulation.

Expression of EP400NL resulted in a 3.2-fold increase in PD-L1 mRNA in the presence of serum stimulation. Conversely, the polyclonal EP400NL indel cells showed compromised transcript induction profiles with only about 30-fold at the same time interval compared to the control cells which displayed a 100-fold increase. These results indicate that EP400NL requires simultaneous signals from serum treatment to exert its strong coactivator function in the activation of PD-L1. On the other hand, the loss of function studies using CRISPR/Cas9-mediated indels confirm the critical role of EP400NL in driving serum mediated PD-L1 transactivation.

However, despite the upregulated PD-L1 protein expression under both serum stimulation and tetracycline induction, the protein levels of PD-L1 in the EP400NL indel mutation cells remained unchanged, as did Myc protein levels under serum stimulation, indicating that EP400NL does not co-activate Myc in this *in vitro* system. It is therefore likely that EP400NL interacts with other unknown factors in the serum for upregulating PD-L1 expression and seeking those EP400NL interactors in the serum require further investigation.

Taken together, these data suggest that EP400NL promotes transcriptional upregulation by forming a functional protein complex that deposits H2A.Z onto the nucleosomes in an ATP-dependent manner and transforms the closed chromatin into a relaxed open structure. EP400NL complex subsequently coordinates cMyc by binding to the target gene promoter together with multiple additional functional protein candidates such as the ATPases RuvBL1/2 and BRG1 for regulating target gene expression (Figure 7. 1). Interestingly, BRG1 has not been identified as a component of either the hNuA4 complex or EP400 complex which suggests that the EP400NL containing complex may exhibit unique nuclear activities.

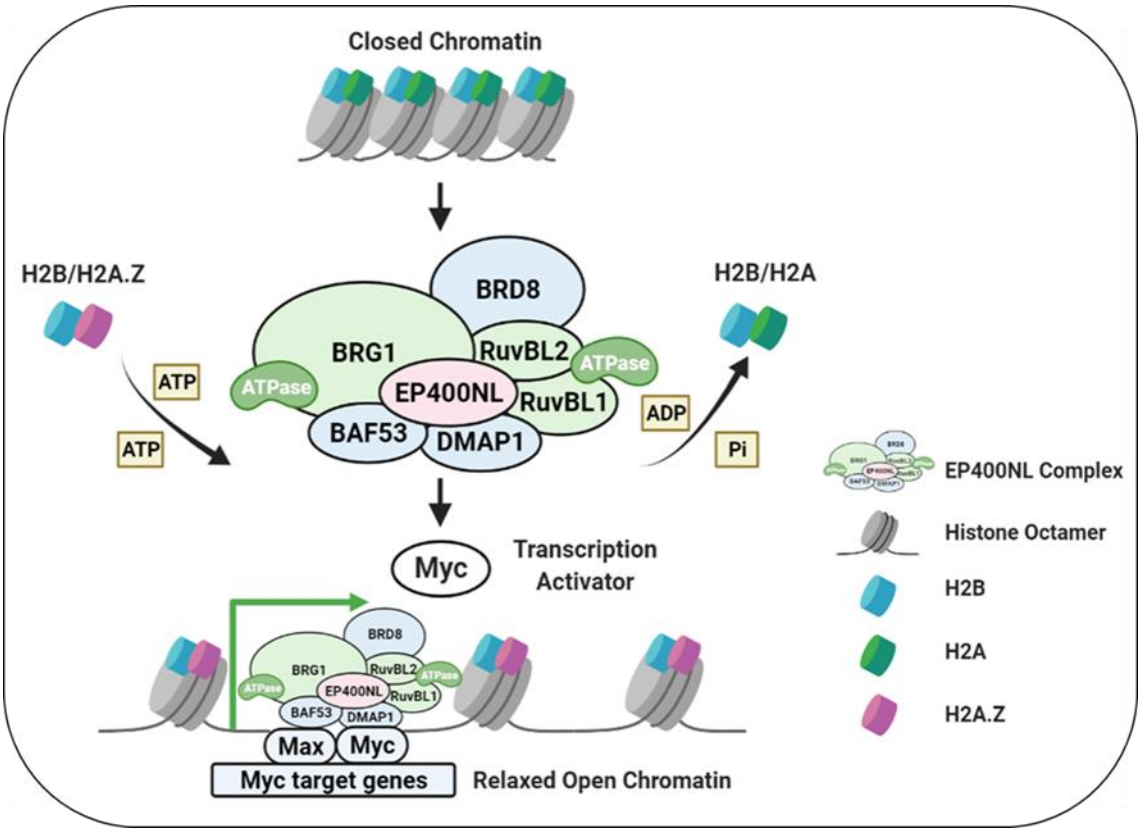

Figure 7. 1 Working model of cMyc-dependent recruitment of EP400NL complex and transcriptional activation of target genes

EP400NL forms a unique chromatin remodelling complex that can transform closed chromatin into open chromatin via its ATP-dependent H2A.Z deposition activity. Sequence-specific DNA binding transcription activators such as Myc recruit the EP400NL complex at the target promoter to allow localised chromatin remodelling for transcriptional activation.

7. 1 CONCLUSION AND FUTURE DIRECTIONS

In this study, we found EP400NL forms a chromatin-remodelling complex similar to the hNuA4 histone acetyltransferase complex or EP400 complex but with a unique interaction with BRG1. EP400NL is not an ATPase and displays no histone acetyltransferase activity, but our studies demonstrate that its nuclear multi-protein complex can catalyse an ATP-dependent H2A.Z deposition which may be due to the association with multiple ATPases including RuvBL1, RuvBL2, and BRG1. In addition, upregulation of EP400NL enhances PD-L1 gene expression mediated by cMyc and IFNγ-regulated transcription factors. Collectively, our studies show that EP400NL plays a role as a transcription coactivator for both cMyc and IFNγ mediated gene expression and provides a potential target to modulate PD-L1 expression in cancer immunotherapy.

EP400NL is only 13.4% the size of EP400 but with a 92% sequence similarity to the N-terminal domain of the EP400. Despite being annotated as an EP400 pseudogene 1 (EP400P1), not only can it be transcribed and translated but the data presented in this thesis show that the EP400NL complex exhibits H2A.Z deposition activity. Moreover, unlike its neighbouring paralog, EP400, it is a novel transcriptional activation complex with a unique interaction with BRG1.

Future studies should be conducted *in vivo* (cultured cells or animal models) to determine whether EP00NL deposits H2A.Z *in vivo* and if this is required for PD-L1 transcriptional activation. Moreover, it would be also pertinent to determine whether BRG1 or RuVBL1/2 directly contribute to the ATP-dependent exchange of H2A.Z-H2B. Since neither the presence of EP400 nor EP400NL was detected from an anti-EP400NL or an anti-EP400 immunoblot after immunoprecipitation (Figure 4. 14). Given the fact that EP400NL-associated proteins incorporate H2A.Z into the assembled chromatin, thus, in addition to the EP400NL associated ATPases such as BRG1 or RuVBL1/2, future investigations need to be carried

out to understand if SRCAP or other known H2A.Z-incorporating enzymes can potentially interact with EP400NL.

Given that most experiments in this research rely on the overexpression of EP400NL, the function of the endogenous protein should be investigated in the future. Even though the expression of the endogenous EP400NL and the TAP-EP400NL are both enriched in the soluble nuclear fraction, they do not seem to have the same partitions between the various fractions (Figure 3. 5, left panel). It is an important point given that it may indicate that the overexpressed protein does not completely recapitulate features of the endogenous protein. The established polyclonal EP400NL indel mutation cells provided some insights on how the partial loss of the endogenous expression of EP400NL affects the transcriptional regulation of both Myc and IFNγ mediated PD-L1 expression. Further studies using monoclonal EP400NL indel cells would provide more solid evidence to show how the complete loss of the endogenous expression of EP400NL defects the transcription, it would be meaningful to further confirm if the ectopic expression of EP400NL complements the defects observed in the genome-edited cell line by CRISPR/Cas9.

A different approach to investigating the loss of function of EP400NL in transcription is by using the deletion mutants of EP400NL, two deletion mutants (Δ246-260 and Δ360-419) which are defective for GAL4Myc co-activator activity were found from the dual luciferase assay (Figure 5. 12 and Figure 5. 13). These data indicate that these two regions might be critical for interacting with BAF53 for the oncogenic transformation and Myc mediated transcription. As the assumption of EP400NL being one of the coactivators of Myc which is a global transcription factor, EP400NL needs to be colocalized with Myc in the nuclei for participating in multiple Myc mediated nuclear events. Regardless of the technical difficulties in the explicit separation between the cytoplasmic and the soluble nuclear fractions which may cause such observations: a very low level of endogenous EP400NL was detected in the cytoplasmic fraction from the

fractionation results despite both the endogenous EP400NL and the induced TAP-EP400NL is predominantly from the soluble nuclear fraction. Thus, deciphering the subcellular localization of these mutants might answer questions including if these mutants are unable to be transported back into the nuclei after being produced in the cytoplasm as lacking these domains or if they are more likely to shuffle between the nuclei and cytoplasmic rather than stabilized in the nuclei due to the lack of these two specific regions comparing to the full-length EP400NL. Since dimerized Myc/Max binds specifically to the E-box of the promoter region for promoting Myc targeted PD-L1 expression, it is of interest to investigate if EP400NL coactivates PD-L1 expression in a Myc dependent manner when the E-box region was either mutated or deleted. The coactivator function of EP400NL was also studied by exploiting cell proliferation assays. The proliferation rate significantly increased under both serum stimulation and tetracycline induction in Flp-In™ T-REx™ cells and correspondingly decreased when EP400NL was indel mutated by CRISPR/Cas9 in H1299 cells. To apply this result and connect it to the field of translational research, other non-small cell lung cancer cell lines such as (H1437, H1568, and H1395) which exhibit comparable PD-L1 expression should be tested to see if the loss of EP400NL can decrease the proliferation rate and potentially slow the process of the cancer progression.

Gene expression profiling of 54 tissues from GTEx RNA-sequence shows that EP400 is ubiquitously expressed at a high level in many tissues whereas higher EP400NL expression is restricted only in the testis and pituitary gland, suggesting a specialised function in those tissues. The exon regions of EP400NL are highly conserved across mammals, suggesting that the unique function is conferred by EP400NL may not be redundant with EP400. Although EP400NL modifies Myc and IFNγ mediated PD-L1 expression by forming a unique nuclear complex, the specific functional domains and direct binding partners of EP400NL remain to be identified. Therefore, elucidating the binding domains of EP400NL and how these

interacting candidate proteins are recruited into the complex will be a focus of future work. Thus, investigation of EP400NL-induced whole transcriptome changes and genome-wide ChIP-sequencing will provide better insight into how EP400NL contributes to human epigenome maintenance and gene regulation, especially in connection with Myc-dependent cellular proliferation and oncogenic transformation.

8. BIBLIOGRAPHY

Aasland, R., Stewart, A. F. & Gibson, T. 1996. The SANT domain: A putative DNA-binding domain in the SWI-SNF and ADA complexes, the transcriptional corepressor N-CoR and TFIIIB. *Trends in Biochemical Sciences,* 21, 87-88. Available: Doi 10.1016/S0968-0004(96)30009-1

Adams, C. C. & Workman, J. L. 1995. Binding of disparate transcriptional activators to nucleosomal DNA is inherently cooperative. *Mol Cell Biol,* 15, 1405-21. Available: 10.1128/mcb.15.3.1405

Ahmad, K. & Henikoff, S. 2002. The histone variant H3.3 marks active chromatin by replication-independent nucleosome assembly. *Mol Cell,* 9, 1191-200.

Akbay, E. A., Koyama, S., Carretero, J., Altabef, A., Tchaicha, J. H., Christensen, C. L., Mikse, O. R., Cherniack, A. D., Beauchamp, E. M., Pugh, T. J., Wilkerson, M. D., Fecci, P. E., Butaney, M., Reibel, J. B., Soucheray, M., Cohoon, T. J., Janne, P. A., Meyerson, M., Hayes, D. N., Shapiro, G. I., Shimamura, T., Sholl, L. M., Rodig, S. J., Freeman, G. J., Hammerman, P. S., Dranoff, G. & Wong, K. K. 2013. Activation of the PD-1 Pathway Contributes to Immune Escape in EGFR-Driven Lung Tumors. *Cancer Discovery,* 3, 1355-1363. Available: 10.1158/2159-8290.Cd-13-0310

Akhtar, A., Zink, D. & Becker, P. B. 2000. Chromodomains are protein-RNA interaction modules. *Nature,* 407, 405-409. Available: Doi 10.1038/35030169

Alatwi, H. E. & Downs, J. A. 2015. Removal of H2A.Z by INO80 promotes homologous recombination. *Embo Reports,* 16, 986-994.

Allard, S., Utley, R. T., Savard, J., Clarke, A., Grant, P., Brandl, C. J., Pillus, L., Workman, J. L. & Cote, J. 1999. NuA4, an essential transcription adaptor/histone H4 acetyltransferase complex containing Esa1p and the ATM-related cofactor Tra1p. *Embo Journal,* 18, 5108-5119. Available: DOI 10.1093/emboj/18.18.5108

Allis, C. D. & Jenuwein, T. 2016. The molecular hallmarks of epigenetic control. *Nature Reviews Genetics,* 17, 487-500. Available: 10.1038/nrg.2016.59

Altaf, M., Auger, A., Monnet-Saksouk, J., Brodeur, J., Piquet, S., Cramet, M., Bouchard, N., Lacoste, N., Utley, R. T., Gaudreau, L. & Cote, J. 2010. NuA4-dependent Acetylation of Nucleosomal Histones H4 and H2A Directly Stimulates Incorporation of H2A.Z by the SWR1 Complex. *Journal of Biological Chemistry,* 285, 15966-15977. Available: 10.1074/jbc.M110.117069

Alvisi, G., Paolini, L., Contarini, A., Zambarda, C., Di Antonio, V., Colosini, A., Mercandelli, N., Timmoneri, M., Palu, G., Caimi, L., Ricotta, D. & Radeghieri, A. 2018. Intersectin goes nuclear: secret life of an endocytic protein. *Biochemical Journal,* 475, 1455-1472. Available: 10.1042/Bcj20170897

Annunziato, A. T. 2005. Split decision: What happens to nucleosomes during DNA replication? *Journal of Biological Chemistry,* 280, 12065-12068. Available: 10.1074/jbc.R400039200

Antonangeli, F., Natalini, A., Garassino, M. C., Sica, A., Santoni, A. & Di Rosa, F. 2020. Regulation of PD-L1 Expression by NF-kappa B in Cancer. *Frontiers in Immunology,* 11. Available: ARTN 584626

Baek, H. J., Kang, Y. K. & Roeder, R. G. 2006. Human mediator enhances basal transcription by facilitating recruitment of transcription factor IIB during preinitiation complex assembly. *Journal of Biological Chemistry,* 281, 15172-15181. Available: 10.1074/jbc.M601983200

Baek, H. J., Malik, S., Qin, J. & Roeder, R. G. 2002. Requirement of TRAP/mediator for both activator-independent and activator-dependent transcription in conjunction with TFIID-associated TAF(II)s. *Molecular and Cellular Biology,* 22, 2842-2852. Available: 10.1128/Mcb.22.8.2842.2852.2002

Bayley, S. T. & Mymryk, J. S. 1994. Adenovirus E1a Proteins and Transformation (Review). *International Journal of Oncology,* 5, 425-444.

Ben-Israel, H. & Kleinberger, T. 2002. Adenovirus and cell cycle control. *Front Biosci,* 7, d1369-95.

Bhaumik, S. R. & Green, M. R. 2001. SAGA is an essential in vivo target of the yeast acidic activator Gal4p. *Genes Dev,* 15, 1935-45. Available: 10.1101/gad.911401

Billon, P. & Cote, J. 2012. Precise deposition of histone H2A.Z in chromatin for genome expression and maintenance. *Biochimica Et Biophysica Acta-Gene Regulatory Mechanisms,* 1819, 290-302. Available: 10.1016/j.bbagrm.2011.10.004

Bird, A. W., Yu, D. Y., Pray-Grant, M. G., Qiu, Q. F., Harmon, K. E., Megee, P. C., Grant, P. A., Smith, M. M. & Christman, M. F. 2002. Acetylation of histone H4 by Esa1 is required for DNA double-strand break repair. *Nature,* 419, 411-415. Available: 10.1038/nature01035

Blackwood, E. M. & Eisenman, R. N. 1991. Max: a helix-loop-helix zipper protein that forms a sequence-specific DNA-binding complex with Myc. *Science,* 251, 1211-7. Available: 10.1126/science.2006410

Bouchard, C., Thieke, K., Maier, A., Saffrich, R., Hanley-Hyde, J., Ansorge, W., Reed, S., Sicinski, P., Bartek, J. & Eilers, M. 1999. Direct induction of cyclin D2 by Myc contributes to cell cycle progression and sequestration of p27. *EMBO J,* 18, 5321-33. Available: 10.1093/emboj/18.19.5321

Brown, C. E., Lechner, T., Howe, L. & Workman, J. L. 2000. The many HATs of transcription coactivators. *Trends in Biochemical Sciences,* 25, 15-19. Available: Doi 10.1016/S0968-0004(99)01516-9

Bruce, D. L., Macartney, T., Yong, W., Shou, W. & Sapkota, G. P. 2012. Protein phosphatase 5 modulates SMAD3 function in the transforming growth factor-beta pathway. *Cell Signal,* 24, 1999-2006. Available: 10.1016/j.cellsig.2012.07.003

Bruno, M., Flaus, A., Stockdale, C., Rencurel, C., Ferreira, H. & Owen-Hughes, T. 2003. Histone H2A/H2B dimer exchange by ATP-dependent chromatin remodeling activities. *Mol Cell,* 12, 1599-606.

Buchanan, L., Durand-Dubief, M., Roguev, A., Sakalar, C., Wilhelm, B., Stralfors, A., Shevchenko, A., Aasland, R., Shevchenko, A., Ekwall, K. & Stewart, A. F. 2009. The Schizosaccharomyces pombe JmjC-Protein, Msc1, Prevents H2A.Z Localization in Centromeric and Subtelomeric Chromatin Domains. *Plos Genetics,* 5. Available: ARTN e1000726

Bulger, M., Ito, T., Kamakaka, R. T. & Kadonaga, J. T. 1995. Assembly of Regularly Spaced Nucleosome Arrays by Drosophila Chromatin Assembly Factor-1 and a 56-Kda Histone-Binding Protein. *Proceedings of the National Academy of*

Sciences of the United States of America, 92, 11726-11730. Available: DOI 10.1073/pnas.92.25.11726

Buschbeck, M. & Hake, S. B. 2017. Variants of core histones and their roles in cell fate decisions, development and cancer. *Nature Reviews Molecular Cell Biology,* 18, 299-314. Available: 10.1038/nrm.2016.166

Cai, Y., Jin, J., Tomomori-Sato, C., Sato, S., Sorokina, I., Parmely, T. J., Conaway, R. C. & Conaway, J. W. 2003a. Identification of new subunits of the multiprotein mammalian TRRAP/TIP60-containing histone acetyltransferase complex. *J Biol Chem,* 278, 42733-6. Available: 10.1074/jbc.C300389200

Cao, X. B., Zhao, Y., Wang, J., Dai, B. B., Gentile, E., Lin, J., Pu, X. X., Ji, L., Wu, S. H., Meraz, I., Majidi, M. & Roth, J. A. 2017b. TUSC2 downregulates PD-L1 expression in non-small cell lung cancer (NSCLC). *Oncotarget,* 8, 107621-107629. Available: 10.18632/oncotarget.22581

Carlson, M., Osmond, B. C., Neigeborn, L. & Botstein, D. 1984. A Suppressor of Snf1 Mutations Causes Constitutive High-Level Invertase Synthesis in Yeast. *Genetics,* 107, 19-32.

Casey, S. C., Tong, L., Li, Y. L., Do, R., Walz, S., Fitzgerald, K. N., Gouw, A. M., Baylot, V., Gutgemann, I., Eilers, M. & Felsher, D. W. 2016. MYC regulates the antitumor immune response through CD47 and PD-L1. *Science,* 352, 227-231. Available: 10.1126/science.aac9935

Cavalheiro, G. R., Matos-Rodrigues, G. E., Zhao, Y., Gomes, A. L., Anand, D., Predes, D., de Lima, S., Abreu, J. G., Zheng, D., Lachke, S. A., Cvekl, A. & Martins, R. A. P. 2017. N-myc regulates growth and fiber cell differentiation in lens development. *Dev Biol,* 429, 105-117. Available: 10.1016/j.ydbio.2017.07.002

Chakraborty, A. A. & Tansey, W. P. 2009. Adenoviral E1A Function through Myc. *Cancer Research,* 69, 6-9. Available: 10.1158/0008-5472.Can-08-3026

Chen, J., Jiang, C. C., Jin, L. & Zhang, X. D. 2016. Regulation of PD-L1: a novel role of pro-survival signalling in cancer. *Annals of Oncology,* 27, 409-416. Available: 10.1093/annonc/mdv615

Chen, J. & Stubbe, J. 2005. Bleomycins: towards better therapeutics. *Nat Rev Cancer,* 5, 102-12. Available: 10.1038/nrc1547

Chen, J. G. & Archer, T. K. 2005. Regulating SWI/SNF subunit levels via protein-protein interactions and proteasomal degradation: BAF155 and BAF170 limit expression of BAF57. *Molecular and Cellular Biology,* 25, 9016-9027. Available: 10.1128/Mcb.25.20.9016-9027.2005

Chen, P., Zhao, J., Wang, Y., Wang, M., Long, H., Liang, D., Huang, L., Wen, Z., Li, W., Li, X., Feng, H., Zhao, H., Zhu, P., Li, M., Wang, Q. F. & Li, G. 2013a. H3.3 actively marks enhancers and primes gene transcription via opening higher-ordered chromatin. *Genes Dev,* 27, 2109-24. Available: 10.1101/gad.222174.113

Chen, P., Zhao, J. C., Wang, Y., Wang, M., Long, H. Z., Liang, D., Huang, L., Wen, Z. Q., Li, W., Li, X., Feng, H. L., Zhao, H. Y., Zhu, P., Li, M., Wang, Q. F. & Li, G. H. 2013b. H3.3 actively marks enhancers and primes gene transcription via opening higher-ordered chromatin. *Genes & Development,* 27, 2109-2124. Available: 10.1101/gad.222174.113

Chiu, L. Y., Gong, F. D. & Miller, K. M. 2017. Bromodomain proteins: repairing DNA damage within chromatin. *Philosophical Transactions of the Royal Society B-Biological Sciences,* 372. Available: ARTN 20160286

Choi, J., Heo, K. & An, W. J. 2009. Cooperative action of TIP48 and TIP49 in H2A.Z exchange catalyzed by acetylation of nucleosomal H2A. *Nucleic Acids Research,* 37, 5993-6007. Available: 10.1093/nar/gkp660

Clapier, C. R., Iwasa, J., Cairns, B. R. & Peterson, C. L. 2017. Mechanisms of action and regulation of ATP-dependent chromatin-remodelling complexes. *Nature Reviews Molecular Cell Biology,* 18, 407-422. Available: 10.1038/nrm.2017.26

Cole, M. D. & McMahon, S. B. 1999. The Myc oncoprotein: a critical evaluation of transactivation and target gene regulation. *Oncogene,* 18, 2916-2924. Available: DOI 10.1038/sj.onc.1202748

Cote, J., Quinn, J., Workman, J. L. & Peterson, C. L. 1994. Stimulation of GAL4 derivative binding to nucleosomal DNA by the yeast SWI/SNF complex. *Science,* 265, 53-60. Available: 10.1126/science.8016655

Courilleau, C., Chailleux, C., Jauneau, A., Grimal, F., Briois, S., Boutet-Robinet, E., Boudsocq, F., Trouche, D. & Canitrot, Y. 2012. The chromatin remodeler p400 ATPase facilitates Rad51-mediated repair of DNA double-strand breaks. *J Cell Biol,* 199, 1067-81. Available: 10.1083/jcb.201205059

Cowling, V. H. & Cole, M. D. 2006. Mechanism of transcriptional activation by the Myc oncoproteins. *Semin Cancer Biol,* 16, 242-52. Available: 10.1016/j.semcancer.2006.08.001

Dang, C. V. 2012. MYC on the Path to Cancer. *Cell,* 149, 22-35. Available: 10.1016/j.cell.2012.03.003

Dean, M., Levine, R. A., Ran, W., Kindy, M. S., Sonenshein, G. E. & Campisi, J. 1986. Regulation of c-myc transcription and mRNA abundance by serum growth factors and cell contact. *J Biol Chem,* 261, 9161-6.

DeSantis, C. E., Lin, C. C., Mariotto, A. B., Siegel, R. L., Stein, K. D., Kramer, J. L., Alteri, R., Robbins, A. S. & Jemal, A. 2014. Cancer Treatment and Survivorship Statistics, 2014. *Ca-a Cancer Journal for Clinicians,* 64, 252-271. Available: 10.3322/caac.21235

Doyon, Y. & Cote, J. 2004a. The highly conserved and multifunctional NuA4 HAT complex. *Current Opinion in Genetics & Development,* 14, 147-154. Available: 10.1016/j.gde.2004.02.009

Doyon, Y., Selleck, W., Lane, W. S., Tan, S. & Cote, J. 2004. Structural and functional conservation of the NuA4 histone acetyltransferase complex from yeast to humans. *Mol Cell Biol,* 24, 1884-96. Available: 10.1128/mcb.24.5.1884-1896.2004

Dryhurst, D., Ishibashi, T., Rose, K. L., Eirin-Lopez, J. M., McDonald, D., Silva-Moreno, B., Veldhoen, N., Helbing, C. C., Hendzel, M. J., Shabanowitz, J., Hunt, D. F. & Ausio, J. 2009. Characterization of the histone H2A.Z-1 and H2A.Z-2 isoforms in vertebrates. *Bmc Biology,* 7. Available: Artn 86

Dunn, C. J., Sarkar, P., Bailey, E. R., Farris, S., Zhao, M. L., Ward, J. M., Dudek, S. M. & Saha, R. N. 2017. Histone Hypervariants H2A.Z.1 and H2A.Z.2 Play Independent and Context-Specific Roles in Neuronal Activity-Induced Transcription of Arc/Arg3.1 and Other Immediate Early Genes. *Eneuro,* 4. Available: UNSP e0040-17.2017

Eilers, M. & Eisenman, R. N. 2008. Myc's broad reach. *Genes Dev,* 22, 2755-66. Available: 10.1101/gad.1712408

El Hadidy, N. & Uversky, V. N. 2019. Intrinsic Disorder of the BAF Complex: Roles in Chromatin Remodeling and Disease Development. *International Journal of Molecular Sciences,* 20. Available: ARTN 5260

Elsesser, O., Frob, F., Kuspert, M., Tamm, E. R., Fujii, T., Fukunaga, R. & Wegner, M. 2019. Chromatin remodeler Ep400 ensures oligodendrocyte survival and is required for myelination in the vertebrate central nervous system. *Nucleic Acids Research,* 47, 6208-6224. Available: 10.1093/nar/gkz376

Engeholm, M., de Jager, M., Flaus, A., Brenk, R., van Noort, J. & Owen-Hughes, T. 2009. Nucleosomes can invade DNA territories occupied by their neighbors. *Nature Structural & Molecular Biology,* 16, 151-158. Available: 10.1038/nsmb.1551

Euskirchen, G., Auerbach, R. K. & Snyder, M. 2012a. SWI/SNF chromatin-remodeling factors: multiscale analyses and diverse functions. *J Biol Chem,* 287, 30897-905. Available: 10.1074/jbc.R111.309302

Farris, S. D., Rubio, E. D., Moon, J. J., Gombert, W. M., Nelson, B. H. & Krumm, A. 2005. Transcription-induced chromatin remodeling at the c-myc gene involves the local exchange of histone H2A.Z. *Journal of Biological Chemistry,* 280, 25298-25303. Available: 10.1074/jbc.M501784200

Fazzio, T. G., Huff, J. T. & Panning, B. 2008. An RNAi screen of chromatin proteins identifies Tip60-p400 as a regulator of embryonic stem cell identity. *Cell,* 134, 162-74. Available: 10.1016/j.cell.2008.05.031

Fernandez, P. C., Frank, S. R., Wang, L. Q., Schroeder, M., Liu, S. X., Greene, J., Cocito, A. & Amati, B. 2003. Genomic targets of the human c-Myc protein. *Genes & Development,* 17, 1115-1129. Available: 10.1101/gad.1067003

Flaus, A. & Owen-Hughes, T. 2004. Mechanisms for ATP-dependent chromatin remodelling: farewell to the tuna-can octamer? *Curr Opin Genet Dev,* 14, 165-73. Available: 10.1016/j.gde.2004.01.007

Frank, S. R., Parisi, T., Taubert, S., Fernandez, P., Fuchs, M., Chan, H. M., Livingston, D. M. & Amati, B. 2003. MYC recruits the TIP60 histone acetyltransferase complex to chromatin. *Embo Reports,* 4, 575-580. Available: 10.1038/sj.embor.embor861

Frank, S. R., Schroeder, M., Fernandez, P., Taubert, S. & Amati, B. 2001. Binding of c-Myc to chromatin mediates mitogen-induced acetylation of histone H4 and gene activation. *Genes & Development,* 15, 2069-2082. Available: DOI 10.1101/gad.906601

Fuchs, M., Gerber, J., Drapkin, R., Sif, S., Ikura, T., Ogryzko, V., Lane, W. S., Nakatani, Y. & Livingston, D. M. 2001. The p400 complex is an essential E1A transformation target. *Cell,* 106, 297-307. Available: 10.1016/s0092-8674(01)00450-0

Fujisawa, T. & Filippakopoulos, P. 2017. Functions of bromodomain-containing proteins and their roles in homeostasis and cancer. *Nature Reviews Molecular Cell Biology,* 18, 246-262. Available: 10.1038/nrm.2016.143

Gallant, P. 2005. Myc, cell competition, and compensatory proliferation. *Cancer Res,* 65, 6485-7. Available: 10.1158/0008-5472.CAN-05-1101

Garcia-Diaz, A., Shin, D. S., Moreno, B. H., Saco, J., Escuin-Ordinas, H., Rodriguez, G. A., Zaretsky, J. M., Sun, L., Hugo, W., Wang, X. Y., Parisi, G., Saus, C. P., Torrejon, D. Y., Graeber, T. G., Comin-Anduix, B., Hu-Lieskovan, S.,

Damoiseaux, R., Lo, R. S. & Ribas, A. 2019. Interferon Receptor Signaling Pathways Regulating PD-L1 and PD-L2 Expression (vol 19, pg 1189, 2017). *Cell Reports,* 29, 3766-3766. Available: 10.1016/j.celrep.2019.11.113

Garcia-Gutierrez, L., Delgado, M. D. & Leon, J. 2019. MYC Oncogene Contributions to Release of Cell Cycle Brakes. *Genes,* 10. Available: ARTN 244

Gargano, B., Amente, S., Majello, B. & Lania, L. 2007. P-TEFb is a crucial co-factor for Myc transactivation. *Cell Cycle,* 6, 2031-2037. Available: DOI 10.4161/cc.6.16.4554

Gerstein, M. B., Kundaje, A., Hariharan, M., Landt, S. G., Yan, K. K., Cheng, C., Mu, X. J., Khurana, E., Rozowsky, J., Alexander, R., Min, R. Q., Alves, P., Abyzov, A., Addleman, N., Bhardwaj, N., Boyle, A. P., Cayting, P., Charos, A., Chen, D. Z., Cheng, Y., Clarke, D., Eastman, C., Euskirchen, G., Frietze, S., Fu, Y., Gertz, J., Grubert, F., Harmanci, A., Jain, P., Kasowski, M., Lacroute, P., Leng, J., Lian, J., Monahan, H., O'Geen, H., Ouyang, Z. Q., Partridge, E. C., Patacsil, D., Pauli, F., Raha, D., Ramirez, L., Reddy, T. E., Reed, B., Shi, M. Y., Slifer, T., Wang, J., Wu, L. F., Yang, X. Q., Yip, K. Y., Zilberman-Schapira, G., Batzoglou, S., Sidow, A., Farnham, P. J., Myers, R. M., Weissman, S. M. & Snyder, M. 2012. Architecture of the human regulatory network derived from ENCODE data. *Nature,* 489, 91-100. Available: 10.1038/nature11245

Gevry, N., Chan, H. M., Laflamme, L., Livingston, D. M. & Gaudreau, L. 2007. p21 transcription is regulated by differential localization of histone H2A.Z. *Genes Dev,* 21, 1869-81. Available: 10.1101/gad.1545707

Ghosh, K., Tang, M., Kumari, N., Nandy, A., Basu, S., Mall, D. P., Rai, K. & Biswas, D. 2018. Positive Regulation of Transcription by Human ZMYND8 through Its Association with P-TEFb Complex. *Cell Reports,* 24, 2141-+. Available: 10.1016/j.celrep.2018.07.064

Giaimo, B. D., Ferrante, F., Herchenrother, A., Hake, S. B. & Borggrefe, T. 2019. The histone variant H2A.Z in gene regulation. *Epigenetics & Chromatin,* 12. Available: ARTN 37

Goldberg, A. D., Banaszynski, L. A., Noh, K. M., Lewis, P. W., Elsaesser, S. J., Stadler, S., Dewell, S., Law, M., Guo, X. Y., Li, X., Wen, D. C., Chapgier, A., DeKelver, R. C., Miller, J. C., Lee, Y. L., Boydston, E. A., Holmes, M. C., Gregory, P. D., Greally, J. M., Rafii, S., Yang, C. W., Scambler, P. J., Garrick, D., Gibbons, R. J., Higgs, D. R., Cristea, I. M., Urnov, F. D., Zheng, D. Y. & Allis, C. D. 2010. Distinct Factors Control Histone Variant H3.3 Localization at Specific Genomic Regions. *Cell,* 140, 678-691. Available: 10.1016/j.cell.2010.01.003

Gong, J., Chehrazi-Raffle, A., Reddi, S. & Salgia, R. 2018. Development of PD-1 and PD-L1 inhibitors as a form of cancer immunotherapy: a comprehensive review of registration trials and future considerations. *Journal for Immunotherapy of Cancer,* 6. Available: ARTN 8

Goodman, R. H. & Smolik, S. 2000. CBP/p300 in cell growth, transformation, and development. *Genes & Development,* 14, 1553-1577.

Gowrishankar, K., Gunatilake, D., Gallagher, S., Tiffen, J. & Hersey, P. 2014. Regulation of PD-L1 expression in human melanoma by NF-kappa B. *Cancer Research,* 74. Available: 10.1158/1538-7445.Am2014-2947

Grant, P. A., Duggan, L., Cote, J., Roberts, S. M., Brownell, J. E., Candau, R., Ohba, R., OwenHughes, T., Allis, C. D., Winston, F., Berger, S. L. & Workman, J. L. 1997. Yeast Gcn5 functions in two multisubunit complexes to acetylate nucleosomal histones: Characterization of an Ada complex and the SAGA (Spt/Ada) complex. *Genes & Development,* 11, 1640-1650. Available: DOI 10.1101/gad.11.13.1640

Guccione, E., Martinato, F., Finocchiaro, G., Luzi, L., Tizzoni, L., Dall' Olio, V., Zardo, G., Nervi, C., Bernard, L. & Amati, B. 2006a. Myc-binding-site recognition in the human genome is determined by chromatin context. *Nat Cell Biol,* 8, 764-70. Available: 10.1038/ncb1434

Hahn, S. 2004. Structure and mechanism of the RNA polymerase II transcription machinery. *Nat Struct Mol Biol,* 11, 394-403. Available: 10.1038/nsmb763

Haiman, C. A., Le Marchand, L., Yamamato, J., Stram, D. O., Sheng, X., Kolonel, L. N., Wu, A. H., Reich, D. & Henderson, B. E. 2007. A common genetic risk factor for colorectal and prostate cancer. *Nature Genetics,* 39, 954-956. Available: 10.1038/ng2098

Hainer, S. J. & Fazzio, T. G. 2015. Regulation of Nucleosome Architecture and Factor Binding Revealed by Nuclease Footprinting of the ESC Genome. *Cell Reports,* 13, 61-69. Available: 10.1016/j.celrep.2015.08.071

Hake, S. B., Garcia, B. A., Duncan, E. M., Kauer, M., Dellaire, G., Shabanowitz, J., Bazett-Jones, D. P., Allis, C. D. & Hunt, D. F. 2006. Expression patterns and post-translational modifications associated with mammalian histone H3 variants. *Journal of Biological Chemistry,* 281, 559-568. Available: DOI 10.1074/jbc.M509266200

Han, Y., Luo, J., Ranish, J. & Hahn, S. 2014. Architecture of the Saccharomyces cerevisiae SAGA transcription coactivator complex. *EMBO J,* 33, 2534-46. Available: 10.15252/embj.201488638

Hart, T., Chandrashekhar, M., Aregger, M., Steinhart, Z., Brown, K. R., MacLeod, G., Mis, M., Zimmermann, M., Fradet-Turcotte, A., Sun, S., Mero, P., Dirks, P., Sidhu, S., Roth, F. P., Rissland, O. S., Durocher, D., Angers, S. & Moffat, J. 2015. High-Resolution CRISPR Screens Reveal Fitness Genes and Genotype-Specific Cancer Liabilities. *Cell,* 163. Available: 10.1016/j.cell.2015.11.015

Hayward, W. S., Neel, B. G. & Astrin, S. M. 1981. Activation of a cellular onc gene by promoter insertion in ALV-induced lymphoid leukosis. *Nature,* 290, 475-80. Available: 10.1038/290475a0

He, X. & Xu, C. Q. 2020. Immune checkpoint signaling and cancer immunotherapy. *Cell Research,* 30, 660-669. Available: 10.1038/s41422-020-0343-4

He, X. N., Zhang, C., Shi, C. & Lu, Q. Q. 2018. Meta-analysis of mRNA expression profiles to identify differentially expressed genes in lung adenocarcinoma tissue from smokers and non-smokers. *Oncology Reports,* 39, 929-938. Available: 10.3892/or.2018.6197

Hirschhorn, J. N., Brown, S. A., Clark, C. D. & Winston, F. 1992. Evidence That Snf2/Swi2 and Snf5 Activate Transcription in Yeast by Altering Chromatin Structure. *Genes & Development,* 6, 2288-2298. Available: DOI 10.1101/gad.6.12a.2288

Hodges, C., Kirkland, J. G. & Crabtree, G. R. 2016. The Many Roles of BAF (mSWI/SNF) and PBAF Complexes in Cancer. *Cold Spring Harbor Perspectives in Medicine,* 6. Available: ARTN a026930

Ikura, T., Ogryzko, V. V., Grigoriev, M., Groisman, R., Wang, J., Horikoshi, M., Scully, R., Qin, J. & Nakatani, Y. 2000. Involvement of the TIP60 histone acetylase complex in DNA repair and apoptosis. *Cell,* 102, 463-473. Available: Doi 10.1016/S0092-8674(00)00051-9

Imbalzano, A. N., Kwon, H., Green, M. R. & Kingston, R. E. 1994. Facilitated binding of TATA-binding protein to nucleosomal DNA. *Nature,* 370, 481-5. Available: 10.1038/370481a0

Ito, T., Ikehara, T., Nakagawa, T., Kraus, W. L. & Muramatsu, M. 2000. p300-mediated acetylation facilitates the transfer of histone H2A-H2B dimers from nucleosomes to a histone chaperone. *Genes Dev,* 14, 1899-907.

Iwamori, N., Tominaga, K., Sato, T., Riehle, K., Iwamori, T., Ohkawa, Y., Coarfa, C., Ono, E. & Matzuk, M. M. 2016. MRG15 is required for pre-mRNA splicing and spermatogenesis. *Proceedings of the National Academy of Sciences of the United States of America,* 113, E5408-E5415. Available: 10.1073/pnas.1611995113

Iyer, V. R. 2020. The specificity of H2A.Z occupancy in the yeast genome and its relationship to transcription. *Current Genetics,* 66, 939-944. Available: 10.1007/s00294-020-01087-7

Jackson, J. D., Falciano, V. T. & Gorovsky, M. A. 1996. A likely histone H2A.F/Z variant in Saccharomyces cerevisiae. *Trends in Biochemical Sciences,* 21, 466-467. Available: Doi 10.1016/S0968-0004(96)20028-3

Jensen, K., Santisteban, M. S., Urekar, C. & Smith, M. M. 2011. Histone H2A.Z acid patch residues required for deposition and function. *Molecular Genetics and Genomics,* 285, 287-296. Available: 10.1007/s00438-011-0604-5

Jiang, C. Z. & Pugh, B. F. 2009. Nucleosome positioning and gene regulation: advances through genomics. *Nature Reviews Genetics,* 10, 161-172. Available: 10.1038/nrg2522

Jiang, X., Wang, J., Deng, X., Xiong, F., Ge, J., Xiang, B., Wu, X., Ma, J., Zhou, M., Li, X., Li, Y., Li, G., Xiong, W., Guo, C. & Zeng, Z. 2019a. Role of the tumor microenvironment in PD-L1/PD-1-mediated tumor immune escape. *Mol Cancer,* 18, 10. Available: 10.1186/s12943-018-0928-4

Jiang, X. F., Xu, Y. & Price, B. D. 2010. Acetylation of H2AX on lysine 36 plays a key role in the DNA double-strand break repair pathway. *Febs Letters,* 584, 2926-2930. Available: 10.1016/j.febslet.2010.05.017

Jiang, X. J., Wang, J., Deng, X. Y., Xiong, F., Ge, J. S., Xiang, B., Wu, X., Ma, J., Zhou, M., Li, X. L., Li, Y., Li, G. Y., Xiong, W., Guo, C. & Zeng, Z. Y. 2019b. Role of the tumor microenvironment in PD-L1/PD-1-mediated tumor immune escape. *Molecular Cancer,* 18. Available: ARTN 10

Jin, C. Y. & Felsenfeld, G. 2007. Nucleosome stability mediated by histone variants H3.3 and H2A.Z. *Genes & Development,* 21, 1519-1529. Available: 10.1101/gad.1547707

Jin, C. Y., Zang, C. Z., Wei, G., Cui, K. R., Peng, W. Q., Zhao, K. J. & Felsenfeld, G. 2009. H3.3/H2A.Z double variant-containing nucleosomes mark 'nucleosome-free

regions' of active promoters and other regulatory regions. *Nature Genetics,* 41, 941-U112. Available: 10.1038/ng.409

Jones, S. 2004. An overview of the basic helix-loop-helix proteins. *Genome Biology,* 5. Available: ARTN 226

Josling, G. A., Selvarajah, S. A., Petter, M. & Duffy, M. F. 2012. The Role of Bromodomain Proteins in Regulating Gene Expression. *Genes,* 3, 320-343. Available: 10.3390/genes3020320

Kanazawa, S., Soucek, L., Evan, G., Okamoto, T. & Peterlin, B. M. 2003. c-Myc recruits P-TEFb for transcription, cellular proliferation and apoptosis. *Oncogene,* 22, 5707-5711. Available: 10.1038/sj.onc.1206800

Karachaliou, N., Gonzalez-Cao, M., Crespo, G., Drozdowskyj, A., Aldeguer, E., Gimenez-Capitan, A., Teixido, C., Molina-Vila, M. A., Viteri, S., Gil, M. D., Algarra, S. M., Perez-Ruiz, E., Marquez-Rodas, I., Rodriguez-Abreu, D., Blanco, R., Puertolas, T., Royo, M. A. & Rosell, R. 2018. Interferon gamma, an important marker of response to immune checkpoint blockade in non-small cell lung cancer and melanoma patients. *Therapeutic Advances in Medical Oncology,* 10. Available: 10.1177/1758834017749748

Keir, M. E., Butte, M. J., Freeman, G. J. & Sharpel, A. H. 2008. PD-1 and its ligands in tolerance and immunity. *Annual Review of Immunology,* 26, 677-704. Available: 10.1146/annurev.immunol.26.021607.090331

Khammanit, R., Chantakru, S., Kitiyanant, Y. & Saikhun, J. 2008. Effect of serum starvation and chemical inhibitors on cell cycle synchronization of canine dermal fibroblasts. *Theriogenology,* 70, 27-34. Available: 10.1016/j.theriogenology.2008.02.015

Kim, E. Y., Kim, A., Kim, S. K. & Chang, Y. S. 2017. MYC expression correlates with PD-L1 expression in non-small cell lung cancer. *Lung Cancer,* 110, 63-67. Available: 10.1016/j.lungcan.2017.06.006

Kimura, H. & Cook, P. R. 2001. Kinetics of core histones in living human cells: little exchange of H3 and H4 and some rapid exchange of H2B. *J Cell Biol,* 153, 1341-53. Available: 10.1083/jcb.153.7.1341

Kojima, K., Sakamoto, T., Kasai, T., Kagawa, T., Yoon, H. & Atagi, S. 2021. PD-L1 expression as a predictor of postoperative recurrence and the association between the PD-L1 expression and EGFR mutations in NSCLC. *Scientific Reports,* 11. Available: ARTN 17522

Komarnitsky, P., Cho, E. J. & Buratowski, S. 2000. Different phosphorylated forms of RNA polymerase II and associated mRNA processing factors during transcription. *Genes & Development,* 14, 2452-2460. Available: DOI 10.1101/gad.824700

Kraushaar, D. C., Jin, W. F., Maunakea, A., Abraham, B., Ha, M. & Zhao, K. J. 2016. Genome-wide incorporation dynamics reveal distinct categories of turnover for the histone variant H3.3 (vol 14, R121, 2013). *Genome Biology,* 17. Available: ARTN 21

Krogan, N. J., Kim, M., Tong, A., Golshani, A., Cagney, G., Canadien, V., Richards, D. P., Beattie, B. K., Emili, A., Boone, C., Shilatifard, A., Buratowski, S. & Greenblatt, J. 2003. Methylation of histone H3 by Set2 in Saccharomyces

cerevisiae is linked to transcriptional elongation by RNA polymerase II. *Mol Cell Biol,* 23, 4207-18. Available: 10.1128/mcb.23.12.4207-4218.2003

Kufe, D. W., MA, US). 2020. *COMPOSITIONS AND METHODS OF TREATING CANCER.* United States patent application 20200056174.

Kundu, T. K. & Rao, M. R. S. 1999. CpG islands in chromatin organization and gene expression. *Journal of Biochemistry,* 125, 217-222. Available: DOI 10.1093/oxfordjournals.jbchem.a022276

Kwon, H., Imbalzano, A. N., Khavari, P. A., Kingston, R. E. & Green, M. R. 1994. Nucleosome disruption and enhancement of activator binding by a human SW1/SNF complex. *Nature,* 370, 477-81. Available: 10.1038/370477a0

Lalonde, M. E., Cheng, X. & Cote, J. 2014. Histone target selection within chromatin: an exemplary case of teamwork. *Genes & Development,* 28, 1029-1041. Available: 10.1101/gad.236331.113

Land, H., Parada, L. F. & Weinberg, R. A. 1983. Tumorigenic conversion of primary embryo fibroblasts requires at least two cooperating oncogenes. *Nature,* 304, 596-602. Available: 10.1038/304596a0

Lans, H., Marteijn, J. A. & Vermeulen, W. 2012. ATP-dependent chromatin remodeling in the DNA-damage response. *Epigenetics & Chromatin,* 5. Available: Artn 4

Lastwika, K. J., Wilson, W., Li, Q. K., Norris, J., Xu, H. Y., Ghazarian, S. R., Kitagawa, H., Kawabata, S., Taube, J. M., Yao, S., Liu, L. N., Gills, J. J. & Dennis, P. A. 2016. Control of PD-L1 Expression by Oncogenic Activation of the AKT-mTOR Pathway in Non-Small Cell Lung Cancer. *Cancer Research,* 76, 227-238. Available: 10.1158/0008-5472.Can-14-3362

Lee, C. K., Shibata, Y., Rao, B., Strahl, B. D. & Lieb, J. D. 2004. Evidence for nucleosome depletion at active regulatory regions genome-wide. *Nat Genet,* 36, 900-5. Available: 10.1038/ng1400

Lee, T. & Pelletier, J. 2016. The biology of DHX9 and its potential as a therapeutic target. *Oncotarget,* 7, 42716-42739. Available: 10.18632/oncotarget.8446

Leon, J., Ferrandiz, N., Acosta, J. C. & Delgado, M. D. 2009. Inhibition of cell differentiation: a critical mechanism for MYC-mediated carcinogenesis? *Cell Cycle,* 8, 1148-57. Available: 10.4161/cc.8.8.8126

Leung, J. Y., Ehmann, G. L., Giangrande, P. H. & Nevins, J. R. 2008. A role for Myc in facilitating transcription activation by E2F1. *Oncogene,* 27, 4172-4179. Available: 10.1038/onc.2008.55

Li, B., Carey, M. & Workman, J. L. 2007. The role of chromatin during transcription. *Cell,* 128, 707-19. Available: 10.1016/j.cell.2007.01.015

Li, B., Pattenden, S. G., Lee, D., Gutierrez, J., Chen, J., Seidel, C., Gerton, J. & Workman, J. L. 2005a. Preferential occupancy of histone variant H2AZ at inactive promoters influences local histone modifications and chromatin remodeling. *Proc Natl Acad Sci U S A,* 102, 18385-90. Available: 10.1073/pnas.0507975102

Li, Z. R., Van Calcar, S., Qu, C. X., Cavenee, W. K., Zhang, M. Q. & Ren, B. 2003. A global transcriptional regulatory role for c-Myc in Burkitt's lymphoma cells. *Proceedings of the National Academy of Sciences of the United States of America,* 100, 8164-8169. Available: 10.1073/pnas.1332764100

Lickert, H., Takeuchi, J. K., von Both, I., Walls, J. R., McAuliffe, F., Adamson, S. L., Henkelman, R. M., Wrana, J. L., Rossant, J. & Bruneau, B. G. 2004. Baf60c is essential for function of BAF chromatin remodelling complexes in heart development. *Nature,* 432, 107-112. Available: 10.1038/nature03071

Lin, C. H., Jackson, A. L., Guo, J., Linsley, P. S. & Eisenman, R. N. 2009. Myc-regulated microRNAs attenuate embryonic stem cell differentiation. *EMBO J,* 28, 3157-70. Available: 10.1038/emboj.2009.254

Lin, C. Y., Loven, J., Rahl, P. B., Paranal, R. M., Burge, C. B., Bradner, J. E., Lee, T. I. & Young, R. A. 2012. Transcriptional Amplification in Tumor Cells with Elevated c-Myc. *Cell,* 151, 56-67. Available: 10.1016/j.cell.2012.08.026

Lin, Y. M., Sung, W. W., Hsieh, M. J., Tsai, S. C., Lai, H. W., Yang, S. M., Shen, K. H., Chen, M. K., Lee, H., Yeh, K. T. & Chen, C. J. 2015. High PD-L1 Expression Correlates with Metastasis and Poor Prognosis in Oral Squamous Cell Carcinoma. *Plos One,* 10. Available: ARTN e0142656

Liu, X. H., Tesfai, J., Evrard, Y. A., Dent, S. Y. R. & Martinez, E. 2003. C-Myc transformation domain recruits the human STAGA complex and requires TRRAP and GCN5 acetylase activity for transcription activation. *Journal of Biological Chemistry,* 278, 20405-20412. Available: 10.1074/jbc.M211795200

Lopez-Perrote, A., Alatwi, H. E., Torreira, E., Ismail, A., Ayora, S., Downs, J. A. & Llorca, O. 2014. Structure of Yin Yang 1 Oligomers That Cooperate with RuvBL1-RuvBL2 ATPases. *Journal of Biological Chemistry,* 289, 22614-22629. Available: 10.1074/jbc.M114.567040

Lotterman, C. D., Kent, O. A. & Mendell, J. T. 2008. Functional integration of microRNAs into oncogenic and tumor suppressor pathways. *Cell Cycle,* 7, 2493-9. Available: 10.4161/cc.7.16.6452

Lu, P. Y. T., Levesque, N. & Kobor, M. S. 2009. NuA4 and SWR1-C: two chromatin-modifying complexes with overlapping functions and components. *Biochemistry and Cell Biology,* 87, 799-815. Available: 10.1139/O09-062

Luco, R. F., Pan, Q., Tominaga, K., Blencowe, B. J., Pereira-Smith, O. M. & Misteli, T. 2010. Regulation of Alternative Splicing by Histone Modifications. *Science,* 327, 996-1000. Available: 10.1126/science.1184208

Luger, K., Mader, A. W., Richmond, R. K., Sargent, D. F. & Richmond, T. J. 1997. Crystal structure of the nucleosome core particle at 2.8 A resolution. *Nature,* 389, 251-60. Available: 10.1038/38444

Martin, G. R. & Evans, M. J. 1975. Differentiation of Clonal Lines of Teratocarcinoma Cells - Formation of Embryoid Bodies Invitro. *Proceedings of the National Academy of Sciences of the United States of America,* 72, 1441-1445. Available: DOI 10.1073/pnas.72.4.1441

Martinez-Lostao, L., Anel, A. & Pardo, J. 2015. How Do Cytotoxic Lymphocytes Kill Cancer Cells? *Clinical Cancer Research,* 21, 5047-5056. Available: 10.1158/1078-0432.Ccr-15-0685

Mathew, R., Hartmuth, K., Mohlmann, S., Urlaub, H., Ficner, R. & Luhrmann, R. 2008. Phosphorylation of human PRP28 by SRPK2 is required for integration of the U4/U6-U5 tri-snRNP into the spliceosome. *Nature Structural & Molecular Biology,* 15, 435-443. Available: 10.1038/nsmb.1415

Matsuda, R., Hori, T., Kitamura, H., Takeuchi, K., Fukagawa, T. & Harata, M. 2010. Identification and characterization of the two isoforms of the vertebrate H2A.Z

histone variant. *Nucleic Acids Research,* 38, 4263-4273. Available: 10.1093/nar/gkq171

Mattera, L., Escaffit, F., Pillaire, M. J., Selves, J., Tyteca, S., Hoffmann, J. S., Gourraud, P. A., Chevillard-Briet, M., Cazaux, C. & Trouche, D. 2009. The p400/Tip60 ratio is critical for colorectal cancer cell proliferation through DNA damage response pathways. *Oncogene,* 28, 1506-1517. Available: 10.1038/onc.2008.499

Mattiroli, F., D'Arcy, S. & Luger, K. 2015. The right place at the right time: chaperoning core histone variants. *Embo Reports,* 16, 1454-1466. Available: DOI 10.15252/embr.201540840

Maze, I., Noh, K. M., Soshnev, A. A. & Allis, C. D. 2014. Every amino acid matters: essential contributions of histone variants to mammalian development and disease. *Nature Reviews Genetics,* 15, 259-271. Available: 10.1038/nrg3673

McCracken, S., Fong, N., Rosonina, E., Yankulov, K., Brothers, G., Siderovski, D., Hessel, A., Poster, S., Shuman, S., Bentley, D. L. & Program, A. E. 1997. 5 '-capping enzymes are targeted to pre-mRNA by binding to the phosphorylated carboxy-terminal domain of RNA polymerase II. *Genes & Development,* 11, 3306-3318. Available: DOI 10.1101/gad.11.24.3306

McMahon, S. B., Van Buskirk, H. A., Dugan, K. A., Copeland, T. D. & Cole, M. D. 1998. The novel ATM-related protein TRRAP is an essential cofactor for the c-Myc and E2F oncoproteins. *Cell,* 94, 363-374. Available: Doi 10.1016/S0092-8674(00)81479-8

Mito, Y., Henikoff, J. G. & Henikoff, S. 2005. Genome-scale profiling of histone H3.3 replacement patterns. *Nature Genetics,* 37, 1090-1097. Available: 10.1038/ng1637

Mizuguchi, G., Shen, X., Landry, J., Wu, W. H., Sen, S. & Wu, C. 2004a. ATP-driven exchange of histone H2AZ variant catalyzed by SWR1 chromatin remodeling complex. *Science,* 303, 343-8. Available: 10.1126/science.1090701

Mizuguchi, G., Wu, W. H., Alami, S. & Luk, E. 2012. Biochemical Assay for Histone H2A.Z Replacement by the Yeast SWR1 Chromatin Remodeling Complex. *Nucleosomes, Histones & Chromatin, Pt A,* 512, 275-291. Available: 10.1016/B978-0-12-391940-3.00012-3

Monden, T., Wondisford, F. E. & Hollenberg, A. N. 1997. Isolation and characterization of a novel ligand-dependent thyroid hormone receptor-coactivating protein. *Journal of Biological Chemistry,* 272, 29834-29841. Available: DOI 10.1074/jbc.272.47.29834

Moon, J. W., Kong, S. K., Kim, B. S., Kim, H. J., Lim, H., Noh, K., Kim, Y., Choi, J. W., Lee, J. H. & Kim, Y. S. 2017. IFN gamma induces PD-L1 overexpression by JAK2/STAT1/IRF-1 signaling in EBV-positive gastric carcinoma. *Scientific Reports,* 7. Available: ARTN 17810

Muchir, A., Medioni, J., Laluc, M., Massart, C., Arimura, T., Van Der Kooi, A. J., Desguerre, I., Mayer, M., Ferrer, X., Briault, S., Hirano, M., Worman, H. J., Mallet, A., Wehnert, M., Schwartz, K. & Bonne, G. 2004. Nuclear envelope alterations in fibroblasts from patients with muscular dystrophy, cardiomyopathy, and partial lipodystrophy carrying lamin A/C gene mutations. *Muscle & Nerve,* 30, 444-450. Available: 10.1002/mus.20122

Muratcioglu, S., Presman, D. M., Pooley, J. R., Grontved, L., Hager, G. L., Nussinov, R., Keskin, O. & Gursoy, A. 2015. Structural Modeling of GR Interactions with the SWI/SNF Chromatin Remodeling Complex and C/EBP. *Biophysical Journal,* 109, 1227-1239. Available: 10.1016/j.bpj.2015.06.044

Murr, R., Loizou, J. I., Yang, Y. G., Cuenin, C., Li, H., Wang, Z. Q. & Herceg, Z. 2006. Histone acetylation by Trrap-Tip60 modulates loading of repair proteins and repair of DNA double-strand breaks. *Nature Cell Biology,* 8, 91-U36. Available: 10.1038/ncb1343

Mustata, G., Follis, A. V., Hammoudeh, D. I., Metallo, S. J., Wang, H., Prochownik, E. V., Lazo, J. S. & Bahar, I. 2009. Discovery of novel Myc-Max heterodimer disruptors with a three-dimensional pharmacophore model. *J Med Chem,* 52, 1247-50. Available: 10.1021/jm801278g

Nesvizhskii, A. I. & Aebersold, R. 2005. Interpretation of shotgun proteomic data: the protein inference problem. *Mol Cell Proteomics,* 4, 1419-40. Available: 10.1074/mcp.R500012-MCP200

Nevins, J. R. 1992. E2f - a Link between the Rb Tumor Suppressor Protein and Viral Oncoproteins. *Science,* 258, 424-429.

Nikiforov, M. A., Chandriani, S., Park, J., Kotenko, I., Matheos, D., Johnsson, A., McMahon, S. B. & Cole, M. D. 2002. TRRAP-dependent and TRRAP-independent transcriptional activation by Myc family oncoproteins. *Mol Cell Biol,* 22, 5054-63. Available: 10.1128/mcb.22.14.5054-5063.2002

Nowicki, T. S., Hu-Lieskovan, S. & Ribas, A. 2018. Mechanisms of Resistance to PD-1 and PD-L1 Blockade. *Cancer Journal,* 24, 47-53.

Oberstrass, F. C., Auweter, S. D., Erat, M., Hargous, Y., Henning, A., Wenter, P., Reymond, L., Amir-Ahmady, B., Pitsch, S., Black, D. L. & Allain, F. H. T. 2005. Structure of PTB bound to RNA: Specific binding and implications for splicing regulation. *Science,* 309, 2054-2057. Available: 10.1126/science.1114066

Ogorman, S., Fox, D. T. & Wahl, G. M. 1991. Recombinase-Mediated Gene Activation and Site-Specific Integration in Mammalian-Cells. *Science,* 251, 1351-1355. Available: DOI 10.1126/science.1900642

Orlando, K. A., Nguyen, V., Raab, J. R., Walhart, T. & Weissman, B. E. 2019. Remodeling the cancer epigenome: mutations in the SWI/SNF complex offer new therapeutic opportunities. *Expert Rev Anticancer Ther,* 19, 375-391. Available: 10.1080/14737140.2019.1605905

Oster, S. K., Mao, D. Y., Kennedy, J. & Penn, L. Z. 2003. Functional analysis of the N-terminal domain of the Myc oncoprotein. *Oncogene,* 22, 1998-2010. Available: 10.1038/sj.onc.1206228

Owen-Hughes, T., Utley, R. T., Cote, J., Peterson, C. L. & Workman, J. L. 1996. Persistent site-specific remodeling of a nucleosome array by transient action of the SWI/SNF complex. *Science,* 273, 513-6. Available: 10.1126/science.273.5274.513

Park, J., Kunjibettu, S., McMahon, S. B. & Cole, M. D. 2001. The ATM-related domain of TRRAP is required for histone acetyltransferase recruitment and Myc-dependent oncogenesis. *Genes & Development,* 15, 1619-1624. Available: DOI 10.1101/gad.900101

Park, J., Wood, M. A. & Cole, M. D. 2002. BAF53 forms distinct nuclear complexes and functions as a critical c-Myc-interacting nuclear cofactor for oncogenic

transformation. *Molecular and Cellular Biology,* 22, 1307-1316. Available: Doi 10.1128/Mcb.22.5.1307-1316.2002

Park, J. H., Sun, X. J. & Roeder, R. G. 2010. The SANT Domain of p400 ATPase Represses Acetyltransferase Activity and Coactivator Function of TIP60 in Basal p21 Gene Expression. *Molecular and Cellular Biology,* 30, 2750-2761. Available: 10.1128/Mcb.00804-09

Patel, J. H., Loboda, A. P., Showe, M. K., Showe, L. C. & McMahon, S. B. 2004. Analysis of genomic targets reveals complex functions of MYC. *Nat Rev Cancer,* 4, 562-8. Available: 10.1038/nrc1393

Perna, D., Faga, G., Verrecchia, A., Gorski, M. M., Barozzi, I., Narang, V., Khng, J., Lim, K. C., Sung, W. K., Sanges, R., Stupka, E., Oskarsson, T., Trumpp, A., Wei, C. L., Muller, H. & Amati, B. 2012. Genome-wide mapping of Myc binding and gene regulation in serum-stimulated fibroblasts. *Oncogene,* 31, 1695-1709. Available: 10.1038/onc.2011.359

Peterson, C. L. & Herskowitz, I. 1992. Characterization of the Yeast Swi1, Swi2, and Swi3 Genes, Which Encode a Global Activator of Transcription. *Cell,* 68, 573-583. Available: Doi 10.1016/0092-8674(92)90192-F

Pokholok, D. K., Harbison, C. T., Levine, S., Cole, M., Hannett, N. M., Lee, T. I., Bell, G. W., Walker, K., Rolfe, P. A., Herbolsheimer, E., Zeitlinger, J., Lewitter, F., Gifford, D. K. & Young, R. A. 2005. Genome-wide map of nucleosome acetylation and methylation in yeast. *Cell,* 122, 517-27. Available: 10.1016/j.cell.2005.06.026

Pradhan, S. K., Su, T., Yen, L., Jacquet, K., Huang, C., Cote, J., Kurdistani, S. K. & Carey, M. F. 2016a. EP400 Deposits H3.3 into Promoters and Enhancers during Gene Activation. *Mol Cell,* 61, 27-38. Available: 10.1016/j.molcel.2015.10.039

Pradhan, S. K., Su, T., Yen, L. D., Jacquet, K., Cote, J., Kurdistani, S. & Carey, M. 2016b. Chromatin Remodeler EP400 Deposits H3.3 into Promoters and Enhancers During Gene Activation. *Faseb Journal,* 30.

Puri, T., Wendler, P., Sigala, B., Saibil, H. & Tsaneva, I. R. 2007. Dodecameric structure and ATPase activity of the human TIP48/TIP49 complex. *Journal of Molecular Biology,* 366, 179-192. Available: 10.1016/j.jmb.2006.11.030

Qin, T., Zeng, Y. D., Qin, G., Xu, F., Lu, J. B., Fang, W. F., Xue, C., Zhan, J. H., Zhang, X. K., Zheng, Q. F., Peng, R. J., Yuan, Z. Y., Zhang, L. & Wang, S. S. 2015. High PD-L1 expression was associated with poor prognosis in 870 Chinese patients with breast cancer. *Oncotarget,* 6, 33972-33981. Available: 10.18632/oncotarget.5583

Raisner, R. M., Hartley, P. D., Meneghini, M. D., Bao, M. Z., Liu, C. L., Schreiber, S. L., Rando, O. J. & Madhani, H. D. 2005. Histone variant H2A.Z marks the 5' ends of both active and inactive genes in euchromatin. *Cell,* 123, 233-48. Available: 10.1016/j.cell.2005.10.002

Rakhra, K., Bachireddy, P., Zabuawala, T., Zeiser, R., Xu, L. W., Kopelman, A., Fan, A. C., Yang, Q. W., Braunstein, L., Crosby, E., Ryeom, S. & Felsher, D. W. 2010. CD4(+) T Cells Contribute to the Remodeling of the Microenvironment Required for Sustained Tumor Regression upon Oncogene Inactivation. *Cancer Cell,* 18, 485-498. Available: 10.1016/j.ccr.2010.10.002

Ranjan, A., Mizuguchi, G., FitzGerald, P. C., Wei, D., Wang, F., Huang, Y. Z., Luk, E., Woodcock, C. L. & Wu, C. 2013. Nucleosome-free Region Dominates

Histone Acetylation in Targeting SWR1 to Promoters for H2A.Z Replacement. *Cell,* 154, 1232-1245. Available: 10.1016/j.cell.2013.08.005

Richman, A. & Hayday, A. 1989a. Serum-inducible expression of transfected human c-myc genes. *Mol Cell Biol,* 9, 4962-9. Available: 10.1128/mcb.9.11.4962-4969.1989

Rountree, M. R., Bachman, K. E. & Baylin, S. B. 2000. DNMT1 binds HDAC2 and a new co-repressor, DMAP1, to form a complex at replication foci. *Nature Genetics,* 25, 269-277. Available: Doi 10.1038/77023

Ruhl, D. D., Jin, J., Cai, Y., Swanson, S., Florens, L., Washburn, M. P., Conaway, R. C., Conaway, J. W. & Chrivia, J. C. 2006. Purification of a human SRCAP complex that remodels chromatin by incorporating the histone variant H2A.Z into nucleosomes. *Biochemistry,* 45, 5671-7. Available: 10.1021/bi060043d

Saha, A., Wittmeyer, J. & Cairns, B. R. 2006. Chromatin remodelling: the industrial revolution of DNA around histones. *Nat Rev Mol Cell Biol,* 7, 437-47. Available: 10.1038/nrm1945

Schildberg, F. A., Klein, S. R., Freeman, G. J. & Sharpe, A. H. 2016. Coinhibitory Pathways in the B7-CD28 Ligand-Receptor Family. *Immunity,* 44, 955-972. Available: 10.1016/j.immuni.2016.05.002

Schmidt, E. V. 1999. The role of c-myc in cellular growth control. *Oncogene,* 18, 2988-2996. Available: DOI 10.1038/sj.onc.1202751

Schroeder, S. C., Schwer, B., Shuman, S. & Bentley, D. 2000. Dynamic association of capping enzymes with transcribing RNA polymerase II. *Genes & Development,* 14, 2435-2440. Available: DOI 10.1101/gad.836300

Sekinger, E. A., Moqtaderi, Z. & Struhl, K. 2005. Intrinsic histone-DNA interactions and low nucleosome density are important for preferential accessibility of promoter regions in yeast. *Mol Cell,* 18, 735-48. Available: 10.1016/j.molcel.2005.05.003

Seliger, B. 2019. Basis of PD1/PD-L1 Therapies. *Journal of Clinical Medicine,* 8. Available: ARTN 2168

Senoo, M., Takijiri, T., Yoshida, N., Ozawa, M. & Ikawa, M. 2019. PTBP1 contributes to spermatogenesis through regulation of proliferation in spermatogonia. *Journal of Reproduction and Development,* 65, 37-46. Available: DOI 10.1262/jrd.2018-109

Shivaswamy, S., Bhinge, A., Zhao, Y. J., Jones, S., Hirst, M. & Iyer, V. R. 2008. Dynamic remodeling of individual nucleosomes across a eukaryotic genome in response to transcriptional perturbation. *Plos Biology,* 6, 618-630. Available: ARTN e65

Siegel, R., Ma, J. M., Zou, Z. H. & Jemal, A. 2014. Cancer Statistics, 2014. *Ca-a Cancer Journal for Clinicians,* 64, 9-29. Available: 10.3322/caac.21208

Singhi, A. D., Cimino-Mathews, A., Jenkins, R. B., Lan, F., Fink, S. R., Nassar, H., Vang, R., Fetting, J. H., Hicks, J., Sukumar, S., De Marzo, A. M. & Argani, P. 2012. MYC gene amplification is often acquired in lethal distant breast cancer metastases of unamplified primary tumors. *Mod Pathol,* 25, 378-87. Available: 10.1038/modpathol.2011.171

Slaymaker, I. M., Gao, L. Y., Zetsche, B., Scott, D. A., Yan, W. X. & Zhang, F. 2016. Rationally engineered Cas9 nucleases with improved specificity. *Science,* 351, 84-88. Available: 10.1126/science.aad5227

Smith, R. J., Savoian, M. S., Weber, L. E. & Park, J. H. 2016. Ataxia telangiectasia mutated (ATM) interacts with p400 ATPase for an efficient DNA damage response. *BMC Mol Biol,* 17, 22. Available: 10.1186/s12867-016-0075-7

Soucek, L. & Evan, G. I. 2010. The ups and downs of Myc biology. *Curr Opin Genet Dev,* 20, 91-5. Available: 10.1016/j.gde.2009.11.001

Stern, M., Jensen, R. & Herskowitz, I. 1984. 5 Swi Genes Are Required for Expression of the Ho Gene in Yeast. *Journal of Molecular Biology,* 178, 853-868. Available: Doi 10.1016/0022-2836(84)90315-2

Sterner, D. E. & Berger, S. L. 2000. Acetylation of histones and transcription-related factors. *Microbiology and Molecular Biology Reviews,* 64, 435-+. Available: Doi 10.1128/Mmbr.64.2.435-459.2000

Stine, Z. E., Walton, Z. E., Altman, B. J., Hsieh, A. L. & Dang, C. V. 2015. MYC, Metabolism, and Cancer. *Cancer Discovery,* 5, 1024-1039. Available: 10.1158/2159-8290.Cd-15-0507

Strahl, B. D., Grant, P. A., Briggs, S. D., Sun, Z. W., Bone, J. R., Caldwell, J. A., Mollah, S., Cook, R. G., Shabanowitz, J., Hunt, D. F. & Allis, C. D. 2002. Set2 is a nucleosomal histone H3-selective methyltransferase that mediates transcriptional repression. *Molecular and Cellular Biology,* 22, 1298-1306. Available: Doi 10.1128/Mcb.22.5.1298-1306.2002

Sun, C., Mezzadra, R. & Schumacher, T. N. 2018. Regulation and Function of the PD-L1 Checkpoint. *Immunity,* 48, 434-452. Available: 10.1016/j.immuni.2018.03.014

Szerlong, H., Hinata, K., Viswanathan, R., Erdjument-Bromage, H., Tempst, P. & Cairns, B. R. 2008. The HSA domain binds nuclear actin-related proteins to regulate chromatin-remodeling ATPases. *Nature Structural & Molecular Biology,* 15, 469-476. Available: 10.1038/nsmb.1403

Tagami, H., Ray-Gallet, D., Almouzni, G. & Nakatani, Y. 2004. Histone H3.1 and H3.3 complexes mediate nucleosome assembly pathways dependent or independent of DNA synthesis. *Cell,* 116, 51-61. Available: Doi 10.1016/S0092-8674(03)01064-X

Tang, Y. Y., He, Y., Shi, L., Yang, L. T., Wang, J. P., Lian, Y., Fan, C. M., Zhang, P., Guo, C., Zhang, S. S., Gong, Z. J., Li, X. Y., Xiong, F., Li, X. L., Li, Y., Li, G. Y., Xiong, W. & Zeng, Z. Y. 2017. Co-expression of AFAP1-AS1 and PD-1 predicts poor prognosis in nasopharyngeal carcinoma. *Oncotarget,* 8, 39001-39011. Available: 10.18632/oncotarget.16545

Taylor, I. C., Workman, J. L., Schuetz, T. J. & Kingston, R. E. 1991. Facilitated binding of GAL4 and heat shock factor to nucleosomal templates: differential function of DNA-binding domains. *Genes Dev,* 5, 1285-98. Available: 10.1101/gad.5.7.1285

Teperino, R., Schoonjans, K. & Auwerx, J. 2010. Histone Methyl Transferases and Demethylases; Can They Link Metabolism and Transcription? *Cell Metabolism,* 12, 321-327. Available: 10.1016/j.cmet.2010.09.004

Thakar, A., Gupta, P., Ishibashi, T., Finn, R., Silva-Moreno, B., Uchiyama, S., Fukui, K., Tomschik, M., Ausio, J. & Zlatanova, J. 2009. H2A.Z and H3.3 Histone Variants Affect Nucleosome Structure: Biochemical and Biophysical Studies. *Biochemistry,* 48, 10852-10857. Available: 10.1021/bi901129e

Thomas, M. C. & Chiang, C. M. 2006. The general transcription machinery and general cofactors. *Crit Rev Biochem Mol Biol,* 41, 105-78. Available: 10.1080/10409230600648736

Tokarew, N., Ogonek, J., Endres, S., von Bergwelt-Baildon, M. & Kobold, S. 2019. Teaching an old dog new tricks: next-generation CAR T cells. *British Journal of Cancer,* 120, 26-37. Available: 10.1038/s41416-018-0325-1

Trotter, K. W. & Archer, T. K. 2008. The BRG1 transcriptional coregulator. *Nucl Recept Signal,* 6, e004. Available: 10.1621/nrs.06004

Tworkowski, K. A., Chakraborty, A. A., Samuelson, A. V., Seger, Y. R., Narita, M., Hannon, G. J., Lowe, S. W. & Tansey, W. P. 2008. Adenovirus E1A targets p400 to induce the cellular oncoprotein Myc. *Proc Natl Acad Sci U S A,* 105, 6103-8. Available: 10.1073/pnas.0802095105

Ueda, T., Watanabe-Fukunaga, R., Ogawa, H., Fukuyama, H., Higashi, Y., Nagata, S. & Fukunaga, R. 2007. Critical role of the p400/mDomino chromatin-remodeling ATPase in embryonic hematopoiesis. *Genes Cells,* 12, 581-92. Available: 10.1111/j.1365-2443.2007.01080.x

Uribesalgo, I., Buschbeck, M., Gutierrez, A., Teichmann, S., Demajo, S., Kuebler, B., Nomdedeu, J. F., Martin-Caballero, J., Roma, G., Benitah, S. A. & Di Croce, L. 2011. E-box-independent regulation of transcription and differentiation by MYC. *Nature Cell Biology,* 13, 1443-U149. Available: 10.1038/ncb2355

Vaquero, A., Loyola, A. & Reinberg, D. 2003. The constantly changing face of chromatin. *Sci Aging Knowledge Environ,* 2003, RE4. Available: 10.1126/sageke.2003.14.re4

Vardabasso, C., Hasson, D., Ratnakumar, K., Chung, C. Y., Duarte, L. F. & Bernstein, E. 2014. Histone variants: emerging players in cancer biology. *Cellular and Molecular Life Sciences,* 71, 379-404. Available: 10.1007/s00018-013-1343-z

Venkatesh, S. & Workman, J. L. 2015. Histone exchange, chromatin structure and the regulation of transcription. *Nat Rev Mol Cell Biol,* 16, 178-89. Available: 10.1038/nrm3941

Vita, M. & Henriksson, M. 2006. The Myc oncoprotein as a therapeutic target for human cancer. *Seminars in Cancer Biology,* 16, 318-330. Available: 10.1016/j.semcancer.2006.07.015

Volle, C. & Dalal, Y. 2014. Histone variants: the tricksters of the chromatin world. *Current Opinion in Genetics & Development,* 25, 8-14. Available: 10.1016/j.gde.2013.11.006

Wang, A. Y., Aristizabal, M. J., Ryan, C., Krogan, N. J. & Kobor, M. S. 2011. Key Functional Regions in the Histone Variant H2A.Z C-Terminal Docking Domain. *Molecular and Cellular Biology,* 31, 3871-3884. Available: 10.1128/Mcb.05182-11

Wang, J. & Manley, J. L. 1997. Regulation of pre-mRNA splicing in metazoa. *Current Opinion in Genetics & Development,* 7, 205-211. Available: Doi 10.1016/S0959-437x(97)80130-X

Wang, W. D. & Crabtree, G. R. 1997. Diversity and specialization of mammalian SWI/SNF complexes. *Faseb Journal,* 11, A1300-A1300.

Wang, W. D., Xue, Y. T., Zhou, S., Kuo, A., Cairns, B. R. & Crabtree, G. R. 1996. Diversity and specialization of mammalian SWI/SNF complexes. *Genes & Development,* 10, 2117-2130. Available: DOI 10.1101/gad.10.17.2117

Wang, X., Ahmad, S., Zhang, Z., Cote, J. & Cai, G. 2018. Architecture of the Saccharomyces cerevisiae NuA4/TIP60 complex. *Nat Commun,* 9, 1147. Available: 10.1038/s41467-018-03504-5

Wang, X., Teng, F. F., Kong, L. & Yu, J. M. 2016. PD-L1 expression in human cancers and its association with clinical outcomes. *Oncotargets and Therapy,* 9, 5023-5039. Available: 10.2147/Ott.S105862

Wang, Z., Wang, P., Li, Y., Peng, H., Zhu, Y., Mohandas, N. & Liu, J. 2021. Interplay between cofactors and transcription factors in hematopoiesis and hematological malignancies. *Signal Transduct Target Ther,* 6, 24. Available: 10.1038/s41392-020-00422-1

Watanabe, R., Kanno, S., Roushandeh, A. M., Ui, A. & Yasui, A. 2017. Nucleosome remodelling, DNA repair and transcriptional regulation build negative feedback loops in cancer and cellular ageing. *Philosophical Transactions of the Royal Society B-Biological Sciences,* 372. Available: ARTN 20160473

Weber, C. M., Ramachandran, S. & Henikoff, S. 2014. Nucleosomes Are Context-Specific, H2A.Z-Modulated Barriers to RNA Polymerase. *Molecular Cell,* 53, 819-830. Available: 10.1016/j.molcel.2014.02.014

Weidensdorfer, D., Stohr, N., Baude, A., Lederer, M., Kohn, M., Schierhorn, A., Buchmeier, S., Wahle, E. & Huttelmaier, S. 2009. Control of c-myc mRNA stability by IGF2BP1-associated cytoplasmic RNPs. *Rna,* 15, 104-115. Available: 10.1261/rna.1175909

West, K. A., Linnoila, I. R., Belinsky, S. A., Harris, C. C. & Dennis, P. A. 2004. Tobacco carcinogen-induced cellular transformation increases activation of the phosphatidylinositol 3 '-Kinase/Akt pathway in vitro and in vivo. *Cancer Research,* 64, 446-451. Available: Doi 10.1158/0008-5472.Can-03-3241

Wolpaw, A. J. & Dang, C. V. 2018. MYC-induced metabolic stress and tumorigenesis. *Biochim Biophys Acta Rev Cancer,* 1870, 43-50. Available: 10.1016/j.bbcan.2018.05.003

Wong, M. M., Cox, L. K. & Chrivia, J. C. 2007. The chromatin remodeling protein, SRCAP, is critical for deposition of the histone variant H2A.Z at promoters. *Journal of Biological Chemistry,* 282, 26132-26139. Available: 10.1074/jbc.M703418200

Workman, J. L. 2006. Nucleosome displacement in transcription. *Genes & Development,* 20, 2009-2017. Available: 10.1101/gad.1435706

Workman, J. L. & Kingston, R. E. 1998. Alteration of nucleosome structure as a mechanism of transcriptional regulation. *Annu Rev Biochem,* 67, 545-79. Available: 10.1146/annurev.biochem.67.1.545

Wu, Q., Lian, J. B., Stein, J. L., Stein, G. S., Nickerson, J. A. & Imbalzano, A. N. 2017. The BRG1 ATPase of human SWI/SNF chromatin remodeling enzymes as a driver of cancer. *Epigenomics,* 9, 919-931. Available: 10.2217/epi-2017-0034

Wu, Y. L., Chen, W. Y., Xu, Z. P. & Gu, W. Y. 2019. PD-L1 Distribution and Perspective for Cancer Immunotherapy-Blockade, Knockdown, or Inhibition. *Frontiers in Immunology,* 10. Available: ARTN 2022

Xiao, R., Tang, P., Yang, B., Huang, J., Zhou, Y., Shao, C. W., Li, H. R., Sun, H., Zhang, Y. & Fu, X. D. 2012. Nuclear Matrix Factor hnRNP U/SAF-A Exerts a Global Control of Alternative Splicing by Regulating U2 snRNP Maturation. *Molecular Cell,* 45, 656-668. Available: 10.1016/j.molcel.2012.01.009

Xu, D. W., Popov, N., Hou, M., Wang, Q., Bjorkholm, M., Gruber, A., Menkel, A. R. & Henriksson, M. 2001. Switch from Myc/Max to Mad1/Max binding and decrease in histone acetylation at the telomerase reverse transcriptase promoter

during differentiation of HL60 cells. *Proceedings of the National Academy of Sciences of the United States of America,* 98, 3826-3831. Available: DOI 10.1073/pnas.071043198

Xu, P., Li, C. M., Chen, Z. H., Jiang, S. Y., Fan, S. L., Wang, J. W., Dai, J. B., Zhu, P. & Chen, Z. C. 2016. The NuA4 Core Complex Acetylates Nucleosomal Histone H4 through a Double Recognition Mechanism. *Molecular Cell,* 63, 965-975. Available: 10.1016/j.molcel.2016.07.024

Xu, Y., Ayrapetov, M. K., Xu, C., Gursoy-Yuzugullu, O., Hu, Y. D. & Price, B. D. 2012. Histone H2A.Z Controls a Critical Chromatin Remodeling Step Required for DNA Double-Strand Break Repair. *Molecular Cell,* 48, 723-733. Available: 10.1016/j.molcel.2012.09.026

Xu, Y., Sun, Y. L., Jiang, X. F., Ayrapetov, M. K., Moskwa, P., Yang, S. H., Weinstock, D. M. & Price, B. D. 2010. The p400 ATPase regulates nucleosome stability and chromatin ubiquitination during DNA repair. *Journal of Cell Biology,* 191, 31-43. Available: 10.1083/jcb.201001160

Xue, Y. C., Zhou, Y., Wu, T. B., Zhu, T., Ji, X., Kwon, Y. S., Zhang, C., Yeo, G., Black, D. L., Sun, H., Fu, X. D. & Zhang, Y. 2009. Genome-wide Analysis of PTB-RNA Interactions Reveals a Strategy Used by the General Splicing Repressor to Modulate Exon Inclusion or Skipping. *Molecular Cell,* 36, 996-1006. Available: 10.1016/j.molcel.2009.12.003

Yague-Sanz, C., Vazquez, E., Sanchez, M., Antequera, F. & Hermand, D. 2017. A conserved role of the RSC chromatin remodeler in the establishment of nucleosome-depleted regions. *Current Genetics,* 63, 187-193. Available: 10.1007/s00294-016-0642-y

Yamada, H. Y. 2012. Human Tip60 (NuA4) complex and cancer. *Colorectal Cancer Biology-From Genes to Tumor.* Intechopen.

Yamazaki, T., Akiba, H., Iwai, H., Matsuda, H., Aoki, M., Tanno, Y., Shin, T., Tsuchiya, H., Pardoll, D. M., Okumura, K., Azuma, M. & Yagita, H. 2002. Expression of programmed death 1 ligands by murine T cells and APC. *Journal of Immunology,* 169, 5538-5545. Available: DOI 10.4049/jimmunol.169.10.5538

Yan, L., Xie, S., Du, Y. M. & Qian, C. M. 2017. Structural Insights into BAF47 and BAF155 Complex Formation. *Journal of Molecular Biology,* 429, 1650-1660. Available: 10.1016/j.jmb.2017.04.008

Yuan, G. C., Liu, Y. J., Dion, M. F., Slack, M. D., Wu, L. F., Altschuler, S. J. & Rando, O. J. 2005. Genome-scale identification of nucleosome positions in S. cerevisiae. *Science,* 309, 626-30. Available: 10.1126/science.1112178

Yugami, M., Kabe, Y., Yamaguchi, Y., Wada, T. & Handa, H. 2007. hnRNP-U enhances the expression of specific genes by stabilizing mRNA. *Febs Letters,* 581, 1-7. Available: 10.1016/j.febslet.2006.11.062

Yukawa, M., Akiyama, T., Franke, V., Mise, N., Isagawa, T., Suzuki, Y., Suzuki, M. G., Vlahovicek, K., Abe, K., Aburatani, H. & Aoki, F. 2014. Genome-Wide Analysis of the Chromatin Composition of Histone H2A and H3 Variants in Mouse Embryonic Stem Cells. *Plos One,* 9. Available: ARTN e92689

Zanton, S. J. & Pugh, B. F. 2006. Full and partial genome-wide assembly and disassembly of the yeast transcription machinery in response to heat shock. *Genes Dev,* 20, 2250-65. Available: 10.1101/gad.1437506

Zeller, K. I., Zhao, X. D., Lee, C. W. H., Chiu, K. P., Yao, F., Yustein, J. T., Ooi, H. S., Orlov, Y. L., Shahab, A., Yong, H. C., Fu, Y. T., Weng, Z. P., Kuznetsov, V. A., Sung, W. K., Ruan, Y. J., Dang, C. V. & Wei, C. L. 2006. Global mapping of c-Myc binding sites and target gene networks in human B cells. *Proceedings of the National Academy of Sciences of the United States of America,* 103, 17834-17839. Available: 10.1073/pnas.0604129103

Zhang, H., Roberts, D. N. & Cairns, B. R. 2005. Genome-wide dynamics of Htz1, a histone H2A variant that poises repressed/basal promoters for activation through histone loss. *Cell,* 123, 219-31. Available: 10.1016/j.cell.2005.08.036

Zhang, P. Y., Torres, K., Liu, X. P., Liu, C. G. & Pollock, R. E. 2016. An Overview of Chromatin-Regulating Proteins in Cells. *Current Protein & Peptide Science,* 17, 401-410. Available: 10.2174/1389203717666160122120310

Zhang, S. S. & Grosse, F. 1994. Nuclear-DNA Helicase-Ii Unwinds Both DNA and Rna. *Biochemistry,* 33, 3906-3912. Available: DOI 10.1021/bi00179a016

Zhang, Z. H., Wippo, C. J., Wal, M., Ward, E., Korber, P. & Pugh, B. F. 2011. A Packing Mechanism for Nucleosome Organization Reconstituted Across a Eukaryotic Genome. *Science,* 332, 977-980. Available: 10.1126/science.1200508

Zhao, H., Xue, J., Liu, J., Liu, Y. & Cheng, Y. 2016. Effect of metastasis suppressor 1 on H1299 cells and its clinical significance in non-small cell lung cancer. *Oncol Rep,* 36, 2814-2822. Available: 10.3892/or.2016.5081

Zhao, K. J., Wang, W. D., Rando, O. J., Xue, Y. T., Swiderek, K., Kuo, A. & Crabtree, G. R. 1998. Rapid and phosphoinositol-dependent binding of the SWI/SNF-like BAF complex to chromatin after T lymphocyte receptor signaling. *Cell,* 95, 625-636. Available: Doi 10.1016/S0092-8674(00)81633-5

Zhao, L. J., Loewenstein, P. M. & Green, M. 2017. Enhanced MYC association with the NuA4 histone acetyltransferase complex mediated by the adenovirus E1A N-terminal domain activates a subset of MYC target genes highly expressed in cancer cells. *Genes Cancer,* 8, 752-761. Available: 10.18632/genesandcancer.160

Zhou, Y. J., Miao, J. J., Wu, H. J., Tang, H., Kuang, J., Zhou, X. Y., Peng, Y., Hu, D. S., Shi, D. B., Deng, W. G., Cao, X. Y., Zhao, C. & Xie, C. H. 2017. PD-1 and PD-L1 expression in 132 recurrent nasopharyngeal carcinoma: the correlation with anemia and outcomes. *Oncotarget,* 8, 51210-51223. Available: 10.18632/oncotarget.17214

9. APPENDIX 1

9. 1 HRM primers and protocol

Name	Orientation	Sequence (5' → 3')	Amplicon (bps)	Annealing Temperature (°C)
EP400NL INDELs	Forward	TTTCCCTTCTTCCTCCCTTC	94	55
	Reverse	GCTATGGCAACAGGAGTC		

Table A. 1 HRM primer sequences used for detecting indel mutations in the coding region of EP400NL

HRM primers (indicated as black arrows) were designed to amplify specifically at the exon 4 of the EP400NL (DNA sequence labelled in dark green), EP400NL targeted guide RNA sequence (First red sequence) was utilized to create indel mutations (Chapter 2. 6. 4).

Figure A. 1 Genomic location of the HRM primers

HRM PCR reactions were carried out using Luna® Universal qPCR Master Mix as described below. Forward and reverse primers were premixed to a final concentration of 10 µM and 1 µL was used for each reaction. Annealing temperatures for primer pairs are shown in table A.3. Reactions were in a total volume of 10 µL.

Table A. 2 Luna® Universal qPCR reaction composition

Component	Volume (µL)
Luna® Universal qPCR Master Mix	5
Forward Primer (10 µM)	0.5
Reverse Primer (10 µM)	0.5
Template DNA (20 ng/µL)	1.5
PCR Grade Water	2.5

Table A. 3 HRM PCR protocol using Luna® Universal qPCR Master Mix

Temperature	Time	Cycles
Denaturing (95°C)	5 min	1
Amplification (95°C)	5 sec	40
Amplification (63°C)	30 sec	
Amplification (72°C)	4 sec	
Melting Curve (95°C)	Continuous	1
Cool Down (40°C)	Hold	1

9. 2 Protocol for Real-Time qRT-PCR

HRM PCR Protocol Reactions were carried out using SensiFAST™ SYBR® No-ROX One-Step Kit as described below and Chapter 2. 6. Forward and reverse primers were premixed to a final concentration of 10 µM and 2 µL was used in each reaction. Reaction programs were set up in the qPCR machine for unbiased cDNA synthesis and followed by highly sensitive, real-time PCR detection in a single PCR tube. Reactions were in a total volume of 20 µL.

Table A. 4 SensiFAST™ SYBR® No-ROX One-Step qPCR reaction composition

Component	Volume (µL)
SensiFAST SYBR® Lo-ROX One-Step Mix (2x)	10
Primer pairs (10 µM) (Forward + Reverse Primer)	2
RiboSafe RNase Inhibitor	0.4
Reverse transcriptase	0.2
Template mRNA (10-30 ng/µL)	4
DEPC-H2O	3.4

Table A. 5 Real-Time qRT-PCR protocol using SensiFAST™ SYBR® No-ROX One-Step Kit

Temperature	Time	Cycles
Program 1 (45°C)	20 min	1
Program 1 (95°C)	5 min	
Program 2 (95°C)	5 sec	40
Program 2 (63°C)	20 sec	
Program 3 (95°C)	1 sec	1
Program 3 (65°C)	1 sec	
Program 3 (97°C)	Continuous	

9. 3 Protocol for ChIP-qPCR

ChIP-qPCR reactions were carried out using Luna® Universal qPCR Master Mix as described below and in Chapter 2. 6. 2. Forward and reverse primers were premixed to a final concentration of 5 µM (10 ×) and 2.5 µL was used per reaction. Annealing temperatures for primer pairs are shown in table A.3. Annealing 1 was employed for FLAG-GAL4Myc enrichment, annealing 2 was employed for the enrichment of candidate proteins that interacted with EP400NL. Reactions were in a total volume of 25 µL.

Table A. 6 Luna® Universal ChIP-qPCR reaction composition

Component	Volume (µL)
Luna® Universal qPCR Master Mix	12.5
Primer pairs (5 µM) (Forward + Reverse Primer)	2.5
Immunoprecipitated Template DNA	4
PCR Grade Water	6

Table A. 7 ChIP-qPCR protocol using Luna® Universal qPCR Master Mix

Temperature	Time	Cycles
Initiation (95°C)	5 min	1
Denaturing (95°C)	5 sec	45
Annealing 1 (63°C)	30 sec	
Annealing 2 (68°C)	30 sec	
Program (95°C)	1 sec	1
Program (65°C)	1 sec	
Program (97°C)	Continuous	

9. 4 Protocol for Lentiviral Titration using qRT-PCR

Lentiviral Titration using qRT-PCR was carried out using Abcam's qPCR Lentivirus Titer Kit as described below. Viruses were collected, centrifuged at 1000 rpm (100 rcf) for 5 minutes and lysed with viral lysis buffer in a ratio of 1:9 followed by room temperature incubation for 3 minutes. Virus samples were tested with the standards (STD1 and STD2) provided by the lentivirus titer kit. Reactions were in a total volume of 25 µL. The lentiviral titer was calculated based on the Abcam lentivirus titer calculator from their official website. https://old.abmgood.com/viralexp/lentivirus-calculator.php.

Table A. 8 Abcam's lentiviral titration qRT-PCR reaction composition

Component	Volume (µL)
BlasTaq™ 2X qPCR Titer MasterMix	12.5
Primer Mix (5 µM) (WPRE Primer Pair)	2.5
Enzyme Mix	0.2
Collected Viral samples	2.5
Nuclease-Free Water	7.3

Table A. 9 Lentiviral titration protocol using Abcam's qPCR Lentivirus Titer Kit

Temperature	Time	Cycles
Program 1 (42°C)	20 min	1
Program 1 (95°C)	10 min	
Program 2 (95°C)	15 sec	40
Program 2 (60°C)	1 min	
Program 3 (95°C)	1 sec	1
Program 3 (65°C)	1 sec	
Program 3 (97°C)	Continuous	

10. APPENDIX 2

CbF plasmid map

Vector map determined from Invitrogen Vector NTI software. The backbone of all the FLAG-tagged plasmids in this research.

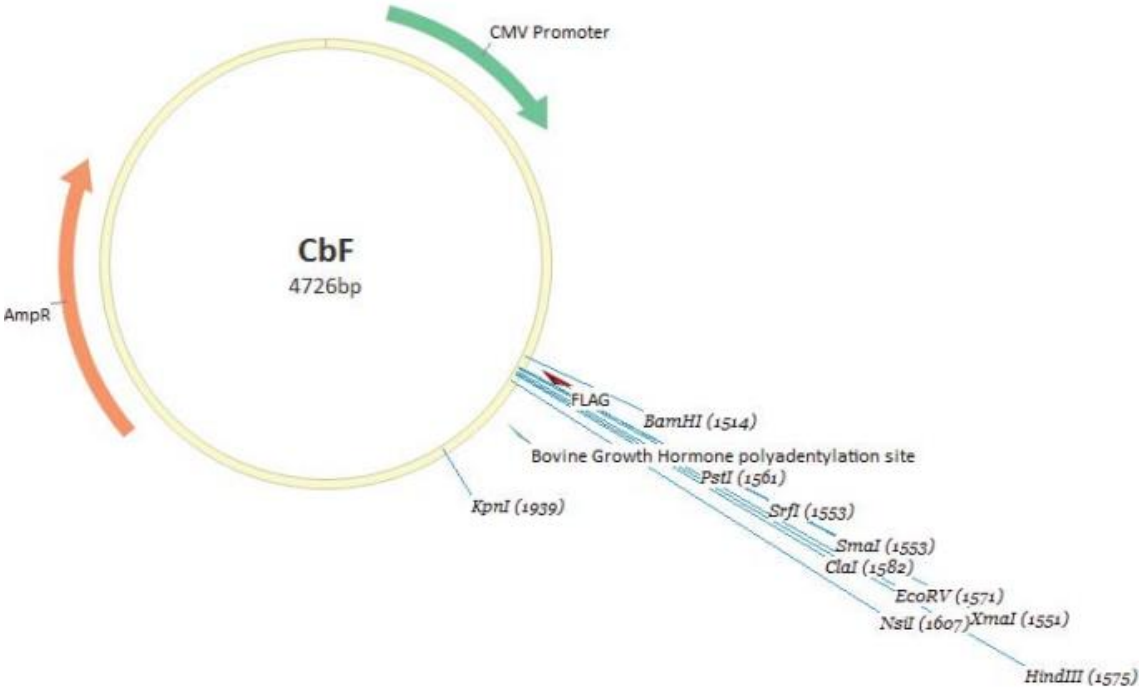

Figure A. 2 A vector map of the CbF transient mammalian expression vector for the expression of the FLAG tagged proteins

11. APPENDIX 3

11. 1 Melting curves and melting peaks of GUSB and PD-L1

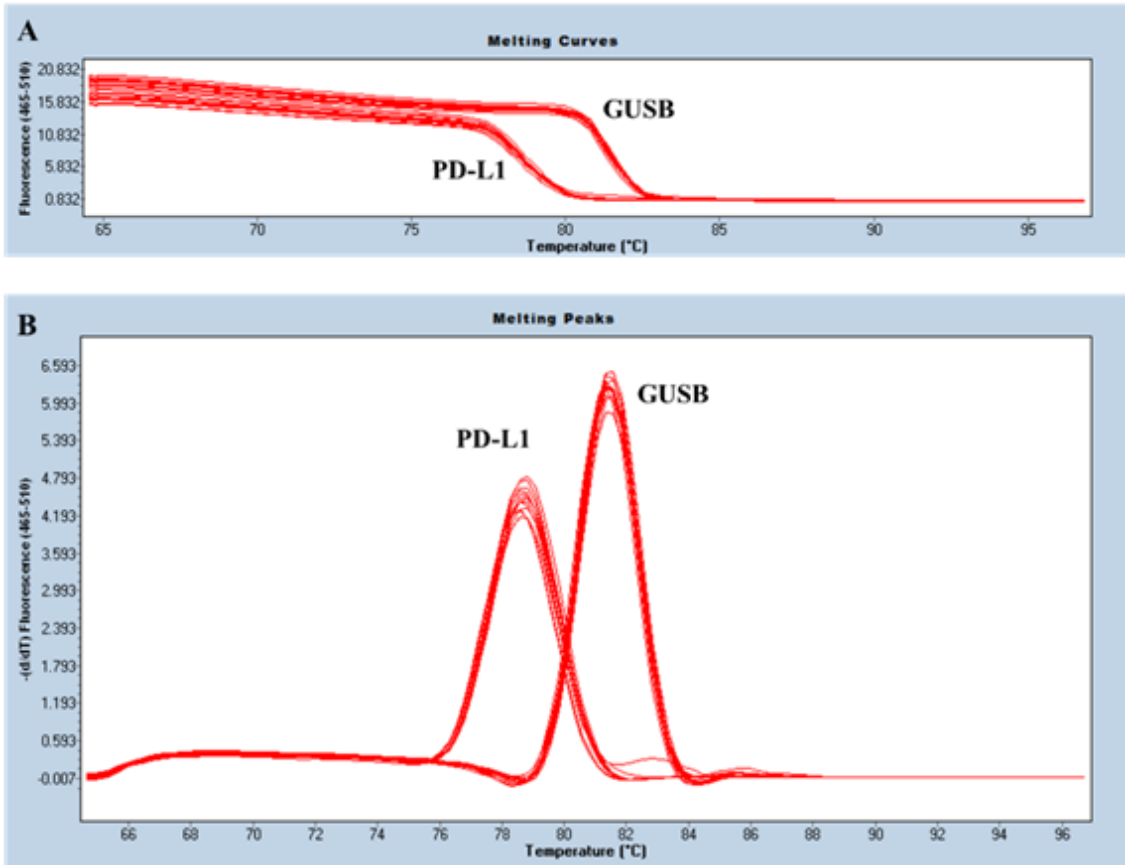

Figure A. 3 Melting curve and melting peak of GUSB gene and PD-L1 gene in quantitative real-rime PCR.

Melting curves (A), Melting peaks (B). A single amplicon of either PD-L1 or GUSB was generated, verifying a single PCR product for each gene. The melting temperature for PD-L1 and GUSB is around 78 °C and 82 °C respectively in the Real-Time qRT-PCR.

11. 2 Melting curves and melting peaks of DBS and p21

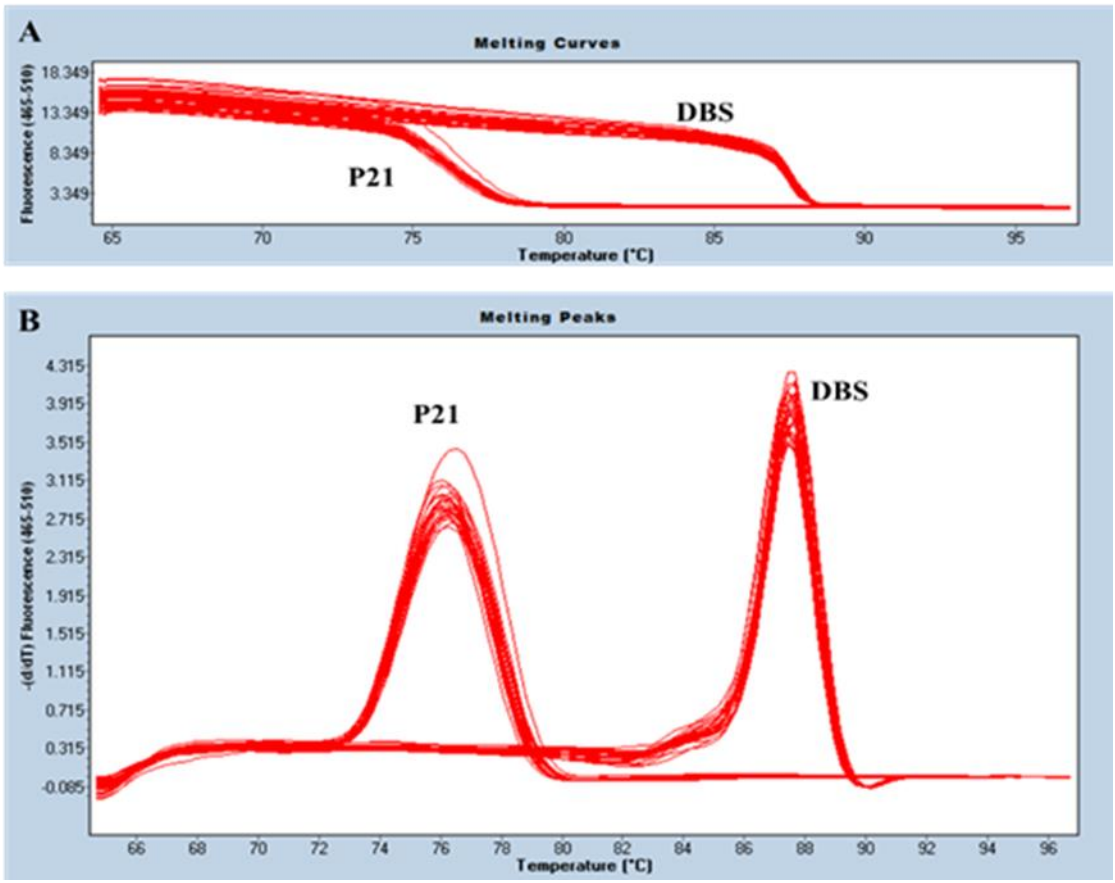

Figure A. 4 Melting curve and melting peak of DBS and p21 in chromatin immunoprecipitation quantitative PCR

Melting curves (A), Melting peaks (B). A single amplicon of either DBS or p21 was generated, verifying a single PCR product for each genetic region. The melting temperature for p21 and DBS (DNA binding site) is around 76 °C and 88 °C respectively in the ChIP-qPCR.

11. 3 Melting curves and melting peaks of PD-L1 and GAPDH

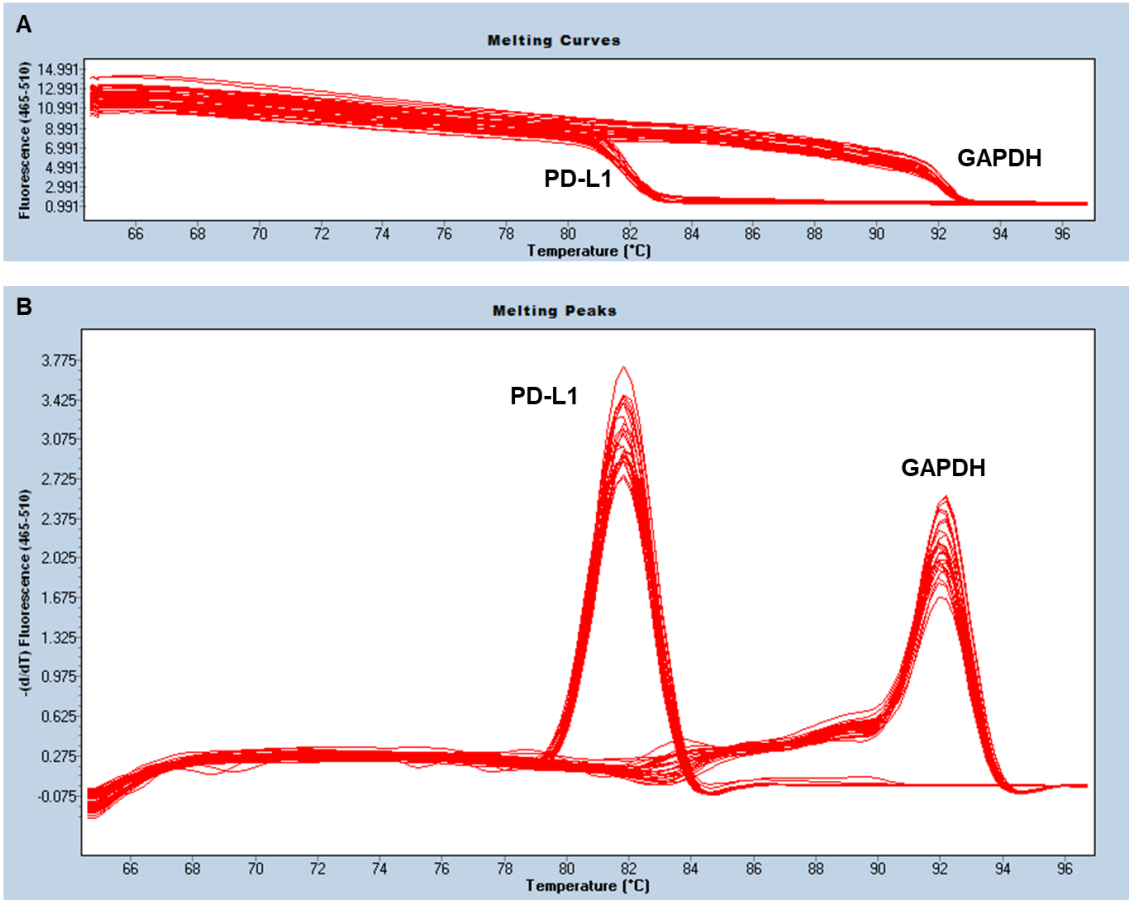

Figure A. 5 Melting curve and melting peak of PD-L1 and GAPDH in chromatin immunoprecipitation quantitative PCR

Melting curves (A), Melting peaks (B). A single amplicon of either PD-L1 or GAPDH was generated, verifying a single PCR product for each genetic region. The melting temperature for PD-L1 and GAPDH is around 82 °C and 92 °C respectively in the ChIP-qPCR.

11. 4 Melting curves and melting peaks of WPRE in lentiviral titration

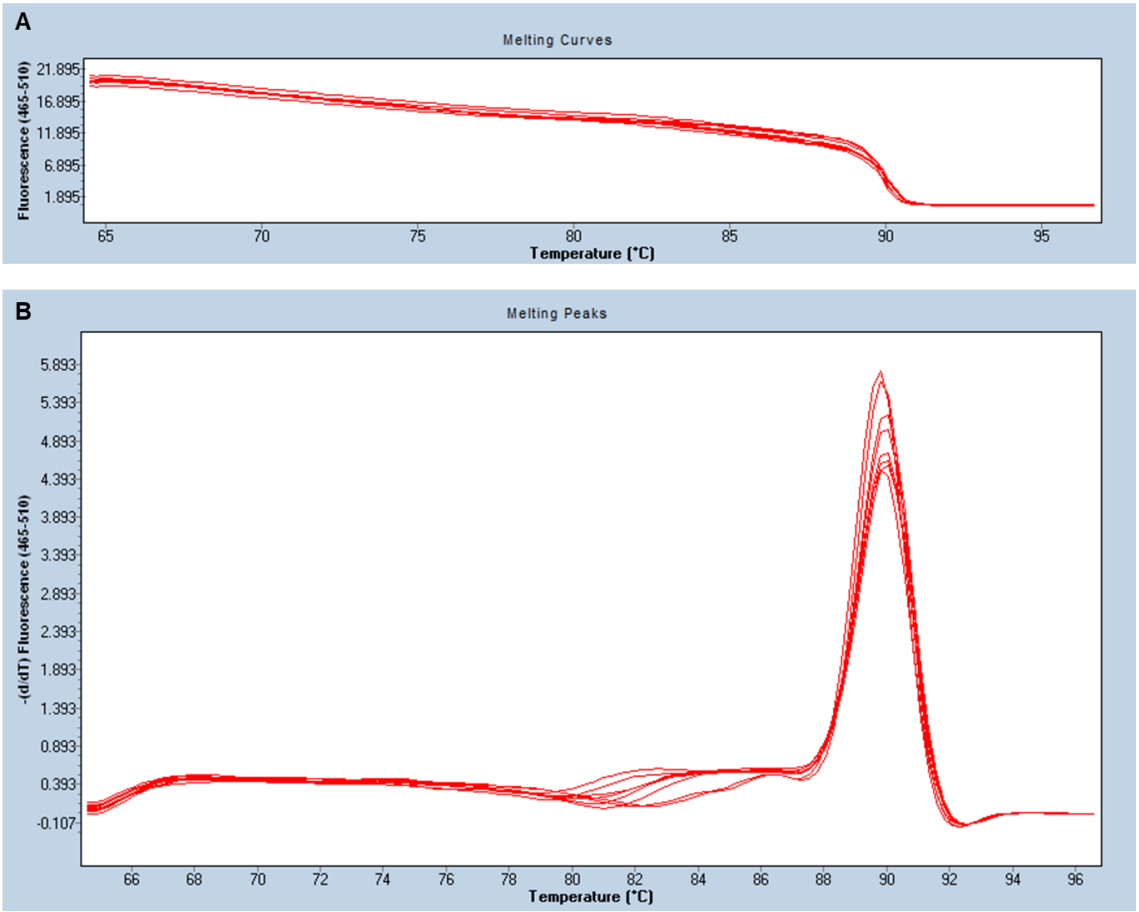

Figure A. 6 Melting curve and melting peak of WPRE in Lentiviral Titration

Melting curves (A), Melting peaks (B). The melting temperature for WPRE is around 90 °C in the qPCR analysis for lentiviral titration.

12. APPENDIX 4

The identification and quantification of proteins using Thermo Scientific™ Proteome Discoverer™ software

The mass spectrometry analysis was performed by Trevor Loo in the School of Natural Sciences Mass Spectrometry Lab. Peptides were analyzed using a bottom-up proteomic methodology, which is a proteomic technique capable of identifying a very low abundance of proteins or peptides in a sample. It measures the accurate masses within a sample by ionizing the chemical species and sorting the ions based on their mass-to-charge ratio for specific peptide detection. The cleavage of the peptide bond primarily leads to either an acylium ion, when the charge was retained on the N-terminal side of the peptide or a protonated peptide when the charge was retained at the C-terminal side of the peptide and these ions were indicated as 'bn' and 'yn' ions, respectively. The unknown amino acid sequence can be read from the two complementary series of ions in the mass spectrum. The identified peptides were assigned back to a comprehensive protein database using a method called protein inference (Nesvizhskii and Aebersold, 2005).

Proteome Discoverer™ Software 2.2 (Thermo Scientific™) was utilized for the identification of peptide sequences. Given a relatively low abundance of the protein sample, the coverage of the peptides is around 15%-20% but with all the specific unique peptides detected and have been recognized as "true" detections rather than "false" detections in the software default setting. The "true" labelled peptides were the real interacting candidates, and the "false" labelled ones were the contaminants. An embedded file of contaminants listed in this software summarized proteins commonly found in proteomics experiments that are present either by accident or through unavoidable contamination of protein samples. PSM (peptide-spectrum match) was also being monitored and the number was either equal or higher than the unique peptides which was a good indicator suggesting multiple encounters of the same unique peptides were found in the sorting process,

however, the number is generally lower than 10 suggesting a relatively low abundance of the protein sample.

A total of 17 gel pieces were trypsinized and followed by the mass spectrometric analysis. No functional proteins were identified from gel slices No.1 and No.2. The eighteen EP400NL associated functional protein candidates have been identified from gel slice No.3 to gel slice No17. Identified protein candidates that are known to be involved in either chromatin remodelling, or transcriptional regulation were specifically analysed.

Table A. 10 Proteins identified from gel slice No.3

Description	Coverage [%]	Contaminant	# Peptides	# PSMs	# Unique Peptides	# AAs	MW [kDa]
Keratin, type II cytoskeletal 1 OS=Homo sapiens OX=9606 GN=KRT1 PE=1 SV=6	16	FALSE	8	10	8	644	66
Bromodomain-containing protein 8 OS=Homo sapiens OX=9606 GN=BRD8 PE=1 SV=2	4	FALSE	3	3	3	1235	135.3
Trypsin OS=Sus scrofa PE=1 SV=1 Tax_Id=9823 [Sus scrofa]	12	TRUE	2	3	2	231	24.4
Keratin, type I cytoskeletal 9 OS=Homo sapiens OX=9606 GN=KRT9 PE=1 SV=3	7	FALSE	3	3	3	623	62
Keratin, type II cytoskeletal 5 OS=Homo sapiens OX=9606 GN=KRT5 PE=1 SV=3	3	FALSE	2	2	2	590	62.3
Keratin, type I cytoskeletal 10 OS=Homo sapiens OX=9606 GN=KRT10 PE=1 SV=6	5	FALSE	2	2	2	584	58.8
Chromodomain-helicase-DNA-binding protein 4 OS=Homo sapiens OX=9606 GN=CHD4 PE=1 SV=1	1	FALSE	2	2	2	1937	220.3
Serum albumin OS=Homo sapiens OX=9606 GN=ALB PE=1 SV=2	2	FALSE	1	1	1	609	69.3
Filamin-A OS=Homo sapiens OX=9606 GN=FLNA PE=1 SV=4	1	FALSE	1	1	1	2647	280.6
Spectrin alpha chain, non-erythrocytic 1 OS=Homo sapiens OX=9606 GN=SPTAN1 PE=1 SV=1	2	FALSE	3	3	3	2498	287.4
Actin, cytoplasmic 1 OS=Homo sapiens OX=9606 GN=ACTB PE=1 SV=1	5	FALSE	1	1	1	375	41.7
Pre-mRNA-processing-splicing factor 8 OS=Homo sapiens OX=9606 GN=PRPF8 PE=1 SV=2	1	FALSE	1	1	1	2335	273.4
Spectrin beta chain OS=Homo sapiens OX=9606 GN=SPTBN1 PE=1 SV=1	0	FALSE	1	1	1	2366	274.7

Table A. 11 Proteins identified from gel slice No.4

Description	Coverage [%]	Contaminant	# Peptides	# PSMs	# Unique Peptides	# AAs	MW [kDa]
Trypsin OS=Sus scrofa PE=1 SV=1 Tax_Id=9823 [Sus scrofa]	22	TRUE	4	10	4	231	24.4
Pre-mRNA-processing-splicing factor 8 OS=Homo sapiens OX=9606 GN=PRPF8 PE=1 SV=2	7	FALSE	13	13	13	2335	273.4
Keratin, type I cytoskeletal 9 OS=Homo sapiens OX=9606 GN=KRT9 PE=1 SV=3	11	FALSE	3	4	3	623	62
Keratin, type II cytoskeletal 1 OS=Homo sapiens OX=9606 GN=KRT1 PE=1 SV=6	12	FALSE	6	6	6	644	66
U5 small nuclear ribonucleoprotein 200 kDa helicase OS=Homo sapiens OX=9606 GN=SNRNP200 PE=1 SV=2	6	FALSE	9	9	9	2136	244.4
Bromodomain-containing protein 8 OS=Homo sapiens OX=9606 GN=BRD8 PE=1 SV=2	7	FALSE	5	5	5	1235	135.3
Serum albumin OS=Bos taurus GN=ALB PE=1 SV=4 Tax_Id=9913 [Bos taurus]	6	TRUE	3	3	3	607	69.2
Acetyl-CoA carboxylase 1 OS=Homo sapiens OX=9606 GN=ACACA PE=1 SV=2	4	FALSE	5	5	5	2346	265.4
Nuclear mitotic apparatus protein 1 OS=Homo sapiens OX=9606 GN=NUMA1 PE=1 SV=2	7	FALSE	9	9	9	2115	238.1
Transcription activator BRG1 OS=Homo sapiens OX=9606 GN=SMARCA4 PE=1 SV=1	4	FALSE	5	5	5	1681	188.7
Keratin, type II cytoskeletal 5 OS=Homo sapiens OX=9606 GN=KRT5 PE=1 SV=3	2	FALSE	1	1	1	590	62.3
Protein virilizer homolog OS=Homo sapiens OX=9606 GN=VIRMA PE=1 SV=2	1	FALSE	2	2	2	1812	201.9
DNA-directed RNA polymerase I subunit RPA1 OS=Homo sapiens OX=9606 GN=POLR1A PE=1 SV=2	1	FALSE	1	1	1	1720	194.7
Keratin, type I cytoskeletal 10 OS=Homo sapiens OX=9606 GN=KRT10 PE=1 SV=6	2	TRUE	1	1	1	584	58.8
Heterogeneous nuclear ribonucleoprotein U OS=Homo sapiens OX=9606 GN=HNRNPU PE=1 SV=6	2	FALSE	1	1	1	825	90.5
Structural maintenance of chromosomes flexible hinge domain-containing protein 1 OS=Homo sapiens OX=9606 GN=SMCHD1 PE=1 SV=2	1	FALSE	1	1	1	2005	226.2
Transmembrane anterior posterior transformation protein 1 homolog OS=Homo sapiens OX=9606 GN=TAPT1 PE=1 SV=1	3	FALSE	1	1	1	567	64.2
Rubber elongation factor protein OS=Hevea brasiliensis PE=1 SV=2 Tax_Id=3981 [Hevea brasiliensis]	8	TRUE	1	1	1	138	14.7
Keratin, type II cytoskeletal 2 epidermal OS=Homo sapiens OX=9606 GN=KRT2 PE=1 SV=2	7	FALSE	1	1	1	639	65.4
Unconventional myosin-XVIIIa OS=Homo sapiens OX=9606 GN=MYO18A PE=1 SV=3	1	FALSE	1	1	1	2054	233
Putative EP400-like protein OS=Homo sapiens OX=9606 GN=EP400P1 PE=5 SV=2	2	FALSE	1	1	1	488	51.7
Protein PRRC2A OS=Homo sapiens OX=9606 GN=PRRC2A PE=1 SV=3	3	FALSE	2	2	2	2157	228.7

Table A. 12 Proteins identified from gel slice No.5

Description	Coverage [%]	Contaminant	# Peptides	# PSMs	# Unique Peptides	# AAs	MW [kDa]
Bromodomain-containing protein 8 OS=Homo sapiens OX=9606 GN=BRD8 PE=1 SV=1	38	FALSE	19	32	2	878	95.3
Bromodomain-containing protein 8 (Fragment) OS=Homo sapiens OX=9606 GN=BRD8 PE=1 SV=1	34	FALSE	19	30	2	892	96.8
Trypsin OS=Sus scrofa PE=1 SV=1 Tax_Id=9823 [Sus scrofa]	22	TRUE	3	8	3	231	24.4
Serum albumin OS=Homo sapiens OX=9606 GN=ALB PE=1 SV=2	2	TRUE	1	1	1	609	69.3
Keratin, type II cytoskeletal 1 OS=Homo sapiens OX=9606 GN=KRT1 PE=1 SV=6	6	FALSE	3	3	3	644	66
Structural maintenance of chromosomes protein 4 OS=Homo sapiens OX=9606 GN=SMC4 PE=1 SV=2	2	FALSE	2	2	2	1288	147.1
B2 bradykinin receptor OS=Homo sapiens OX=9606 GN=BDKRB2 PE=1 SV=2	9	FALSE	1	3	1	391	44.4
Keratin, type I cytoskeletal 9 OS=Homo sapiens OX=9606 GN=KRT9 PE=1 SV=3	1	FALSE	1	1	1	623	62
MyoD family inhibitor domain-containing protein 2 OS=Homo sapiens OX=9606 GN=MDFIC2 PE=2 SV=1	17	FALSE	1	1	1	189	21.5
Mitogen-activated protein kinase 14 OS=Homo sapiens OX=9606 GN=MAPK14 PE=1 SV=3	11	FALSE	1	2	1	360	41.3
Clathrin heavy chain OS=Homo sapiens OX=9606 GN=CLTC PE=1 SV=1	1	FALSE	1	1	1	1679	191.9
Transcription factor p65 OS=Homo sapiens OX=9606 GN=RELA PE=1 SV=2	5	FALSE	1	1	1	551	60.2
Adenylate kinase 9 OS=Homo sapiens OX=9606 GN=AK9 PE=1 SV=2	2	FALSE	1	1	1	1911	221.3
Keratin, type I cytoskeletal 10 OS=Homo sapiens OX=9606 GN=KRT10 PE=1 SV=6	2	TRUE	1	1	1	584	58.8
Rubber elongation factor protein OS=Hevea brasiliensis PE=1 SV=2 Tax_Id=3981 [Hevea brasiliensis]	8	TRUE	1	1	1	138	14.7
Ras GTPase-activating-like protein IQGAP1 OS=Homo sapiens OX=9606 GN=IQGAP1 PE=1 SV=1	1	FALSE	2	2	2	1657	189.1
Keratin, type II cytoskeletal 5 OS=Homo sapiens OX=9606 GN=KRT5 PE=1 SV=3	4	FALSE	2	2	2	590	62.3

Table A. 13 Proteins identified from gel slice No.6

Description	Coverage [%]	Contaminant	# Peptides	# PSMs	# Unique Peptides	# AAs	MW [kDa]
Bromodomain-containing protein 8 OS=Homo sapiens OX=9606 GN=BRD8 PE=1 SV=2	7	FALSE	5	8	1	1235	135.3
Bromodomain-containing protein 8 (Fragment) OS=Homo sapiens OX=9606 GN=BRD8 PE=1 SV=1	8	FALSE	5	8	1	892	96.8
Trypsin OS=Sus scrofa PE=1 SV=1 Tax_Id=9823 [Sus scrofa]	25	TRUE	4	5	4	231	24.4
Keratin, type II cytoskeletal 1 OS=Homo sapiens OX=9606 GN=KRT1 PE=1 SV=6	6	FALSE	3	3	3	644	66
Keratin, type II cytoskeletal 5 OS=Homo sapiens OX=9606 GN=KRT5 PE=1 SV=3	4	FALSE	2	2	1	590	62.3
Serum albumin OS=Homo sapiens OX=9606 GN=ALB PE=1 SV=2	4	TRUE	2	2	2	609	69.3
Eukaryotic translation initiation factor 3 subunit A OS=Homo sapiens OX=9606 GN=EIF3A PE=1 SV=1	2	FALSE	2	2	2	1382	166.5
Lysozyme C OS=Homo sapiens OX=9606 GN=LYZ PE=1 SV=1	8	FALSE	1	1	1	148	16.5
Keratin, type II cytoskeletal 2 epidermal OS=Homo sapiens OX=9606 GN=KRT2 PE=1 SV=2	5	FALSE	2	2	1	639	65.4
Keratin, type II cytoskeletal 6A OS=Homo sapiens OX=9606 GN=KRT6A PE=1 SV=3	7	FALSE	3	3	2	564	60
Cleavage and polyadenylation specificity factor subunit 1 OS=Homo sapiens OX=9606 GN=CPSF1 PE=1 SV=2	3	FALSE	3	3	3	1443	160.8
Deleted in malignant brain tumors 1 protein OS=Homo sapiens OX=9606 GN=DMBT1 PE=1 SV=2	7	FALSE	1	1	1	2413	260.6
Keratin, type I cytoskeletal 10 OS=Homo sapiens OX=9606 GN=KRT10 PE=1 SV=6	6	FALSE	3	3	3	584	58.8
Protein S100-A8 OS=Homo sapiens OX=9606 GN=S100A8 PE=1 SV=1	12	FALSE	1	1	1	93	10.8
Fatty acid-binding protein 5 OS=Homo sapiens OX=9606 GN=FABP5 PE=1 SV=3	7	FALSE	1	1	1	135	15.2
Cilia- and flagella-associated protein 47 OS=Homo sapiens OX=9606 GN=CFAP47 PE=2 SV=5	0	FALSE	1	1	1	3187	361.4
Immunoglobulin heavy constant alpha 1 (Fragment) OS=Homo sapiens OX=9606 GN=IGHA1 PE=1 SV=1	4	FALSE	1	1	1	398	42.8
TBC1 domain family member 19 OS=Homo sapiens OX=9606 GN=TBC1D19 PE=1 SV=2	4	FALSE	1	2	1	526	60.2

Table A. 14 Proteins identified from gel slice No.7

Description	Coverage [%]	Contaminant	# Peptides	# PSMs	# Unique Peptides	# AAs	MW [kDa]
Bromodomain-containing protein 8 OS=Homo sapiens OX=9606 GN=BRD8 PE=1 SV=2	8	FALSE	6	10	6	1235	135.3
Trypsin OS=Sus scrofa PE=1 SV=1 Tax_Id=9823 [Sus scrofa]	25	TRUE	4	11	4	231	24.4
Keratin, type II cytoskeletal 1 OS=Homo sapiens OX=9606 GN=KRT1 PE=1 SV=6	9	FALSE	4	4	4	644	66
Structural maintenance of chromosomes protein 1A OS=Homo sapiens OX=9606 GN=SMC1A PE=1 SV=2	4	FALSE	6	6	6	1233	143.1
Serum albumin OS=Bos taurus GN=ALB PE=1 SV=4 Tax_Id=9913 [Bos taurus]	4	TRUE	2	2	2	607	69.2
pre-mRNA 3' end processing protein WDR33 OS=Homo sapiens OX=9606 GN=WDR33 PE=1 SV=2	1	FALSE	1	1	1	1336	145.8
Keratin, type II cytoskeletal 6A OS=Homo sapiens OX=9606 GN=KRT6A PE=1 SV=3	3	FALSE	1	1	1	564	60
Rubber elongation factor protein OS=Hevea brasiliensis PE=1 SV=2 Tax_Id=3981 [Hevea brasiliensis]	8	TRUE	1	1	1	138	14.7
Paired amphipathic helix protein Sin3a OS=Homo sapiens OX=9606 GN=SIN3A PE=1 SV=2	1	FALSE	1	1	1	1273	145.1
Probable E3 ubiquitin-protein ligase makorin-3 OS=Homo sapiens OX=9606 GN=MKRN3 PE=1 SV=1	13	FALSE	1	1	1	182	19.6
U3 small nucleolar RNA-interacting protein 2 OS=Homo sapiens OX=9606 GN=RRP9 PE=1 SV=1	7	FALSE	1	3	1	475	51.8
DNA repair protein RAD50 OS=Homo sapiens OX=9606 GN=RAD50 PE=1 SV=1	2	FALSE	3	3	3	1312	153.8
Scaffold attachment factor B2 OS=Homo sapiens OX=9606 GN=SAFB2 PE=1 SV=1	1	FALSE	1	1	1	953	107.4
Coatomer subunit alpha OS=Homo sapiens OX=9606 GN=COPA PE=1 SV=2	2	FALSE	2	2	2	1224	138.3
Transcription elongation regulator 1 OS=Homo sapiens OX=9606 GN=TCERG1 PE=1 SV=2	1	FALSE	1	1	1	1098	123.8

Table A. 15 Proteins identified from gel slice No.8

Description	Coverage [%]	Contaminant	# Peptides	# PSMs	# Unique Peptides	# AAs	MW [kDa]
ATP-dependent RNA helicase A OS=Homo sapiens OX=9606 GN=DHX9 PE=1 SV=4	13	FALSE	11	12	11	1270	140.9
Trypsin OS=Sus scrofa PE=1 SV=1 Tax_Id=9823 [Sus scrofa]	22	TRUE	3	7	3	231	24.4
General transcription factor II-I OS=Homo sapiens OX=9606 GN=GTF2I PE=1 SV=2	14	FALSE	9	9	9	998	112.3
Structural maintenance of chromosomes protein 3 OS=Homo sapiens OX=9606 GN=SMC3 PE=1 SV=2	6	FALSE	5	5	5	1217	141.5
Keratin, type II cytoskeletal 1 OS=Homo sapiens OX=9606 GN=KRT1 PE=1 SV=6	8	FALSE	4	4	4	644	66
Cell cycle and apoptosis regulator protein 2 OS=Homo sapiens OX=9606 GN=CCAR2 PE=1 SV=2	15	FALSE	9	10	9	923	102.8
Structural maintenance of chromosomes protein 2 OS=Homo sapiens OX=9606 GN=SMC2 PE=1 SV=2	2	FALSE	2	2	2	1197	135.6
Splicing factor 3B subunit 1 OS=Homo sapiens OX=9606 GN=SF3B1 PE=1 SV=3	7	FALSE	5	6	5	1304	145.7
Keratin, type I cytoskeletal 9 OS=Homo sapiens OX=9606 GN=KRT9 PE=1 SV=3	12	FALSE	3	3	3	623	62
Splicing factor 3B subunit 2 OS=Homo sapiens OX=9606 GN=SF3B2 PE=1 SV=2	1	FALSE	1	1	1	895	100.2
Bromodomain-containing protein 8 OS=Homo sapiens OX=9606 GN=BRD8 PE=1 SV=2	2	FALSE	1	1	1	1235	135.3
Serum albumin OS=Homo sapiens OX=9606 GN=ALB PE=1 SV=2	2	TRUE	1	1	1	609	69.3
Inter-alpha-trypsin inhibitor heavy chain H2 OS=Homo sapiens OX=9606 GN=ITIH2 PE=1 SV=2	1	FALSE	1	1	1	946	106.4
Heterogeneous nuclear ribonucleoprotein U OS=Homo sapiens OX=9606 GN=HNRNPU PE=1 SV=6	1	FALSE	1	1	1	825	90.5
Keratin, type II cytoskeletal 2 epidermal OS=Homo sapiens OX=9606 GN=KRT2 PE=1 SV=2	3	FALSE	1	1	1	639	65.4
THO complex subunit 2 OS=Homo sapiens OX=9606 GN=THOC2 PE=1 SV=2	1	FALSE	1	1	1	1593	182.7
Splicing factor 3B subunit 3 OS=Homo sapiens OX=9606 GN=SF3B3 PE=1 SV=4	1	FALSE	1	1	1	1217	135.5
Pre-mRNA-processing factor 40 homolog A OS=Homo sapiens OX=9606 GN=PRPF40A PE=1 SV=1	1	FALSE	1	1	1	994	112.3
Putative EP400-like protein OS=Homo sapiens OX=9606 GN=EP400P1 PE=5 SV=2	2	FALSE	1	1	1	488	51.7
Keratin, type II cytoskeletal 6A OS=Homo sapiens OX=9606 GN=KRT6A PE=1 SV=3	3	FALSE	1	1	1	564	60
Dermcidin OS=Homo sapiens OX=9606 GN=DCD PE=1 SV=2	10	FALSE	1	1	1	110	11.3
DNA-directed RNA polymerase II subunit RPB2 OS=Homo sapiens OX=9606 GN=POLR2B PE=1 SV=1	1	FALSE	1	1	1	1174	133.8
Keratin, type I cytoskeletal 10 OS=Homo sapiens OX=9606 GN=KRT10 PE=1 SV=6	3	FALSE	1	1	1	584	58.8
Vimentin OS=Homo sapiens OX=9606 GN=VIM PE=1 SV=4	3	FALSE	1	1	1	466	53.6
Xin actin-binding repeat-containing protein 2 OS=Homo sapiens OX=9606 GN=XIRP2 PE=1 SV=2	1	FALSE	1	2	1	3374	382.1
RNA-binding protein 26 OS=Homo sapiens OX=9606 GN=RBM26 PE=1 SV=1	1	FALSE	1	1	1	1009	113.7
Keratin, type II cytoskeletal 5 OS=Homo sapiens OX=9606 GN=KRT5 PE=1 SV=3	7	FALSE	3	3	3	590	62.3

Table A. 16 Proteins identified from gel slice No.9

Description	Coverage [%]	Contaminant	# Peptides	# PSMs	# Unique Peptides	# AAs	MW [kDa]
Heterogeneous nuclear ribonucleoprotein U OS=Homo sapiens OX=9606 GN=HNRNPU PE=1 SV=6	10	FALSE	6	8	6	825	90.5
Trypsin OS=Sus scrofa PE=1 SV=1 Tax_Id=9823 [Sus scrofa]	25	TRUE	4	10	4	231	24.4
Keratin, type II cytoskeletal 1 OS=Homo sapiens OX=9606 GN=KRT1 PE=1 SV=6	9	FALSE	5	5	5	644	66
Matrin-3 OS=Homo sapiens OX=9606 GN=MATR3 PE=1 SV=1	7	FALSE	5	6	5	895	99.9
116 kDa U5 small nuclear ribonucleoprotein component OS=Homo sapiens OX=9606 GN=EFTUD2 PE=1 SV=1	8	FALSE	6	6	6	972	109.4
Lipocalin-1 OS=Homo sapiens OX=9606 GN=LCN1 PE=1 SV=1	13	FALSE	2	2	2	176	19.2
Lysozyme C OS=Homo sapiens OX=9606 GN=LYZ PE=1 SV=1	8	FALSE	1	1	1	148	16.5
Serrate RNA effector molecule homolog OS=Homo sapiens OX=9606 GN=SRRT PE=1 SV=1	1	FALSE	1	1	1	876	100.6
Serum albumin OS=Bos taurus GN=ALB PE=1 SV=4 Tax_Id=9913 [Bos taurus]	4	TRUE	3	3	1	607	69.2
ATP-dependent RNA helicase A OS=Homo sapiens OX=9606 GN=DHX9 PE=1 SV=4	3	FALSE	3	3	3	1270	140.9
Eukaryotic translation initiation factor 3 subunit B OS=Homo sapiens OX=9606 GN=EIF3B PE=1 SV=3	9	FALSE	5	5	5	814	92.4
Lactotransferrin OS=Homo sapiens OX=9606 GN=LTF PE=1 SV=6	3	FALSE	2	2	2	710	78.1
Splicing factor 3A subunit 1 OS=Homo sapiens OX=9606 GN=SF3A1 PE=1 SV=1	6	FALSE	3	4	3	793	88.8
Keratin, type I cytoskeletal 9 OS=Homo sapiens OX=9606 GN=KRT9 PE=1 SV=3	5	FALSE	2	2	2	623	62
Heterogeneous nuclear ribonucleoprotein U-like protein 2 OS=Homo sapiens OX=9606 GN=HNRNPUL2 PE=1 SV=1	6	FALSE	3	3	3	747	85.1
RNA-binding protein 25 OS=Homo sapiens OX=9606 GN=RBM25 PE=1 SV=3	1	FALSE	1	1	1	843	100.1
Poly [ADP-ribose] polymerase 1 OS=Homo sapiens OX=9606 GN=PARP1 PE=1 SV=4	2	FALSE	2	2	2	1014	113
Keratin, type II cytoskeletal 6A OS=Homo sapiens OX=9606 GN=KRT6A PE=1 SV=3	3	FALSE	1	1	1	564	60
Keratin, type I cytoskeletal 10 OS=Homo sapiens OX=9606 GN=KRT10 PE=1 SV=6	7	FALSE	2	2	2	584	58.8
Keratin, type II cytoskeletal 2 epidermal OS=Homo sapiens OX=9606 GN=KRT2 PE=1 SV=2	2	FALSE	1	1	1	639	65.4
Serum albumin OS=Homo sapiens OX=9606 GN=ALB PE=1 SV=2	4	FALSE	3	3	1	609	69.3
Polymeric immunoglobulin receptor OS=Homo sapiens OX=9606 GN=PIGR PE=1 SV=4	1	FALSE	1	1	1	764	83.2
Keratin, type II cytoskeletal 5 OS=Homo sapiens OX=9606 GN=KRT5 PE=1 SV=3	4	FALSE	2	2	2	590	62.3

Table A. 17 Proteins identified from gel slice No.10

Description	Coverage [%]	Contaminant	# Peptides	# PSMs	# Unique Peptides	# AAs	MW [kDa]
Trypsin OS=Sus scrofa PE=1 SV=1 Tax_Id=9823 [Sus scrofa]	22	TRUE	4	11	4	231	24.4
Keratin, type II cytoskeletal 1 OS=Homo sapiens OX=9606 GN=KRT1 PE=1 SV=6	14	FALSE	7	7	7	644	66
Interleukin enhancer-binding factor 3 OS=Homo sapiens OX=9606 GN=ILF3 PE=1 SV=3	11	FALSE	6	7	6	894	95.3
Keratin, type I cytoskeletal 9 OS=Homo sapiens OX=9606 GN=KRT9 PE=1 SV=3	12	FALSE	4	4	4	623	62
X-ray repair cross-complementing protein 5 OS=Homo sapiens OX=9606 GN=XRCC5 PE=1 SV=3	9	FALSE	4	4	4	732	82.7
Keratin, type I cytoskeletal 10 OS=Homo sapiens OX=9606 GN=KRT10 PE=1 SV=6	11	FALSE	3	3	3	584	58.8
Transcription intermediary factor 1-beta OS=Homo sapiens OX=9606 GN=TRIM28 PE=1 SV=5	9	FALSE	4	4	4	835	88.5
Pre-mRNA-processing factor 6 OS=Homo sapiens OX=9606 GN=PRPF6 PE=1 SV=1	3	FALSE	3	3	3	941	106.9
Nucleolar RNA helicase 2 OS=Homo sapiens OX=9606 GN=DDX21 PE=1 SV=5	6	FALSE	4	4	4	783	87.3
Heterogeneous nuclear ribonucleoprotein U OS=Homo sapiens OX=9606 GN=HNRNPU PE=1 SV=6	3	FALSE	2	2	2	825	90.5
Statherin OS=Homo sapiens OX=9606 GN=STATH PE=1 SV=2	53	FALSE	1	1	1	62	7.3
Bromodomain-containing protein 8 OS=Homo sapiens OX=9606 GN=BRD8 PE=1 SV=2	2	FALSE	1	1	1	1235	135.3
Testis-expressed protein 10 OS=Homo sapiens OX=9606 GN=TEX10 PE=1 SV=2	2	FALSE	1	1	1	929	105.6
Serum albumin OS=Homo sapiens OX=9606 GN=ALB PE=1 SV=2	2	TRUE	1	1	1	609	69.3
Poly [ADP-ribose] polymerase 1 OS=Homo sapiens OX=9606 GN=PARP1 PE=1 SV=4	5	FALSE	4	4	4	1014	113
Pre-mRNA-splicing factor ATP-dependent RNA helicase DHX15 OS=Homo sapiens OX=9606 GN=DHX15 PE=1 SV=2	2	FALSE	1	1	1	795	90.9
Keratin, type II cytoskeletal 5 OS=Homo sapiens OX=9606 GN=KRT5 PE=1 SV=3	2	FALSE	1	1	1	590	62.3
Splicing factor, proline- and glutamine-rich OS=Homo sapiens OX=9606 GN=SFPQ PE=1 SV=2	8	FALSE	4	4	4	707	76.1
Nuclear pore complex protein Nup98-Nup96 OS=Homo sapiens OX=9606 GN=NUP98 PE=1 SV=1	3	FALSE	1	2	1	1348	143.4
DNA-directed RNA polymerase II subunit RPB1 OS=Homo sapiens OX=9606 GN=POLR2A PE=1 SV=2	2	FALSE	1	4	1	1970	217
Lethal(2) giant larvae protein homolog 1 OS=Homo sapiens OX=9606 GN=LLGL1 PE=1 SV=3	3	FALSE	1	1	1	1064	115.3
Mediator of RNA polymerase II transcription subunit 16 OS=Homo sapiens OX=9606 GN=MED16 PE=1 SV=2	2	FALSE	1	1	1	877	96.7
Eukaryotic translation initiation factor 3 subunit B OS=Homo sapiens OX=9606 GN=EIF3B PE=1 SV=3	1	FALSE	1	1	1	814	92.4
MAP kinase-activated protein kinase 2 OS=Homo sapiens OX=9606 GN=MAPKAPK2 PE=1 SV=1	3	FALSE	1	1	1	400	45.5
Vimentin OS=Homo sapiens OX=9606 GN=VIM PE=1 SV=4	3	FALSE	1	1	1	466	53.6
U4/U6.U5 tri-snRNP-associated protein 1 OS=Homo sapiens OX=9606 GN=SART1 PE=1 SV=1	7	FALSE	3	3	3	800	90.2
Metastasis-associated protein MTA1 OS=Homo sapiens OX=9606 GN=MTA1 PE=1 SV=2	2	FALSE	1	1	1	715	80.7
5'-3' exoribonuclease 2 OS=Homo sapiens OX=9606 GN=XRN2 PE=1 SV=1	1	FALSE	1	1	1	950	108.5
ATP-binding cassette sub-family A member 9 OS=Homo sapiens OX=9606 GN=ABCA9 PE=1 SV=1	1	FALSE	1	3	1	1624	184.2
Heterogeneous nuclear ribonucleoprotein U-like protein 1 OS=Homo sapiens OX=9606 GN=HNRNPUL1 PE=1 SV=2	2	FALSE	1	1	1	856	95.7
Matrin-3 OS=Homo sapiens OX=9606 GN=MATR3 PE=1 SV=1	2	FALSE	1	1	1	895	99.9

Table A. 18 Proteins identified from gel slice No.11

Description	Coverage [%]	Contaminant	# Peptides	# PSMs	# Unique Peptides	# AAs	MW [kDa]
Trypsin OS=Sus scrofa PE=1 SV=1 Tax_Id=9823 [Sus scrofa]	25	TRUE	5	13	5	231	24.4
Splicing factor, proline- and glutamine-rich OS=Homo sapiens OX=9606 GN=SFPQ PE=1 SV=2	14	FALSE	7	12	7	707	76.1
Keratin, type I cytoskeletal 9 OS=Homo sapiens OX=9606 GN=KRT9 PE=1 SV=3	17	FALSE	5	5	5	623	62
Keratin, type II cytoskeletal 1 OS=Homo sapiens OX=9606 GN=KRT1 PE=1 SV=6	8	FALSE	4	4	4	644	66
Cleavage and polyadenylation specificity factor subunit 2 OS=Homo sapiens OX=9606 GN=CPSF2 PE=1 SV=2	5	FALSE	3	3	3	782	88.4
Serum albumin OS=Bos taurus GN=ALB PE=1 SV=4 Tax_Id=9913 [Bos taurus]	4	TRUE	2	2	2	607	69.2
Cell division cycle 5-like protein OS=Homo sapiens OX=9606 GN=CDC5L PE=1 SV=2	3	FALSE	2	2	2	802	92.2
Nucleolar RNA helicase 2 OS=Homo sapiens OX=9606 GN=DDX21 PE=1 SV=5	2	FALSE	1	1	1	783	87.3
Probable ATP-dependent RNA helicase DDX23 OS=Homo sapiens OX=9606 GN=DDX23 PE=1 SV=3	6	FALSE	4	5	4	820	95.5
Heterogeneous nuclear ribonucleoprotein U OS=Homo sapiens OX=9606 GN=HNRNPU PE=1 SV=6	3	FALSE	2	2	2	825	90.5
Nebulin OS=Homo sapiens OX=9606 GN=NEB PE=1 SV=1	0	FALSE	1	1	1	8560	990.2
Condensin complex subunit 2 OS=Homo sapiens OX=9606 GN=NCAPH PE=1 SV=3	3	FALSE	2	2	2	741	82.5
Intersectin-2 OS=Homo sapiens OX=9606 GN=ITSN2 PE=1 SV=3	1	FALSE	1	1	1	1697	193.3
Pre-mRNA-processing factor 6 OS=Homo sapiens OX=9606 GN=PRPF6 PE=1 SV=1	1	FALSE	1	1	1	941	106.9
Bromodomain-containing protein 8 OS=Homo sapiens OX=9606 GN=BRD8 PE=1 SV=2	1	FALSE	1	1	1	1235	135.3
Cilia- and flagella-associated protein 47 OS=Homo sapiens OX=9606 GN=CFAP47 PE=2 SV=5	0	FALSE	1	1	1	3187	361.4
Tuftelin-interacting protein 11 OS=Homo sapiens OX=9606 GN=TFIP11 PE=1 SV=1	1	FALSE	1	1	1	837	96.8
Rubber elongation factor protein OS=Hevea brasiliensis PE=1 SV=2 Tax_Id=3981 [Hevea brasiliensis]	8	TRUE	1	1	1	138	14.7
CCR4-NOT transcription complex subunit 4 OS=Homo sapiens OX=9606 GN=CNOT4 PE=1 SV=3	4	FALSE	1	3	1	575	63.5
Keratin, type II cytoskeletal 2 epidermal OS=Homo sapiens OX=9606 GN=KRT2 PE=1 SV=2	5	FALSE	2	2	2	639	65.4
INO80 complex subunit C OS=Homo sapiens OX=9606 GN=INO80C PE=4 SV=1	29	FALSE	1	4	1	89	9.4
YTH domain-containing protein 1 OS=Homo sapiens OX=9606 GN=YTHDC1 PE=1 SV=1	1	FALSE	1	1	1	735	85.5
Transcription intermediary factor 1-beta OS=Homo sapiens OX=9606 GN=TRIM28 PE=1 SV=5	1	FALSE	1	1	1	835	88.5
Keratin, type II cytoskeletal 5 OS=Homo sapiens OX=9606 GN=KRT5 PE=1 SV=3	2	FALSE	1	1	1	590	62.3

Table A. 19 Proteins identified from gel slice No.12

Description	Contaminant	Coverage [%]	# Peptides	# PSMs	# Unique Peptides	# AAs	MW [kDa]
Trypsin OS=Sus scrofa PE=1 SV=1 Tax_Id=9823 [Sus scrofa]	TRUE	21	4	11	4	231	24.4
Keratin, type II cytoskeletal 1 OS=Homo sapiens OX=9606 GN=KRT1 PE=1 SV=6	FALSE	24	10	11	10	644	66
Heat shock 70 kDa protein 1B OS=Homo sapiens OX=9606 GN=HSPA1B PE=1 SV=1	FALSE	22	8	8	7	642	70.1
Heterogeneous nuclear ribonucleoprotein R OS=Homo sapiens OX=9606 GN=HNRNPR PE=1 SV=1	FALSE	9	5	6	4	633	70.9
Heat shock cognate 71 kDa protein OS=Homo sapiens OX=9606 GN=HSPA8 PE=1 SV=1	FALSE	14	6	6	5	646	70.9
Keratin, type I cytoskeletal 9 OS=Homo sapiens OX=9606 GN=KRT9 PE=1 SV=3	FALSE	8	3	3	3	623	62
Uncharacterized protein OS=Homo sapiens OX=9606 PE=3 SV=1	FALSE	3	3	3	3	849	94.6
X-ray repair cross-complementing protein 6 OS=Homo sapiens OX=9606 GN=XRCC6 PE=1 SV=2	FALSE	13	7	7	7	609	69.8
Methylcrotonoyl-CoA carboxylase subunit alpha, mitochondrial OS=Homo sapiens OX=9606 GN=MCCC1 PE=1 SV=3	FALSE	11	5	5	5	725	80.4
Keratin, type II cytoskeletal 2 epidermal OS=Homo sapiens OX=9606 GN=KRT2 PE=1 SV=2	FALSE	5	2	2	1	639	65.4
Keratin, type II cytoskeletal 5 OS=Homo sapiens OX=9606 GN=KRT5 PE=1 SV=3	FALSE	4	2	2	1	590	62.3
Double-strand break repair protein MRE11 OS=Homo sapiens OX=9606 GN=MRE11 PE=1 SV=3	FALSE	5	3	3	3	708	80.5
Heterogeneous nuclear ribonucleoprotein Q OS=Homo sapiens OX=9606 GN=SYNCRIP PE=1 SV=2	FALSE	9	4	4	3	623	69.6
Exocyst complex component 3 OS=Homo sapiens OX=9606 GN=EXOC3 PE=1 SV=3	FALSE	6	3	3	3	745	85.5
Endoplasmic reticulum chaperone BiP OS=Homo sapiens OX=9606 GN=HSPA5 PE=1 SV=2	FALSE	4	2	2	2	654	72.3
Heterogeneous nuclear ribonucleoprotein M OS=Homo sapiens OX=9606 GN=HNRNPM PE=1 SV=1	FALSE	4	3	3	3	730	77.5
Stress-70 protein, mitochondrial OS=Homo sapiens OX=9606 GN=HSPA9 PE=1 SV=2	FALSE	4	2	2	2	679	73.6
Heterogeneous nuclear ribonucleoprotein U OS=Homo sapiens OX=9606 GN=HNRNPU PE=1 SV=6	FALSE	2	1	1	1	825	90.5
Probable ATP-dependent RNA helicase DDX5 OS=Homo sapiens OX=9606 GN=DDX5 PE=1 SV=1	FALSE	3	2	2	2	614	69
Replication protein A 70 kDa DNA-binding subunit OS=Homo sapiens OX=9606 GN=RPA1 PE=1 SV=2	FALSE	9	3	3	3	616	68.1
Matrin-3 OS=Homo sapiens OX=9606 GN=MATR3 PE=1 SV=1	FALSE	2	1	1	1	895	99.9
Metastasis-associated protein MTA2 OS=Homo sapiens OX=9606 GN=MTA2 PE=1 SV=1	FALSE	3	2	2	2	668	75
Propionyl-CoA carboxylase alpha chain, mitochondrial OS=Homo sapiens OX=9606 GN=PCCA PE=1 SV=4	FALSE	4	2	2	2	728	80
Eukaryotic translation initiation factor 3 subunit D OS=Homo sapiens OX=9606 GN=EIF3D PE=1 SV=1	FALSE	5	3	3	3	548	63.9
Serum albumin OS=Homo sapiens OX=9606 GN=ALB PE=1 SV=2	TRUE	2	1	1	1	609	69.3
RNA-binding protein 14 OS=Homo sapiens OX=9606 GN=RBM14 PE=1 SV=2	FALSE	4	2	2	2	669	69.4
Metastasis-associated protein MTA1 OS=Homo sapiens OX=9606 GN=MTA1 PE=1 SV=2	FALSE	2	1	1	1	715	80.7
Nucleolar protein 56 OS=Homo sapiens OX=9606 GN=NOP56 PE=1 SV=4	FALSE	2	1	1	1	594	66
U4/U6.U5 tri-snRNP-associated protein 2 OS=Homo sapiens OX=9606 GN=USP39 PE=1 SV=2	FALSE	3	1	1	1	565	65.3
Regulatory factor X-associated protein OS=Homo sapiens OX=9606 GN=RFXAP PE=1 SV=1	FALSE	8	1	2	1	272	28.2
Pentatricopeptide repeat domain-containing protein 3, mitochondrial OS=Homo sapiens OX=9606 GN=PTCD3 PE=1 SV=3	FALSE	2	1	1	1	689	78.5
STAGA complex 65 subunit gamma OS=Homo sapiens OX=9606 GN=SUPT7L PE=1 SV=1	FALSE	2	1	1	1	414	46.2
Nucleolar RNA helicase 2 OS=Homo sapiens OX=9606 GN=DDX21 PE=1 SV=5	FALSE	2	1	1	1	783	87.3

Table A. 20 Proteins identified from gel slice No.13

Description	Coverage [%]	Contaminant	# Peptides	# PSMs	# Unique Peptides	# AAs	MW [kDa]
Trypsin OS=Sus scrofa PE=1 SV=1 Tax_Id=9823 [Sus scrofa]	25	TRUE	5	17	5	231	24.4
Putative EP400-like protein OS=Homo sapiens OX=9606 GN=EP400P1 PE=5 SV=2	24	FALSE	6	10	6	488	51.7
Keratin, type I cytoskeletal 9 OS=Homo sapiens OX=9606 GN=KRT9 PE=1 SV=3	13	FALSE	4	4	4	623	62
Keratin, type II cytoskeletal 1 OS=Homo sapiens OX=9606 GN=KRT1 PE=1 SV=6	8	FALSE	4	4	4	644	66
Serum albumin OS=Bos taurus GN=ALB PE=1 SV=4 Tax_Id=9913 [Bos taurus]	4	TRUE	2	2	2	607	69.2
Splicing factor 3A subunit 3 OS=Homo sapiens OX=9606 GN=SF3A3 PE=1 SV=1	2	FALSE	1	1	1	501	58.8
T-complex protein 1 subunit gamma OS=Homo sapiens OX=9606 GN=CCT3 PE=1 SV=4	6	FALSE	3	3	3	545	60.5
Heterogeneous nuclear ribonucleoprotein L OS=Homo sapiens OX=9606 GN=HNRNPL PE=1 SV=2	2	FALSE	1	1	1	589	64.1
Keratin, type II cytoskeletal 2 epidermal OS=Homo sapiens OX=9606 GN=KRT2 PE=1 SV=2	9	FALSE	4	4	3	639	65.4
Splicing factor U2AF 65 kDa subunit OS=Homo sapiens OX=9606 GN=U2AF2 PE=1 SV=4	12	FALSE	4	4	4	475	53.5
Alpha-internexin OS=Homo sapiens OX=9606 GN=INA PE=1 SV=2	4	FALSE	2	2	1	499	55.4
Probable ATP-dependent RNA helicase DDX17 OS=Homo sapiens OX=9606 GN=DDX17 PE=1 SV=1	2	FALSE	1	1	1	731	80.4
Eukaryotic translation initiation factor 3 subunit L OS=Homo sapiens OX=9606 GN=EIF3L PE=1 SV=1	3	FALSE	2	2	2	607	70.9
26S proteasome non-ATPase regulatory subunit 3 OS=Homo sapiens OX=9606 GN=PSMD3 PE=1 SV=2	2	FALSE	1	1	1	534	60.9
T-complex protein 1 subunit zeta OS=Homo sapiens OX=9606 GN=CCT6A PE=1 SV=3	2	FALSE	1	1	1	531	58
Transcription elongation factor SPT6 OS=Homo sapiens OX=9606 GN=SUPT6H PE=1 SV=2	1	FALSE	1	1	1	1726	198.9
Heterogeneous nuclear ribonucleoprotein Q OS=Homo sapiens OX=9606 GN=SYNCRIP PE=1 SV=2	4	FALSE	2	2	2	623	69.6
Keratin, type II cytoskeletal 5 OS=Homo sapiens OX=9606 GN=KRT5 PE=1 SV=3	6	FALSE	3	3	2	590	62.3
T-complex protein 1 subunit alpha OS=Homo sapiens OX=9606 GN=TCP1 PE=1 SV=1	8	FALSE	3	3	3	556	60.3
Eukaryotic translation initiation factor 3 subunit D OS=Homo sapiens OX=9606 GN=EIF3D PE=1 SV=1	3	FALSE	1	1	1	548	63.9
Keratin, type I cytoskeletal 10 OS=Homo sapiens OX=9606 GN=KRT10 PE=1 SV=6	6	FALSE	3	3	3	584	58.8
Rubber elongation factor protein OS=Hevea brasiliensis PE=1 SV=2 Tax_Id=3981 [Hevea brasiliensis]	8	TRUE	1	1	1	138	14.7
Vimentin OS=Homo sapiens OX=9606 GN=VIM PE=1 SV=4	5	FALSE	2	2	1	466	53.6
U4/U6.U5 tri-snRNP-associated protein 2 OS=Homo sapiens OX=9606 GN=USP39 PE=1 SV=2	2	FALSE	1	1	1	565	65.3
Myosin light chain kinase 2, skeletal/cardiac muscle OS=Homo sapiens OX=9606 GN=MYLK2 PE=1 SV=3	2	FALSE	1	1	1	596	64.6
Far upstream element-binding protein 1 OS=Homo sapiens OX=9606 GN=FUBP1 PE=1 SV=1	1	FALSE	1	1	1	655	68.9

Table A. 21 Proteins identified from gel slice No.14

Description	Coverage [%]	Contaminant	# Peptide	# PSMs	# Unique Peptides	# AAs	MW [kDa]
Vimentin OS=Homo sapiens OX=9606 GN=VIM PE=1 SV=4	49	FALSE	23	67	23	466	53.6
Tubulin beta chain OS=Homo sapiens OX=9606 GN=TUBB PE=1 SV=2	32	FALSE	11	15	4	444	49.6
Tubulin alpha chain OS=Homo sapiens OX=9606 GN=TUBA1C PE=1 SV=1	34	FALSE	11	14	11	519	57.7
Trypsin OS=Sus scrofa PE=1 SV=1 Tax_Id=9823 [Sus scrofa]	22	TRUE	4	12	4	231	24.4
Tubulin beta-2A chain OS=Homo sapiens OX=9606 GN=TUBB2A PE=1 SV=1	23	FALSE	8	11	1	445	49.9
Propionyl-CoA carboxylase beta chain, mitochondrial OS=Homo sapiens OX=9606 GN=PCCB PE=1 SV=1	22	FALSE	9	12	9	570	61.6
Keratin, type I cytoskeletal 9 OS=Homo sapiens OX=9606 GN=KRT9 PE=1 SV=3	15	FALSE	6	7	6	623	62
Keratin, type I cytoskeletal 10 OS=Homo sapiens OX=9606 GN=KRT10 PE=1 SV=6	24	FALSE	9	9	9	584	58.8
DNA methyltransferase 1-associated protein 1 OS=Homo sapiens OX=9606 GN=DMAP1 PE=1 SV=1	16	FALSE	6	7	6	467	53
Polypyrimidine tract-binding protein 1 OS=Homo sapiens OX=9606 GN=PTBP1 PE=1 SV=1	15	FALSE	4	4	4	588	62.4
Keratin, type II cytoskeletal 1 OS=Homo sapiens OX=9606 GN=KRT1 PE=1 SV=6	16	FALSE	8	9	6	644	66
Non-POU domain-containing octamer-binding protein OS=Homo sapiens OX=9606 GN=NONO PE=1 SV=4	5	FALSE	2	3	2	471	54.2
Keratin, type II cytoskeletal 2 epidermal OS=Homo sapiens OX=9606 GN=KRT2 PE=1 SV=2	7	FALSE	4	5	2	639	65.4
Keratin, type II cytoskeletal 8 OS=Homo sapiens OX=9606 GN=KRT8 PE=1 SV=7	6	FALSE	3	3	1	483	53.7
Serum albumin OS=Bos taurus GN=ALB PE=1 SV=4 Tax_Id=9913 [Bos taurus]	4	TRUE	2	2	2	607	69.2
Splicing factor 3A subunit 3 OS=Homo sapiens OX=9606 GN=SF3A3 PE=1 SV=1	2	FALSE	1	1	1	501	58.8
Heterogeneous nuclear ribonucleoprotein K OS=Homo sapiens OX=9606 GN=HNRNPK PE=1 SV=1	8	FALSE	3	3	3	463	50.9
Pre-mRNA-processing factor 19 OS=Homo sapiens OX=9606 GN=PRPF19 PE=1 SV=1	27	FALSE	8	8	8	504	55.1
U4/U6 small nuclear ribonucleoprotein Prp4 OS=Homo sapiens OX=9606 GN=PRPF4 PE=1 SV=2	11	FALSE	3	3	3	522	58.4
Keratin, type II cytoskeletal 5 OS=Homo sapiens OX=9606 GN=KRT5 PE=1 SV=3	3	FALSE	2	2	1	590	62.3
Keratin, type II cytoskeletal 6A OS=Homo sapiens OX=9606 GN=KRT6A PE=1 SV=3	4	FALSE	2	2	1	564	60
Myosin light chain kinase 2, skeletal/cardiac muscle OS=Homo sapiens OX=9606 GN=MYLK2 PE=1 SV=3	2	FALSE	1	1	1	596	64.6
H/ACA ribonucleoprotein complex subunit DKC1 OS=Homo sapiens OX=9606 GN=DKC1 PE=1 SV=3	2	FALSE	1	1	1	514	57.6
Sphingolipid delta(4)-desaturase/C4-monooxygenase DES2 OS=Homo sapiens OX=9606 GN=DEGS2 PE=1 SV=1	19	FALSE	1	1	1	54	5.9
Dynactin subunit 4 OS=Homo sapiens OX=9606 GN=DCTN4 PE=1 SV=1	3	FALSE	1	1	1	460	52.3
Rubber elongation factor protein OS=Hevea brasiliensis PE=1 SV=2 Tax_Id=3981 [Hevea brasiliensis]	8	TRUE	1	1	1	138	14.7
U11/U12 small nuclear ribonucleoprotein 35 kDa protein OS=Homo sapiens OX=9606 GN=SNRNP35 PE=1 SV=1	4	FALSE	1	1	1	246	29.4
Histone-binding protein RBBP4 OS=Homo sapiens OX=9606 GN=RBBP4 PE=1 SV=3	3	FALSE	1	1	1	425	47.6
SWI/SNF-related matrix-associated actin-dependent regulator of chromatin subfamily E member 1 OS=Homo sapiens OX=9606 GN=SMARCE1 PE=1 SV=2	3	FALSE	1	1	1	411	46.6
F-box-like/WD repeat-containing protein TBL1XR1 OS=Homo sapiens OX=9606 GN=TBL1XR1 PE=1 SV=1	4	FALSE	1	1	1	514	55.6
Dermcidin OS=Homo sapiens OX=9606 GN=DCD PE=1 SV=2	10	FALSE	1	1	1	110	11.3
Aspartate--tRNA ligase, cytoplasmic OS=Homo sapiens OX=9606 GN=DARS PE=1 SV=2	2	FALSE	1	1	1	501	57.1
Transmembrane anterior posterior transformation protein 1 homolog OS=Homo sapiens OX=9606 GN=TAPT1 PE=1 SV=1	3	FALSE	1	1	1	567	64.2
Parafibromin OS=Homo sapiens OX=9606 GN=CDC73 PE=1 SV=1	2	FALSE	1	1	1	531	60.5
Putative EP400-like protein OS=Homo sapiens OX=9606 GN=EP400P1 PE=5 SV=2	6	FALSE	2	4	2	488	51.7
OR8G5 OS=Homo sapiens OX=9606 GN=OR8G5 PE=3 SV=1	6	FALSE	1	1	1	311	34.6
Thyroid hormone receptor-associated protein 3 OS=Homo sapiens OX=9606 GN=THRAP3 PE=1 SV=2	2	FALSE	1	1	1	955	108.6

Table A. 22 Proteins identified from gel slice No.15

Description	Contamin	Coverage [%]	# Peptides	# PSMs	# Unique Peptides	# AAs	MW [kDa]
Trypsin OS=Sus scrofa PE=1 SV=1 Tax_Id=9823 [Sus scrofa]	TRUE	25	5	16	5	231	24.4
Vimentin OS=Homo sapiens OX=9606 GN=VIM PE=1 SV=4	FALSE	34	15	17	14	466	53.6
Keratin, type II cytoskeletal 1 OS=Homo sapiens OX=9606 GN=KRT1 PE=1 SV=6	FALSE	24	11	17	9	644	66
Keratin, type I cytoskeletal 9 OS=Homo sapiens OX=9606 GN=KRT9 PE=1 SV=3	FALSE	17	8	8	8	623	62
Tubulin alpha chain OS=Homo sapiens OX=9606 GN=TUBA1C PE=1 SV=1	FALSE	23	7	8	7	519	57.7
Elongation factor 1-alpha 1 OS=Homo sapiens OX=9606 GN=EEF1A1 PE=1 SV=1	FALSE	16	5	5	5	462	50.1
Tubulin beta chain OS=Homo sapiens OX=9606 GN=TUBB PE=1 SV=2	FALSE	27	9	10	2	444	49.6
Tubulin beta-4B chain OS=Homo sapiens OX=9606 GN=TUBB4B PE=1 SV=1	FALSE	26	8	8	1	445	49.8
Keratin, type II cytoskeletal 8 OS=Homo sapiens OX=9606 GN=KRT8 PE=1 SV=7	FALSE	11	5	6	3	483	53.7
Keratin, type I cytoskeletal 10 OS=Homo sapiens OX=9606 GN=KRT10 PE=1 SV=6	FALSE	23	8	8	7	584	58.8
Interleukin enhancer-binding factor 2 OS=Homo sapiens OX=9606 GN=ILF2 PE=1 SV=2	FALSE	25	7	8	7	390	43
Polymerase delta-interacting protein 3 OS=Homo sapiens OX=9606 GN=POLDIP3 PE=1 SV=1	FALSE	11	3	3	3	438	48.1
Lipoamide acyltransferase component of branched-chain alpha-keto acid dehydrogenase complex, mitochondrial OS=Homo sapiens	FALSE	15	6	6	6	482	53.5
39S ribosomal protein L37, mitochondrial OS=Homo sapiens OX=9606 GN=MRPL37 PE=1 SV=1	FALSE	23	7	8	7	483	54.9
Histone-binding protein RBBP4 OS=Homo sapiens OX=9606 GN=RBBP4 PE=1 SV=3	FALSE	21	6	6	3	425	47.6
Actin, cytoplasmic 1 OS=Homo sapiens OX=9606 GN=ACTB PE=1 SV=1	FALSE	18	4	5	2	375	41.7
Keratin, type II cytoskeletal 2 epidermal OS=Homo sapiens OX=9606 GN=KRT2 PE=1 SV=2	FALSE	11	6	7	3	639	65.4
Actin-like protein 6A OS=Homo sapiens OX=9606 GN=ACTL6A PE=1 SV=1	FALSE	26	8	9	8	429	47.4
Actin, alpha cardiac muscle 1 OS=Homo sapiens OX=9606 GN=ACTC1 PE=1 SV=1	FALSE	11	3	3	1	377	42
Polypyrimidine tract-binding protein 1 OS=Homo sapiens OX=9606 GN=PTBP1 PE=1 SV=1	FALSE	9	3	3	3	588	62.4
Protein S100-A7 OS=Homo sapiens OX=9606 GN=S100A7 PE=1 SV=4	FALSE	35	4	5	4	101	11.5
Keratin, type I cytoskeletal 18 OS=Homo sapiens OX=9606 GN=KRT18 PE=1 SV=2	FALSE	12	4	5	3	430	48
Histone-binding protein RBBP7 OS=Homo sapiens OX=9606 GN=RBBP7 PE=1 SV=1	FALSE	20	5	5	2	425	47.8
Zinc finger protein ubi-d4 OS=Homo sapiens OX=9606 GN=DPF2 PE=1 SV=1	FALSE	13	3	3	3	405	45.8
Serum albumin OS=Homo sapiens OX=9606 GN=ALB PE=1 SV=2	FALSE	9	4	4	3	609	69.3
Alpha-centractin OS=Homo sapiens OX=9606 GN=ACTR1A PE=1 SV=1	FALSE	22	5	5	5	376	42.6
Elongation factor 1-gamma OS=Homo sapiens OX=9606 GN=EEF1G PE=1 SV=3	FALSE	11	4	4	4	437	50.1
39S ribosomal protein L38, mitochondrial OS=Homo sapiens OX=9606 GN=MRPL38 PE=1 SV=2	FALSE	7	3	3	3	380	44.6
RuvB-like 2 OS=Homo sapiens OX=9606 GN=RUVBL2 PE=1 SV=3	FALSE	5	2	2	2	463	51.1
26S proteasome regulatory subunit 8 OS=Homo sapiens OX=9606 GN=PSMC5 PE=1 SV=1	FALSE	10	3	3	3	406	45.6
Keratin, type I cytoskeletal 19 OS=Homo sapiens OX=9606 GN=KRT19 PE=1 SV=4	FALSE	10	4	4	1	400	44.1
Keratin, type II cytoskeletal 5 OS=Homo sapiens OX=9606 GN=KRT5 PE=1 SV=3	FALSE	5	3	3	1	590	62.3
Bystin OS=Homo sapiens OX=9606 GN=BYSL PE=1 SV=3	FALSE	8	3	3	3	437	49.6
Rubber elongation factor protein OS=Hevea brasiliensis PE=1 SV=2 Tax_Id=3981 [Hevea brasiliensis]	TRUE	15	2	2	2	138	14.7
Keratin, type I cytoskeletal 14 OS=Homo sapiens OX=9606 GN=KRT14 PE=1 SV=4	FALSE	8	3	3	1	472	51.5
Spliceosome RNA helicase DDX39B OS=Homo sapiens OX=9606 GN=DDX39B PE=1 SV=1	FALSE	6	2	2	2	428	49
Splicing factor 3B subunit 4 OS=Homo sapiens OX=9606 GN=SF3B4 PE=1 SV=1	FALSE	3	1	1	1	424	44.4

Table A. 23 Proteins identified from gel slice No.16

Description	Coverage [%]	Contaminant	# Peptides	# PSMs	# Unique Peptides	# AAs	MW [kDa]
Mortality factor 4-like protein 1 OS=Homo sapiens OX=9606 GN=MORF4L1 PE=1 SV=1	37	FALSE	14	19	13	348	40
Heterogeneous nuclear ribonucleoproteins A2/B1 OS=Homo sapiens OX=9606 GN=HNRNPA2B1 PE=1 SV=2	22	FALSE	5	7	4	353	37.4
Trypsin OS=Sus scrofa PE=1 SV=1 Tax_Id=9823 [Sus scrofa]	25	TRUE	5	15	5	231	24.4
rRNA 2'-O-methyltransferase fibrillarin OS=Homo sapiens OX=9606 GN=FBL PE=1 SV=2	23	FALSE	4	5	4	321	33.8
Heterogeneous nuclear ribonucleoprotein A3 OS=Homo sapiens OX=9606 GN=HNRNPA3 PE=1 SV=2	13	FALSE	4	4	3	378	39.6
Keratin, type II cytoskeletal 1 OS=Homo sapiens OX=9606 GN=KRT1 PE=1 SV=6	7	FALSE	3	3	3	644	66
U5 small nuclear ribonucleoprotein 40 kDa protein OS=Homo sapiens OX=9606 GN=SNRNP40 PE=1 SV=1	16	FALSE	3	3	3	357	39.3
Mortality factor 4-like protein 2 OS=Homo sapiens OX=9606 GN=MORF4L2 PE=1 SV=1	10	FALSE	2	3	1	288	32.3
Heterogeneous nuclear ribonucleoprotein A1 OS=Homo sapiens OX=9606 GN=HNRNPA1 PE=1 SV=5	6	FALSE	2	2	1	372	38.7
Heterogeneous nuclear ribonucleoproteins C1/C2 OS=Homo sapiens OX=9606 GN=HNRNPC PE=1 SV=1	19	FALSE	4	4	3	292	32.2
Heterogeneous nuclear ribonucleoprotein C-like 4 OS=Homo sapiens OX=9606 GN=HNRNPCL4 PE=4 SV=1	10	FALSE	2	2	1	293	32
Keratin, type I cytoskeletal 10 OS=Homo sapiens OX=9606 GN=KRT10 PE=1 SV=6	4	FALSE	1	1	1	584	58.8
Splicing factor U2AF 35 kDa subunit OS=Homo sapiens OX=9606 GN=U2AF1 PE=1 SV=3	15	FALSE	2	2	2	240	27.9
28S ribosomal protein S22, mitochondrial OS=Homo sapiens OX=9606 GN=MRPS22 PE=1 SV=1	3	FALSE	1	1	1	360	41.3
Rubber elongation factor protein OS=Hevea brasiliensis PE=1 SV=2 Tax_Id=3981 [Hevea brasiliensis]	15	TRUE	2	2	2	138	14.7
Keratin, type II cytoskeletal 2 epidermal OS=Homo sapiens OX=9606 GN=KRT2 PE=1 SV=2	5	FALSE	2	2	2	639	65.4
Aminoacyl tRNA synthase complex-interacting multifunctional protein 1 OS=Homo sapiens OX=9606 GN=AIMP1 PE=1 SV=2	14	FALSE	3	3	3	312	34.3
Keratin, type II cytoskeletal 5 OS=Homo sapiens OX=9606 GN=KRT5 PE=1 SV=3	4	FALSE	2	2	2	590	62.3
DNA-directed RNA polymerases I and III subunit RPAC1 OS=Homo sapiens OX=9606 GN=POLR1C PE=1 SV=1	5	FALSE	1	1	1	346	39.2
Serum albumin OS=Homo sapiens OX=9606 GN=ALB PE=1 SV=2	2	TRUE	1	1	1	609	69.3
Elongation factor 1-delta OS=Homo sapiens OX=9606 GN=EEF1D PE=1 SV=1	2	FALSE	1	1	1	697	76.5
Tetratricopeptide repeat domain 12, isoform CRA_d OS=Homo sapiens OX=9606 GN=TTC12 PE=1 SV=1	6	FALSE	1	3	1	711	79.4
Serine/threonine-protein phosphatase PP1-beta catalytic subunit OS=Homo sapiens OX=9606 GN=PPP1CB PE=1 SV=3	4	FALSE	1	1	1	327	37.2
Dermcidin OS=Homo sapiens OX=9606 GN=DCD PE=1 SV=2	10	FALSE	1	1	1	110	11.3
Replication factor C subunit 2 OS=Homo sapiens OX=9606 GN=RFC2 PE=1 SV=3	5	FALSE	1	1	1	354	39.1
Deoxynucleotidyltransferase terminal-interacting protein 1 OS=Homo sapiens OX=9606 GN=DNTTIP1 PE=1 SV=2	4	FALSE	1	1	1	329	37
Keratin, type I cytoskeletal 9 OS=Homo sapiens OX=9606 GN=KRT9 PE=1 SV=3	5	FALSE	1	1	1	623	62
Eukaryotic translation initiation factor 3 subunit I OS=Homo sapiens OX=9606 GN=EIF3I PE=1 SV=1	8	FALSE	2	2	2	325	36.5
Keratin, type I cytoskeletal 19 OS=Homo sapiens OX=9606 GN=KRT19 PE=1 SV=4	6	FALSE	2	2	2	400	44.1
Keratin, type II cytoskeletal 6A OS=Homo sapiens OX=9606 GN=KRT6A PE=1 SV=3	3	FALSE	1	1	1	564	60

Table A. 24 Proteins identified from gel slice No.17

Description	Contaminant	Coverage [%]	# Peptides	# PSMs	# Unique Peptides	# AAs	MW [kDa]
Trypsin OS=Sus scrofa PE=1 SV=1 Tax_Id=9823 [Sus scrofa]	TRUE	25	5	15	5	231	24.4
Mortality factor 4-like protein 2 OS=Homo sapiens OX=9606 GN=MORF4L2 PE=1 SV=1	FALSE	29	9	12	7	288	32.3
Keratin, type II cytoskeletal 1 OS=Homo sapiens OX=9606 GN=KRT1 PE=1 SV=6	FALSE	22	11	13	11	644	66
Keratin, type I cytoskeletal 9 OS=Homo sapiens OX=9606 GN=KRT9 PE=1 SV=3	FALSE	13	4	4	4	623	62
ELAV-like protein 1 OS=Homo sapiens OX=9606 GN=ELAVL1 PE=1 SV=2	FALSE	12	3	3	3	326	36.1
Keratin, type I cytoskeletal 10 OS=Homo sapiens OX=9606 GN=KRT10 PE=1 SV=6	FALSE	13	4	4	4	584	58.8
Heterogeneous nuclear ribonucleoprotein A1 OS=Homo sapiens OX=9606 GN=HNRNPA1 PE=1 SV=5	FALSE	7	2	2	2	372	38.7
THO complex subunit 4 OS=Homo sapiens OX=9606 GN=ALYREF PE=1 SV=1	FALSE	11	2	2	2	264	27.5
28S ribosomal protein S7, mitochondrial OS=Homo sapiens OX=9606 GN=MRPS7 PE=1 SV=1	FALSE	13	3	3	3	271	31.7
40S ribosomal protein S3 OS=Homo sapiens OX=9606 GN=RPS3 PE=1 SV=2	FALSE	7	2	2	2	243	26.7
Keratin, type II cytoskeletal 2 epidermal OS=Homo sapiens OX=9606 GN=KRT2 PE=1 SV=2	FALSE	10	2	2	2	639	65.4
Heterogeneous nuclear ribonucleoproteins A2/B1 OS=Homo sapiens OX=9606 GN=HNRNPA2B1 PE=1 SV=2	FALSE	3	1	1	1	353	37.4
Mortality factor 4-like protein 1 OS=Homo sapiens OX=9606 GN=MORF4L1 PE=1 SV=2	FALSE	13	4	4	2	362	41.4
U2 small nuclear ribonucleoprotein A' OS=Homo sapiens OX=9606 GN=SNRPA1 PE=1 SV=2	FALSE	15	3	3	3	255	28.4
rRNA 2'-O-methyltransferase fibrillarin OS=Homo sapiens OX=9606 GN=FBL PE=1 SV=2	FALSE	4	1	1	1	321	33.8
MRG/MORF4L-binding protein OS=Homo sapiens OX=9606 GN=MRGBP PE=1 SV=1	FALSE	17	2	2	2	204	22.4
40S ribosomal protein S5 OS=Homo sapiens OX=9606 GN=RPS5 PE=1 SV=4	FALSE	10	1	1	1	204	22.9
60S ribosomal protein L23a OS=Homo sapiens OX=9606 GN=RPL23A PE=1 SV=1	FALSE	7	1	1	1	194	21.9
U2 small nuclear ribonucleoprotein B" OS=Homo sapiens OX=9606 GN=SNRPB2 PE=1 SV=1	FALSE	8	1	1	1	225	25.5
Serum albumin OS=Bos taurus GN=ALB PE=1 SV=4 Tax_Id=9913 [Bos taurus]	TRUE	4	2	2	2	607	69.2
Histone H2A.Z OS=Homo sapiens OX=9606 GN=H2AFZ PE=1 SV=2	FALSE	8	1	1	1	128	13.5
Elongation factor 1-beta OS=Homo sapiens OX=9606 GN=EEF1B2 PE=1 SV=3	FALSE	7	1	1	1	225	24.7
Serine/arginine-rich splicing factor 7 OS=Homo sapiens OX=9606 GN=SRSF7 PE=1 SV=1	FALSE	4	1	1	1	238	27.4
Keratin, type II cytoskeletal 5 OS=Homo sapiens OX=9606 GN=KRT5 PE=1 SV=3	FALSE	4	2	2	2	590	62.3
YEATS domain-containing protein 4 OS=Homo sapiens OX=9606 GN=YEATS4 PE=1 SV=1	FALSE	4	1	1	1	227	26.5
Serine/arginine-rich-splicing factor 1 OS=Homo sapiens OX=9606 GN=SRSF1 PE=1 SV=1	FALSE	4	1	2	1	253	28.3
39S ribosomal protein L13, mitochondrial OS=Homo sapiens OX=9606 GN=MRPL13 PE=1 SV=1	FALSE	6	1	1	1	178	20.7
Protein NYNRIN OS=Homo sapiens OX=9606 GN=NYNRIN PE=2 SV=3	FALSE	2	1	1	1	1898	208.2
Heterogeneous nuclear ribonucleoprotein A0 OS=Homo sapiens OX=9606 GN=HNRNPA0 PE=1 SV=1	FALSE	5	1	1	1	305	30.8
Rubber elongation factor protein OS=Hevea brasiliensis PE=1 SV=2 Tax_Id=3981 [Hevea brasiliensis]	TRUE	20	2	2	2	138	14.7
40S ribosomal protein S8 OS=Homo sapiens OX=9606 GN=RPS8 PE=1 SV=2	FALSE	3	1	1	1	208	24.2
28S ribosomal protein S23, mitochondrial OS=Homo sapiens OX=9606 GN=MRPS23 PE=1 SV=2	FALSE	5	1	1	1	190	21.8
U11/U12 small nuclear ribonucleoprotein 35 kDa protein OS=Homo sapiens OX=9606 GN=SNRNP35 PE=1 SV=1	FALSE	8	2	2	2	246	29.4
Splicing factor U2AF 35 kDa subunit OS=Homo sapiens OX=9606 GN=U2AF1 PE=1 SV=3	FALSE	8	1	1	1	240	27.9
BAG family molecular chaperone regulator 2 OS=Homo sapiens OX=9606 GN=BAG2 PE=1 SV=1	FALSE	5	1	1	1	211	23.8
28S ribosomal protein S2, mitochondrial OS=Homo sapiens OX=9606 GN=MRPS2 PE=1 SV=1	FALSE	3	1	1	1	296	33.2
60S ribosomal protein L27 (Fragment) OS=Homo sapiens OX=9606 GN=RPL27 PE=1 SV=1	FALSE	6	1	1	1	144	16.5

13. APPENDIX 5

Cell cycle analysis and doublets/multiplets discrimination in flow cytometry

13. 1 Flp-In™ T-REx™ cells in four different conditions (±Serum/± Tetracycline)

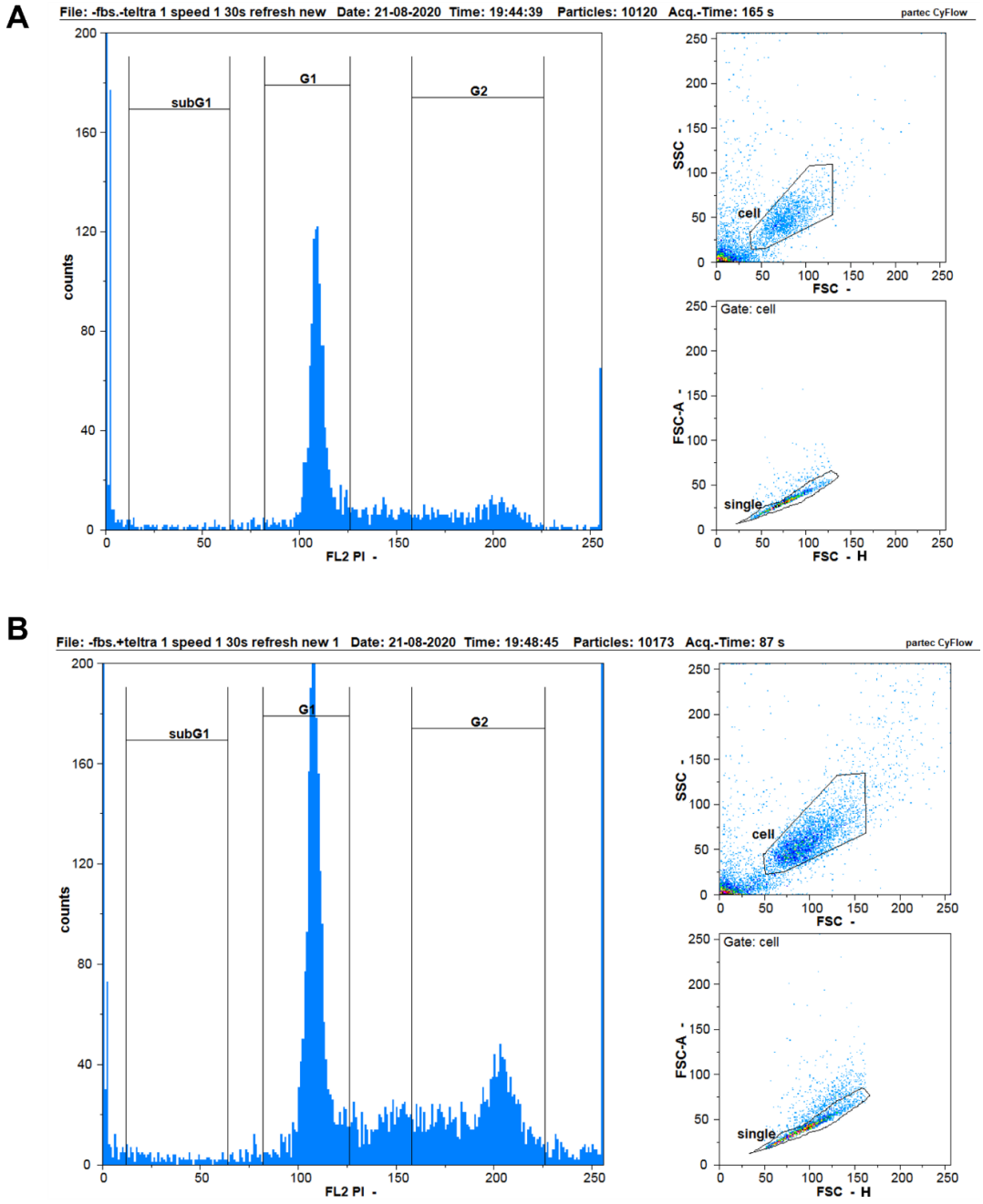

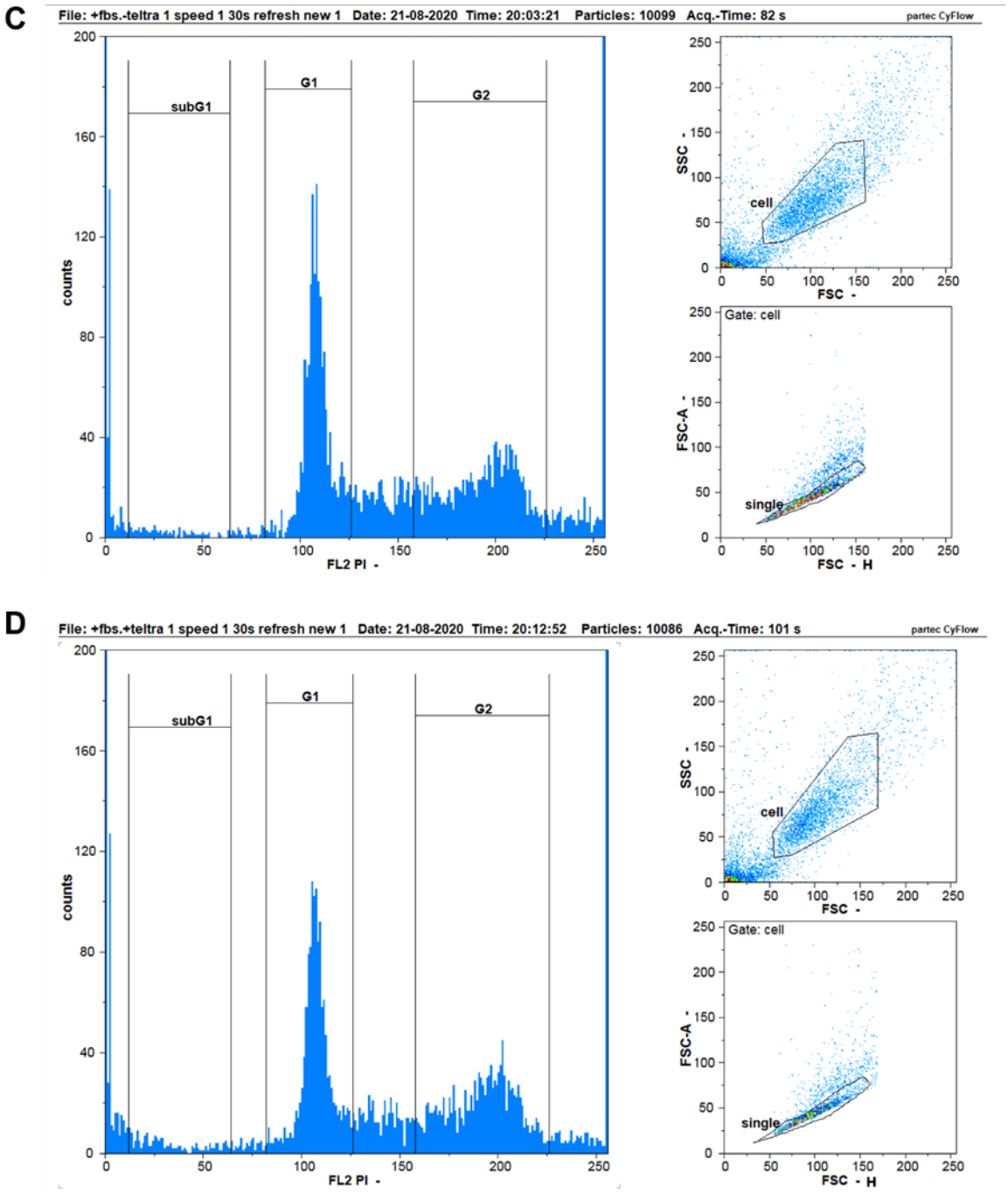

Figure A. 7 Cell cycle analysis of Flp-In™ T-REx™ cells using propidium iodide
Three fractions (subG1, G1, and G2/M) were separated based on the software manual. Approximately 10000 particles were applied in each analysis. Partec CyFlow software identifies two peaks in G1 and G2/M. No peaks were identified from the subG1 phase (Left panels). Cells were simultaneously separated by forward scatter (FSC) and side scatter (SSC) (Right top panels). Doublets and multiplets were subsequently eliminated by plotting the height (H) against the area (A) (Right bottom panels). A: -Serum/-Tetracycline; B: -Serum/+Tetracycline; C +Serum/-Tetracycline; D: +Serum/+Tetracycline.

13. 2 Cell cycle analysis using wild type and EP400NL indel mutated H1299 cells

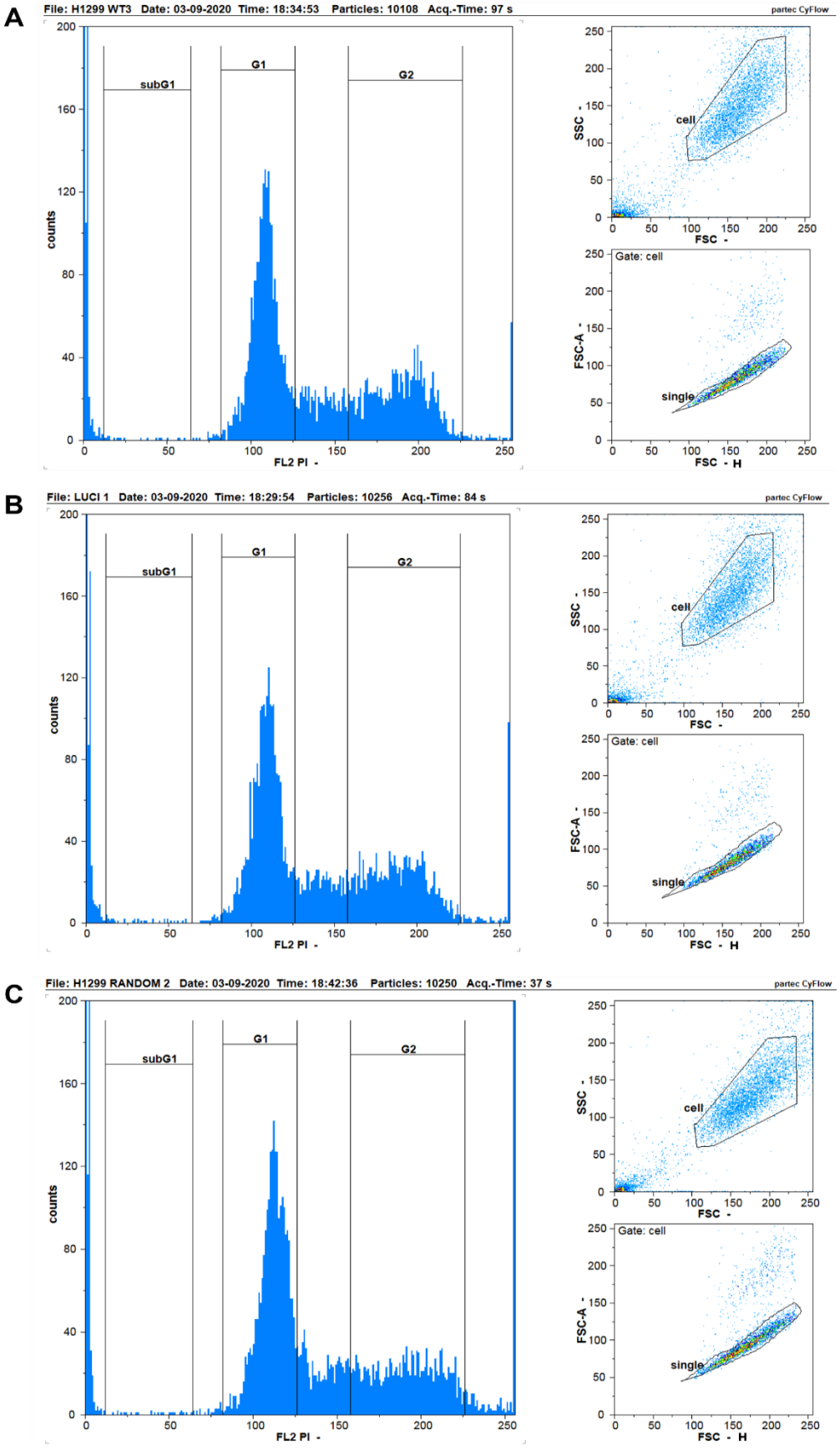

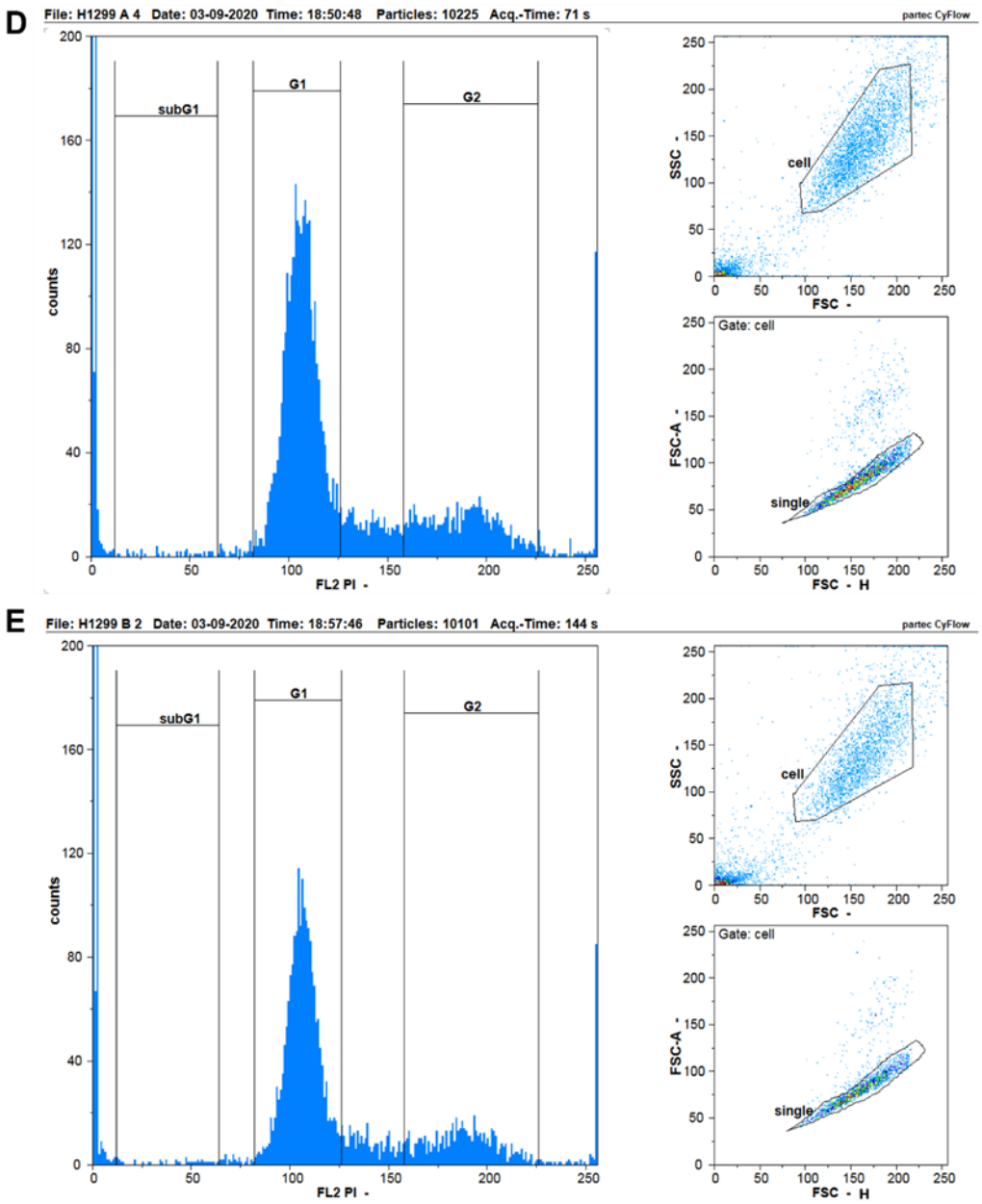

Figure A. 8 Cell cycle analysis of H1299 cells using propidium iodide

Three fractions (subG1, G1, and G2/M) were separated based on the software manual. Approximately 10000 particles were applied in each analysis. Partec CyFlow software identifies two peaks in G1 and G2/M. No peaks were identified from the subG1 phase. Cell counts decreased in the G2/M phase in EP400NL indel cell lines (D, E) compared to the wild type H1299 (A) and two negative controls (B, C) (Left panels). Cells were simultaneously separated by forward scatter (FSC) and side scatter (SSC) (Right top panels). Doublets and multiplets were subsequently eliminated by plotting the height (H) against the area (A) (Right bottom panels). A: Wild type H1299; B: Luciferase, gRNA-luciferase; C: Scramble, gRNA-scrambled random sequence; D: Indel mutation A, gRNA-EP400NL-A; E: Indel mutation B, gRNA-EP400NL-B.

14. APPENDIX 6

14. 1 Raw data for quantifying PD-L1 mRNA by RT-qPCR

Table A. 25 CT values of housekeeping gene (GUSB) and data analysis for constructing a standard curve for GUSB

GUSB	CT	CT	AVERAGE	Log	Rel. conc
80ng/ul	14.76	14.67	14.715	2	100
16ng/ul	16.68	16.76	16.72	1.30103	20
3.2ng/ul	19.29	19.01	19.15	0.60206	4

GUSB	CT	CT	AVERAGE	Y	CT (Norm)	
HA-GST	16.68	16.76	16.72	1.346276	22.19607	1
FLAG-Myc 0.4	16.62	16.73	16.675	1.360415	22.93058	0.967967999
FLAG-Myc 0.8	16.84	16.83	16.835	1.310143	20.4241	1.086758386
FLAG-Myc 1.2	17.26	17.57	17.415	1.127907	13.42477	1.65336599
FLAG-Myc 1.6	16.84	17.32	17.08	1.233164	17.10661	1.297513843
FLAG-Myc 2.0	17.1	17.73	17.415	1.127907	13.42477	1.65336599

Table A. 26 CT values of target gene (PD-L1), data analysis for constructing a standard curve for PD-L1, and fold change normalization (PD-L1) against GUSB

PDL1	CT	CT	AVERAGE		Rel. conc
80ng/ul	18.13	17.95	18.04	2	100
16ng/ul	20.13	20.22	20.175	1.30103	20
3.2ng/ul	22.38	22.4	22.39	0.60206	4

PDL1	CT	CT	AVERAGE	Y	CT (Norm)	Norm to GUSB		
HA-GST	20.13	20.22	20.175	1.310173	20.42549	1	20.42549	1
FLAG-Myc 0.4	20.02	20.08	20.05	1.350335	22.40449	0.967967999	21.68683	1.061753
FLAG-Myc 0.8	19.83	19.75	19.79	1.433873	27.15645	1.086758386	29.5125	1.444886
FLAG-Myc 1.2	19.78	20.26	20.02	1.359974	22.90731	1.65336599	37.87416	1.854259
FLAG-Myc 1.6	19.7	19.59	19.645	1.480462	30.23163	1.297513843	39.22595	1.920441
FLAG-Myc 2.0	19.79	19.83	19.81	1.427447	26.75759	1.65336599	44.24009	2.165925

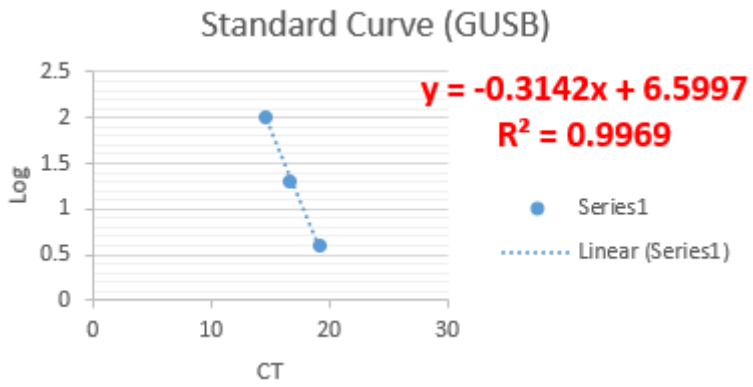

Figure A. 9 Standard curve of the housekeeping gene GUSB

Standard curve quantification is performed by constructing a standard curve for the reference gene GUSB, and plotting the CT values against log[quantity] of a dilution series of known amounts (80 ng/µL, 16 ng/µL, 3.2 ng/µL)

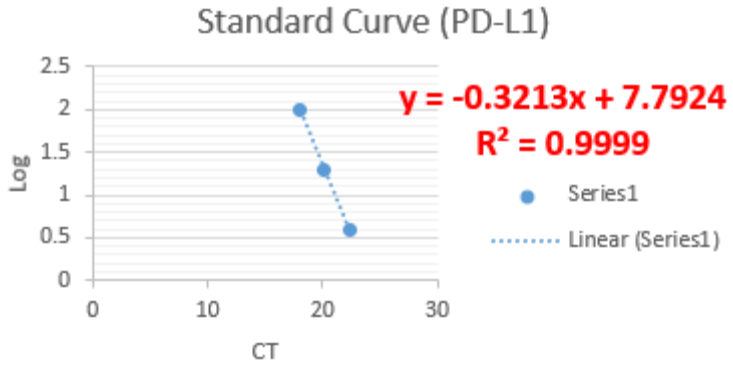

Figure A. 10 Standard curve of the target gene PD-L1

Standard curve quantification is performed by constructing a standard curve for target gene PD-L1, and plotting the CT values against log[quantity] of a dilution series of known amounts (80 ng/µL, 16 ng/µL, 3.2 ng/µL)

14. 2 Raw data for quantifying PD-L1 mRNA in Flp-In™ T-REx™ cells

Table A. 27 CT values of housekeeping gene (GUSB) and data analysis for constructing a standard curve for GUSB

GUSB	CT	CT	AVERAGE	Log	
500ng/ul	12.95	13.49	13.22	2	100
100ng/ul	14.12	14.57	14.345	1.30103	20
20ng/ul	16.47	16.39	16.43	0.60206	4

GUSB	CT	CT	AVERAGE	Y	CT (Norm)	
0h	14.12	14.57	14.345	1.4362	27.302317	1
6h	14.97	14.72	14.845	1.22475	16.77836	1.627233963
12h	14.74	14.92	14.83	1.231093	17.02523	1.603638595
24h	14.81	14.82	14.815	1.237437	17.275734	1.580385368
36h	14.91	14.89	14.9	1.20149	15.903401	1.716759661

Table A. 28 CT values of target gene (PD-L1), data analysis for constructing a standard curve for PD-L1, and fold change normalization (PD-L1) against GUSB

PDL1	CT	CT	AVERAGE	Log	
500ng/ul	20.43	20.91	20.67	2	100
100ng/ul	22.74	22.63	22.685	1.30103	20
20ng/ul	24.07	23.96	24.015	0.60206	4

PDL1	CT	CT	AVERAGE	Y	CT (Norm)	Norm to GUSB		set 0h to 1
0h	22.74	22.63	22.685	1.206243	16.078406	1	16.07841	1
6h	22	21.93	21.965	1.503027	31.843955	1.627233963	51.81756	3.2228048
12h	21.72	21.82	21.77	1.583406	38.318279	1.603638595	61.44867	3.8218136
24h	21.59	22.19	21.89	1.533942	34.193377	1.580385368	54.03871	3.3609496
36h	21.65	21.82	21.735	1.597833	39.612568	1.716759661	68.00526	4.229602

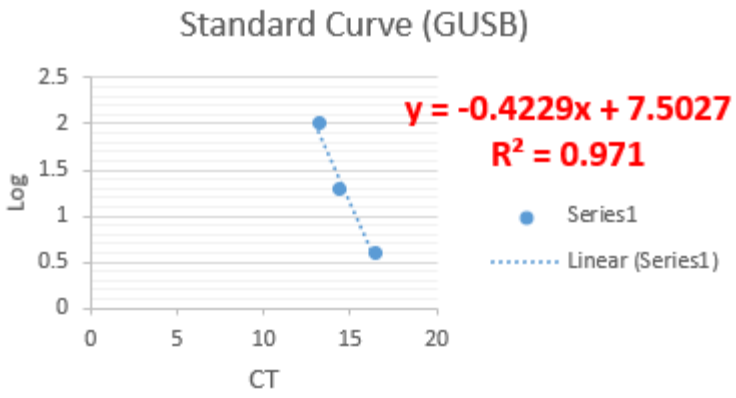

Figure A. 11 Standard curve of the housekeeping gene GUSB

Standard curve quantification is performed by constructing a standard curve for the reference gene GUSB, and plotting the CT values against log[quantity] of a dilution series of known amounts (500 ng/µL, 100 ng/µL, 20 ng/µL)

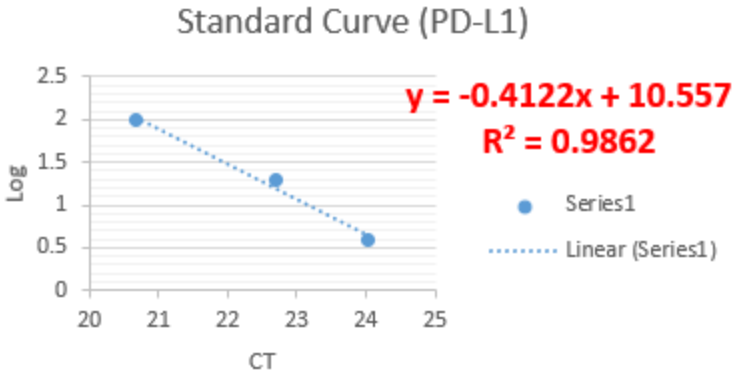

Figure A. 12 Standard curve of the target gene PD-L1

Standard curve quantification is performed by constructing a standard curve for target gene PD-L1, and plotting the CT values against log[quantity] of a dilution series of known amounts (500 ng/µL, 100 ng/µL, 20 ng/µL)

14. 3 Raw data for quantifying PD-L1 mRNA in H1299 cells

Table A. 29 CT values of housekeeping gene (GUSB) and data analysis for constructing a standard curve for GUSB

H1299					
GUSB	CT	CT	AVERAGE	Log	
30ng/ul	14.54	14.48	14.51	2	100
6ng/ul	16.46	16.78	16.62	1.30103	20
1.2ng/ul	18.84	18.17	18.505	0.60206	4

GUSB	CT	CT	AVERAGE	Y	CT (Norm)	
0h	16.46	16.78	16.62	1.274048	18.79525	1
6h	16.82	16.9	16.86	1.190144	15.4933	1.213120663
12h	17.03	17.21	17.12	1.099248	12.56747	1.495546773
24h	16.13	16.28	16.205	1.419132	26.25016	0.716004909
36h	16.32	16.25	16.285	1.391164	24.61297	0.76363179

Table A. 30 CT values of target gene (PD-L1), data analysis for constructing a standard curve for PD-L1, and fold change normalization (PD-L1) against GUSB

PDL1	CT	CT	AVERAGE		
30ng/ul	19.36	19.5	19.43	2	100
6ng/ul	21.32	21.24	21.28	1.30103	20
1.2ng/ul	23.5	23.45	23.475	0.60206	4

PDL1	CT	CT	AVERAGE	Y	CT (Norm)	Norm to GUSB		set 0h to 1
0h	21.32	21.24	21.28	1.339856	21.87036	1	21.87036	1
6h	18.95	19.14	19.045	2.110484	128.9686	1.213120663	156.4545	7.153721
12h	19.49	19.55	19.52	1.946704	88.45126	1.495546773	132.283	6.0485044
24h	19.16	19.5	19.33	2.012216	102.8528	0.716004909	73.64309	3.3672549
36h	19.97	20.3	20.135	1.734652	54.28152	0.76363179	41.45109	1.8953089

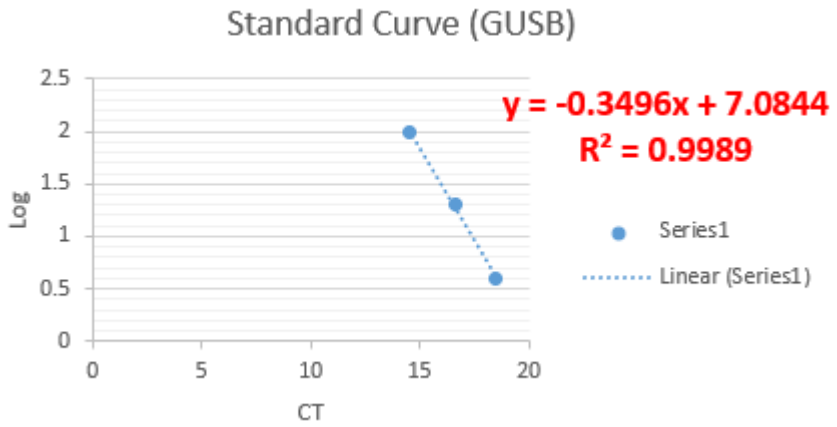

Figure A. 13 Standard curve of the housekeeping gene GUSB

Standard curve quantification is performed by constructing a standard curve for the reference gene GUSB and plotting the CT values against log[quantity] of a dilution series of known amounts (30 ng/µL, 6 ng/µL, 1.2 ng/µL).

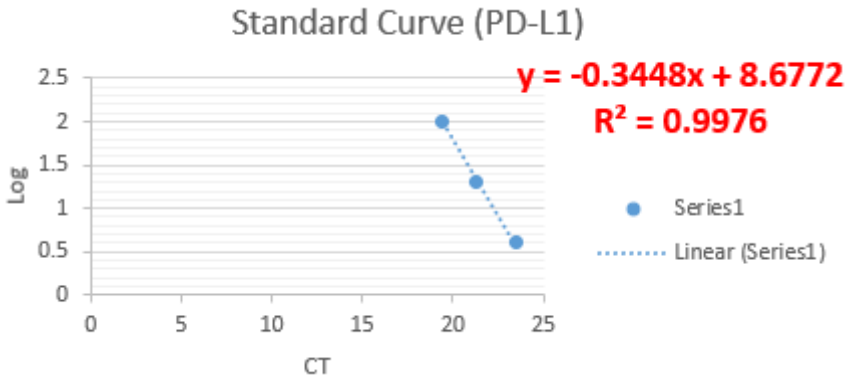

Figure A. 14 Standard curve of the target gene PD-L1

Standard curve quantification is performed by constructing a standard curve for target gene PD-L1 and plotting the CT values against log[quantity] of a dilution series of known amounts (30 ng/µL, 6 ng/µL, 1.2 ng/µL).

14. 4 Raw data for quantifying PD-L1 mRNA in response to serum stimulation and EP400NL induction

Table A. 31 CT values of housekeeping gene (GUSB) and data analysis for constructing a standard curve for GUSB

GUSB	CT	CT	AVERAGE		Rel. conc
100ng/ul	13.69	13.93	13.81	2	100
20ng/ul	15.47	15.45	15.46	1.30103	20
4ng/ul	17.79	17.62	17.705	0.60206	4

GUSB	CT	CT	AVERAGE	Y	CT (Norm)	
no Serum no Tet.	15.47	15.45	15.46	1.372194	23.56102	1
with Serum no Tet.	16.46	16.29	16.375	1.046363	11.1266	2.117539401
no Serum with Tet.	15.82	15.97	15.895	1.217291	16.49265	1.428576494
with Serum with Tet.	16.33	15.89	16.11	1.140729	13.82703	1.703981989

Table A. 32 CT values of target gene (PD-L1), data analysis for constructing a standard curve for PD-L1, and fold change normalization (PD-L1) against GUSB

PDL1	CT	CT	AVERAGE		Rel. conc
100ng/ul	23.21	23.49	23.35	2	100
20ng/ul	25.47	25.74	25.605	1.30103	20
4ng/ul	27.65	27.58	27.615	0.60206	4

PDL1	CT	CT	AVERAGE	Y	CT (Norm)	Norm to GUSB		
no Serum no Tet.	25.47	25.74	25.605	1.274523	18.81581	1	18.81581	1
with Serum no Tet.	25.65	25.54	25.595	1.277797	18.9582	2.117539401	40.14473	2.133563
no Serum with Tet.	25.28	25.12	25.2	1.40712	25.53407	1.428576494	36.47737	1.938655
with Serum with Tet.	24.75	24.81	24.78	1.544628	35.04516	1.703981989	59.71631	3.17373

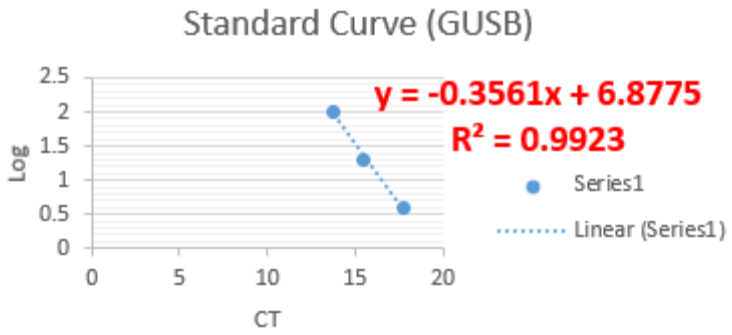

Figure A. 15 Standard curve of the housekeeping gene GUSB

Standard curve quantification is performed by constructing a standard curve for the reference gene GUSB, and plotting the CT values against log[quantity] of a dilution series of known amounts (100 ng/µL, 20 ng/µL, 4 ng/µL)

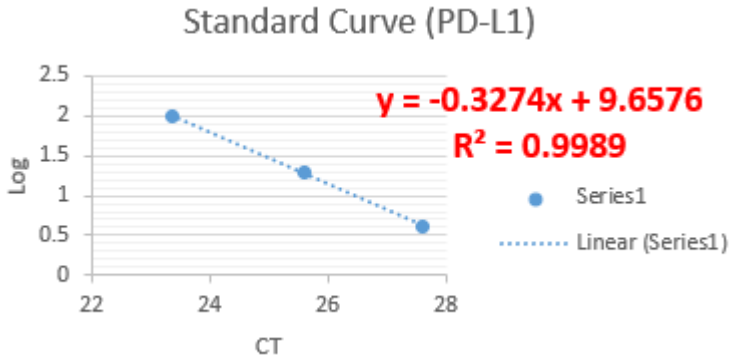

Figure A. 16 Standard curve of the target gene PD-L1

Standard curve quantification is performed by constructing a standard curve for target gene PD-L1 and plotting the CT values against log[quantity] of a dilution series of known amounts (100 ng/µL, 20 ng/µL, 4 ng/µL).

14. 5 Raw data for quantifying PD-L1 mRNA in response to IFNγ sensitization, serum stimulation, and tetracycline induction

Table A. 33 CT values of housekeeping gene (GUSB) and data analysis for constructing a standard curve for GUSB

GUSB	CT	CT	AVERAGE	Log	Rel. conc
100ng/ul	17.8	17.93	17.865	2	100
20ng/ul	19.54	20.09	19.815	1.301029996	20
4ng/ul	21	21.16	21.08	0.602059991	4

GUSB	CT	CT	AVERAGE	Y	CT (Norm)	
no Serum no Tet.	19.54	20.09	19.815	1.2039355	15.9932	1
no Serum no Tet.with IFNγ	19.41	19.49	19.45	1.360265	22.92266	0.697702855
no Serum with Tet.with IFNγ	20.49	20.86	20.675	0.8355975	6.848532	2.335274838
with Serum no Tet.with IFNγ	19.17	19.74	19.455	1.3581235	22.80991	0.701151714
with Serum with Tet.with IFNγ	19.07	20.4	19.735	1.2381995	17.30611	1.324541287

Table A. 34 CT values of target gene (PD-L1), data analysis for constructing a standard curve for PD-L1, and fold change normalization (PD-L1) against GUSB

PDL1	CT	CT	AVERAGE		Rel. conc
100ng/ul	23.89	23.48	23.685	2	100
20ng/ul	24.87	25.01	24.94	1.301029996	20
4ng/ul	26.99	26.84	26.915	0.602059991	4

PD-L1	Replicate1	Y		Normalization 1	Final	Fold change
no Serum no Tet.	24.87	1.433841	27.15445	1	27.15445	1
no Serum no Tet.with IFNγ	24.04	1.787172	61.2593	0.697702855	42.74079	1.573988301
no Serum with Tet.with IFNγ	24.3	1.67649	47.47774	2.335274838	110.8736	4.08307164
with Serum no Tet.with IFNγ	23.23	2.131989	135.5155	0.701151714	95.01693	3.499129374
with Serum with Tet.with IFNγ	23.14	2.170302	148.0137	1.324541287	196.0503	7.219822159

PD-L1	Replicate2	Y		Normalization 2	Final	Fold change
no Serum no Tet.	25.01	1.374243	23.67244	1	23.67244	1
no Serum no Tet.with IFNγ	24.15	1.740345	54.99776	0.697702855	38.37209	1.62096075
no Serum with Tet.with IFNγ	24.19	1.723317	52.88311	2.335274838	123.4966	5.21689385
with Serum no Tet.with IFNγ	23.24	2.127732	134.1937	0.701151714	94.09012	3.9746693
with Serum with Tet.with IFNγ	23.15	2.166045	146.57	1.324541287	194.138	8.20101299

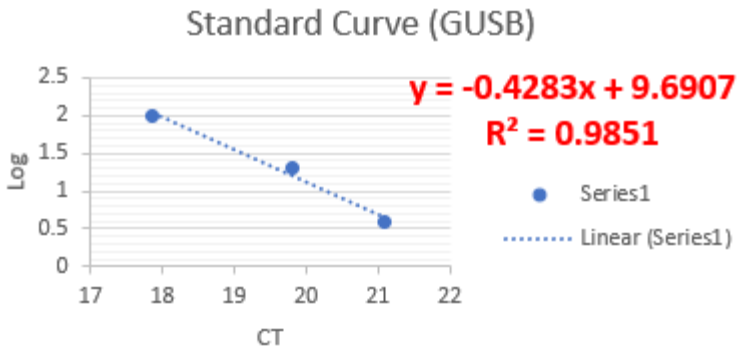

Figure A. 17 Standard curve of the housekeeping gene GUSB

Standard curve quantification is performed by constructing a standard curve for the reference gene GUSB, and plotting the CT values against log[quantity] of a dilution series of known amounts (100 ng/µL, 20 ng/µL, 4 ng/µL)

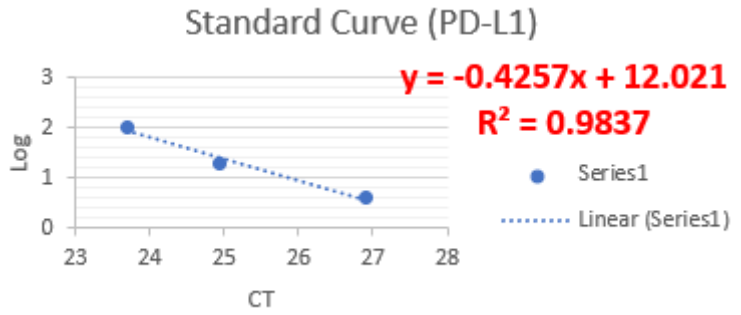

Figure A. 18 Standard curve of the target gene PD-L1

Standard curve quantification is performed by constructing a standard curve for target gene PD-L1 and plotting the CT values against log[quantity] of a dilution series of known amounts (100 ng/µL, 20 ng/µL, 4 ng/µL).